Reconstruction of changes in the Southern Ocean Overturning Circulation using radiogenic Pb and Nd isotopes in marine sediments and a Fe-Mn crust for the past 19 Ma

Dissertation
zur Erlangung des Doktorgrades
Dr. rer. nat.

der Mathematisch-Naturwissenschaftlichen Fakultät der
Christian-Albrechts-Universität zu Kiel

vorgelegt von
Huang Huang
Kiel, 2019

Gutacher und Betreuer: Prof. Dr. Anton Eisenhauer

2. Gutachter: Prof. Dr. Samuel Jaccard (Univ. Bern. Switzerland)

Eingereicht am:

Datum der Disputation: 28.10.2019

Zum Druck genehmigt:

gez. (Titel, Vor- und Zuname), Dekan

Statement

I hereby assure on oath that I am doing this dissertation independently and only with help of the specified sources and tools. Furthermore, I assure you that the contents of this document, neither in this nor in modified form, another Examining authority. The work is good in compliance with the rules scientific practice of the Deutsche Research Foundation.

Kiel, 2019

Huang Huang

Context

Abstract

Radiogenic lead (Pb) and neodymium (Nd) isotopes are sensitive paleoceanographic proxies for the reconstruction of ocean circulation changes in the past. The goal of this dissertation is to develop improved approaches to recover past seawater Pb and Nd isotope signals from marine sediments and ferromanganese (Fe-Mn) crust, and apply it for tracing water mass sourcing changes in the Southern Ocean at (sub-)millennial resolution.

Chemical reductive leaching of hydrogenentic Fe-Mn oxyhydroxides from bulk marine sediments offers an efficient and easily accessible way to recover past seawater Pb and Nd isotope signatures. However, the leached seawater derived Pb and Nd isotope signal could be compromised if substantial quantities of Pb and Nd were released from non-hydrogenentic sediment fractions during leaching. In Chapter 3, a fast and reliable vortexing leaching method is presented for extracting porewater Pb and Nd isotope signals from sediment samples in the Atlantic sector of the Southern Ocean. The effect of a previously introduced $MgCl_2$ prewash is investigated, as well as the role of chelate ligands and length of leaching time. In order to validate the vortexing leaching method, Pb and Nd isotope signatures were analysed in actual seawater and underlying porewater and sediment leachates from three stations in front of the Filchner-Rønne Ice Shelf, Antarctica. The well-matching results between water sample and leachates corroborate the robustness of this method. Moreover, using the newly developed vortexing leaching method, I generated authigenic Pb and Nd isotopic maps from 70 Southern Ocean coretop sediment samples to help select suitable sites for paleoceanographic and paleoclimatic reconstructions.

In Chapter 4, seawater-derived downcore sedimentary Nd and Pb isotope records are presented from three Southern Ocean sites inside and outside the Weddell Sea to resolve changes in Southern Ocean overturning circulation for the past two glacial terminations. The data provide strong evidence for the absence of Weddell Sea

AABW outside the Weddell Sea during the last and penultimate glacial maximum. The successive southward displacement of the SO overturning cell following glacial maxima is recorded by increasing contributions of Weddell Sea derived Pb admixtures to regions outside the Weddell Sea during both glacial terminations. The export of Weddell Sea AABW resumed late during glacial terminations, coinciding with the last major atmospheric CO_2 rise in the transition to the Holocene and the Eemian. While Holocene AABW formation and export out of the Weddell Sea took place without major perturbations, our new records lend strong support for a previously inferred overturning stagnation event during the peak Eemian interglacial.

In Chapter 5, an unprecedented continuous high-resolution Pb isotope record was recovered from a Fe-Mn crust grown on the Marie Byrd Seamont in the Pacific sector of the Southern Ocean using laser ablation coupled MC-ICPMS. The Pb isotope data document the ACC history for the past 19 million years and indicate that the final establishment of clockwise (eastward) circulating Antarctic Circumpolar Currents took place at 14 Ma. The Pb isotopic evolution also suggest five large-scale ocean circulation reorganization events which are likely related to changes in Antarctic Bottom Water formation and tectonic events in ocean gateway regions, i.e. Panama Seaway and Drake Passage.

Overall, the results presented in this dissertation show deep sea Pb and Nd isotope records are able to resolve the changes in the glacial/interglacial Southern Ocean overturning circulation front shifting and the Antarctic Bottom Water evolution. The Pb isotope system also shows great potential in tracking Antarctic ice dynamics and ocean circulation changes on Cenozoic timescales. Applying these approaches employed in this dissertation to different key locations and into different time period will help resolving more ocean circulation mysteries.

Kurzzusammenfassung

Radiogene Blei- (Pb) und Neodym- (Nd) Isotopenverhältnisse sind sensitive paläozeanographische Werkzeuge für die Rekonstruktion von Ozeanzirkulationsmustern der Vergangenheit. Das Ziel dieser Doktorarbeit ist, einen verbesserten methodischen Ansatz zu entwickeln, um vergangene Pb- und Nd-Isotopensignale aus marinen Sedimenten und aus Eisenmangankrusten (Fe-Mn-Krusten) zu gewinnen und diese für die Rekonstruktion der Änderungen der Südozeans-Zirkulation mit einer zeitlichen Auflösung von bis zu unter tausend Jahren anzuwenden.

Das chemisch reduzierende Lösen von hydrogenetischen Fe-Mn Oxyhydroxiden aus marinen Sedimenten ist ein effizienter und einfacher Weg, um vergangene Pb- und Nd-Meerwasserisotopensignaturen zu gewinnen. Allerdings könnten die gelösten Pb- und Nd-Isotopensignale verfälscht werden, falls während des chemischen Lösungsvorgangs erhebliche Mengen an Pb und Nd aus nicht-hydrogenetischen Sedimentkomponenten gelöst werden. In Kapitel 3 wird eine schnelle und zuverlässige „Vortexing"-Lösungssmethode für die Extrahierung von Pb- und Nd-Isotopensignalen aus Sedimentproben des atlantischen Sektors des Südozeans präsentiert. Sowohl der Effekt einer vorherigen Vorreinigung mit $MgCl_2$ wird untersucht, als auch die Rolle von Chelatliganden und die Länge der Lösungsdauer. Um die „Vortexing"-Lösungsmethode zu validieren, wurden die Pb- und Nd-Isotopensignaturen in Meerwasserproben, sowie im sedimentären Porenwasser und in chemisch gelösten Fe-Mn Oxyhydroxiden an drei Stationen vor dem Filchner-Rønne-Eisschelf in der Antarktis analysiert und verglichen. Die gut zueinanderpassenden Ergebnisse zwischen Wasserproben und gelösten Fe-Mn Oxyhydroxiden belegen die Zuverlässigkeit dieser Methode. Zudem habe ich mithilfe der neu entwickelten „Vortexing"-Lösungsmethode authigene Pb- und Nd-Isotopenkarten mittels 70 Oberflächensedimentproben aus dem Südozean

generiert, die helfen sollen, geeignete Orte für paläozeanographische und paläoklimatische Rekonstruktionen auszuwählen.

In Kapitel 4 werden Meerwasser-Nd- und Pb-Isotopendatensätze aus Sedimentkernen präsentiert. Sie stammen von drei Südozeanlokalitäten innerhalb und außerhalb des Weddellmeeres und sollen Änderungen in der Südozean-Umwälzzirkulation der letzten zwei Deglaziationen aufzeigen. Die neuen Daten belegen die Abwesenheit von aus dem Weddellmeer stammenden Antarktischen Bodenwassers (AABW) im atlantischen Sektor des Südozeans während des letzten und vorletzten glazialen Maximums. Die schrittweise Verlagerung der Zirkulationszelle des Südozeans nach Süden im Anschluss an glaziale Maxima wird durch erhöhte Anteile von Pb-Beimischungen aus dem Weddellmeer in Regionen außerhalb des Weddellmeeres während beider Deglaziationen aufgezeichnet. Der Export von Weddellmeer-AABW setzte spät während der jeweiligen Deglaziationen wieder ein und ereignete sich zeitgleich mit dem letzten größeren Anstieg des atmosphärischen CO_2-Gehalts während des Überganges ins Holozän und in die Eem-Warmzeit. Während die Bildung und der Export Antarktischen Bodenwassers aus dem Weddellmeer während des Holozäns ohne größere Störungen erfolgte, bekräftigen die neuen Datensätze eine frühere Studie, laut derer sich eine Stagnation des AABW-Exports aus dem Weddellmeer während des Höhepunktes des Eem-Interglazials ereignete.

In Kapitel 5 wurde ein bisher einmaliger kontinuierlicher Pb-Isotopendatensatz in hoher zeitlicher Auflösung aus einer Fe-Mn-Kruste gewonnen, die von dem Marie Byrd Seamount im pazifischen Sektor des Südozeans stammt. Dieser Datensatz wurde mit Hilfe einer Laserablations-Methode, gekoppelt an ein Multikollektor-Massenspektrometer, gemessen. Die Pb-Isotopendaten dokumentieren die Entwicklung des Antarktischen Zirkumpolarstroms während der letzten 19 Millionen Jahre und belegen die Etablierung des im Uhrzeigersinn (ostwärts) fließenden Antarktischen Zirkumpolarstroms vor 14 Ma. Die Pb-Isotopenentwicklung deutet außerdem auf fünf umfassende regionale Zirkulationsänderungen im

pazifischen Sektion des Südozeans hin. Diese stehen wahrscheinlich mit der Entstehung des Rossmeer-Tiefenwassers und tektonischen Ereignissen in Ozean-Gateway-Regionen wie der Schließung des Panamaseewegs und der Öffnung der Drakepassage in Verbindung.

Insgesamt erlauben die in dieser Doktorarbeit präsentierten Ergebnisse Einblicke in die deglazialen Änderungen der Zirkulation des Südozeans mithilfe einer Kombination aus tiefmarinen Pb- und Nd-Isotopendatensätzen. Das Pb-Isotopensystem birgt zudem großes Potential, um die antarktische Eisdynamik sowie känozoische Ozeanzirkulationsänderungen nachzuverfolgen. Die Anwendung der in dieser Doktorarbeit verwendeten Ansätze auf verschiedene Schlüssellokationen und auf verschiedene Zeitspannen kann helfen, weitere Rätsel der Ozeanzirkulation zu lösen.

Acknowledgements

First and foremost I want to thank my advisor Marcus Gutjahr. He is a dedicated and modest scientist model which I wish oneday I can shape myself into. I appreciate all his contributions of time, ideas, and effort to make my Ph.D. experience productive and stimulating. His office door is constantly open and he is always very patient with my daily basic questions since the beginning of my Ph.D study. Whenever I have an abstract or manuscript asking him for comments or revisions, he can quickly and properly give me feedbacks. I really enjoyed sharing the carbin with Marcus during Polarstern cruise PS111 in 2018 and am grateful to his help when the sea sickness took me down.

I want to thank my advisor Anton Eisenhauer for welcoming me as a member of his group and providing funding to support my Ph.D. study. He secured the free research environment around me which plays an essential role in my scientific work in GROMAR. I also benefit from his scientific advice and his group has been a source of friendships as well as collaboration during my Ph.D. study.

I am especially grateful of the support from my co-advisor Gerhard Kuhn. He invited me twice for Polarstern cruises to the Weddell Sea where the scenary is phenomenal. I couldn't even image me to have this fantastic life experience before I came to Germany. He also kindly provided me important sediment samples which are the foundation of my Ph.D. work.

It's my honour to have Martin Frank as my co-advisor as well. He has been always very supportive, and especially in the last two years he offered me a lot help during paper revisions and Fe-Mn crust dating.

I would like to thank Sam Jaccard for giving me important comments and suggestions for my first manuscript. Also, it is a great pleasure to have you as my external examiner.

I would like to thank all the members in our reseach group. I need to firstly give many thanks to Tyler Goepfert for his outstanding technical assistance and also for being a wonderful neighbour of mine. I also benefited a lot from the discussion with Jan Fietzke when he was having a cigarette in the smoking hotspot. I really appreciate the lab support and the concentration measurements by Ana Kolevica. I enjoyed the time spent with Volker Liebetrau, Florian Böhm and Isabelle Taubner no matter for scientific topics or dinners in the restaurants in Kiel.

With great appreciation I shall acknowledge Ed Hathorne and Christian Schlosser for their help of seaFAST measurement, and Chris Siebert for giving me the lab introduction tours at my first arrival. I also want to thank Sevasti Modestou for kindly providing me the USGS NOD standard pellets for my laser ablation work, Mario Thöner for the microprobe measurement. and Lisa Bretschneider for helping me translate the abstract into German.

In the end, I am grateful to my parents and friends. They always gave me enough support, encouragement and motivation to accomplish my goals.

1 Introduction

1.1 The present-day Southern Ocean overturning circulation

The Southern Ocean has a profound influence on the world's ocean and climate. It connects the three major oceans, Altlantic, Indian and Pacific, and shapes the characteristics of the global ocean in temperature, salinity, and chemical properties (Carter et al. 2008). Circulation in the Southern Ocean is taking place via the Antarctic Circumpolar Current (ACC), which is the most prominent current in the Southern Hemisphere transferring about 134 million m^3 s^{-1} (134 Sv) of seawater from west to east (Gordon 2001). To the north the ACC is bound by the Subtropical Front (STF) and its southern boundary is characterized by large clockwise flowing gyres within embayments of Antarctica, notably the Weddell and Ross Seas.

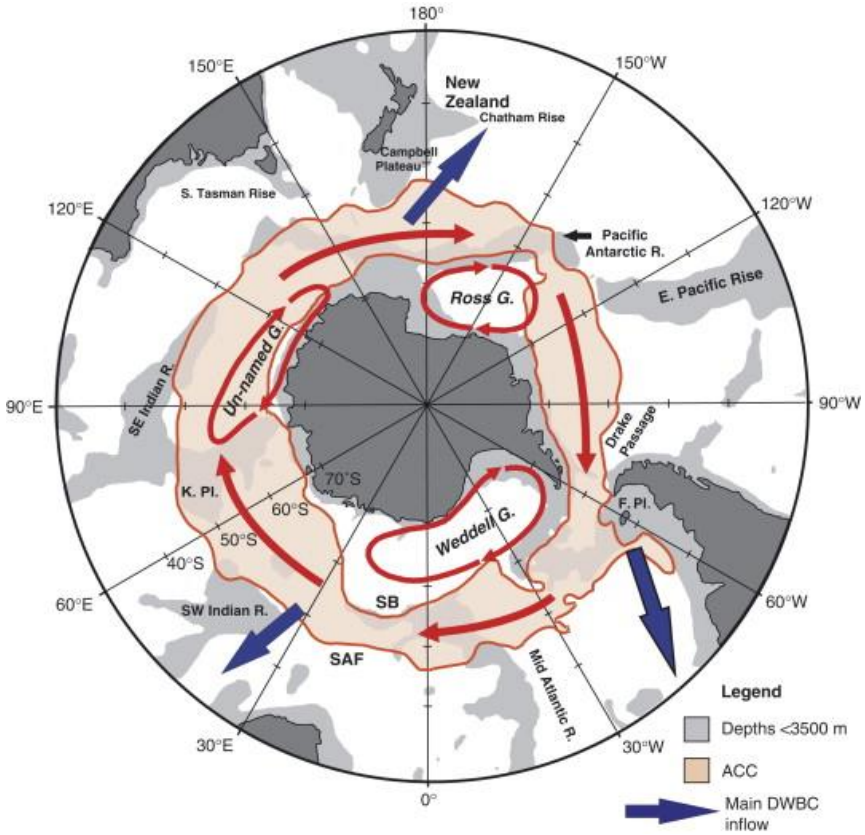

Figure 1.1 The main oceanographic elements of the Southern Ocean. The ACC is constrained by the Subantarctic Front (SAF) and its southern boundary (SB). The blue arrows indicate main exit routes of Deep Western Boundary Currents (DWBC) from the Southern Ocean. The Ross, Weddell and other gyres are also presented. Bathymetric elevations are annotated as R., ridge; K. Pl., Kerguelen Plateau; and F. Pl., Falkland Plateau (Figure from Carter et al. 2008).

From surface to abyss, the major water masses in the Southern Ocean can be divided into Antarctic Surface Water (ASW), Antarctic Intermediate Water (AAIW), Circumpolar Deep Water (CDW) and Antarctic Bottom Waters (AABW). Strong westerly winds control the motion of the surface ACC and the maximum westerlies occur near 55°S, which roughly coincides with the axis of the ACC (Gordon 2001) . Equally at 55°S latitude, surface water sinks underneath the more buoyant surface water to the north, producing AAIW. To the south of this latitude, wind-induced northward Ekman transport of surface water results in a wide region of upwelling. Upwelling poleward of the maximum westerlies brings deep water to the sea surface to compensate for the sinking of AABW to the south and AAIW to the north (Orsi et al. 1995, Orsi et al. 1999). Modern AABW is formed by two main processes: (i) in ice-free polynyas, surface water cools to freezing and increases salinity due to sea-ice formation, sinking down the continental slope, and (ii) water drawn underneath the ice shelves cools down to temperatures below surface freezing temperature and is

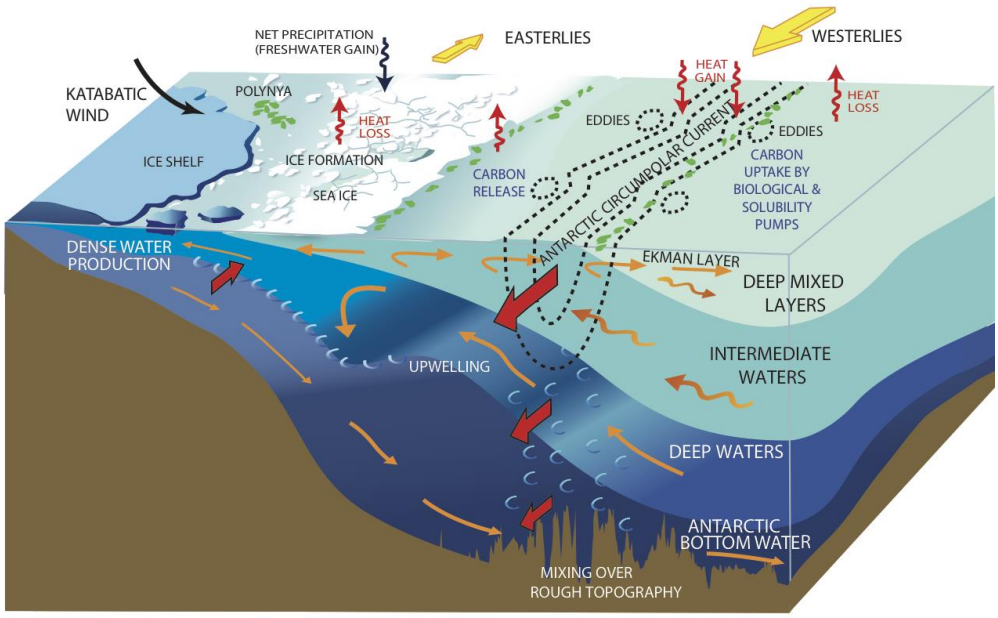

Figure 1.2 Schematic section of the main water masses and their meridional transport (Figure from Talley 2018).

exported from the ice shelf front as super-cooled Ice Shelf Water (ISW) (Jacobs 2004). The exported AABW from the Weddell Sea is incorporated into the ACC and mixes

with polarward moving deep waters from lower latitudes, i.e. North Atlantic Deep Water (NADW), which in turn produces CDW that occupies the major part of deep ACC (Orsi et al. 1999).

1.2 Southern Ocean circulation in the past

The development of the first continental-scale ice sheet on Antarctica occurred at ~34 Ma, coincident with a ~1.5‰ increase in benthic foraminiferal $\delta^{18}O$ (Zachos et al. 2001, Coxall et al. 2005), which was interpreted as a 4°C cooling in deep ocean temperature (Liu et al. 2009) with 80 m of sea level equivalent in ice volume on the Antarctic continent (DeConto et al. 2008). The development of a deep ACC is widely

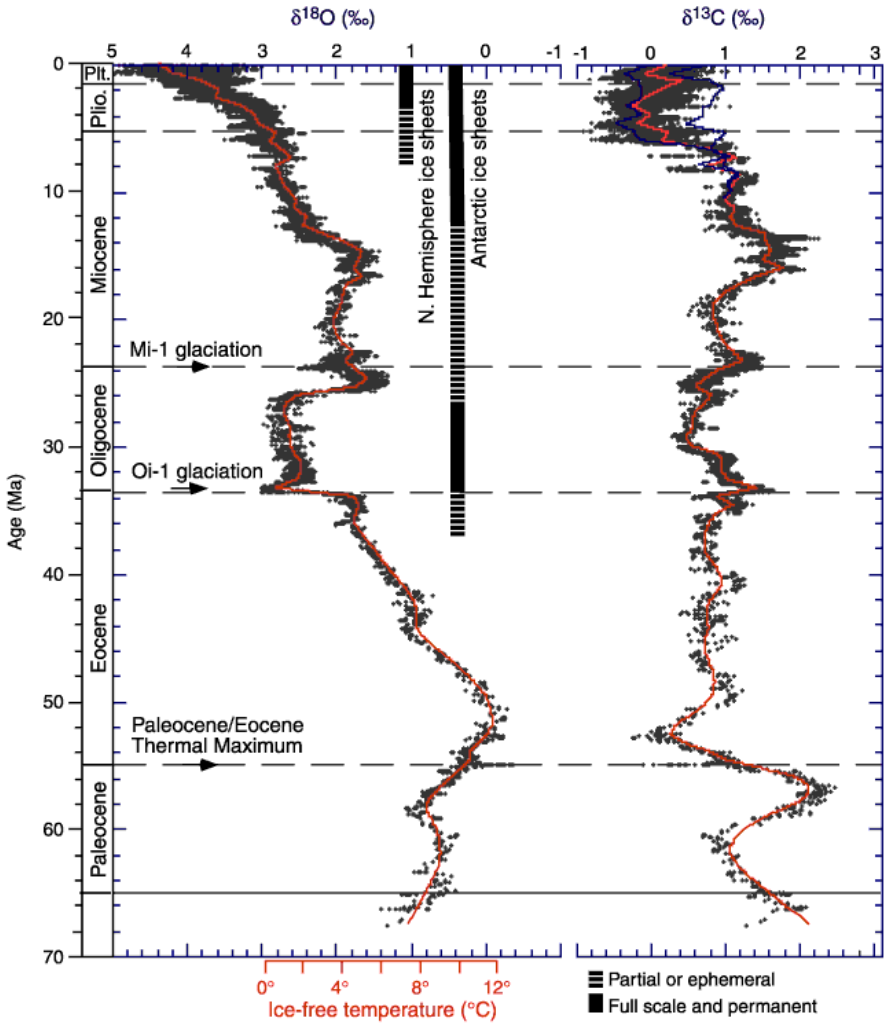

Figure 1.3 Global deep-sea oxygen and carbon isotope records for the past 70 Ma (Figure modified from Zachos et al. 2001).

understood to have been a key factor in the history of Antarctic glaciation on Cenozoic timescales (Kennett 1977, Zachos et al. 2001, Barker and Thomas 2004), but the timing of onset of the ACC is still uncertain. The formation of a deep ACC requires seawater to pass around the Antarctic continent both through the Tasman Gateway (TG) south of Australia and the Drake Passage (DP) south of South America. Therefore, the progressive tectonic opening of these two gateways exerted a key control on ACC evolution. Tasman Gateway deepening started around 35.5 Ma and was completed by ~30.2 Ma (Stickley et al. 2004), and the existence of deep seawater within the TG was also confirmed by a seawater Nd isotope record (Scher et al. 2015). However, the timing of deep water advection following gateway establishment through the DP and ACC is still unresolved, even though the first influx of shallow Pacific seawater from Pacific to Atlantic through the DP was found at approximately 41 Ma. The two alternative estimated age ranges for the deep opening of DP – based mainly on palaeomagnetic tectonic reconstructions – are ~31–28.5 Ma (Lawver and Gahagan 2003) and ~22–17 Ma (Barker 2001), and both these time-frames have their supporters within the geologic community (Pfuhl and McCave 2005).

On shorter glacial-interglacial timescales, Southern Ocean overturning circulation in the late Pleistocene plays an important role in regulating atmospheric carbon dioxide concentrations (CO_2) (Anderson et al. 2009, Sigman et al. 2010, Skinner et al. 2010, Jaccard et al. 2016). In the modern Atlantic sector of the Southern Ocean, AABW generated from Weddell Sea occupies the deep ocean and spreads to the South Atlantic Ocean (van Sebille et al. 2013, Ferrari et al. 2014). The deep ocean waters with high CO_2 and nutrient content are brought to the surface by wind-driven upwelling and density-driven overturning resulting in elevated atmospheric CO_2. In contrast to the modern scenario, the glacial Southern Ocean circulation was found to be very different. A stratified and poorly ventilated deep Southern Ocean during the Last Glacial Maximum (LGM) was suggested, which led to elevated carbon sequestration in the deep ocean and reduced atmospheric CO_2 concentrations (Broecker and Henderson 1998, Anderson et al. 2009, Skinner et al. 2010, Burke and

Robinson 2012), but the origin of deep waters in the glacial Southern Ocean remains unresolved at present. Presumably, glacial Weddell Sea derived AABW occupied large parts of the deeper Atlantic Ocean at the expense of NADW during the LGM and major Northern Hemisphere Stadials, a finding mainly based on salinity and temperature reconstructions in the deep sea from ODP Site 1093 which is far away from its AABW source in the Weddell Sea (Adkins et al. 2002). However, the seawater Nd isotope records in deep South Atlantic Ocean during the LGM were more radiogenic than modern seawater Nd signature of Weddell Sea derived AABW, indicating possibly more Pacific sourced water contribution instead of full dominated glacial Weddell Sea derived AABW (Skinner et al. 2013, Hu et al. 2016, Lippold et al. 2016, Wei et al. 2016). Even more, the glacial-interglacial variability of AABW

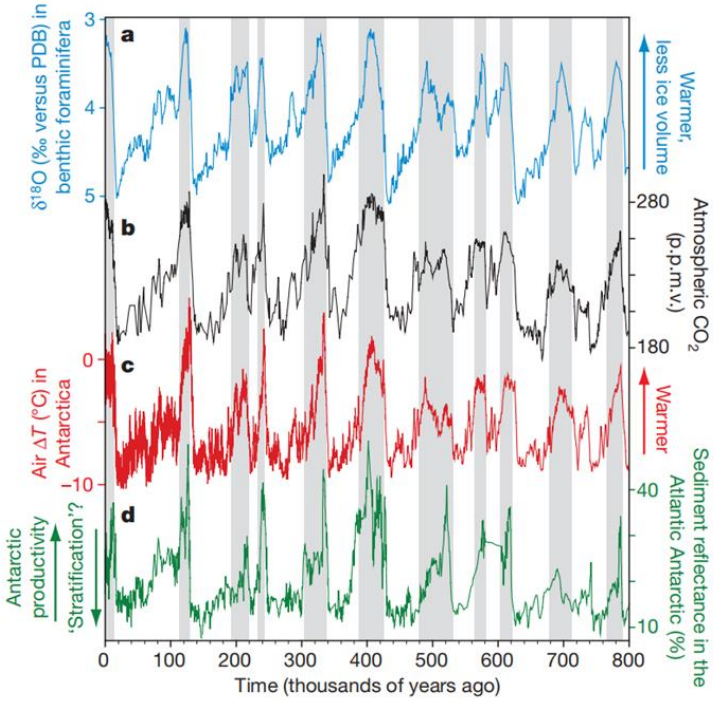

Figure 1.4 Compilated records of deep sea oxygen isotope, atmospheric pCO_2, and Southern Ocean conditions over the last 800 thousand years. a, Benthic foraminiferal $\delta^{18}O$ records (Lisiecki and Raymo 2005) which reflect changes in continental glaciation and deep ocean temperature. b, Atmospheric CO_2 concentrations in the past were reconstructed from Antarctic ice cores (Lüthi et al. 2008). c, Antarctic air temperature as reconstructed from the deuterium content of an Antarctic ice core (Jouzel et al. 2007). d, The sediment reflectance of an Antarctic deep sea sediment record from Site ODP 1094 (Hodell et al. 2002), providing a measure of the export of biogenic material (including organic carbon) out of the surface ocean. Grey bars indicate warm intervals ('interglacials') (Figure from Sigman et al. 2010).

formation and its export history are also barely understood.

1.3 Radiogenic Nd and Pb isotopes as paleoceanographic proxies

Radiogenic Nd and Pb isotopes have been successfully applied as paleoceanographic proxies on both long Cenozoic and short (sub-)millennial, or even decadal, timescales for decades (Frank 2002). They are excellent water mass tracers for reconstructing circulation changes in the past since (1) they have a suitable seawater residence time, which is shorter than seawater mixing time (1000 yrs, or more) but still long enough to travel for a distance (Schaule and Patterson 1981, Cochran et al. 1990, Tachikawa et al. 1999, Henderson and Maier-Reimer 2002, Tachikawa et al. 2003); (2) different water masses have distinguishable Nd and Pb isotope signatures, supplied by variably aged continental sources with distinct chemical composition (Martin 2002, Goldstein and Hemming 2003); 3) Dissolved Nd and Pb in seawater are scavenged and preserved into fish tooth (Staudigel et al. 1985, Martin and Scher 2004), corals (Shen and Boyle 1987, van de Flierdt et al. 2006, Colin et al. 2010, van de Flierdt et al. 2010, Lee et al. 2014, Wilson et al. 2014, Lee et al. 2017, Struve et al. 2017, Wilson et al. 2017), foraminifera (Vance and Burton 1999, Klevenz et al. 2008, Roberts et al. 2010), ferromanganese (Fe-Mn) crusts or nodules (Burton et al. 1997, Christensen et al. 1997, Goldstein and Hemming 2003) and authigenic sedimentary Fe-Mn oxyhydroxides (Piotrowski et al. 2004, Gutjahr et al. 2007).

Nd has only one radiogenic isotope, ^{143}Nd, generated by radioactive decay of ^{147}Sm with a half-life 106 Gyr. Therefore, the abundance of ^{143}Nd in a rock relative to that of other stable isotopes of Nd, such as ^{144}Nd, varies as a function of age and Sm/Nd ratio. Because of the very small differences among ^{143}Nd/^{144}Nd ratios, which are mostly at the fourth decimal place, Nd isotope ratios are expressed as ε_{Nd} values:

$$\varepsilon_{\mathrm{Nd}} = \left(\frac{\left(\frac{^{143}\mathrm{Nd}}{^{144}\mathrm{Nd}}\mathrm{Sample}\right) - \left(\frac{^{143}\mathrm{Nd}}{^{144}\mathrm{Nd}}\mathrm{CHUR}\right)}{\left(\frac{^{143}\mathrm{Nd}}{^{144}\mathrm{Nd}}\mathrm{CHUR}\right)} \right) * 10000$$

where CHUR is the $^{143}Nd/^{144}Nd$ of the chondritic uniform reservoir (presently 0.512638). Early studies suggested dissolved Nd in the ocean acquires its isotopic signature mainly from rivers and dust (Goldstein et al. 1984, Goldstein and Jacobsen 1987, Frank 2002), but these alone are insufficient to close the mass balance of Nd in the ocean (Bertram and Elderfield 1993, van de Flierdt et al. 2004, Rempfer et al. 2011). Recently, a growing number of studies have shown that Nd can be exchanged, released and adsorbed in continental margin settings, which is commonly called boundary exchange (Lacan and Jeandel 2005, Lacan et al. 2012). Several studies

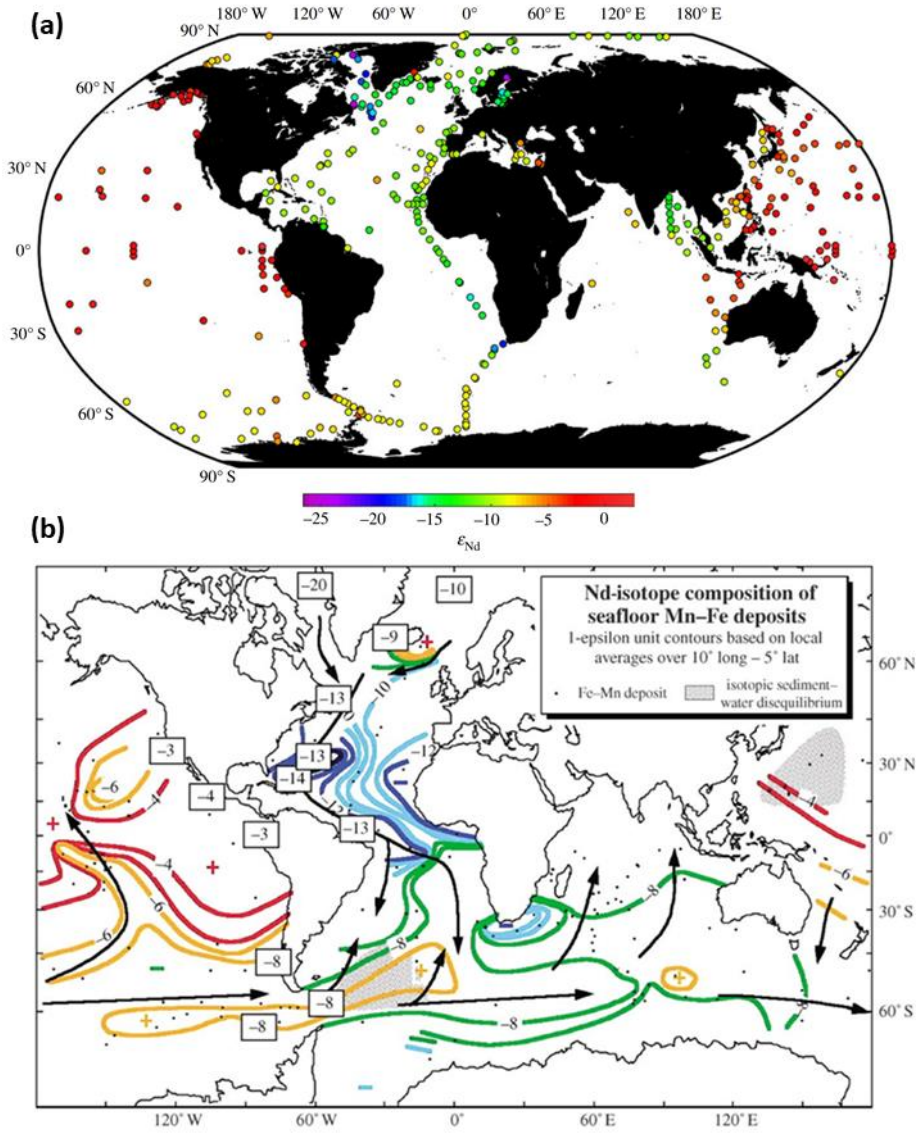

Figure 1.5 Map of Nd isotopic compositions in (a) surface (or shallow subsurface) seawater and (b) surface Fe-Mn deposits (Modified from Goldstein and Hemming 2003 and van de Flierdt et al. 2016).

suggested that boundary exchange is even dominating the oceanic Nd budget (Tachikawa et al. 2003, Arsouze et al. 2009, Jeandel and Oelkers 2015). Although the Nd budget in the Ocean is not yet fully constrained, the unique Nd signatures found in different modern oceans suggest that Nd isotopes are a promising tracer for water mass mixing and global ocean circulation. In general, North Pacific water masses feature very radiogenic ε_{Nd}=-3 (Fröllje et al. 2016) and North Atlantic Deep Water in the vicinity of the Labrador Sea has an unradiogenic ε_{Nd}=-14 (Lacan and Jeandel 2005), while the Southern Ocean has ε_{Nd} signatures ranging from -7 to -9 (Stichel et al. 2012, Rickli et al. 2014, Basak et al. 2015). The average oceanic Nd residence time between 600 and 2000 years (Tachikawa et al. 1999, Tachikawa et al. 2003) allows radiogenic Nd to serve as a 'quasi-conservative' water mass tracer, whereby variable Nd isotope signatures are resolvable between different water masses as found in the Northern Atlantic (Lambelet et al. 2016).

In contrast to Nd, Pb has three stable isotopes (^{206}Pb, ^{207}Pb, ^{208}Pb) which are the final products of the three uranium decay series with the parent isotopes ^{238}U, ^{235}U and ^{232}Th (respective half-lives are: 4.47 Gyr, 0.704 Gyr, and 14 Gyr, respectively). Pb

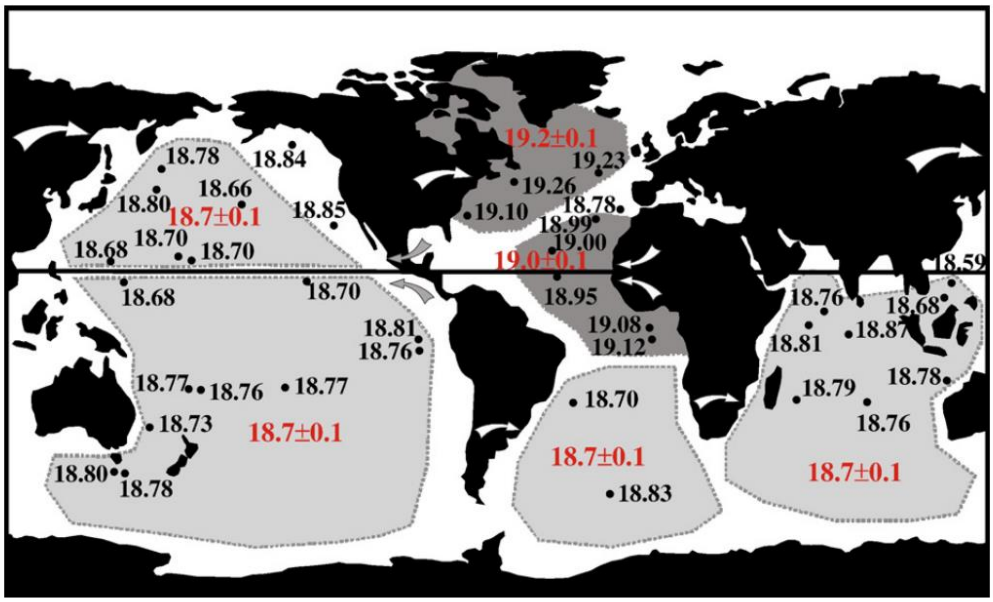

Figure 1.6 ^{206}Pb/^{204}Pb of ferromanganese crust surfaces which represent pre-industrial values. Figure from Klemm et al. 2007.

isotopic compositions are commonly expressed as $^{206}Pb/^{204}Pb$, $^{207}Pb/^{204}Pb$ and $^{208}Pb/^{204}Pb$. Pre-industrial dissolved Pb in the ocean is mainly supplied by riverine input so that the regional seawater Pb isotopic signatures are depending on the Pb isotopic compositions of the source areas (Frank 2002). Unfortunately, the modern seawater Pb isotope composition is heavily overprinted by anthropogenic contaminations and pre-industrial seawater Pb signature can only be recovered from either ferromanganese crusts and nodules or authigenic Fe-Mn oxyhydroxides in sediments (Gutjahr et al. 2007, Klemm et al. 2007, Gutjahr et al. 2009).

Dissolved Pb in seawater behaves differently compared with Nd. Because Pb is more particle-reactive than Nd, its residence time in seawater is significantly shorter on the order of few tens of years (Schaule and Patterson 1981, Cochran et al. 1990, Henderson and Maier-Reimer 2002), compared with several hundreds of years for dissolved Nd (Tachikawa et al. 1999, Tachikawa et al. 2003), leading to a short transport distance of Pb in the ocean. The high particle-reactivity of Pb also leads to its special behaviour in seawater. A recent studies showed that Pb isotopic changes in surface seawater can leave a footprint in the underlying deep water Pb isotopes signal even without vertical water mass mixing because of the seawater-particle Pb exchange mechanism (Wu et al. 2010). Overall, taking advantage of different behaviours of Pb and Nd in seawater, the combination of deep sea Pb and Nd isotope records enables us to resolve circulation changes affecting the entire water column.

1.4 Outline of the Thesis

This dissertation addresses three main scientific objectives, starting from establishing a reliable method to extract hydrogenetic Pb and Nd from the Fe-Mn oxyhydroxide fraction in Southern Ocean sediments, and then using seawater-derived Pb and Nd isotope records to reconstruct both upper and lower Southern Ocean overturning processes for the past two glacial-interglacial transitions. Finally, a high-resolution laser ablation-based seawater Pb isotope record extending back to the Miocene is presented and discussed.

Chapter 2 presents the principal sampling processes during the two Polarstern cruises (PS111 and PS118), and chemical procedures applied to extract and purify Pb and Nd from marine sediments and seawater. The laser ablation as well as electron microprobe analytical procedures and mass spectrometric approaches for Pb and Nd isotopes are also described in detail.

Chapter 3 discusses the ideal reductive leaching protocol for extracting hydrogenetic Pb and Nd in sediments derived from the Atlantic sector of the Southern Ocean. The modified leaching method is validated by comparison with corresponding Pb and Nd isotope signatures in sediment leachates and corresponding seawater and porewater from three stations in front of the Filchner-Rønne Ice Shelf. The Pb and Nd isotopic maps generated from 70 coretop sediment samples in the studied area are also presented to help select suitable core sites for potential paleoceanographic studies.

Chapter 4 presents sub-millennial-resolution seawater Pb and Nd isotope records to reconstruct changes in Southern Ocean circulation during the past two glacial terminations. Combination of deep sea Pb and Nd isotope records allows resolving the evolution of both the upper and lower Southern Ocean overturning cells during glacial terminations. Because East and West Antarctica supply very unique Pb isotope signatures into the Weddell Sea, the deep sea Pb isotope record also provides the potential to reveal different Antarctic ice dynamics between the past two glacial-interglacial transitions.

In Chapter 5, a high-resolution seawater Pb isotope signals in Fe-Mn crust for past 19 Ma from Pacific sector of Southern Ocean were analysed by laser ablation technique. This unprecedented Pb isotope record revealed the evolution of the Antarctic Circumpolar Current (ACC) between the Tasman Gateway and Drake Passage from a new perspective, providing time constraints for the onset of a full depth ACC in its modern configuration.

2. Methodology

2.1 Sample collection

Seawater and sediment samples used for this thesis were collected by CTD and multicorer (MUC) during the expedition PS111 from January to March 2018 and PS118 from February to April 2019 on board the German research vessel RV Polarstern.

2.1.1 CTD seawater sampling

Seawater samples were collected for Pb and Nd isotope analysis from different depths in the water column using Niskin bottles mounted on a stainless steel CTD rosette. While seawater sampling for Nd isotopic analyses are commonly undertaken using this seawater sampling approach, for seawater Pb collection usually trace metal-clean approaches are necessary (e.g. Rijkenberg et al., 2015, Marine Chemistry). Since such a sampling device was not available during PS111 and PS118, seawater Pb concentration and isotope results presented within this thesis are to be interpreted with caution as the blank contribution could be quantitatively constrained (yet are considered minor and possibly insignificant). The samples were filtered through a

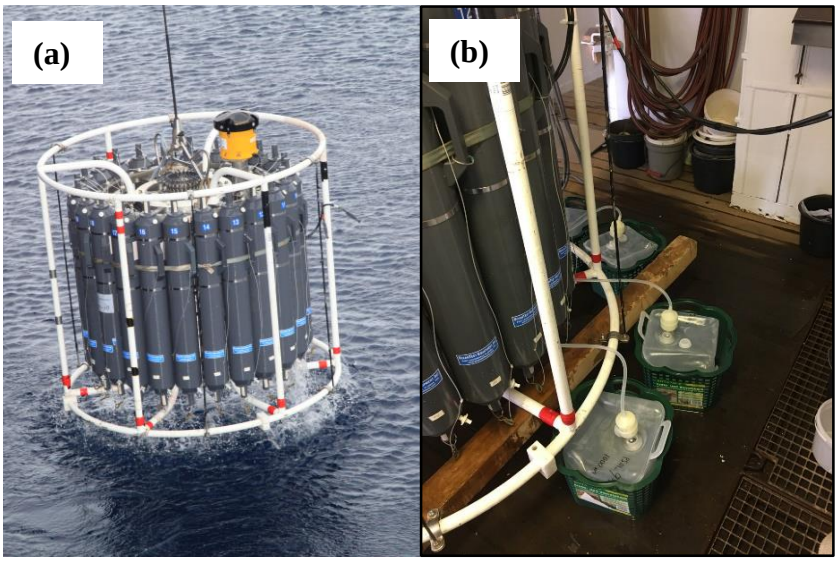

Figure 2.1 CTD seawater sampling. (a) Seawater sampling and (b) seawater filtration.

0.2/0.8 μm Acropak® filter and then acidified to pH ~2 using double distilled concentrated nitric acid. From each depth, ~10-20 L seawater was collected in acid-cleaned 20 L LDPE-collapsible cubitainer for Nd isotopes analysis, 1 L seawater was collected in acid-cleaned 1 L PE bottle for Pb isotope analysis and 250 mL seawater sample was collected in acid-cleaned 250 mL PE bottle for Pb and Rare Earth Element (REE) concentration measurements. Besides the 20 L samples for Nd isotopes analysis, all other samples were only filtered and acidified on board and further processed in the GEOMAR clean lab facilities.

2.1.2 Seawater Nd precipitation

The ~10-20 L seawater samples for Nd isotopic analysis were further processed on board by adding purified dissolved Fe–chloride solution. After 6 hours equilibration time, ammonia solution (25%, Mercksuprapur®) was added to raise the pH to 7.5-8.5 in order to co-precipitate dissolved Nd with iron oxyhydroxides. After settling of the precipitates, most of the supernatant was discarded and the residue was transferred into 1 L acid-cleaned PE-bottles for transport to the home laboratory.

2.1.3 MUC seawater sampling

Bottom seawater samples were also collected during multi core sampling (MUC). About 3 L seawater in total was siphoned out from three MUC sampling tubes at each station for both Pb and Nd isotope analysis (Figure 2.2a). The samples were filtered through a 0.2/0.8 μm Acropak® filter and then acidified to pH ~2 using double distilled concentrated nitric acid before storage. All samples were transported back to clean lab for further work.

2.1.4 MUC porewater sampling

All operations for porewater sampling from MUC sediments were undertaken in a glove bag under oxygen-free conditions in an argon gas atmosphere. The centrifuge tubes and sample bottles were also flushed with argon gas before use. After siphoning

of overlying seawater, the MUC sampling tube was transferred into the glove bag and MUC sediment was sampled in 2 cm increments on a Teflon sampling stand as fast as possible. Each 2 cm sub-sample was transferred in a 50 mL centrifuge tube. The porewater was separated from sediment by centrifugation at 4000 rpm for 60 minutes. Consequently, the porewater was filtered though a pre-cleaned 0.2 μm Supor®filter and acidified to pH~2. About 10-20 mL porewater samples were recovered from each depth from one sample tube. The remaining sediment samples were kept for reductive leaching experiments. All samples were transported back home for further chemistry purification and isotope measurement in the GEOMAR clean labs.

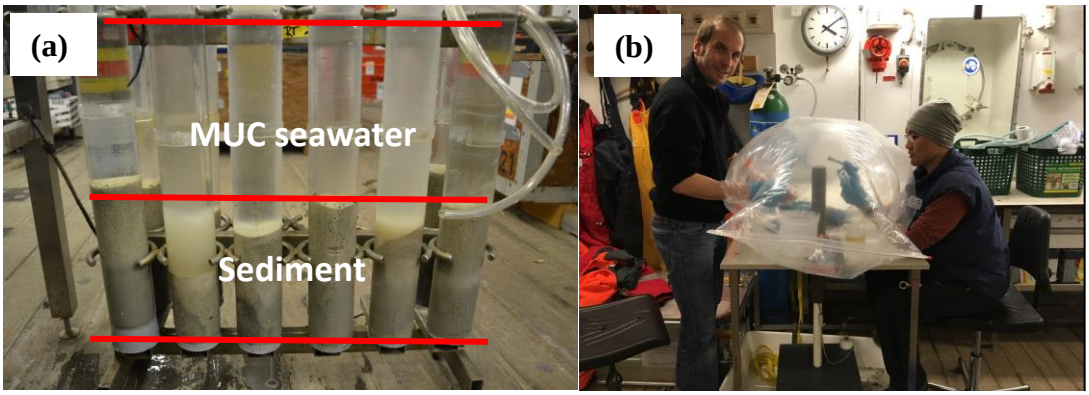

Figure 2.2 MUC porewater sampling. (a) Samples in the MUC and (b) glove bag operation.

2.2 Chemistry pre-concentrating seawater and porewater Pb and Nd

In order to distinguish seawater collected by CTD and MUC, these are referred to as CTD seawater and MUC seawater in the following Chapters.

2.2.1 CTD seawater Nd

After transport back to clean lab, the iron oxyhydroxide precipitates were transferred in acid-cleaned 50 mL centrifuge tubes and centrifuged for 10 minutes at 4000 rpm in the clean lab at GEOMAR in Kiel (Germany). Subsequently samples were rinsed at least two times with Milli-Q water followed by centrifugation to wash out major ions (Ca, Mg, K etc.). Since the majority of the seawater Nd isotope analyses are part of a

separate study (Gutjahr et al. 2019), the subsequent Nd purification was coordinated and realised mainly by Marcus Gutjahr and a student helper yet briefly described below. The precipitates were dissolved in 2 mL 6 M HCl and transferred into 30 ml Teflon vials to dry down on the hotplate. Subsequently, 2 ml aqua regia (HNO_3: HCl = 1:4) were added, refluxed for 24 hours and afterwards dried down. Then 2 ml of 6 M HCl was added and dried down again to transfer back to Cl-form. Before column purification, the excess amount of Fe is separated from the sample by the Fe back extraction procedure. For this step, each dried sample was re-dissolved in 4 ml of 6M HCl and mixed with a suitable amount (about 3 mL) cleaned di-ethyl ether. About 90% iron can be extracted into the organic solution phase and discarded. This Fe-extraction procedure was repeated twice or more often until the sample solutions became pale yellow. Most of the samples formed a jelly-like precipitate, which incorporated about 90 % of the Hf from the sample. This precipitate was separated from the sample by centrifugation and kept for potential future Hf isotope analyses. After evaporation, the seawater samples were re-fluxed in 2 ml 6M HCl and dried down again before the subsequent cation exchange purification step (see section 2.4.4 below).

2.2.2 $Mg(OH)_2$ co-precipitation method for pre-concentrating CTD seawater Pb and MUC seawater Pb and Nd

For pre-concentrating CTD seawater Pb and MUC seawater Pb and Nd, concentrated ammonia solution (25%, Mercksuprapur®) is added into 1 L acidified seawater samples to adjust the pH up to 10. After 2 days of reaction time, white $Mg(OH)_2$ precipitates slowly form. The supernant was then discarded and the white residue dissolved into 6 mL 2M HBr/0.1M HF solution for further Pb and Nd column chemistry purification (see section 2.4.2 and 2.4.3 below).

2.2.3 Porewater Pb

Dissolved Pb contained in sediment porewaters was directly dried down for Pb column purification (see section 2.4.1 below) without any additional procedure in

order to avoid potential contaminations.

2.3 Vortexing leaching for extraction of authigenic Pb and Nd from sediments

Approximately 0.3-0.5 g of bulk sediment sample was weighed and homogenized prior to chemical extraction. Sample and 15 mL leaching solution (0.005M hydroxylamine hydrochloride (HH), 1.5% acetic acid and 0.003M EDTA solution buffered to pH=4 with suprapure ~0.033M NaOH) were transferred in acid-cleaned polypropylene 50 mL centrifuge tubes. Sample solutions were briefly agitated for only 10 s on a vortexing shaker and centrifuged immediately at 4000 rpm for 2 minutes. After centrifugation, 6 mL of the leachate solution was pipetted into a 15 mL Teflon vial to dry down overnight on a hotplate. The residue was redissolved in 0.3 mL concentrated HNO_3 in order to transfer elements into NO_3^- form and oxidise residual hydrolamine hydrochloride. After subsequent drying down, the sample was redissolved in 1 mL 2% HNO_3, from which 0.1 mL (i.e. 10%) was taken for elemental ratio analysis while the rest was dried down for further column chemistry purification (see section 2.4.1 and 2.4.3 below).

2.4 Ion exchange chromatography

2.4.1 General Pb Purification

Before column chemistry, samples were redissolved three times in 0.3 mL HBr. Subsequently, the residue was dissolved in 0.3mL 0.5 M HNO_3/0.2 M HBr solution for loading onto the resin.

Table 2.1 Column chemistry procedure for the separation of Pb for isotope compositions measurements by ICP-MS

volume	Eluate	Stage
1 mL	1 M HNO_3	Clean the column
1 mL	Milli Q water	Clean the column
0.5 mL	2% HNO_3	Load the resin
0.1 mL	AG1X8 resin, 100–200 mesh	Load the resin
0.1 mL	0.5 M HNO_3/0.2 M HBr	Pre-conditioning

0.1 mL	**0.5 M HNO_3/0.2 M HBr**	**Pre-conditioning**
0.3 mL	**in 0.5 M HNO_3/0.2 M HBr**	**Load the sample**
0.1 mL	**0.5 M HNO_3/0.2 M HBr**	**Elute matrix (collect Nd)**
0.1 mL	**0.5 M HNO_3/0.2 M HBr**	**Elute matrix (collect Nd)**
0.15 mL	**0.5 M HNO_3/0.2 M HBr**	**Elute matrix (collect Nd)**
0.15 mL	**0.5 M HNO_3/0.2 M HBr**	**Elute matrix (collect Nd)**
0.15 mL	**0.5 M HNO_3/0.03 M HBr**	**Collect pure Pb**
0.3 mL	**0.5 M HNO_3/0.03 M HBr**	**Collect pure Pb**
0.2 mL	**0.5 M HNO_3/0.03 M HBr**	**Collect pure Pb**

After column purification, the Pb cut was dried down at 90°C overnight and redissolved in 2% HNO_3 for isotope analysis. The Nd cut was also dried and then 0.7 mL 6 M HCl was added to dissolve residues. After 3 hours reflux time and drying down, the Nd cut was redissolved in 0.5 mL 1 M HCl for Nd purification.

2.4.2 Purification of Pb co-precipitated in $Mg(OH)_2$

This protocol was required for MUC seawater and CTD seawater Pb samples because these were pre-concentrated using the $Mg(OH)_2$ co-precipitation method, which can form substantial quantities of silicate gel during normal Pb chromatography. In order to dissolve the silicate gel, 6 mL 2 M HBr/0.1 M HF was added to the $Mg(OH)_2$ precipitate from each 1L seawater sample. Since the small Pb columns can only contain about maximal 2 mL solution, loading 6 mL sample solution on the the resin requires several runs. The protocol is shown below:

Table 2.2: Column purification procedure for the separation of Pb co-precipitated in $Mg(OH)_2$ from MUC seawater and CTD seawater

volume	Eluate	Stage
1 mL	**1 M HNO_3**	**Clean the column**
1 mL	**Milli Q water**	**Clean the column**
0.5 mL	**2% HNO_3**	**Load the resin**
0.1 mL	**AG1X8 resin, 100–200 mesh**	**Load the resin**
0.2 mL	**2 M HBr/0.1 M HF**	**Pre-conditioning**
0.2 mL	**2 M HBr/0.1 M HF**	**Pre-conditioning**
3x 2 mL	**In 2 M HBr/0.1 M HF**	**Load the sample**
0.5 mL	**2 M HBr/0.1 M HF**	**Elute matrix (collect Nd)**
0.5 mL	**2 M HBr/0.1 M HF**	**Elute matrix (collect Nd)**

0.1 mL	**0.5 M HNO_3/0.2 M HBr**	**Elute matrix (collect Nd)**
0.1 mL	**0.5 M HNO_3/0.2 M HBr**	**Elute matrix (collect Nd)**
0.15 mL	**0.5 M HNO_3/0.2 M HBr**	**Elute matrix (collect Nd)**
0.15 mL	**0.5 M HNO_3/0.2 M HBr**	**Elute matrix (collect Nd)**
0.15 mL	**0.5 M HNO_3/0.03 M HBr**	**Collect pure Pb**
0.3 mL	**0.5 M HNO_3/0.03 M HBr**	**Collect pure Pb**
0.2 mL	**0.5 M HNO_3/0.03 M HBr**	**Collect pure Pb**

After column chemistry, the Pb cut was dried down at 90°C overnight and redissolved in 0.5 mL 2% HNO_3 for isotope analysis. The Nd cut was also dried and then 0.7 mL 6 M HCl was added to dissolve residues. After 3 hours reflux time and subsequent drying, the Nd cut was redissolved into 0.5 mL 1 M HCl for Nd purification.

2.4.3 General Nd purification

The Nd was purified by two steps. Separation of the Rare Earth Element (REE) from matrix and purification of Nd (Pin and Zalduegui 1997, Carsten et al. 2001), which are described as below.

Table 2.3: REE separation using AG50W-X12 (200-400µm).

volume	Eluate	Stage
8 mL	**6 M HCl**	**Clean the column**
0.5 mL	**1 M HCl**	**Pre-conditioning**
1 mL	**1 M HCl**	**Pre-conditioning**
0.5 mL	**In 1 M HCl**	**Load the sample**
0.6 mL	**1 M HCl**	**Elute matrix**
0.6 mL	**1 M HCl**	**Elute matrix**
0.6 mL	**1 M HCl**	**Elute matrix**
10 mL	**3 M HCl**	**Elute matrix**
1 mL	**Milli Q water**	**Conditioning**
1 mL	**Milli Q water**	**Conditioning**
8 mL	**2.5 M HNO_3**	**Elute Ba**
6 mL	**6 M HNO_3**	**Collect REE**
6 mL	**6 M HNO_3**	**Clean column**
1 mL	**Milli Q water**	**Conditioning**
1 mL	**Milli Q water**	**Conditioning**
1 mL	**1 M HCl**	**Storage**

The REE aliquot was dried down and redissolved in 0.5 mL 0.1 M HCl for the next

Nd purification step as following:

Table 2.4: Nd purification by Eichrim®LN-Spec (50-100µm)

volume	Eluate	Stage
8 mL	6 M HCl	Clean the column
0.5 mL	0.1 M HCl	Pre-conditioning
1 mL	0.1 M HCl	Pre-conditioning
0.5 mL	in 0.1 M HCl	Load the sample
0.5 mL	0.1 M HCl	Elute Ba
8 mL	0.25 M HCl	Elute REE
5 mL	0.25 M HCl	Collect Nd
6 mL	6 M HNO_3	Clean column
1 mL	0.4 M HCl	Conditioning
1 mL	0.4 M HCl	Storage

After column chemistry, the purified Nd was dried down at 120°C overnight and redissolved in 0.5 mL 2% HNO_3 for isotopic analysis.

2.4.4 Seawater Nd purification

The general Nd purification protocol was modified to separate REE and Hf in the sample.

Table 2.5: REE and Hf separation using AG50W-X12 (200-400µm).

volume	Eluate	Stage
8 mL	6 M HCl	Clean the column
2 mL	1 M HCl – 0.1 M HF	Clean the column
0.5 mL	1 M HCl – 0.1 M HF	Pre-conditioning
1 mL	1 M HCl – 0.1 M HF	Pre-conditioning
1 mL	In 1 M HCl – 0.1 M HF	Load the sample
0.6 mL	1 M HCl – 0.1 M HF	Collect Hf
0.6 mL	1 M HCl – 0.1 M HF	Collect Hf
0.6 mL	1 M HCl – 0.1 M HF	Collect Hf
10 mL	3 M HCl	Elute matrix
1 mL	Milli Q water	Conditioning
1 mL	Milli Q water	Conditioning
8 mL	2.5 M HNO_3	Elute Ba
6 mL	6 M HNO_3	Collect REE
6 mL	6 M HNO_3	Clean column
1 mL	Milli Q water	Conditioning
1 mL	Milli Q water	Conditioning
1 mL	1 M HCl	Storage

The Hf aliquots are collected for other people to process further purification and analysis. The REE aliquot was dried down and redissolved in 0.5 mL 0.1 M HCl for the next Nd purification step as the same as in Table 2.4.

2.5 Concentration and isotopic composition determination

2.5.1 Elemental ratios analysis for Fe-Mn oxyhydroxide leachates

In general, element concentrations were measured in a ten-fold dilution of the original leaching supernatants using with an Agilent 7500-CE Quadrupole ICP-MS at GEOMAR, Kiel. Two different standard calibrations were employed to cover samples of high and low trace element concentrations with reproducibilities strongly dependent on the respective element. All concentration results were normalized to the initially used sample weight.

2.5.2 Seawater Pb concentration measurements

Seawater Pb concentration measurements were conducted on an 7 mL sample loop using an online preconcentration technique (OP) ICP-MS at GEOMAR employing an automated "SeaFast" system (Elemental Scientific Inc.) coupled to an Thermo Scientific Element XR. The Pb concentration was analysed analogue to the procedure according to established method for the rare earth element concentration measurements (Hathorne et al. 2012). During the measurements, reference seawater BATS, CAB and MF-20 were used to track the reproducibility and accuracy of the data.

2.5.3 Pb and Nd isotopic composition determination on MC-ICP-MS

Pb and Nd isotope measurements were performed on a Thermo Scientific Neptune Plus MC-ICP-MS at GEOMAR, Kiel. Mass bias correction during Pb isotope measurements was done externally using the Tl-doping technique (Thirlwall 2002, Süfke et al. 2019) with added NIST997 Tl standard solution (the used Pb/Tl ratios are shown in Table 2.6). Given that Tl and Pb fractionate slightly differently during

ionization, $^{205}Tl/^{203}Tl$ were determined on a session-by-session basis so that NBS981 Pb isotope compositions matched published compositions (Baker et al. 2004, Süfke et al. 2019). Total Pb procedural blanks in leachates and seawater samples were below 50 pg (n=30) and are hence negligible. The total Pb procedural blanks for in the porewater were below 2 pg (n=2) and the sample were between 50 and 100 pg, so the blank Pb contaminations were lower than 4%. The reproducibility of the secondary standard USGS NOD-A-1 is listed in Table 2.5. As shown in the table, all measured standard Pb isotopic ratios are within the error of literature value.

Table 2.6 The reproducibility of the secondary standard USGS NOD-A-1 for seawater, porewater and leachates Pb isotopic compositions.

			$^{206}Pb/^{204}Pb$	$^{207}Pb/^{204}Pb$	$^{208}Pb/^{204}Pb$	$^{208}Pb/^{206}Pb$	$^{207}Pb/^{206}Pb$	$^{208}Pb/^{207}Pb$
Leachate standards (n=169)	28ppb Pb:7ppb Tl	NOD-A-1	18.959	15.679	38.933	2.0535	0.8270	2.4831
		2 S.D.	0.009	0.010	0.035	0.0009	0.0002	0.0006
Seawater standards (n=16)	1ppb Pb:1ppb Tl	NOD-A-1	18.960	15.680	38.942	2.0539	0.8270	2.4836
		2 S.D.	0.015	0.015	0.043	0.0013	0.0003	0.0012
Porewater standards (n=11)	20ppt Pb:20ppt Tl	NOD-A-1	18.864	15.587	38.558	2.0486	0.8256	2.4825
		2 S.D.	1.924	1.467	3.614	0.0145	0.0074	0.0185
Literature value		Baker et al. 2004	18.964	15.685	38.956	2.0542	0.8271	2.4836

Instrumental mass fractionation for Nd isotopes was corrected by normalizing the measured ratio of $^{143}Nd/^{144}Nd$ to $^{146}Nd/^{144}Nd = 0.7219$ using the mass bias correction procedure of (Vance and Thirlwall 2002). The measured Nd isotope ratios were normalized to the published $^{143}Nd/^{144}Nd$ value of 0.512115 for JNdi-1 (Tanaka et al. 2000). Total procedural blanks for Nd are below 30 pg and hence negligible (n=20). Secondary standard solution NIST 3135a were run with the sample to check the external reproducibility. The reproducibility of the secondary standard NIST 3135a is listed in Table 2.7.

Table 2.7 Reproducibility of the secondary standard NIST 3135a for seawater and leachate Nd isotopic compositions

			$^{143}Nd/^{144}Nd$	εNd
Regular standards (n=98)	50 ppb Nd	NIST 3135a	0.512450	-3.67
		2 S.D.	0.000010	0.20
MUC seawater standards (n=5)	2 ppb Nd	NIST 3135a	0.512436	-3.94
		2 S.D.	0.000064	1.25

2.6 Fe-Mn crust sample preparation

The original Fe-Mn crust surface was first enclosed by resin before cutting. After each cut, the sample was embedded into resin to protect the sample structure from fracturing. Eventually, an approximately 5 cm long, 2 cm wide and 1 cm thick section of the sample was cut following the main growth direction (see Figure 5.1). Sections were polished using sandpaper ranging from 400 to 4000 grit. Finally, the sample was carbon-coated preceding electron microprobe analysis.

2.7 Laser ablation coupled MC-ICP-MS

The Pb isotopic compositions were determined via laser ablation coupled MC-ICP-MS (LA-ICP-MS) using an Analyte Excite Excimer Laser Ablation System connected to a Thermo Scientific Neptune Plus MC-ICP-MS at GEOMAR, Kiel. The instrumental parameters used are listed as below:

Table 2.8 Collector array

L4	L3	L2	L1	Axial	H1	H2	H3	H4
	202	203	204	205	206	207	208	

Table 2.9 Instrumental parameters of the LA-MC-ICP-MS.

Laser settings	
Ablation cell gas	0.7 l min^{-1} (He)
Spot size	15-150µm
Fluence	3 J cm^{-2}

Repetition rate	20 Hz
Scan mode	Line with 1 mm s^{-1} scan speed/ scaned 10 spots in a line
Neptune settings	
Cool gas	16 l min^{-1} (Ar)
Auxiliary gas	0.9 l min^{-1} (Ar)
Nebulizer gas	0.8 l min^{-1} (Ar)
RF power	1200W
Cones	Jet cone/skimmer H cone

2.8 Pb isotopic composition determined by LA-MC-ICPMS

Before laser ablation measurement, the sample surface was pre-ablated by triple laser pulses with 3 J cm^{-2} laser power density in order to eliminate potential surface contamination. Two different laser ablation operation settings were applied for different timescale resolution analysis (Table 2.10). Each analysis consisted of a 30-second gas blank and 60-second sample acquisition signal and all signals were collected for isotopic composition analysis. The instrumental mass fractionation was corrected using the linear regression normalisation method (Fietzke et al. 2008) bracketing samples with NIST610, NOD-A and NOD-P standards. During the LA experiments, we found that the ^{204}Hg interference and Pb isotope signal intensities were the two most critical factors which controlled the data quality, so the standards were analysed with different LA unit settings (Table 2.11) to match the Pb isotope signal intensity of the sample. NIST610 glass showed similar low ^{204}Hg interference contributions as the sample crust material while providing comparable sample LA Pb isotope signal intensities. Pellets made by pressed USGS ferromanganese nodule powder standards NOD-A-1 and NOD-P-1 have a similar matrix composition as the samples. Therefore, the combination of these three different standards (NIST610, NOD-A-1 and NOD-P-1) can best evaluate the accuracy and precision of the measurement covering similar ^{204}Hg interference proportions, Pb isotope signal intensities and considering matrix compositions.

Table 2.10 Instrumental parameters during LA Pb isotope analyses used for samples

	50 microns LA	**15 microns LA**
Laser power density	3 J cm^{-2}	3 J cm^{-2}
Repetition rate	20 Hz	20 Hz
Spot size	50 μm	15 μm
Carrier gas	He	He
Scan mode	LA for a 60 μm line with 1 μm/s moving speed	LA for 10 spots in a line (2 s LA and 4 s gas blank for each spot)

Table 2.11 Instrumental parameters during LA Pb isotope analyses used for standards

	NIST610	**NOD-A**	**NOD-P**
Laser power density	3 J cm^{-2}	3 J cm^{-2}	3 J cm^{-2}
Repetition rate	20 Hz	8 Hz	8 Hz
Spot size	140 μm	120 μm	120 μm
Carrier gas	He	He	He
Scan mode	LA at one for 60 seconds	LA for a 300 μm line with 5 μm/s moving speed	LA for a 300 μm line with 5 μm/s moving speed

The LA-MC-ICPMS data reduction in this study comprised three parts: 1) blank correction, 2) Hg interference correction and 3) instrumental mass bias correction. We here use the data processing for the normalisation of $^{206}Pb/^{204}Pb$ ratio as an example to describe the linear regression normalisation method. Firstly, the blank correction for measured $^{206}Pb/(^{204}Pb+^{204}Hg)$ ratios of the standards was achieved by plotting the raw LA data of standards and corresponding gas blank data collected by amu 206 and amu 204 (Figure 2.3). The slope value is the background (blank) corrected $^{206}Pb/(^{204}Pb+^{204}Hg)$ ratio (Fietzke et al. 2008). Secondly, ^{202}Hg detected during the analysis was used to correct ^{204}Hg interference for ^{204}Pb with an optimal $^{202}Hg/^{204}Hg$ ratio (R_{Hg}). The standards and sample Fe-Mn crust have different Hg/Pb ratios (NIST610: Hg/Pb ~ 0.04%; NOD-A: Hg/Pb ~ 0.06%; NOD-P: Hg/Pb ~ 3.00%; PS75/247-2: Hg/Pb ~ 0.05%). Since the standards contain variable concentrations of interfering Hg, the Goal Seek analysis in Excel software was used to determine the

optimal R_{Hg}. An hypothesized R_{Hg}= 4 was used to calculate measured $^{206}Pb/^{204}Pb$ ratios of the three standards from $^{206}Pb/(^{204}Pb+^{204}Hg)$ ratios at the begining, and then the average value of the instrumental fractionation factor of these three standards based on hypothesized R_{Hg} was applied for the mass bias correction of the standards' $^{206}Pb/^{204}Pb$ ratios. The total offset of the mass bias corrected $^{206}Pb/^{204}Pb$ ratios of three standards to literature values (NIST610: $^{206}Pb/^{204}Pb$ = 17.052; NOD-A: $^{206}Pb/^{204}Pb$ = 18.964; NOD-P: $^{206}Pb/^{204}Pb$ = 18.700 (Baker et al. 2004)) was set to be zero in the Goal Seek analysis with the R_{Hg} value as variable factor. After the Goal Seek analysis, because the optimal

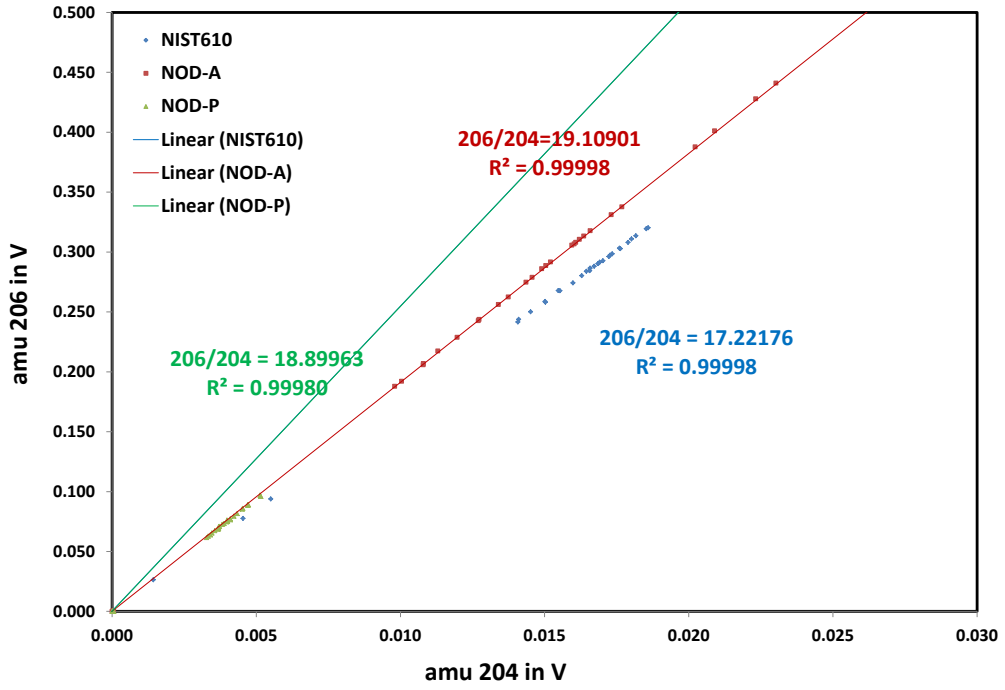

Figure 2.3 Simultaneous responses of the signals of amu 206 vs. amu 204 for NIST610, NOD-A and NOD-P. The 206/204 show uncorrected $^{206}Pb/(^{204}Pb+^{204}Hg)$ ratios.

R_{Hg} is linked to the mass fraction factor for $^{206}Pb/^{204}Pb$, both the optimal R_{Hg} and the optimal average value of the instrumental fractionation factor were determined. Finally, assuming Pb isotope fractionation under the same ICP-MS analytical condition was identical for all standards and sample, the average value of the instrumental fractionation factor of the three standards through the entire measurements (n=230) was also used for the mass bias correction for the $^{206}Pb/^{204}Pb$ ratio of sample data after blank and Hg interference correction. This method was then

used for normalizing other Pb isotopic ratios, i.e $^{208}Pb/^{204}Pb$ and $^{208}Pb/^{206}Pb$, but for the Pb isotopic ratios not using ^{204}Pb, the Hg intereference correction is not needed.

2.9 Electron microprobe analysis

The concentrations of Fe, Mn and the signal intensity of Co in the sample slide were measured by electron microprobe after laser ablation analysis and the results are shown in Chapter 5. The measurement was carried out at GEOMAR Kiel, Germany, using a JEOL JXA 8200 "Superprobe". WDS (wavelength dispersive X-ray spectroscopy) elemental maps were acquired with 30 µm resolution for the whole sample in three steps under the same conditions.

Table 2.12 Instrumental conditions for electron microprobe analysis.

Acceleration voltage	15 kV
Beam current	100 nA
Probe diameter	5 µm
Dwell time	20 ms
Element (channel, crystal)	1) Co (LIFH)
	2) Mn (PETJ)
	3) Fe (LIFH)

Five standards (PbS, Fe_2O_3, VG-2, KAN1, Rhodonite) were analysed using exactly the same instrumental conditions as 5x5 pixel WDS maps. From these standard measurements the intensity-concentration conversion was calculated for Fe and Mn as outlined below. The Co concentration was not calibrated because of no available Co standards.

Table 2.13 Calibration of the intensity-concentration conversion using 5x5 pixel maps on standards (PbS, Fe_2O_3, VG-2, KAN1, Rhodonite). Concentration (% = percentage weight) is provided as a function of the measured intensity in cts = counts

Element	**Concentration [%]=f(Intensity [cts])**
Fe	C[weight %] = 4.094*I[cts]-0.047
Mn	C[weight %] = 7.159*I[cts]-0.050

3. Efficient extraction of past seawater Pb and Nd isotope signatures from Southern Ocean derived bulk sediments

Under preparation for *Global Biogeochemical Cycles* as: Huang, H., Gutjahr, M., Kuhn, G., Eisenhauer, A. Efficient extraction of past seawater Pb and Nd isotope signatures from bulk sediments in the Southern Ocean.

Abstract

The radiogenic Pb and Nd isotope proxies extracted from marine archives are sensitive tracers for reconstruction of ocean circulation and water mass mixing in the past. The preferred archives for such reconstructions – planktic or benthic fossil foraminifera – are often not available in carbonate-free Southern Ocean sediments. Besides, fossil foraminifera might not be a reliable seawater Pb archive. Chemical reductive leaching of hydrogenentic ferromanganese oxyhydroxides from bulk sediments offers an alternative and easily accessible way to recover past seawater Pb and Nd isotope signatures. However, the leached seawater derived isotope signal could be compromised if substantial quantities of Pb and Nd were released from non-hydrogenentic sediment fractions during chemical extraction. Here we developed a very short 10 seconds vortexing leaching method for extracting reliable porewater Pb and Nd isotope signals from sediment samples in the Atlantic sector of Southern Ocean. The effect of a previously recommended $MgCl_2$ prewash, the role of chelate ligands in the leaching solution and length of leaching time were investigated for sediments of representative locations in the studied area as well as in manganese nodule powder, NOD-A-1, as reference. The results show that 10 seconds leaching on a vortex mixer extracted sufficient and more reliable hydrogenetic Pb and Nd compared with commonly used 30-minutes leaching approaches on a shaker table. Our improved vortexing leaching method was further validated via direct comparison of extracted Pb and Nd isotope signatures with actual seawater, porewater and corresponding sediment leachates from three stations in front of the Antarctic

Filchner-Rønne Ice Shelf. With this improved vortexing leaching method, we generated authigenic Pb and Nd isotope maps of the Atlantic sector of the Southern Ocean from 70 coretop sediment samples to help locate identifying the regional variability in bottom water compositions and to find suitable sites for paleoceanographic and paleoclimatic reconstructions.

3.1 Introduction

Radiogenic Pb and Nd isotopes have been successfully applied as sensitive and powerful palaeoceanographic proxies of circulation change and water mass mixing for decades (Burton et al. 1997, Christensen et al. 1997, Frank 2002) . The radiogenic isotopes ^{206}Pb, ^{207}Pb and ^{208}Pb are produced by the very long half-life decay of ^{238}U, ^{235}U and ^{232}Th, while the radiogenic isotope ^{143}Nd is also produced by a very slow decay reaction of ^{147}Sm. Because of these long half lives, crustal radiogenic/primordial isotopes ratios, i.e. $^{206}Pb/^{204}Pb$ and $^{143}Nd/^{144}Nd$, are constant on relatively short Cenozoic timescales unless crustal reservoirs were mixed. Dissolved Pb and Nd in the oceans are mainly supplied by continental runoff, so Pb and Nd isotope signatures of the water masses are determined by the average regional crustal compositions of weathered continental crust (Martin 2002, Goldstein and Hemming 2003). Seawater Nd is also delivered by sediment-bottom water exchange along continental margins (Lacan and Jeandel 2005, Lacan et al. 2012) or oceanic islands (Stichel et al. 2012, Pearce et al. 2013, Rickli et al. 2014). However, such a mechanism has not been reported for seawater Pb likely because the slow Pb release from continental margins could be quickly readsorbed back due to its high particle-reactivity. The average oceanic Nd residence time between 600 and 2000 years (Tachikawa et al. 1999, Tachikawa et al. 2003) allows radiogenic Nd to serve as a quasi-conservative water mass tracer. In contrast to Nd, Pb is more particle-reactive leading to a shorter residence time (50-200 years) (Schaule and Patterson 1981, Cochran et al. 1990, Henderson and Maier-Reimer 2002), allowing it to track local and generally rather proximal weathering inputs (Gutjahr et al. 2009, Kurzweil et al.

2010, Crocket et al. 2012, Crocket et al. 2013) .

Various archives have been utilized to recover seawater Pb and Nd isotope signals in the past such as fossil fish teeth/debris, fossil foraminifera, Fe-Mn crusts or nodules, sedimentary ferromanganese (Fe-Mn) oxyhydroxides and corals. In very early studies, extracting past seawater Pb and Nd isotope signals were mainly conducted using Fe-Mn crusts (Abouchami et al. 1997, Burton et al. 1997, Frank and O'Nions 1998, O'Nions et al. 1998, Reynolds et al. 1999, Frank et al. 2002, van de Flierdt et al. 2004). However, due to its slow growth rate, Fe-Mn crusts are not suitable for generating records of (sub-) millennial resolution. Fossil fish teeth (Staudigel et al. 1985, Martin and Scher 2004) and fossil foraminifera (Vance and Burton 1999, Klevenz et al. 2008, Roberts et al. 2010) in marine sediments are both reliable archives for sub- or millennial resolution seawater Nd isotope studies but fossil fish debris was found not to be suitable for Pb isotope reconstructions (Basak et al. 2011). In addition, fossil foraminifera and fish debris are often not available in sufficient quantity for a hydrogenetic Nd isotope reconstruction of high precision and temporal resolution, especially in Southern Ocean sediments which are normally carbonate-free. Cold-water corals represent a good alternative because their age can be well constrained. Nevertheless, only recently cold-water corals were shown to be a robust archive both for extracting seawater derived Pb (Shen and Boyle 1987, Lee et al. 2014, Lee et al. 2017, Wilson et al. 2017) and Nd (van de Flierdt et al. 2004, van de Flierdt et al. 2006, Colin et al. 2010, Wilson et al. 2014, Struve et al. 2017) . However, these archives are often only found in shallow and middle water depths, and continuous temporal coverage is often not achievable. Past seawater Pb and Nd isotope reconstructions generated via reductive leaching of sedimentary Fe-Mn oxyhydroxides in bulk sediments has also been established as a robust procedure in various deep marine settings (Gutjahr et al. 2007, Blaser et al. 2016). Since Southern Ocean sediments usually do not contain sufficient biogenic components, reductive leaching is so far the only practical option to extract deep sea Pb and Nd isotope signal, which has been applied in carbonate-free Arctic sediments to obtain reliable

bottom water Pb and Nd signal (Haley et al. 2008).

The previously reported reductive leaching methods for extracting authigenic Pb and Nd isotope signatures from marine sediments are slightly different from each other so some issues need to be addressed before extracting authigenic Pb and Nd together. The first is whether it is necessary to pre-wash a sediment sample with $MgCl_2$ solution. The $MgCl_2$ pre-wash was proposed to remove potentially present contaminating phases prior to reductive Fe-Mn oxyhydroxide leaching. This technique was introduced decades ago (Tessier et al. 1979) and especially used for leaching sedimentary seawater derived Pb (Gutjahr et al. 2007, Gutjahr et al. 2009). However, no study has as yet assessed the necessity of carrying out a $MgCl_2$ pre-wash from an isotopic perspective. Secondly, chelate ligands, like EDTA, were used in reductive leaching to prevent re-adsorption of released authigenically sourced trace metals (Gutjahr et al. 2007, Chen et al. 2012, Blaser et al. 2016), but many other studies did not employ chelate ligands in the leaching (Haley et al. 2008, Basak et al. 2011, Wilson et al. 2013, Du et al. 2016). The benefit of adding EDTA is to counteract a re-adsorption effect (Gutjahr et al. 2007), yet whether adding ligands into the leaching solution may introduce contamination or cause isotopic fractionation is still unclear. Last but not least, the short leaching time, in principle, should result in more reliable data since less contamination from non-hydrogenetic phases may be expected (Gutjahr et al. 2007, Wilson et al. 2013, Blaser et al. 2016, Du et al. 2016). In more recent studies, 30 minutes leaching was usually recommended as a suitable leaching time, without prior chemical carbonate removal. Since shorter leaching time should dissolve less material from the non-hydrogenetic fraction, a very short contact time, i.e. 10 seconds, should theoretically extract even purer hydrogenetic Pb and Nd isotope signal than 30 minutes leaching, especially for Southern Ocean sediments which commonly contain substantial quantities of only physically weathered continental detritus (Diekmann and Kuhn 1999, Michels et al. 2002, Diekmann et al. 2003) .

In this study, we investigated the effects of $MgCl_2$ pre-wash, chelate ligands and leaching time on leaching sediments in the Atlantic sector of Southern Ocean in order to optimise the leaching method. Since the ability that chemical leaching of sedimentary Fe-Mn oxyhydroxides can extract seawater Pb and Nd isotope signals is debated, we also analysed Pb and Nd isotopic compositions in seawater, porewater and leachate at three sampling stations in the front of Filchner-Rønne Ice Shelf in the southernmost accessible Weddell Sea area. Additionally, we generated regional Pb and Nd isotopic maps by leaching 70 coretop sediment samples in the Atlantic sector of Southern Ocean to select suitable sediment cores for potential paleoceanographic studies.

3.2 Material and methods

3.2.1 Sample sites

The locations of seawater, porewater and sediment samples used in this study are

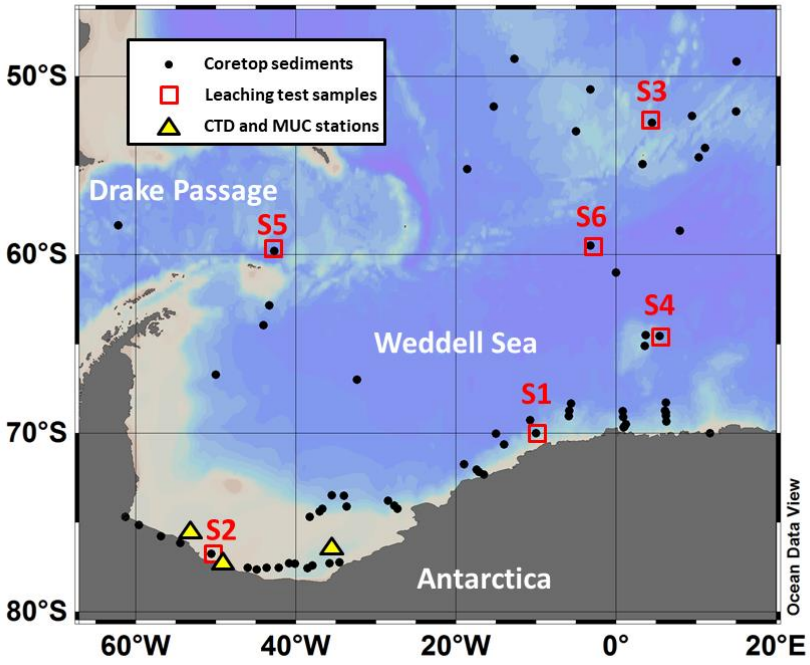

Figure 3.1 The locations of sample sites used in this study. The CTD stations shown in the map are used for Pb and Nd isotopic composition analysis. The seawater stations used for Pb concentration measurements are showed in Figure 3.5.

shown in Figure 3.1. 70 coretop sediment samples were collected for the leaching test and mapping sedimentary seawater-derived Nd and Pb isotopic composition distribution in the Atlantic sector of Southern Ocean from previous Polarstern cruises. The details of the cores are listed in Appendix Table 1. Seawater samples for Pb and Nd isotope analyses were taken from three stations in front of the Filchner-Rønne Ice Shelf using Niskin bottles mounted onto the CTD-rosette during the expedition PS111 from January to March 2018 on board the German research vessel RV Polarstern. Porewater and sediment samples were also retrieved at these three stations by multicore (MUC) sampling during the same cruise. The detailed sampling procedures are described in Chapter 2.1.

3.2.2 Leaching experiments

Although chemical reductive leaching has been applied to extract trace metals from marine Fe-Mn oxyhydroxides since the 1960s (Chester and Hughes 1967), it is still under development to date. One major concern is that the leaching solution applied in the procedure inevitably dissolves both hydrogenetic fractions and non-hydrogenetic sediment components, such as continental detritus and volcanic ash, potentially contaminating the seawater-derived signal. There are two effective ways to minimize contamination: 1) using weak/diluted leaching solution and 2) short leaching time (Gutjahr et al. 2007, Chen et al. 2012, Wilson et al. 2013, Blaser et al. 2016). A smaller solution/solid ratio was also suggested to be an option to reduce contaminations (Wilson et al. 2013). In principal, the leaching reaction consumes chemicals, like hydroxylamine hydrochloride, in the leaching solution and a lower solution/solid ratio would result in a less aggressive leaching solution. Therefore, a lower solution/solid ratio is actually a disguised way of using weaker leaching solution so we do not discuss it in this study. Based on these two principals, a leaching procedure has been recently established for extracting porewater Nd isotopic signature from bulk sediment in the Atlantic Ocean (Blaser et al. 2016). In the following, we adapted this method to extract both seawater-derived Pb and Nd from Soutern Ocean

sediments. Furthermore, we investigated (i) the effect of the $MgCl_2$ pre-wash which was proposed to remove potentially present exchangeable contaminations (Tessier et al. 1979, Gutjahr et al. 2007) and (ii) the effect of chelate ligand used to prevent reabsorption.

Six coretop sediment samples were selected for sequential leaching test in different locations from the Atlantic sector of the Southern Ocean (Figure 3.1). The NOD-A-1 powder, a pure Fe-Mn oxyhydroxide nodule powder, was used as a reference material. The published leaching procedure (Blaser et al. 2016) described below was used as the model to be modified:

Conventional leaching: Approximately 0.5 g of wet bulk sediment or 0.1 g reference material was weighed and homogenized prior to chemical extraction. Samples were immediately exposed to 15 mL leaching solution of 0.005 M hydroxylamine hydrochloride (HH), 1.5 % acetic acid and 0.003 M EDTA solution buffered to pH=4 with suprapure NaOH in acid-cleaned polypropylene 50 mL centrifuge tubes. Sediments were agitated for 10 seconds on a vortex shaker to suspend the sediment and then in a regular shaker for 30 minutes. After centrifugation, 6 mL of the leachate was pipetted out for concentration and isotope analysis.

Following the conventional leaching procedure, a series of control leaching experiments were carried out as followed:

1) *Effect of $MgCl_2$ pre-wash:* before conventional leaching, samples were mixed with 20 mL 1 M $MgCl_2$ solution for 1 hour in a shaker. After centrifugation and decanting of the supernatant, the samples were washed 4 times with 35 mL MilliQ water, followed by centrifugation for 5 minutes at 3000 rpm and decanting of the supernatant.

2) *Effect of chelate ligands:* Two different leaching solutions were modified from conventional leach solution: one used diethylenetriaminepentaacetic acid (DTPA) to replace EDTA and another without chelating ligands inside. Samples were processed

with the conventional leaching method with these two different leaching solutions.

3) *Vortexing leaching (10-seconds leaching only):* samples were only mixed with leaching solution for 10 *seconds* on the vortexing shaker without further 30 min leaching in the regular shaker.

4) *Sequential leaching:* after 30-min conventional leaching, samples were centrifuged, the supernatant extracted, new leaching solution added and samples were leached again with 15 mL new leaching solution for 60 min. Following centrifugation, removal of the supernatant, addition of new leaching solution the samples were leached for another 180 min and this last leachate fraction was subsequentially collected too.

3.2.3 Seawater Pb and Nd

The best way to validate a leaching method is to directly compare the actual seawater isotope signal with corresponding leachate compositions. Unfortunately, the global natural seawater Pb is entirely contaminated by anthropogenic sources but a very recent study showed that seawater very close to Antarctica is still relatively pure containing about 95% natural Pb (Ndungu et al. 2016), implying that seawater Pb in remote Antarctic ocean basins protected under sea ice is expected to be more natural than anywhere else. Therefore, we sampled seawater at around 76° S on the Antarctic shelf in front of Filchner-Rønne Ice Shelf where seawater is covered by sea ice during most of the year. Seawater samples used in this study were both collected with a standard CTD-rosette and multicore (MUC) bottom water for Pb and Nd isotope analysis. In order to distinguish seawater sampled by CTD and MUC, we denote these as CTD seawater and MUC bottom water respectively. The seawater Pb samples were collected by standard CTD-rosette which is not trace metal clean devises, so the potential contamination is a concern. To address this issue, the contamination Pb contribution in the seawater Pb results are discussed in the following section 3.4.1. The sampling and chemical processes are detailed in Chapter 2.1 and 2.2.

3.2.4 MUC sediment and porewater

The analytical approach of sampling MUC sediment and porewater is detailed in Chapter 2.1 and 2.2.

3.2.5 Authigenic Pb and Nd isotopic coretop mapping

The 70 coretop sediment samples were processed using vortexing leaching method for the generation of authigenic Pb and Nd isotopic maps of the Atlantic sector of the Southern Ocean. The method is described in Chapter 2.3. Pb and Nd aliquots were purified by ion chromatography as detailed in Chapter 2.4.

3.2.6 Mass spectrometry

Element concentrations were measured in a ten-fold dilution of the original leaching supernatants using with an Agilent 7500-CE Quadrupole ICP-MS at GEOMAR, Kiel. Pb and Nd isotope measurements were performed on a Thermo Scientific Neptune Plus MC-ICP-MS at GEOMAR, Kiel. Analytical details are described in Chapter 2.5. All data are listed in Appendix Table 1-10.

3.3 Results

3.3.1 Effect of $MgCl_2$ pre-wash

The Pb isotopic compositions of $MgCl_2$ pre-washed samples were all either identical within error or less radiogenic (lower) in $^{206}Pb/^{204}Pb$ compared to the samples processed without $MgCl_2$ pre-wash (Figure 3.2a). Only the Pb isotopic compositions of S7 (i.e. the reference material) and S1 were not affected by $MgCl_2$ pre-wash. Other two Pb isotope ratios, $^{207}Pb/^{204}Pb$ and $^{208}Pb/^{204}Pb$, show similar features with $^{206}Pb/^{204}Pb$ (Appendix Table 7). In contrast to the obtained Pb isotopic results, Pb concentrations recovered by these two approaches were almost identical. On the other hand, both ε_{Nd} and Nd concentrations values extracted from all samples are within

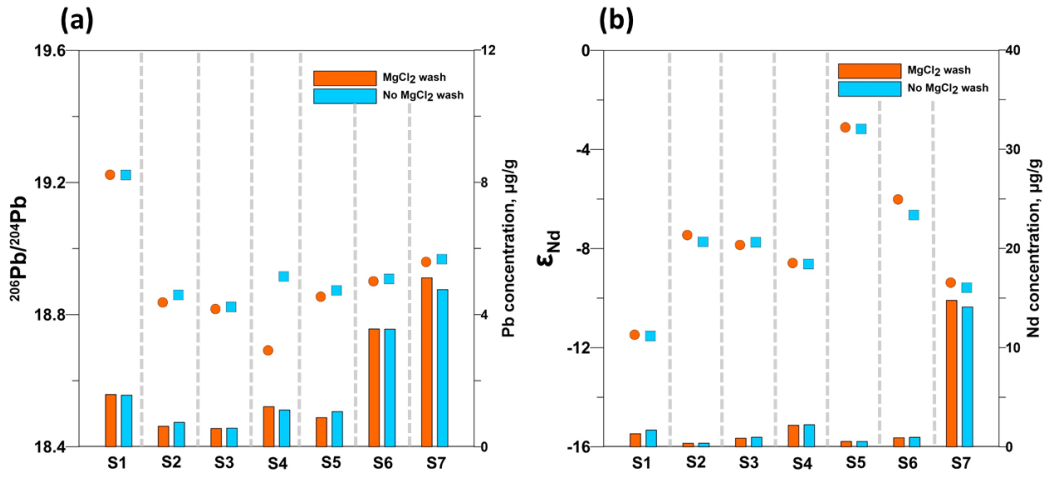

Figure 3.2 Effect of $MgCl_2$ pre-wash. Dots indicate isotopic compositions and bar charts indicate concentrations. (a) $^{206}Pb/^{204}Pb$ and Pb concentration. (b) ε_{Nd} and Nd concentration.

error no matter with or without $MgCl_2$ pre-wash (Figure 3.2b).

3.3.2 Effect of chelate ligand

Leaching solutions containing EDTA and DTPA showed a much higher Pb and Nd recovery rate than solutions without ligands (Figure 3.3a and b). This result clearly shows that adding chelating ligands in the leaching solution can strongly prevent Pb

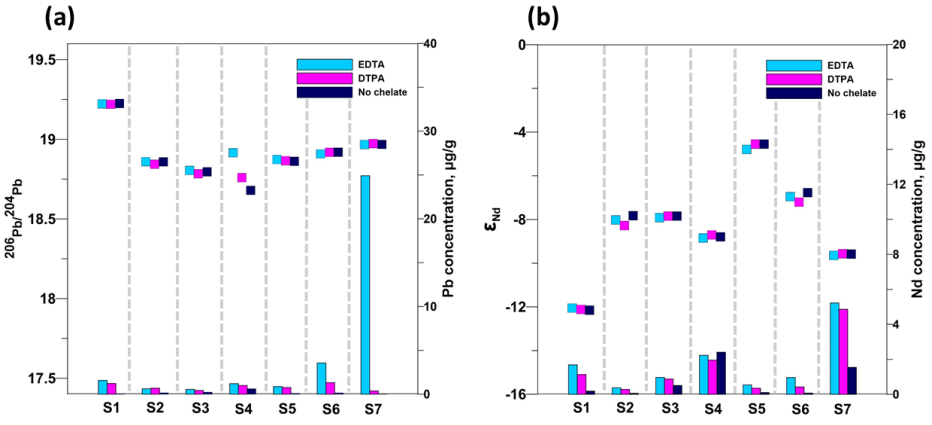

Figure 3.3 Effect of chelate ligands. Square dots illustrate $^{206}Pb/^{204}Pb$ or ε_{Nd}; Bar charts show Pb or Nd concentration values. (a) $^{206}Pb/^{204}Pb$ and Pb concentration. (b) ε_{Nd} and Nd concentration.

and Nd re-adsorption during chemical extraction. Between these two ligands, EDTA shows a stronger complexation ability both towards Nd and Pb than DTPA. Although ligands have a strong influence on the Pb and Nd recovery rate, all ε_{Nd} values and most $^{206}Pb/^{204}Pb$, $^{207}Pb/^{204}Pb$ and $^{208}Pb/^{204}Pb$ ratios produced from these samples are identical within error, indicating that adding ligands neither introduces contamination nor causes isotopic fractionation. Only $^{206}Pb/^{204}Pb$ ratios in S4 leachates produced divergent results, decreasing with increasing re-adsorption effect. $^{207}Pb/^{204}Pb$ and $^{208}Pb/^{204}Pb$ ratios in S4 leachates show similar features with $^{206}Pb/^{204}Pb$ (Appendix Table 8).

3.3.3 Effect of leaching time

A wide range of leaching times, from 10 seconds to 180 minutes, was investigated for all samples. Because $^{207}Pb/^{204}Pb$ and $^{208}Pb/^{204}Pb$ ratios show similar features with $^{206}Pb/^{204}Pb$ (Appendix Table 9), we only discuss $^{206}Pb/^{204}Pb$ here (Figure 3.4a). $^{206}Pb/^{204}Pb$ in the sediment leachates were generally increasing with extended

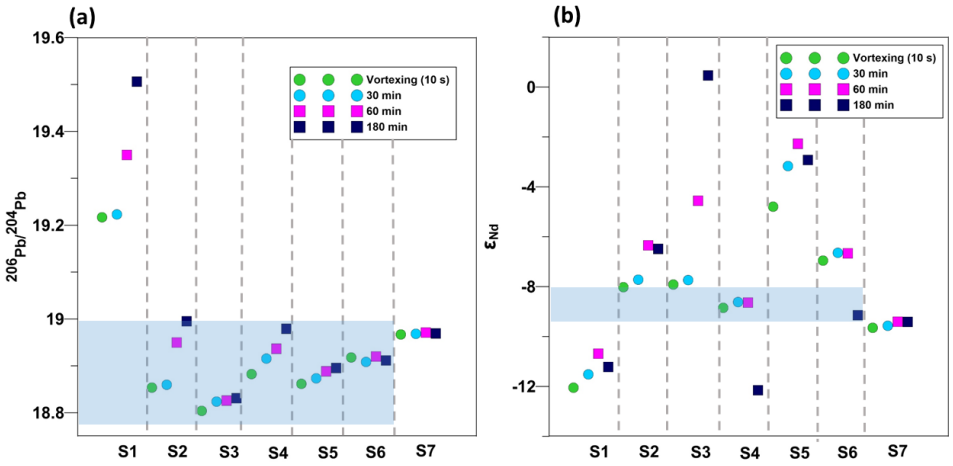

Figure 3.4 Effect of leaching time on Pb and Nd isotopic compositions. (a) $^{206}Pb/^{204}Pb$ and (b) ε_{Nd}. The round dots show results of 10-s vortexing leaching and 30-min conventional leaching each separately with fresh samples. The square dots show sequential leaching results starting by mixing 30-min conventional leaching residues with renewed leaching solution for 60 min, and then remove supernatant and leach again with renewed leaching solution for 180 min. The blue shades indicate seawater Pb and Nd signature (Abouchami and Goldstein 1995, Stichel et al. 2012).

leaching time. S1, S2 and S4 which are close to Antarctica continent showed the most

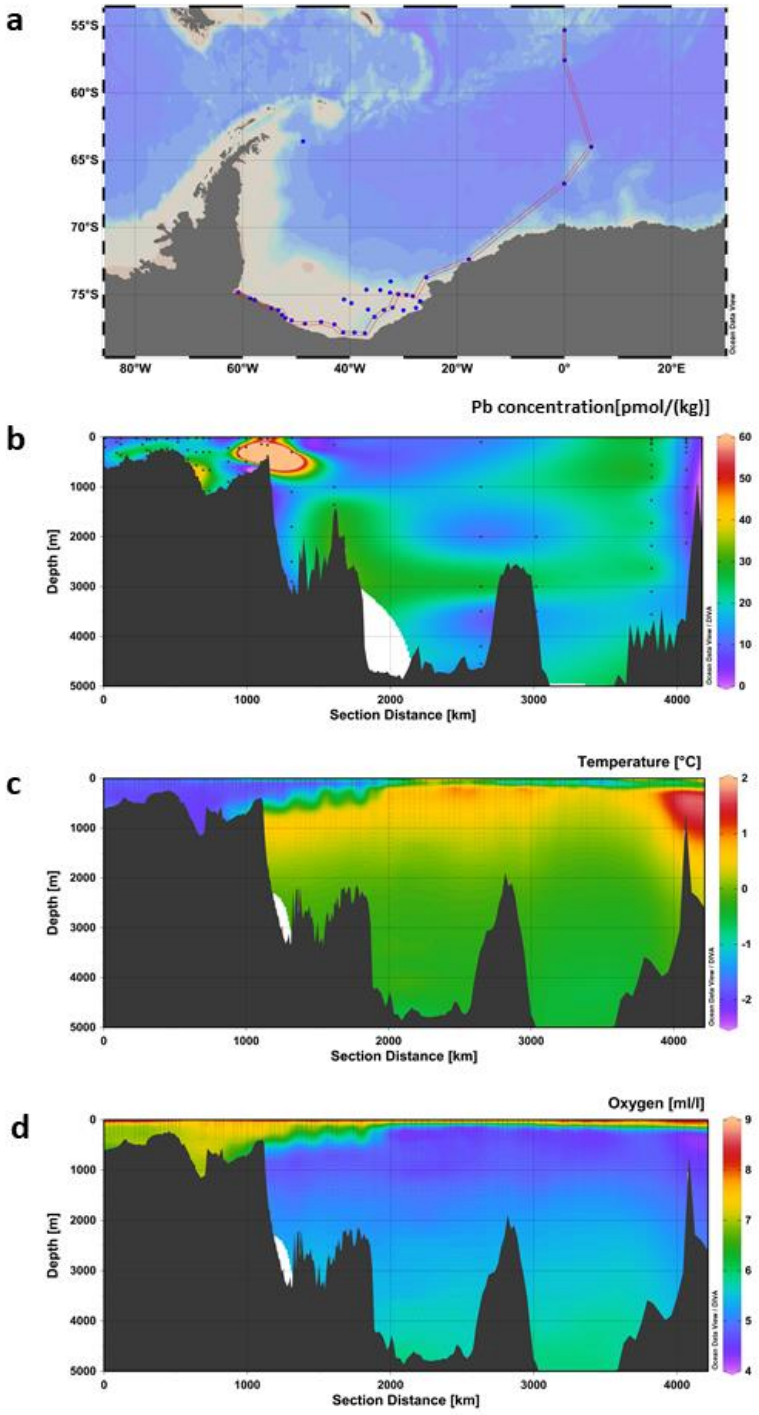

Figure 3.5 Seawater temperature, Pb and oxygen concentrations of a section in the Weddell Sea from south to north. a, The defined section of stations from cruise PS111 and GIPY04 (the two northern most stations in the section) in the Weddell Sea. **b,** seawater Pb concentration. **c,** seawater temperature. **d,** seawater oxygen concentration. The seawater Pb concentration data of GIPY04 were taken from the GEOTRACES database. Color-mapped seawater temperature and oxygen concentration drawn from the 2009 World Ocean Atlas (Garcia et al. 2013, Zweng et al. 2013). The maps were made by Ocean Data View (Schlitzer 2011).

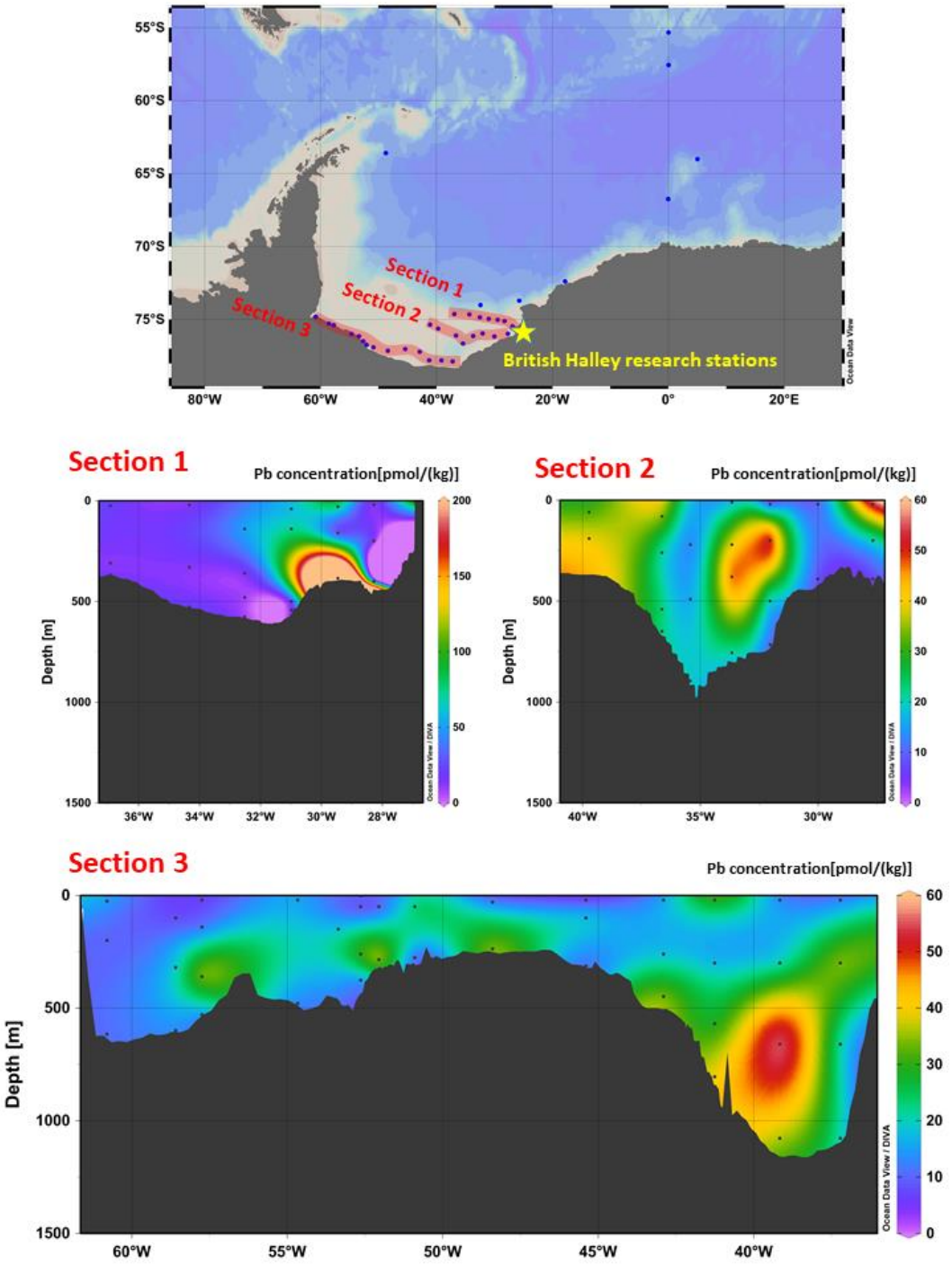

Figure 3.6 Seawater Pb concentrations of three sections in front of the Filchner-Rønne Ice Shelf. Note the expanded Pb concentration range for seawater samples displayed in Section 1 compared with those in Sections 2 and 3. The maps were made by Ocean Data View (Schlitzer 2011).

pronounced offsets with increasing leaching time. In contrast, sequential leaching had only little or no impact on $^{206}Pb/^{204}Pb$ of the samples, S3, S5 and S6, in the open ocean (Figure 3.4a). Similar to $^{206}Pb/^{204}Pb$, ε_{Nd} values in sediment leachates also shifted towards more radiogenic (higher) values from 10 seconds to 60 minutes leaching but reversed to less radiogenic (low) values or increased to very high $\varepsilon_{Nd}>0$ of S3 at 180 minutes, indicating leaching at 180 minutes have attacked different sediment fractions with distinct ε_{Nd} values (Figure 3.4b).

3.3.4 Seawater Pb concentrations in the Weddell Sea

All new seawater Pb concentration data are listed in the appendix (Table 10). As shown in Figure 3.5b, the seawater Pb concentration in the Weddell Sea basin are generally below 30 pmol/kg and very high on the continental shelf in front of Filchner-Rønne Ice Shelf. The northernmost station in the section including Circumpolar Deep Water shows the lowest Pb concentration below 12 pmol/kg (Fig. 3.5b) but the seawater Pb concentrations in the Weddell Sea do not clearly co-vary with hydrographic features. The highest Pb concentrations are observed in the Section 1 (Figure 3.6). The high seawater Pb concentrations are also identifyable in the other two sections within the Filchner trough (eastern part of displayed shelf sections). In the Rønne trough (western side of the displayed shelf sections) the Pb concentrations are low and consistent with the results in the Weddell Sea basin further north.

3.3.5 Filchner-Rønne shelf seawater Pb and Nd isotopic compositions

The Nd isotope compositions of Filchner-Rønne shelf seawater showed remarkably little deviation from an average ε_{Nd} =-9, which agree with published Weddell Sea Deep and Bottom Water ε_{Nd} signatures further north between -8.4 and -9.6 (Stichel et al. 2012). The ε_{Nd} values presented in Figure 3.7 in surface seawater of the station PS111-42-3 and PS111-80-1 are slightly more radiogenic and shift towards a more unradiogenic signal deeper in the water column which is in the opposite of the result in PS111-60-1. The seawater $^{206}Pb/^{204}Pb$ ratios in the sampled water column show

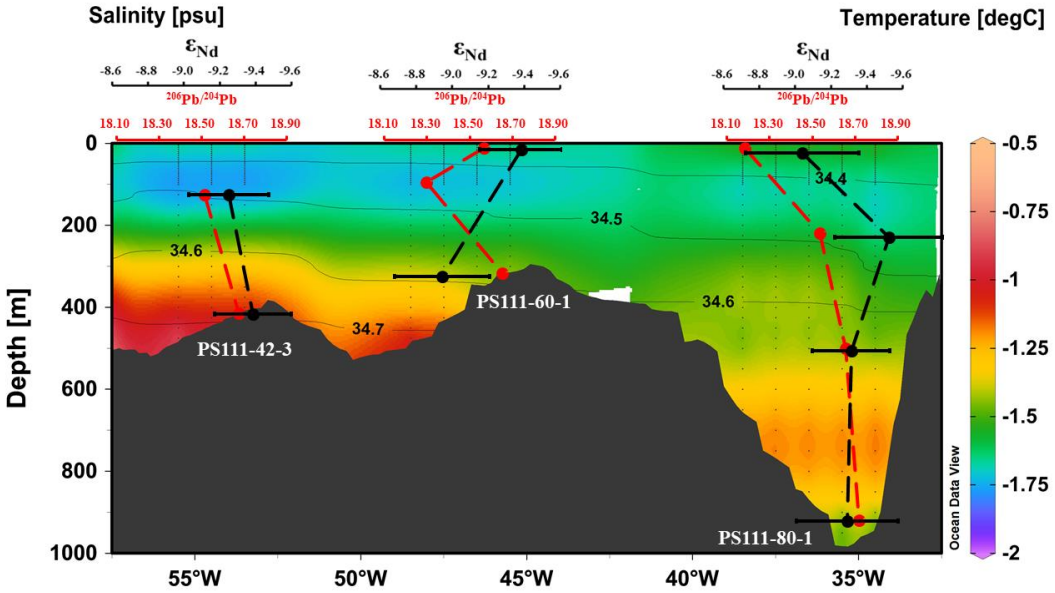

Figure 3.7 Seawater Pb and Nd isotopic compositions with hydrological context in front of Filchner-Rønne Ice Shelf. Color-mapped seawater temperature, with salinity contours overlain, as drawn from the 2009 World Ocean Atlas (Garcia et al. 2013, Zweng et al. 2013).

similar pattern with ε_{Nd} but with larger scale variability range from $^{206}Pb/^{204}Pb$=18.18 to $^{206}Pb/^{204}Pb$=18.72. The $^{206}Pb/^{204}Pb$ ratios in surface seawater are very unradiogenic (low) of the station PS111-42-3 and PS111-80-1 and become radiogenic (high) in the deeper water. The $^{206}Pb/^{204}Pb$ ratio of the surface seawater in the station PS111-60-1 is also unradiogenic (low) and even lower at 100 m water depth. However, $^{206}Pb/^{204}Pb$ in the deepest depth of the water column still shifts towards a radiogenic signal (high) at PS111-60-1.

3.3.6 Pb and Nd isotopic compositions in leachates and MUC porewater

Due to insufficient quantities of available Nd in extracted porewater (below 0.2 ng at each depth), the Nd isotopic compositions in the porewaters were not analyzed. Porewater Pb is also not abundant but Pb isotopic compositions from some depths could still be determined. We only compared $^{208}Pb/^{206}Pb$ in the porewater because ^{208}Pb and ^{206}Pb are the two most enriched Pb isotopes in nature, hence providing the best possible precision among all Pb isotopic ratios. In Figure 3.8a, the MUC bottom water $^{208}Pb/^{206}Pb$ at three stations are identical ($^{208}Pb/^{206}Pb$=2.12) and very distinct from seawater $^{208}Pb/^{206}Pb$ in the water column above. We also noticed more than 10

times

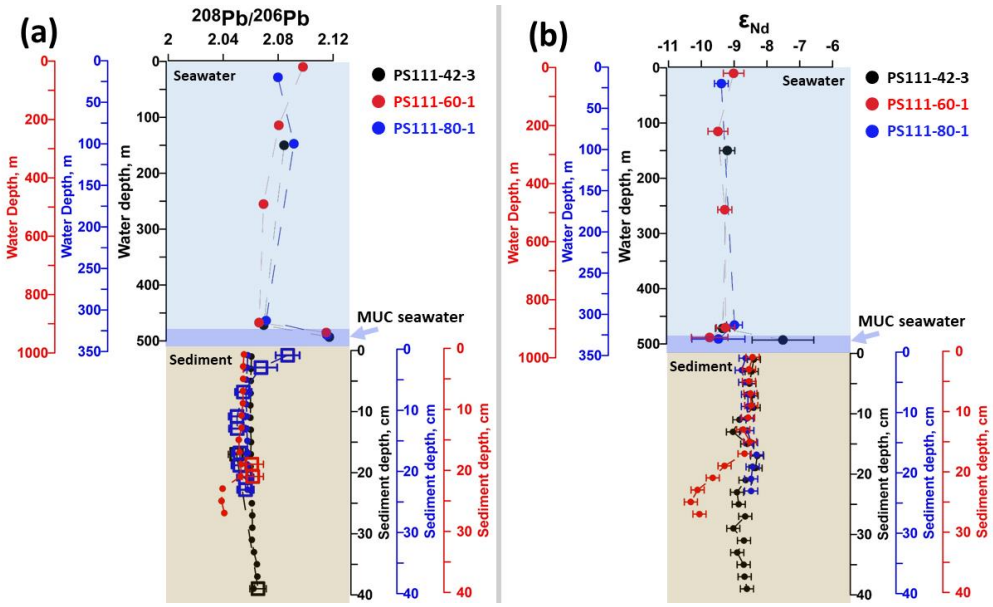

Figure 3.8 Pb and Nd isotopic compositions in sampled shelf seawater, MUC-sampled bottom water, extracted porewater and leachates at three stations in front of Filchner-Rønne Ice Shelf. (a) $^{208}Pb/^{206}Pb$ and (b) ε_{Nd}. The round dots in the seawater and sediment boxes indicate seawater and leachate isotopic compositions. The empty square dots indicate porewater $^{208}Pb/^{206}Pb$ ratios.

higher recovered Pb concentrations in MUC bottom water than in CTD seawater. The suspect MUC seawater Pb isotopic signature is most likely overprinted by Pb comtamination sourced from the MUC sampler itself because Pb bricks are used as a weight mounted on top of the MUC sampling tubes. The $^{208}Pb/^{206}Pb$ in the upper few centimetres within the coretop porewater also shifted towards the distinct Pb contamination signature seen in MUC bottom water, suggesting that Pb derived from the MUC weights also invaded the top centimetres of the sediment porefluids. However, the porewater $^{208}Pb/^{206}Pb$ below about 8 cm were resolvably not affected by this downcore Pb diffusion and agree with $^{208}Pb/^{206}Pb$ values in sediment leachates extracted using the vortexing leaching method. The CTD sampled shelf bottom water $^{208}Pb/^{206}Pb$ at our three sampled stations is consistently in the range of 2.07, which is only slightly offset from the coretop leachate ($^{208}Pb/^{206}Pb$ =2.05 to 2.06). Since the seawater sampling process was not trace metal clean and recovered porewater Pb concentrations were very low, future improved approaches should lead to better match between water samples and corresponding leachates. These results demonstrate that

authigenic Pb extracted from Weddell Sea shelf sediments using the improved reductive leaching reflect the porewater Pb isotope signal derived from bottom water. The low quantities of Nd recovered from MUC seawater resulted in highly expanded measurement uncertainties. The average MUC bottom water ε_{Nd} value of -8.9±2.4 from these three stations, however, is identical to bottom seawater at all three stations. Similar to Pb, the average ε_{Nd} extracted from the top 10 cm of sediment are consistent in all three cores, ranging from -8.4 to -8.8 but are slightly offset from overlying CTD seawater and MUC seawater ε_{Nd} signature (Figure 3.8b) on the order of 0.3 to 0.9 ε_{Nd}.

3.3.7 Authigenic Pb and Nd isotopic variability in the Atlantic sector of the Southern Ocean

In order to identify potential Pb and Nd disturbances which can alter the extracted seawater signal from the sediment at individual sample locations as a function of sedimentary lithology, we mapped the distribution of authigenic Pb and Nd isotopic compositions from 70 coretop sediment samples in the Atlantic sector of the Southern

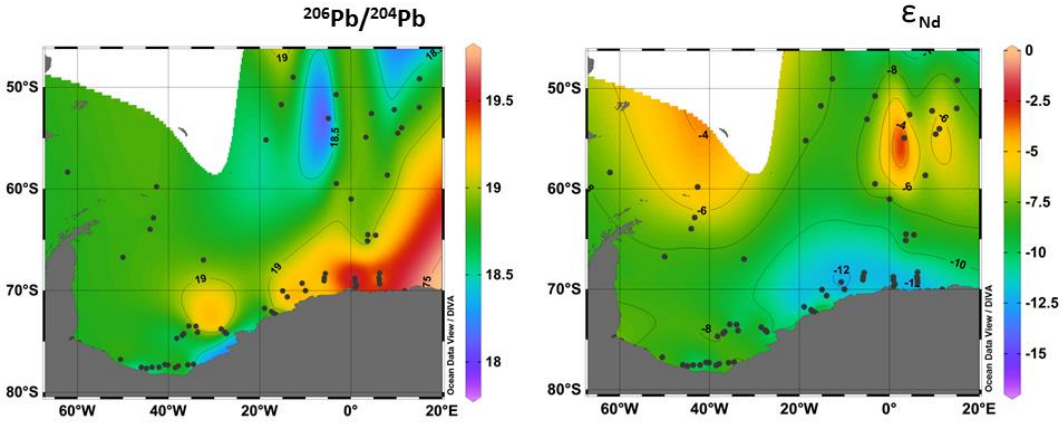

Figure 3.9 Authigenic $^{206}Pb/^{204}Pb$ and ε_{Nd} isotopic maps generated from coretop sediments in the Atlantic sector of the Southern Ocean.

Ocean using the vortexing leaching method. Figure 3.9a shows three different Pb isotope signature regimes on the map: $^{206}Pb/^{204}Pb<18.5$, $^{206}Pb/^{204}Pb>19.0$ along the East Antarctic continental margin and other areas with an average Weddell Sea $^{206}Pb/^{204}Pb$ of about 18.8 (Abouchami and Goldstein 1995). Authigenic ε_{Nd} coretop compositions also allow defining three areas which are slightly different from areas

defined via $^{206}Pb/^{204}Pb$ (Figure 3.9b). Extracted ε_{Nd} found to the east of the Drake Passage and in the northeast at the Bovet Triple Conjunction are very radiogenic with ε_{Nd}>-6. Coretop sediments near the East Antarctic continent have the most unradiogenic ε_{Nd} ranging from -10.3 to -12.5. The rest of the ε_{Nd} values extracted from coretop sediments agree with seawater ε_{Nd} signatures in the literature (Stichel et al. 2012).

3.4 Discussions

3.4.1 Contamination in the seawater Pb samples

The seawater Pb samples collected for this study were sampled by a standard CTD approach, which is not trace metal clean so the samples were likely contaminated to some extent. Moreover, the reseach vesssal Polarstern is also a potential moving Pb comtamination source. One indicator as to whether the sampled seawater Pb is contaminated is the actual seawater Pb concentration, and high seawater Pb concentration values in the sample is a sign of contamination. Reported seawater Pb concentrations in the Atlantic sector of Southern Ocean from previous Geotraces cruises GA10 and GIPY04 are lower than 23 pmol/kg (Schlosser et al. 2019) and 31 pmol/kg (Schlitzer et al. 2018), respectively. Besides several extremly high Pb concentration results in the Filchner trough, Pb in other seawater samples is generally below 31 pmol/kg, indicating no significant comtaminations. The seawater Pb isotopic composition is another indicator for Pb comtamination. Anthropogenic Pb is generally marked by unradiogenic Pb isotope signatures (Bollhöfer and Rosman 2000, Lee et al. 2015). As shown in Figure 3.7, the shelf bottom water $^{206}Pb/^{204}Pb$ ratios at these three stations are very consistent at around 18.7 which agree with the recently reported AABW $^{206}Pb/^{204}Pb$ ratios of 18.68 and 18.78 in the the Indian sector of Southern Ocean (Lee et al. 2015), suggesting that the Pb contamination from our standard CTD sampling process is negligible. The $^{206}Pb/^{204}Pb$ ratio of the surface seawater at these three stations are all very low which can be supplied by unradiogenic anthropogenic Pb derived from dust (Bollhöfer and Rosman 2000,

Bollhöfer and Rosman 2002) as previously found in a nearby ice core (Planchon et al. 2003) or released by ice rafted debris transporting across this area, which also contained very unradiogenic $^{206}Pb/^{204}Pb$ signature (Flowerdew et al. 2013).

The most striking finding of the seawater Pb is the extremly high seawater Pb concentration in the Filchner trough (Figure 3.5 and 3.6) because such high values have not been found in natural settings anywhere else. It is very likely that the high concentrated Pb is derived from anthropogenic sources because Pb is highly particle reactive in seawater and the slow release from natural sources should be quickly scavenged from seawater. One suspicious source is our CTD device since it is not trace metal clean. However, if the CTD itself was the source it should have resulted in high Pb concentration in all stations while only the samples from Filchner trough have high concentrations. Another option would be the abandoned British Halley Research Station (I to V) which were dumped directly into the ocean right at the highest Pb concetration spot in the Section 1 (Figure 3.6).

3.4.2 Reliable extraction of porewater Pb and Nd isotope signals from Southern Ocean sediments

Most Pb isotope signals extracted from the samples pre-treated with $MgCl_2$ were shifted towards less radiogenic Pb isotope compositions in $^{208}Pb/^{204}Pb$-$^{206}Pb/^{204}Pb$ space (Figure 3.10), with this contribution likely being of anthropogenic origin. Because $MgCl_2$ solution is the only variable factor in this experiment, the external Pb contamination was most likely provided from the $MgCl_2$ solution itself. As shown in Figure 3.2a, samples withz low authigenic Pb concentrations (S2 to S5) are more affected due to relatively higher proportions of Pb contamination from $MgCl_2$ solution in the extracted aliquots. However, neither the most affected sample S4 featured the lowest concentration nor did the least affected sample S1 yield the highest concentration. As a result the sample lithology should also play a role in the process as some samples may contain organic matters which can preferencially absorb more Pb (Strawn and Sparks 2000). Interestingly, we did not observe substantial changes in

Pb concentration while the Pb isotopic composition clearly was altered. The process might take place under a solution-particle exchange equilibrium affecting

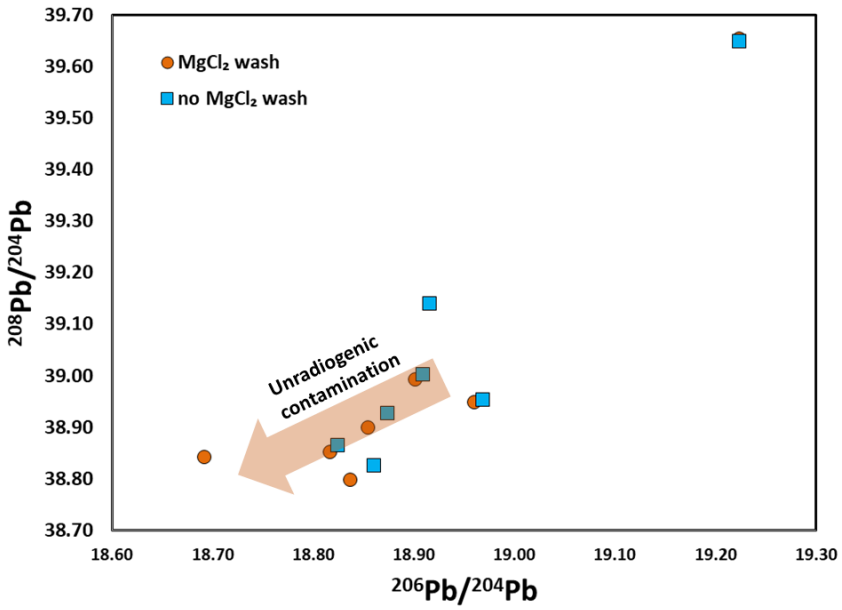

Figure 3.10 $MgCl_2$ pre-wash effects on Pb isotopic composition extracted from leaching test samples in $^{208}Pb/^{204}Pb$-$^{206}Pb/^{204}Pb$ spacing.

only Pb isotope compositions but not concentrations, as seen in seawater (Wu et al. 2010). Background Nd concentrations in inorganic chemicals are commonly much lower than respective Pb contaminations, so neither Nd concentration nor isotopic compositions were altered by $MgCl_2$ pre-wash, which is similar to what has been found before (Haley et al. 2008). Since we found $MgCl_2$ to potentially introduce Pb contamination into the sample, while we conversely observed no significant improvement of extracted Nd signatures, we suggest avoiding the $MgCl_2$ pre-wash step preceding reductive leaching.

Previous leaching protocols that used EDTA required less than one gram of sediment (Gutjahr et al. 2007, Blaser et al. 2016) but an alternative approach without ligands suggested using sometimes more than 10 grams of sediment (Wilson et al. 2013). As shown in Figure 3.3, adding EDTA equally strongly prevents re-adsorption of Nd and we suggest using EDTA in the leaching solution in order to keep sediment usage at a minimum. We also demonstrate that it is safe to use EDTA because no significant contamination and isotopic fractionation was found in our experiments. The only

exception is S4 in which Pb isotopic compositions in the leachats were shifted when using different ligands but ε_{Nd} values remained identical. Although the reason for this effect is not clear, leaching with EDTA still resulted in $^{206}Pb/^{204}Pb$ compositions within the seawater signature range while $^{206}Pb/^{204}Pb$ are too low (<18.76) when used DTPA or no ligands.

One general observation from previous reductive leaching studies for Nd is that shorter leaching times appear to provide more reliable results by dissolving less non-authigenic sedimentary phases (Gutjahr et al. 2007, Gourlan et al. 2010, Wilson et al. 2013, Blaser et al. 2016). Compared with the 10 seconds vortexing leaching approach, both Pb and Nd isotope signals extracted via the recently recommended 30-minute leaching duration are always more radiogenic and closer to the subsequent 1 hour sequential leaching signals which contained a higher proportion non-hydrogenetic Pb and Nd (Figure 3.4a and b), indicating that a 10 second exposure to leaching acquired the purest hydrogenetic signals. Although the ε_{Nd} in S5 and S6 are overprinted by Nd additions from volcanic substrate, 10 seconds leaching still led to ε_{Nd} values closer to actual seawater compositions (Figure 3.4b). One concern of only leaching sediments for 10 seconds is that the Pb and Nd recovered may not be sufficient for isotope analysis. However, we found that 10 seconds vortexing leaching

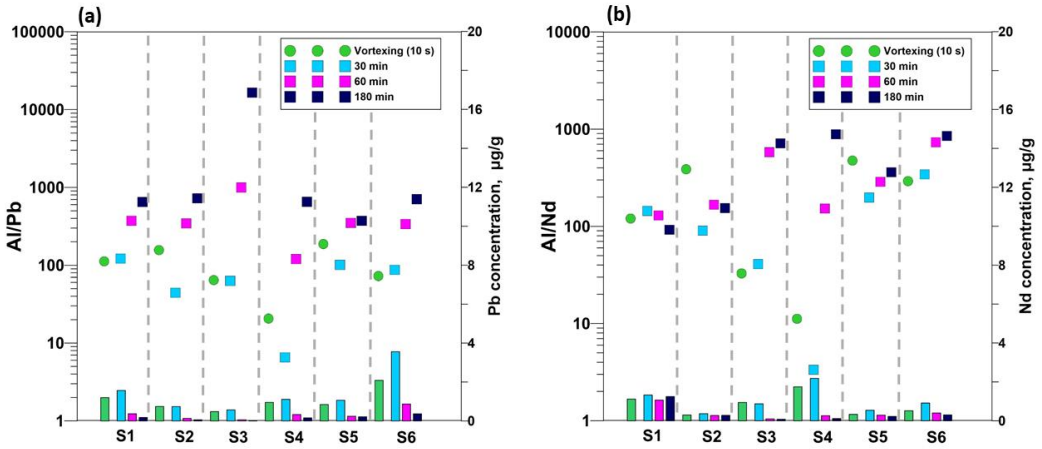

Figure 3.11 Variations of Al/Pb, Al/Nd, Pb and Nd concentrations of sediment samples during the sequential leaching. (a) Al/Pb and Pb concentration. (b) Al/Nd and Nd concentration. Green circle dots indicate Al/Pb or Al/Nd of vortexing leaching. Square dots indicate Al/Pb or Al/Nd of sequential leaching. Bar charts show extracted Pb and Nd concentrations.

surprisingly recovered more or less the same amount of Pb and Nd as extracted during 30 minutes of leaching (Figure 3.11a and b). Given the very good elemental yields and generally most reliable Nd and Pb isotopic results compared with longer leaching approaches, we suggest only to leach sediment for 10 seconds.

It has been found that Nd extracted from the Fe-Mn oxyhydroxide fraction by reductive leaching method in many cases provides identical results to Nd extraction from sedimentary foraminifera, which in turn reflect the porewater origin of the Nd isotope signal (Blaser et al. 2016). The porewater Nd isotope signal is derived from overlying seawater and sometimes modified by benthic exchange processes with the detrital phase (Abbott et al. 2015). We also observed that the ε_{Nd} values extracted by the vortexing leaching method from three MUC sediment cores provided compositions slightly offset from MUC and CTD seawater Nd signature immediately above the sediment (Figure 3.8b). The ε_{Nd} deviation between porewater and overlying seawater is likely caused by settle release of Nd from IRD and/or clays in the sediment because those three MUC sediments are all very muddy with substantial quantities of IRD present inside. Previous studies showed IRD (Pöppelmeier et al. 2018, Blaser et al. 2019) and clays (Ohr et al. 1991) could both release Nd from the terrigenous fraction during early diagenesis. Another important finding of this study is that the Pb isotope signals in the MUC sediment leachates processed by vortexing leaching is identical to the porewater Pb isotope signal and also offset from bottom CTD seawater Pb isotope signature (Figure 3.8a), although the latter may also be induced by the non-trace metal clean water sampling approach. Although it is generally assumed that the Pb isotope signature preserved in sedimentary authigenic Fe-Mn oxyhydroxides records a porewater signal, for the first time this assumption could be validated by actual corresponding porewater Pb isotope compositions.

3.4.3 Elemental ratios as proxies for non-hydrogenetic contamination

Elemental ratios in the leachate were previously used as proxies for monitoring non-hydrogenetic contamination: 1) REE patterns for the origin of the Nd (Bayon et

al., 2002; Martin et al., 2010); 2) Sr/Ca ratios for detrital carbonates (Blaser et al. 2016, Blaser et al. 2019); 3) Al/Pb and Al/Nd for non-hydrogenetic phases (Gutjahr et al. 2007). REE patterns were not investigated in this study because these were recently shown to be unreliable for the identification of contaminating phases (Blaser et al., 2016). The Sr/Ca ratio has been successfully applied for the detection of detrital carbonates in North Atlantic sediments (Blaser et al. 2019). Unfortunately, most of the sediments used in this study are carbonate-free. Al/Pb and Al/Nd were proposed for the evaluation of potential contamination from non-hydrogenetic phases, such as the detrital and potentially present volcanogenic fraction, due to high Al/Pb and Al/Nd ratios in non-hydrogenetic phases and low ratios in hydrogenetic phases (Gutjahr et al. 2007). However, if the degree of re-absorption dominates the element concentration variability, the application of this proxy could be limited and the Al/Pb and Al/Nd ratios then only

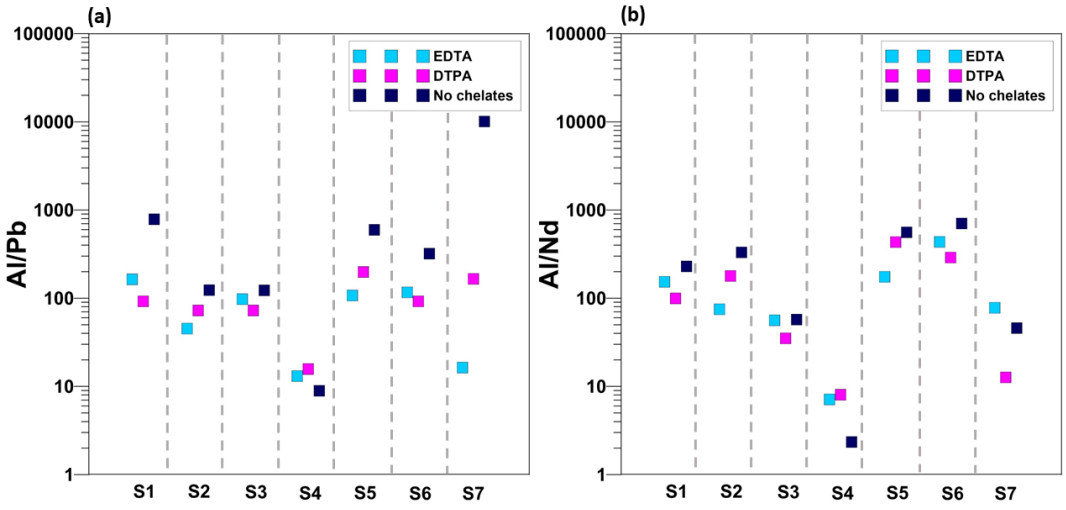

Figure 3.12 Variations of Al/Pb and Al/Nd of all samples using different ligands in the leaching solution. (a) Al/Pb. (b) Al/Nd.

reflect the different re-absorption behaviour of Al, Pb and Nd. As shown during the test constraining the chelating ligands effect, the extracted Pb and Nd isotopic compositions were identical in individual samples (Figure 3.3a and b) but the Al/Pb and Al/Nd dramatically fluctuated, i.e. Al/Pb of S7 ranged from 10 to 10000. Leaching without EDTA, in most caes, led to high Al/Pb and Al/Nd, indicating more Pb and Nd were re-absorbed back onto samples.

When EDTA was used to prevent reabsorption during leaching, Al/Pb and Al/Nd worked well in sequential leaching tests with exposure times from 30 min to 180 min (Figure 3.11a and b). For example, the Nd isotope signals in S5 and S6 were offset by volcanogenic contributions leading to high Al/Nd. Moreover, the ε_{Nd} values in 30 min sediment leachates (S2, S3 and S6) are consistent with seawater ε_{Nd} yielding Al/Nd lower than 100, which is similar to a threshold ratio for good quality Nd isotope data found in previous studies (Gutjahr et al. 2007, Blaser et al. 2016). However, the vortexing leaching method did not always result in lower Al/Pb and Al/Nd than 30 min leaching, although vortexing leaching can extracted a purer hydrogenetic Pb and Nd from the bulk sediments as indicated by the respective isotopic compositions. More specifically, we found, i.e. in S2, the amount of extracted Pb and Nd are similar during 10-second or 30-minute leaching, but the Al concentration extracted by vortexing leaching was much higher than by 30-minute leaching thus resulted in high Al/Pb and Al/Nd ratios using the vortexing leaching approach (Appendix Table 9). Generally, Al^{3+} in the solution starts to precipitate at pH =3.7 and almost quantitatively precipitates at pH = 4.7. The 30-minute leaching consumed more acetic acid than 10-second which leads to higher pH value in the solution, so the lowered Al concentration in the 30-minute leaching was likely caused by Al precipitation due to the pH increase. These considerations reveal that the elemental behaviour during leaching can be complex so that the interpretation based on elemental concentrations and ratios should be made very carefully, even though in the large majority of cases in our experiments the low Al/Pb and Al/Nd ratio (<100) indicated reliable hydrogenetic Pb and Nd extraction.

3.4.4 Selection of suitable sites for paleoceanographic reconstructions in the Atlantic sector of the Southern Ocean

The Nd isotope composition extracted from bulk sediment can be altered by the partial dissolution of sedimentary components, such as volcanic ash (Elmore et al. 2011, Blaser et al. 2016), continental detrital phases (Pöppelmeier et al. 2018, Blaser

et al. 2019) and pre-formed ferromanganese coatings (Bayon et al. 2004, Kraft et al. 2013, Pöppelmeier et al. 2018). As shown in Figure 3.9b, these unwanted Nd disturbances also exist at various sites in Southern Ocean sediments. However, the potential Pb interferences for reductive leaching are to date not as well investigated as for Nd. In this study, we generated corresponding $^{206}Pb/^{204}Pb$ and ε_{Nd} maps from coretop sediments to help identifying potential Pb disturbances in Southern Ocean sediments (Figure 3.9). Firstly, our data showed that both $^{206}Pb/^{204}Pb$ (>19.0) and ε_{Nd} (from -10.3 to -12.5) extracted from the coretop sediments near the East Antarctic continent offset from the neaby actual seawater ε_{Nd} and Pb isotope signature in surface scrapings of Fe-Mn nodules (Abouchami and Goldstein 1995). These could be caused by partially dissolving continental detrital fraction or/and pre-formed ferromanganese coatings during leaching. Dissolution of detrital fraction in the sediment should lead to high Al/Pb and Al/Nd ratios in the leachates (Gutjahr et al. 2007, Blaser et al. 2016), but the Al/Pb and Al/Nd ratios of the 10-s vortexing S1 leachate (Figure 3.11) are low indicating that the leaching did not target significant amounts of the detrital fraction. Therefore, the regional or local continental Pb and Nd isotope signatures in pre-formed ferromanganese oxyhydroxides likely overprinted both extracted seawater-derived Pb and Nd from authigenic Fe-Mn oxyhydroxides in sediments near the Antarctic continental margin because reductive leaching inevitably dissolves both authigenic *and* pre-formed Fe-Mn oxyhydroxides. The pre-formed Fe-Mn oxyhydroxides in the study area could be supplied by nearby ice streams (Rignot et al. 2011). Secondly, the extracted ε_{Nd} from sediments located to the east of Drake Passage and in the Bouvet Triple Conjunction ridge display too radiogenic values compared with ambient deep water compositions due to Nd release from volcanic components within the sediments from nearby volcanic sources (Stichel et al. 2012). The elevated Al/Nd ratios in S5 and S6 (Figure 3.11b) also indicate contributions of volcanic material. Interestingly, Pb in S5 and S6 vortexing leachates seems to be unaffected by volcanic contributions as we did not observe equally elevated Al/Pb in samples S5 and S6 (Figure 3.11a) and $^{206}Pb/^{204}Pb$ extracted from sediments in the area enriched in volcanic materials area did not display compositions

offset from expected seawater signals (Abouchami and Goldstein 1995).

Although extracted Pb is apparently relatively robust against contamination by sedimentary volcanic material, anthropogenic Pb contributions supplied by dust can alter the natural seawater signal. Pb extracted from coretop sediments in the northeast of the research area closest to South Africa are extremely altered by anthropogenic Pb contamination (Figure 3.11a). The lacking of sea ice protection and proximity to the African continent could both result in the strong anthropogenic Pb footprint in these sediment cores, because winter sea ice does not extend that far north and Pb sourced from Africa was found in nearby water masses (Paul et al. 2015). However, as shown in Figure 3.8a, anthropogenic Pb only penetrated the topmost several centimeters in the sediment. Thus, the extracted downcore Pb isotope signals in the lower parts should not be influenced. Overall, the sediment core sites located in the green area in the Figure 3.9a and b are the recommended for downcore Pb and Nd isotope analysis for the purpose of ocean circulation reconstruction because the extracted Pb and Nd isotope signals argee with the seawater signature. In addtion, the sediment cores near the Antractic continent which show distinct continental signal may hold the potential for tracking the local continental weathering changes.

3.5 Conclusions

We developed a fast 10 seconds vortexing leaching method to extract authigenic Pb and Nd isotope signatures from Southern Ocean sediments and validated this method by directly comparing the Pb and Nd isotope signal in the sediment leachates with overlying seawater Nd and Pb isotopic signatures and corresponding Pb porewater compositions. Utilizing the vortexing leaching method established in this study, we screened coretop sediments in the Atlantic sector of Southern Ocean for their hydrogenetic Pb and Nd isotope distribution in order to select suitable sediment core sites for paleoceanographic reconstructions.

The use of a previously employed sedimentary pre-leaching cleaning technique using

$MgCl_2$ was evaluated. Furthermore the effect of using or omitting chelate ligands was assessed, and the optimal leaching time was determined. Our data show that the $MgCl_2$ wash is not necessary and, on the other hand, may potentially contaminate the authigenic Pb isotope signature in sedimentary samples. Experiments to constrain the effect of chelating ligands were carried out by two commonly used ligands, EDTA and DTPA. Adding the chelating ligands during leaching was confirmed to be very important for leaching. When the leaching process was carried out without ligands, both Pb and Nd were substantially readsorbed back to the sediment. Between these two ligands, EDTA most efficiently prevented readsorption both for Pb and Nd, while no mass fractionation or contamination was observed. Moreover, the sequential leaching test indicated that the very short 10-second vortexing leaching extracted the purest hydrogenetic Pb and Nd in all tested sediment samples and recovered sufficient quantities of Pb and Nd for isotope analysis. Therefore, we recommend using vortexing leaching method in combination with EDTA to extract hydrogenetic Pb and Nd in Southern Ocean sediments.

The analysis of Pb and Nd isotope seawater signatures and porewater Pb isotope signatures demonstrated that the extracted hydrogenetic Pb and Nd by vortexing leaching in our settings reflect the porewater isotope signals which may, however, be slightly offset from ambient seawater signal due to early diagenetic porewater processes. The Pb contamination found in MUC seawater indicates that anthropogenic Pb can only penetrate in the topmost several centimeters of the sediment. A similar result was also found in the Pb record from the Lake Grimsel where the Roman smelting Pb signature present only in the topmost sediment layers (Süfke et al. 2019).

The previously suggested leaching quality assessment proxies, Al/Nd and Al/Pb, also provide a critical first insight regarding the nature of the extracted phase for Southern Ocean sediments when EDTA is present during leaching. The low Al/Nd and Al/Pb ratios (<100) in our experiments reflect upon the predominant extraction of a Fe–Mn oxyhydroxide phase but the high Al/Nd and Al/Pb ratios did not necessarily reflect

tapping of the detrital phase since slow pH increase during longer leaching unavoidably induced Al precipitation and complex re-adsorption behaviours.

The vortexing leaching is not omnipotent for extracting hydrogenetic Pb and Nd in all oceanographic settings due to potential presence of a benthic flux and pre-formed continentally derived ferromanganese oxyhydroxides. Therefore, we generated Pb and Nd isotopic maps for the Atlantic sector of Southern Ocean to avoid areas of altered sediment and localise suitable sites for generating authigenic Pb and Nd isotope reconstructions for the late Pleistocene. In general, suitable core sites should be further away from continental margin settings to prevent significant pre-formed ferromanganese oxyhydroxides input and, only applicable for Nd, the sediments should better not contain volcanic material.

Acknowledgements

Sediment material for this study was obtained from the AWI core repository in Bremerhaven. We thank Jutta Heinze, Tyler Goepfert, Ana Kolevica and Micheal Seebeck for technical support. We also thank the chief scientist Michael Schröder, Captain Stefan Schwarze and the crew of Polarstern for their contribution. H. Huang acknowledges the China Scholarship Council (CSC) for providing financial support to his overseas study.

4. Reconstruction of Antarctic Bottom Water export from the Weddell Sea using sedimentary seawater-derived Pb and Nd isotopes during the past two terminations.

Under review at *Nature Communications* as: Huang, H., Gutjahr, M., Eisenhauer, A., Gerhard, K. No Weddell Sea Antarctic Bottom Water export during the Last and Penultimate Glacial Maximum.

Abstract

Weddell Sea derived Antarctic Bottom Water (AABW) is the volumetrically most important deep water mass formed in the Southern Hemisphere and occupies large portions of the deep Southern Ocean (SO) today. While substantial glacial/interglacial changes in SO overturning circulation were suggested in a number of studies, the strength and location of Weddell Sea AABW formation and export to the various deep ocean basins remain enigmatic. Here we report seawater-derived downcore sedimentary Nd and Pb isotope records from three SO sites inside and outside the Weddell Sea that provide strong evidence for the absence of Weddell Sea AABW during the last and penultimate glacial maximum. The successive southward displacement of the SO overturning cell following glacial maxima is recorded by increasing contributions of Weddell Sea derived Pb admixtures to regions outside the Weddell Sea during both glacial terminations. The export of Weddell Sea AABW resumed late during glacial terminations, coinciding with the last major atmospheric CO_2 rise in the transition to the Holocene and the Eemian. While Holocene AABW formation and export out of the Weddell Sea took place without major perturbations, our new records lend strong support for a previously inferred overturning stagnation event during the peak Eemian interglacial. Overall our data suggest that Weddell Sea AABW export can be reduced or absent during both colder and warmer climates than current.

4.1 Introduction

The Southern Ocean (SO) has long been identified as the key driver in regulating

atmospheric CO_2 concentrations on glacial-interglacial timescales, mediating ocean-atmosphere carbon dioxide exchange by the interaction of variable export production (Sigman and Boyle 2000) and circulation changes (Anderson et al. 2009, Skinner et al. 2010, Burke and Robinson 2012, Jaccard et al. 2016). In either deglacial atmospheric carbon dioxide rise scenario, dissolved inorganic carbon (DIC)-enriched deep waters are increasingly upwelled to the SO surface during glacial terminations, where this DIC is degassed to the atmosphere as CO_2. During the last deglaciation (~18-11 ka BP), atmospheric pCO_2 increased during two main intervals between 18-15 ka and 13-11 ka (Monnin et al. 2004) (Fig. 2a), which occurred during Southern Hemispheric warming phases (Shakun et al. 2012). The multi-millennial scale deglacial atmospheric pCO_2 rise was largely a consequence of a southward moving SO overturning cell (Toggweiler 1999, Anderson et al. 2009, Xiao et al. 2016, Menviel et al. 2018) and associated increased upwelling in the Southern Ocean. At least three intervals of centennial-scale atmospheric pCO_2 rise were reported during Termination I (at 16.3 ka, 14.8 ka and 11.7 ka) that can be linked to Northern Hemispheric climate transitions, likely controlled by AMOC re-invigoration and the associated climatic teleconnections (Marcott et al. 2014).

In contrast to the state of knowledge regarding the understanding of deglacial frontal shifts and increasing deep SO overturning, strikingly little is known with respect to changes in water mass *sourcing* before and during glacial terminations. For example, while deep SO water masses at the end of the Last Glacial Maximum (LGM) were identified as being depleted in both $\delta^{13}C$ (Hodell and Venz-Curtis 2006) and radiocarbon (Skinner et al. 2010, Burke and Robinson 2012) alongside relatively low dissolved oxygen concentrations (Jaccard et al. 2016), the geographic origin of this glacial deep SO water mass is unresolved to date. This situation is dissatisfactory since commonly termed Southern Source Waters (SSW) are invoked to occupy large parts of the deeper Atlantic Ocean at the expense of North Atlantic Deep Water (NADW) during the Last Glacial Maximum and major Northern Hemisphere Stadials (Oppo and Lehman 1993, Adkins et al. 2002), with consequences for deep ocean

carbon sequestration (Skinner 2009). No study could as yet unambiguously demonstrate that this SSW is the glacial equivalent of interglacial Antarctic Bottom Water or whether SSW originated from other abyssal parts of the world´s oceans.

Weddell Sea-derived AABW is formed at several locations on the Antarctic shelf today, most prominently in front of the Filchner, Ronne and Larsen ice shelfs in the southern and western Weddell Sea (Foldvik et al. 2004, Huhn et al. 2008). Weddell Sea Bottom Water is the coldest and densest variety of Antarctic Bottom Water formed within the Weddell Sea. It mixes with the overlying Weddell Sea Deep Water and modified Warm Deep Water that is advected into the Weddell Sea within the Weddell Gyre, eventually leaving the basin to the north and northeast as Weddell Sea Deep Water (Naveira Garabato et al. 2002, Kerr et al. 2018, Purkey et al. 2018), which we refer to as Weddell Sea-derived AABW below.

We address the issue of SO water mass sourcing by using two sensitive provenance proxies, the authigenic Fe-Mn oxyhydroxide-bound neodymium (Nd) and lead (Pb) isotope signatures in deep SO sediments. Both trace metals are supplied to the oceans mainly from continental runoff or dust input (Frank 2002). Yet while Nd is also supplied via porewater exchange processes along continental margins (Abbott et al. 2015), such an input mechanism has as yet not been reported for Pb. Both proxies carry the isotopic composition of their continental source area and subsequent alteration through water mass mixing along their flow path. Since Pb is more particle-reactive than Nd, its residence time in seawater is significantly shorter on the order of few tens of years (Henderson and Maier-Reimer 2002), compared with several hundreds of years for dissolved Nd (Tachikawa et al. 2003). The high particle-reactivity of Pb also leads to its special behaviour in seawater in contrast to Nd. A recent study (Wu et al. 2010) demonstrated that even without vertical water mass mixing, temporally changing Pb isotopic compositions in North Pacific surface water left a footprint in the underlying deep water Pb isotope signal through seawater-particle exchange by sinking particles. Consequently, the seawater-derived authigenic Pb isotope signature in deep marine sediments can be controlled both by

bottom water and upper water mass changes. In contrast to authigenic Pb, the Nd isotope signal of the same deep marine authigenic Fe-Mn oxyhydroxide fraction only records bottom or porewater compositions (Du et al. 2016, Blaser et al. 2019). Taking advantage of the different behaviour of Pb and Nd in seawater, past seawater Pb isotopic compositions extracted from the authigenic Fe-Mn oxyhydroxide fraction in deep marine sediments (Gutjahr et al. 2007) hence provide insights into isotopic changes of the *entire* water column, while the Nd isotopic composition extracted from deep marine sediments is controlled by *bottom water* conditions. We generated seawater Pb isotope records ($^{206}Pb/^{204}Pb$ and $^{208}Pb/^{204}Pb$) from a sediment core in the Atlantic sector of the SO (ODP Leg 177, Site 1094, 53.2°S, 5.1°E, water depth 2807 m; Fig. 1), and corresponding bottom water Nd isotope records ($^{143}Nd/^{144}Nd$, expressed as ε_{Nd}) from authigenic Fe-Mn oxyhydroxides of two additional sediment cores: one located very close to ODP Site 1094 (PS1768-8, 53.6°S, 4.5°E, water depth 3299 m) and another located on the northern continental slope of the Antarctic Filchner-Rønne Ice Shelf (PS1599-3, 74.1°S, 27.7°W, water depth 2487 m; Figure 4.1). The two northern sites are ideally located to sensitively record past changes in SO circulation due to their position in the mixing zone between Circumpolar Deep Water (CDW) and Weddell Sea Deep Water (WSDW) (Orsi et al. 1999, Purkey et al. 2018). Specifically, at ODP Site 1094 and PS1768-8, covariation of Pb and Nd isotopic trends dominantly trace variations in Weddell Sea-derived AABW export, while Pb isotopic changes that have no resemblance in the Nd isotopic record reveal upper water column processes. At the same time, the southern core from the East Antarctic margin enables us to monitor the ε_{Nd} water mass signature of cold dense shelf water mixing with ambient water masses on the continental slope to the north of the Filchner-Rønne Ice Shelf (Orsi et al. 1999). In combination, our records resolve changes in the upper and lower SO overturning cells (Orsi et al. 1999, Watson and Garabato 2006) across the two most recent glacial-interglacial transitions (Termination I, TI and Termination II, TII).

4.2 Samples and methods

4.2.1 Core positions

Ocean Drilling Program (ODP, Leg 177) Site 1094 (53.2°S, 5.1°E, water depth 2807 m) and 'RV Polarstern' sediment core PS1768-8 (53.6°S, 4.5°E, water depth 3299 m) were retrieved from the Atlantic sector of the Southern Ocean, south of the modern Antarctic Polar Front (Figure 4.1). Core PS1599-3 (74.1°S, 27.7°E, water depth 2487 m) was retrieved from the continental slope north of the Filchner-Rønne Ice Shelf (Figure 4.1). Additional data from sediment coretops used for seawater Pb isotopic characterization in Figure 4.9 were taken from Chapter 3 and are listed in Appendix Table 14.

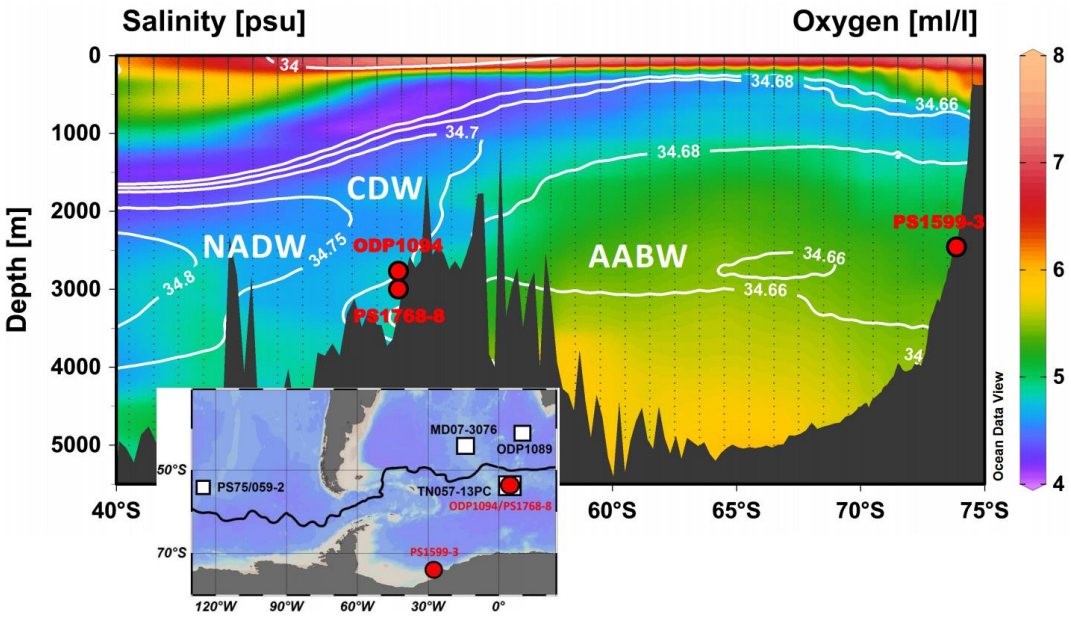

Figure 4. 1 Vertical section of the Atlantic sector of Southern Ocean placing studied sediment core sites into hydrographic context. Colour-mapped oxygen concentrations, with salinity contours overlain, as drawn from the 2013 World Ocean Atlas (Garcia et al. 2013, Zweng et al. 2013). Sediment cores presented here (ODP Site 1094, PS1768-8 and PS1599-3) are marked with red circles. The locations of other cores mentioned in the text are marked as white squares in the inlet map. Figure created with Ocean Data View (Schlitzer 2011).

4.2.2 Age model

For Termination I, existing age models of PS1599-3 (Weber et al. 2011), PS1768-8

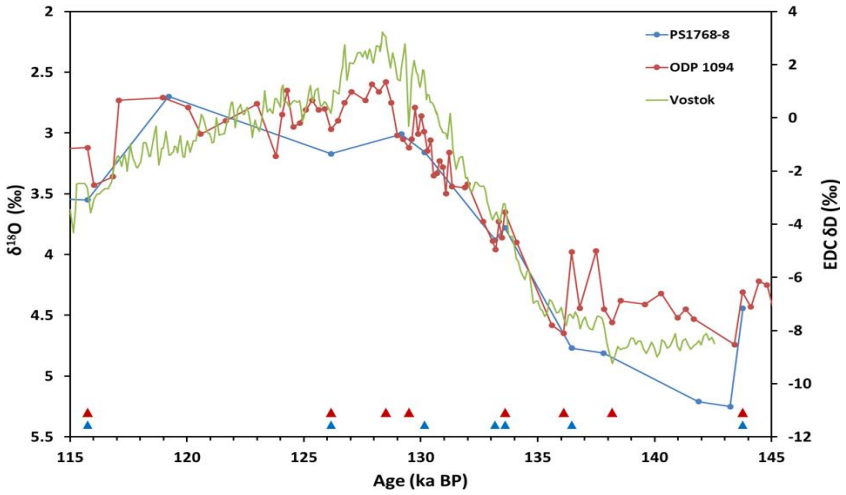

Figure 4.2 Age model found for Termination II from fine-tuning the composite planktonic $\delta^{18}O$ record to Vostok δD (Petit et al. 1999) . The triangles represent the tie-points defined to tune records.

(Frank et al. 1996) and ODP Site 1094 (Hodell et al. 2003) are directly taken from previous studies. For Termination II, the age model for Site ODP 1094 and PS1768-8 was refined via alignment of planktonic foraminiferal $\delta^{18}O$ (Niebler 1995, Hodell et al. 2003) with Antarctic ice δD from Vostok (Petit et al. 1999) assuming an in-phase relationship (Figure 4.2) as described in a recent study (Jaccard et al. 2013).

4.2.3 Pb and Nd isotope measurements

The seawater Pb isotope signal was extracted from bulk sediment of ODP Site 1094 and the seawater Nd isotope signal was extracted from bulk sediment of PS1599-3 and PS1768-8 following the leaching procedure decribed in the Chapter 2.3. Given the lack of foraminifera or fish teeth for comparison to the leachate Nd isotope data in the sediment, past seawater ε_{Nd} was also extracted from the Fe-Mn oxyhydroxide fraction in 10 separated biogenic opal samples picked from core PS1768-8 to confirm the validity of the leaching method (decribed in the Chapter 2.3). The fraction >63 mm was dried and about 0.1g of biogenic opal was picked. The authigenic Fe-Mn oxyhydroxide signal contained in the opal fraction was extracted by the same method we used for bulk sediments leaching. Extracted Pb and Nd were purified by ion

chromatography detailed in Chapter 2.4.1 and 2.4.3. Pb and Nd isotope measurements were performed on a Thermo Scientific Neptune Plus MC-ICP-MS at GEOMAR, Kiel. Analytical details are described in Chapter 2.5. All data are listed in Appendix Tables 11-14.

4.3 Results

4.3.1 Potential impact of Ice Rafted Debris (IRD) on Pb and Nd isotope composition.

Previous studies suggested that Ice Rafted Debris (IRD) may have a substantial impact on both Pb and Nd isotope compositions in high latitude oceans and authigenic phases formed in the sediments during elevated IRD flux in the water column (Kurzweil et al. 2010, Crocket et al. 2012, Roberts and Piotrowski 2015, Blaser et al. 2019).

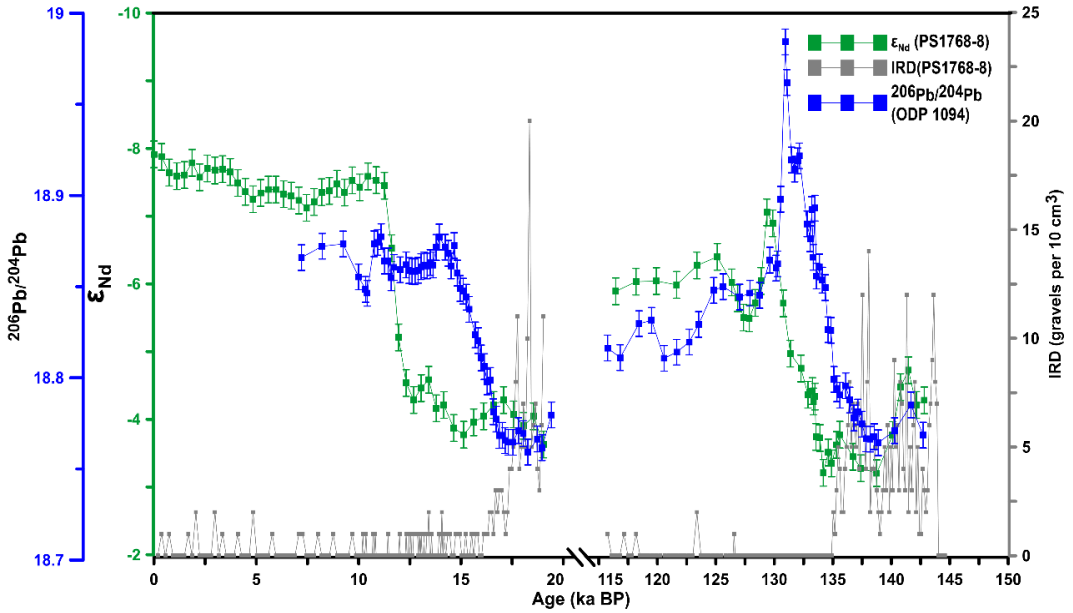

Figure 4.3 Extracted authigenic Fe-Mn oxyhydroxide-derived $^{206}Pb/^{204}Pb$ at ODP Site 1094 and ε_{Nd} in core PS1768-8 compared with its IRD concentrations (Diekmann et al. 2003). Major Pb and Nd isotopic changes did not coincide with changes in IRD concentration during Terminations I and II.

Since ODP Site 1094 and core PS1768-8 were recovered in the flow path of Antarctic Iceberg Alley (Weber et al. 2014), the temporally elevated IRD input may in theory compromise our results. The locations of ODP Site 1094 and core PS1768-8 are very

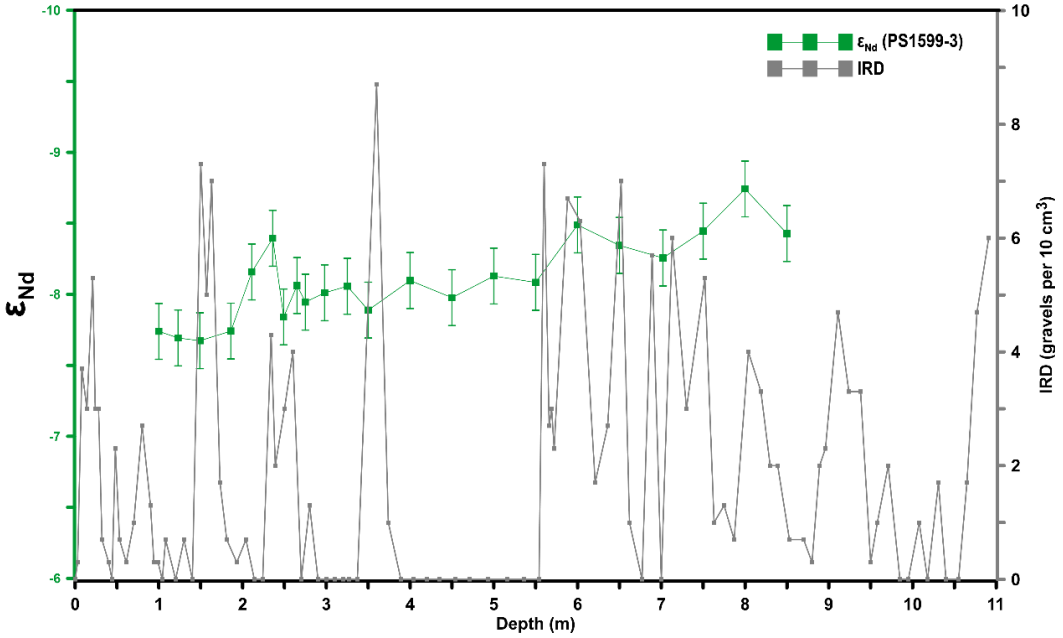

Figure 4.4 Extracted authigenic ε_{Nd} in core PS1599-3 compared with IRD concentrations in the core (Michels et al. 2002). Covariation between Nd isotopic changes and IRD concentration changes are not apparent.

close to each other, for which reason we only compare IRD contents from PS1768-8 to our $^{206}Pb/^{204}Pb$ and ε_{Nd} results. As shown in Figure 4.3, a strong IRD flux was only recorded during glacial times, but in these cold periods our $^{206}Pb/^{204}Pb$ evolution is remarkably smooth, arguing against a significant impact of IRD-sourced Pb on our extracted signal (Kurzweil et al. 2010, Crocket et al. 2012). As shown in Figures 4.3 and 4.4, the variable IRD concentrations only bear a weak correlation with extracted ε_{Nd} records both in core PS1599-3 (Michels et al. 2002) and PS1768-8 (Diekmann et al. 2003). In particular, the ε_{Nd} is almost invariant while the IRD content peaked in various sections throughout the cores. Strikingly, sedimentary sections featuring the major transitions in ε_{Nd} found in our record late during Termination I and II do not contain significant amounts of IRD. We therefore suggest that our ε_{Nd} records are not influenced by IRD-sourced Nd either.

4.3.2 Anthropogenic Pb contamination

Given that the oceanic Pb isotope signal today is largely controlled by anthropogenically sourced Pb (Flegal et al. 1993, Lee et al. 2015), the modern

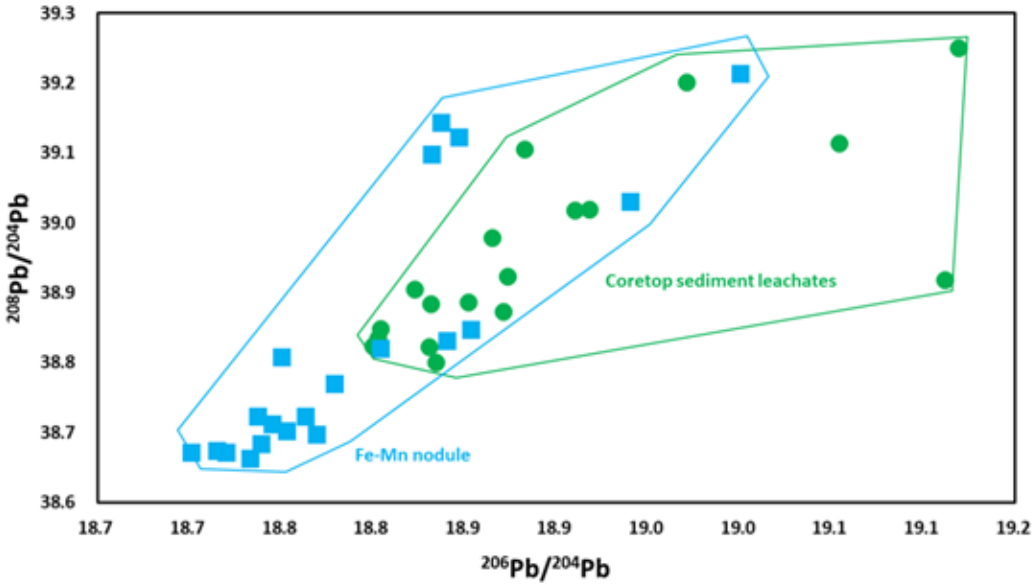

Figure 4.5 Comparison of Pb isotopic compositions between surface Fe-Mn nodules (Abouchami and Goldstein 1995) and core-top sediment leachates in the Weddell Sea, Drake Passage and Atlantic sector of the Southern Ocean. Pb isotope compositions of core-top sediment leachates are more radiogenic (higher) than the Fe-Mn nodule Pb isotope signal, suggesting that anthropogenic Pb contamination does not affect our sedimentary Pb isotope

seawater Pb isotope compositions do not reflect natural Pb isotope signatures of different water masses in the past. To circumvent this problem, we extracted the pre-industrial seawater Pb isotope signature from the authigenic Fe-Mn oxyhydroxide fraction in 20 individual coretop sediment samples in various parts of the Weddell Sea, Drake Passage and Atlantic sector of the Southern Ocean further north (Appendix Table 14). Since Fe-Mn nodules are one of the most reliable Pb isotope archives available, we compare our Pb isotope records with previous Pb isotope datasets based on nearby surface Fe-Mn nodules (Abouchami and Goldstein 1995) (Figure 4.5). Any modern anthropogenic Pb contamination would be detectable via its extremely unradiogenic (low) Pb isotopic signature (Bollhöfer and Rosman 2000, Bollhöfer and Rosman 2002). As shown in Figure 4.5, Pb isotope compositions extracted from sediments are either compositionally identical or systematically more radiogenic (higher) than the Fe-Mn nodule Pb isotope signal, proving strong support that anthropogenic Pb contamination is not controlling our sedimentary Pb isotope records.

4.3.3 Dust influence on Pb isotope compositions

Previous studies found that dust input in the ocean can dominate the seawater Pb isotope signal in the past (Bollhöfer and Rosman 2000). In order to determine the dust influence on dissolved and sedimentary authigenic Pb isotope compositions, we compare the dust record in EPICA Dome C (Lambert et al. 2008, Vallelonga et al. 2010) with our Pb isotope record (Figure 4.6). Most intervals covered within our Pb record correspond to times of insignificant dust deposition. Only the Glacial Maxima were marked by strong dust input. Previously published dust Pb isotope signatures were characterized by frequent and large-amplitude fluctuations between radiogenic and unradiogenic Pb isotope signatures (Vallelonga et al. 2010). Our seawater Pb isotope record extracted from from bulk sediment neither shows any correlation with neither dust intensity nor dust Pb isotopic signatures in the ice core. This suggests that our Pb isotope record is not offset by dust-derived Pb.

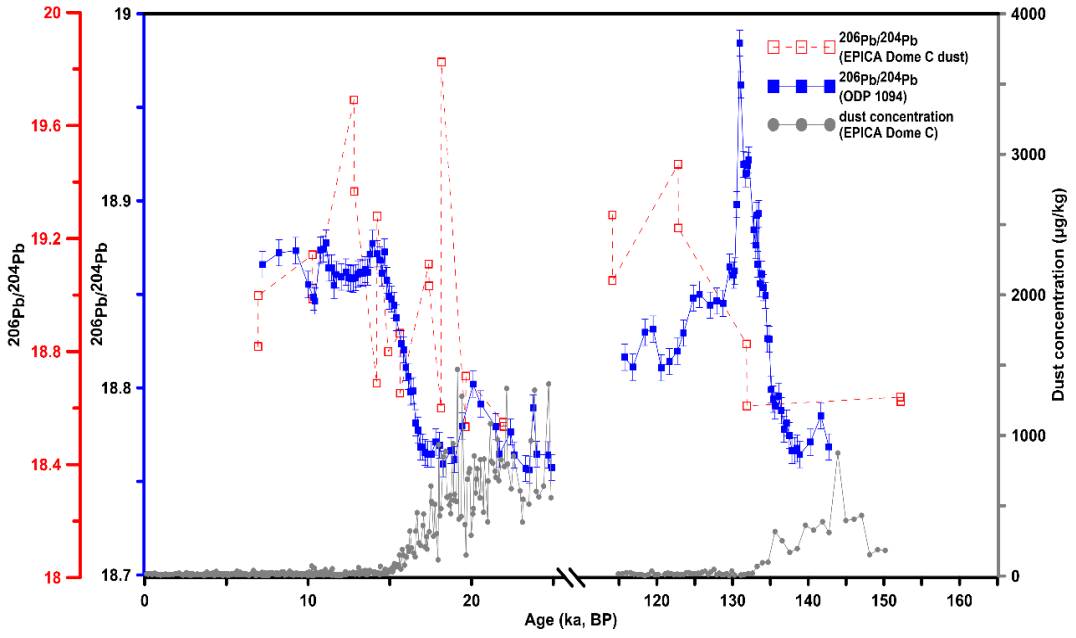

Figure 4.6 Assessment towards the influence of dust on the Pb isotope composition at ODP Site 1094. The $^{206}Pb/^{204}Pb$ record neither co-varies with dust concentrations, nor dust Pb isotopic signatures during Terminations I and II (Vallelonga et al. 2010).

4.3.4 Pb isotopic evolution during Termination I

Least radiogenic (lowest) Pb isotope compositions at ODP Site 1094 were recorded during the Last Glacial Maximum (Figure 4.7 b, c). Both $^{206}Pb/^{204}Pb$ and $^{208}Pb/^{204}Pb$ experienced a major change to significantly more radiogenic Pb isotopic compositions during the early deglaciation until the onset of the Antarctic Cold Reversal (~15 ka BP) during which the ambient ε_{Nd} at Site PS1768-8 was invariant (Figure 4.7g), suggesting changes in the upper SO overturning cell only. The change in Pb isotope composition during this interval is very steady over more than 3 ka. It coincides with the first rise in atmospheric pCO_2 (Figure 4.7a) and correlates with indicators of increasing upwelling in the Atlantic sector of the SO (i.e., a decrease in deep SO radiocarbon reservoir ages (Skinner et al. 2010) (Figure 4.7d), and increasing opal flux (Anderson et al. 2009) (Figure 4.7e)). In $^{206}Pb/^{204}Pb$-$^{208}Pb/^{206}Pb$ isotope space (Figure 4.9), the isotopic signature during the glacial interval of our records resembles most closely hydrogenetic Pb isotope compositions seen at the Drake Passage and the SE Atlantic, trending towards eastern Weddell Sea compositions throughout the deglaciation. We can exclude a dust or IRD control on the observed Pb isotopic changes (see Figure 4.3 and 4.6). The steadiness of the Pb isotopic shift (Figure 4.7b, c) during the early deglaciation argues for a gradual oceanic process operating on millennial timescales and we interpret these changes as corresponding to a gradual southward displacement of major oceanic fronts in the SO during the first half of Termination I until the Antarctic Cold Reversal (ACR) (Xiao et al. 2016) (Figure 4.7b, c).

4.3.5 The ε_{Nd} variation in Termination I

In context of the early deglacial Pb isotopic evolution of the SO water column, a key observation in our records can be made in the bottom water Nd isotopic record of Site PS1768-8. The ε_{Nd} seen during the late LGM and most parts of the deglaciation until 12.7 ka BP is on the order of ~-4 (Figure 4.7g). Such a composition is uncommon for the Atlantic sector of the SO that features a modern composition of -8.5 ± 0.39 ε_{Nd} (Stichel et al. 2012), implying entirely different water mass sourcing and circulation

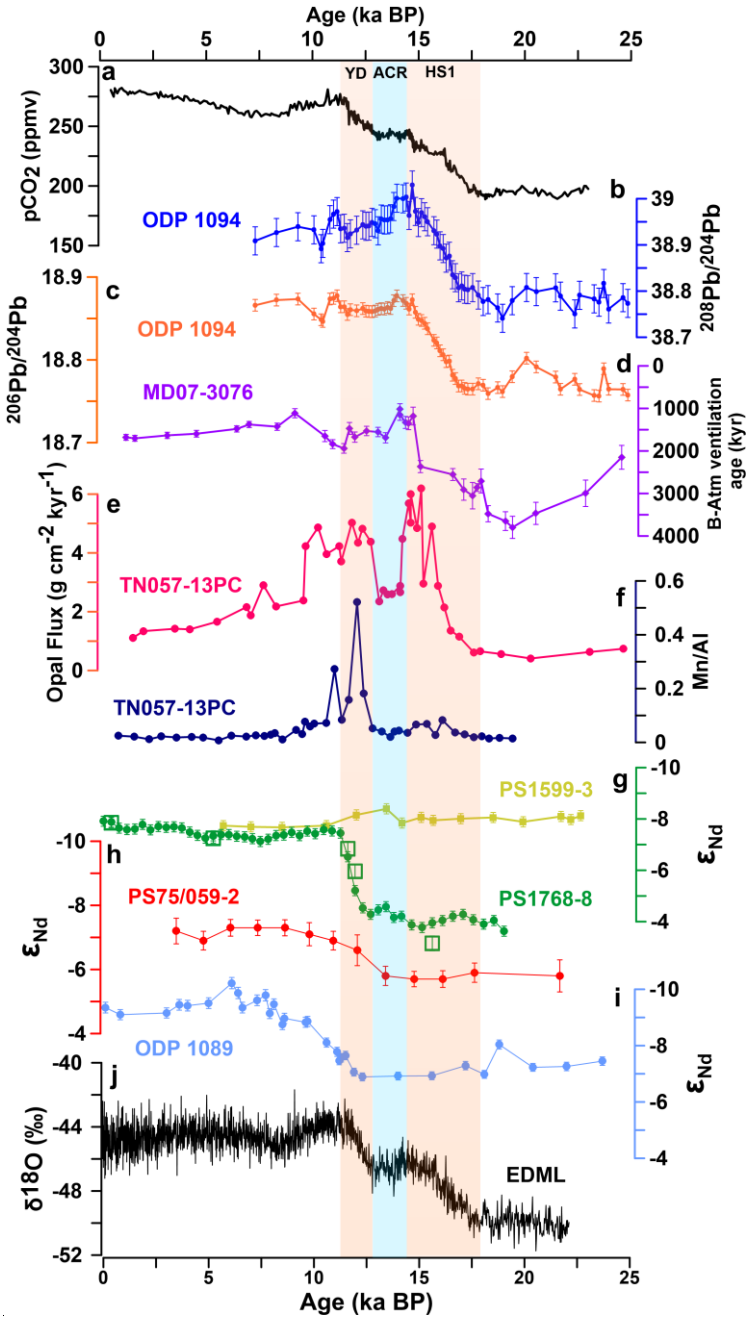

Figure 4.7 Southern Ocean and Antarctic palaeoclimatic reconstructions over the past 25,000 years. a, Atmospheric CO_2 concentrations from Antarctic Dome C ice core (Monnin et al. 2004) and the West Antarctic Ice Sheet Divide ice core (WDC) (Marcott et al. 2014). **b,c,** authigenic Fe-Mn oxyhydroxide-based $^{206}Pb/^{204}Pb$ and $^{208}Pb/^{204}Pb$ records from ODP Site 1094. **d,** Benthic-atmospheric (B-Atm) ventilation age (Skinner et al. 2010). **e,** ^{230}Th-normalized biogenic opal flux (Anderson et al. 2009). **f,** Sedimentary Mn/Al (Jaccard et al. 2016). **g,** ε_{Nd} records extracted from bulk sediment from PS1599-3 (yellow-green circles) and PS1768-8 (darker green circles) and opal from PS1768-8 (open green squares). **h,** Fish teeth and planktic foraminifera ε_{Nd} of South Pacific core PS75/059-2 (Basak et al. 2018). **i,** ε_{Nd} records extracted from core ODP 1089 (Lippold et al. 2016). **j,** EDML ice core $\delta^{18}O$ (Buizert et al. 2018). The orange and blue boxes indicate periods of strong and diminished deglacial CO_2 rise. YD: Younger Dryas; ACR: Antarctic Cold Reversal; HS1: Heinrich Stadial 1.

regime during glacial climate compared with the present-day situation. The ε_{Nd} remained very radiogenic until late into the deglaciation, when it changed to compositions close to modern Lower Circumpolar Deep Water (LCDW) ε_{Nd} within about two thousand years. The clearly defined change in ε_{Nd} was associated with a second smaller excursion towards more radiogenic Pb isotopic compositions (Figure 4.7b, c), an increase in East Antarctic ice core EDML $\delta^{18}O$ (Buizert et al. 2018) (Fig. 2j), the second rise in atmospheric pCO_2 (Figure 4.7a), and coincided with increasing Ross Sea AABW export in the Pacific sector of the SO (Basak et al. 2018) (Figure 4.7h).

4.4 Discussion

4.4.1 Upper overturning cell evolution

The glacial deep water Pb isotopic composition (18 ka - 25 ka) agrees with water mass sourcing from the Drake Passage and the SE Atlantic (Figure 4.9). The contemporaneous very radiogenic ε_{Nd} in PS1768-8 was clearly different from Nd isotope compositions recorded within the Weddell Sea at Site PS1599-3 at the end of the LGM (18 ka-19 ka) (Figure 4.7g). Active export of AABW during the late LGM from the Weddell Sea should transfer Weddell Sea Pb and Nd isotope signatures to our two northern SO sites, yet such a signal is not observed. Our results therefore suggest absence of Weddell Sea-derived AABW export to the Atlantic sector of the SO during the LGM (illustrated in Figure 4.10a). As indicated above, onset or invigoration of AABW export should result in simultaneous changes in our Pb and Nd isotope records. In contrast, the ε_{Nd} in PS1768-8 remained constant and radiogenic until 13 ka whilst only Pb isotope composition attained eastern Weddell Sea signatures already before the onset of the ACR (Figure 4.7b and c). Since the deep marine Pb isotope signal is influenced by changes in the entire water column but the deep Nd isotope signature only responds to transitions in bottom water sourcing, we suggest that the decoupled Pb isotope evolution between 18 ka and 13 ka was merely controlled by circulation changes in the upper overturning cell without significant

Weddell Sea-derived AABW export. Given the striking agreement between the early deglacial Pb isotopic evolution at ODP Site 1094, its co-variation with atmospheric pCO_2 (Figure 4.7a) and correlation with other proxies indicative for increasing upwelling during this interval (Figure 4.7d, e), we regard the steady Pb isotopic shift as tracing the southward displacement of the SO fronts resulting in increasing admixtures of Weddell Sea-sourced near surface waters (illustrated in Figure 4.10b). We also note that the Pb isotope records define a plateau during the early ACR, which corresponds to the timing of Meltwater Pulse 1A (MWP1a). A high-resolution iceberg rafted debris record from the Scotia Sea identified this time interval as the most prominent ice rafting event from the Weddell Sea during TI (Weber et al. 2014). A recent modelling study furthermore suggested increased meltwater rates in the Weddell Sea sector of the Southern Ocean after Heinrich Stadial 1, which may have temporarily affected overturning strength in the SO (Golledge et al. 2014). The Pb isotope evolution at ODP Site 1094 throughout the ACR agrees with such a scenario.

4.4.2 The timing of AABW export

The Nd isotope record from Site PS1768-8 in turn contains key information on abyssal overturning dynamics in the lower SO circulation cell. Generally, Nd isotopic changes in South Atlantic settings are usually more gradual (Piotrowski et al. 2004), while ε_{Nd} changes such as seen at ~13 ka here are commonly observed in the deglacial North Atlantic (Lippold et al. 2016). The rapidity and magnitude of change in ε_{Nd} together with synchronous $^{206}Pb/^{204}Pb$ and $^{208}Pb/^{204}Pb$ excursions hence argues for a local bottom water mass sourcing switch, and we interpret the transition to typical Weddell Sea ε_{Nd} signatures as recording the onset of Weddell Sea Deep Water export into northern reaches of the SO at ~13 ka BP (illustrated in Figure 4.10c). ODP Site 1089 located to the NE of Site PS1768-8 recorded simultaneous changes in ε_{Nd} alongside our site (Figure 4.7i). Yet at Site 1089 this switch is more gradual and offset to less radiogenic ε_{Nd}, reflecting its position further away from the exit route of Weddell Sea AABW and also being located in the export path of NADW into the SO (Piotrowski et al. 2004, Lippold et al. 2016). In contrast to Site PS1768-8, the

southernmost ε_{Nd} record from Site PS1599-3 (Figure 4.7g) situated on the East Antarctic continental rise that continuously monitored Weddell Sea compositions is strikingly invariant over Termination I and converged with northern Site PS1768-8 at

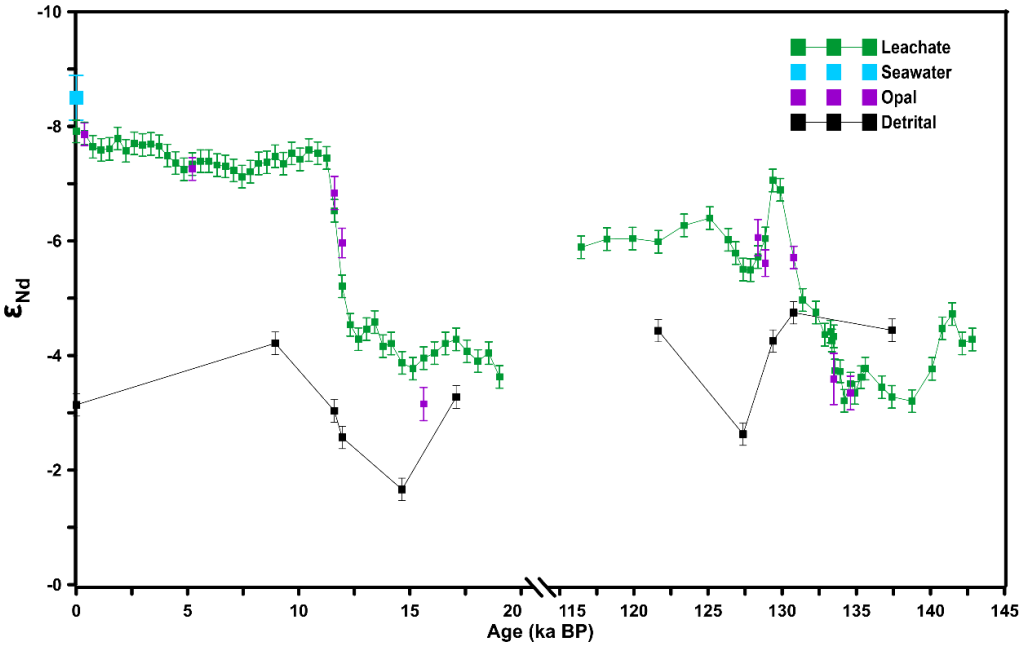

Figure 4.8 Extracted authigenic ε_{Nd} in core PS1768-8 compared with ε_{Nd} in the actual seawater, opal and detrital fraction. The seawater ε_{Nd} is taken from the closest station (Station 113, 53.6°S, 2.0°E, water depth 2400 m) (Stichel et al. 2012).

this time. Last but not least, an earlier study reported a sedimentary Mn/Al spike (Figure 4.7f) in a nearby core of PS1768-8 (Jaccard et al. 2016), interpreted as being driven by an increased ventilation of AABW during this interval.

The absence of Weddell Sea AABW export into the northern reaches of the SO outside the Weddell Sea during glacial climates has not been reported to date. In prior studies a sluggish yet operational glacial AABW water mass presence in the SO was invoked in glacial circulation scenarios (Smith et al. 2010, Adkins 2013, Xiao et al. 2016, Rae et al. 2018), although no study to date could localize the origin of this deep glacial SO water mass. We tested the integrity of our presented Nd isotope signal by extracting the pure opal fraction from the same sediments without adhering terrigenous material and gently extracted the authigenic signature from these. The ε_{Nd} extracted from these opal samples is matching the bulk sediment leach results (Figure 4.7g). The authigenic signal is also different from detrital ε_{Nd} signatures in the

Holocene and late deglacial section of this core (Figure 4.8). Moreover, the ε_{Nd} record appears very clear-cut, suggesting two water mass circulation regimes. We have hence good reason to suggest that the water mass change observed in our record at 13 ka BP is not controlled by analytical artefacts.

However, a second key information contained in our ε_{Nd} record is the glacial deep-water composition with an ε_{Nd} of ~-4. In the modern ocean such a composition is characteristic for North Pacific Deep Water (NPDW) (Fröllje et al. 2016). Although NPDW contributes to LCDW today (Kawabe and Fujio 2010), no resolvable isotopic trace of this ε_{Nd} signature can be found in the present-day Drake Passage water column (Stichel et al. 2012) upstream from Site PS1768-8. Conversely, cold-water coral based glacial and deglacial Upper Circumpolar Deep Water (UCDW) Nd isotope records presented from water depths between 700 to 1750 m water depth suggest that ε_{Nd} within UCDW at the Drake Passage did not become more radiogenic than an ε_{Nd} of ~-6 at any time during Termination I (Struve 2015). Potentially, Nd can be released from marine sediments to deep marine bottom water under very sluggish circulation regimes (Abbott et al. 2015, Blaser et al. 2019). In marine settings such as the North Pacific (Du et al. 2016) or North Atlantic (Blaser et al. 2019), where this process has been observed, the porewater signature (i.e., the ε_{Nd} signal extracted here) is expected to be altered away from bottom water ε_{Nd} towards other non-hydrogenetic sedimentary phases such as volcanic debris within the sediment (Blaser et al. 2019). Since glacial and early deglacial water column Nd isotopic constraints from cold-water corals that grew in intermediate water depth in the Drake Passage (Struve 2015) argue against deep Southern Ocean ε_{Nd} as radiogenic (high) as seen here, we interpret the glacial and deglacial signatures on the order of ~-4 as being controlled by this sedimentary porewater exchange process during which the extracted signature trends towards signatures of particular detrital phases (Figure 4.8). Given that the modern extracted ε_{Nd} compositions at Site PS1768-8 agree with direct seawater data such an alteration was limited to (de)glacial climate stages and significantly reduced SO overturning.

4.4.3 Southern Ocean overturning circulation evolution in TII

To test whether our observed changes are indeed controlled by Milankovitch cycles forcing we also investigated the Pb and Nd isotope evolution at the same sites during Termination II (Figure 4.11). The temporal change in incoming solar radiation during TII was significantly larger than seen during TI (Berger and Loutre 1991), leading to

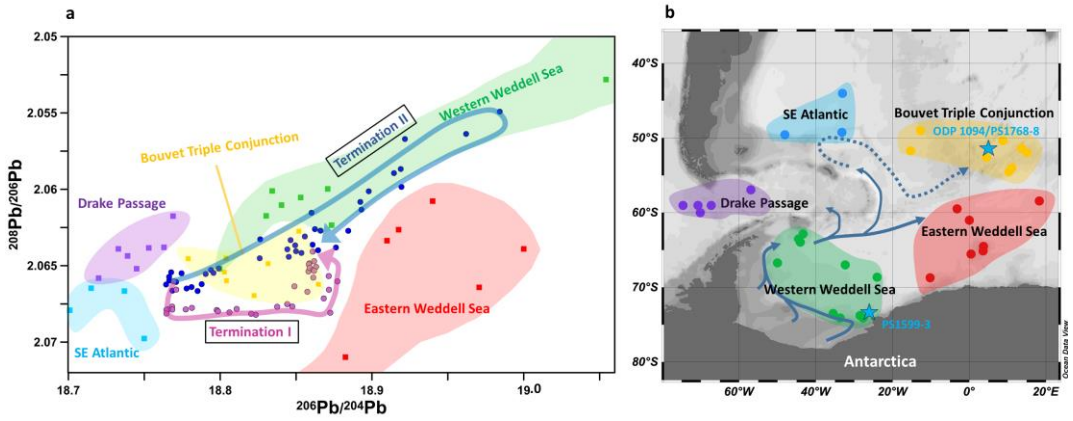

Figure 4.9 Seawater-derived $^{206}Pb/^{204}Pb$-$^{208}Pb/^{206}Pb$ isotopic trends observed at Site 1094 during TI and TII. a, authigenic Fe-Mn oxyhydroxide-based Pb isotopic evolution compared with Pb isotopic signatures in surface Fe-Mn nodules and compositions extracted from core-top sediment samples in different parts of the Atlantic sector of the Southern Ocean. The regionally characteristic Pb isotopic signature for various regions is marked by different colours. The arrows delineate the Pb isotopic evolution across the last two glacial-interglacial transitions (T I arrow covers 12 ka - 18 ka BP and T II arrow covers 125 ka - 142 ka BP). b, Locations of Fe-Mn nodules and core-top sediment samples (Appendix Table 14). The blue arrows in (b) indicate the modern AABW circulation and export path. The dashed blue arrow traces the LCDW flow path after entrainment of Weddell Sea AABW (Hellmer et al. 2016).

monotonic warming over ~8 ka (Broecker and Henderson 1998), peak Eemian temperatures at least 2°C warmer than present and global sea level some 4-6 metres higher than today (Rohling et al. 2007). Furthermore, the atmospheric pCO_2 rise and warming of Antarctica was likely largely completed when Northern Hemisphere ice sheets started to melt (Broecker and Henderson 1998). These different boundary conditions surrounding TII lead to resolvable difference in our Pb and Nd isotopic records yet equally show striking similarities.

First of all, the changes in ε_{Nd} again followed changes seen in Pb isotopes with a delay of several thousand years. Analogously to Termination I, Pb isotope compositions

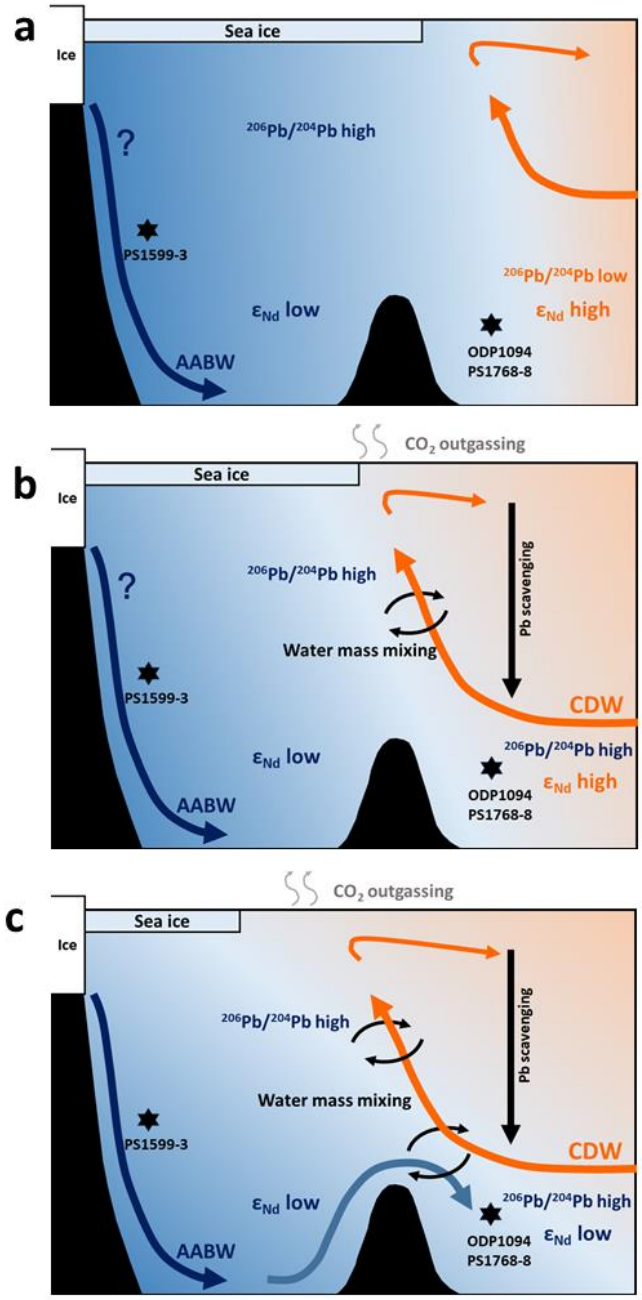

Figure 4.10 Schematic illustration of hypothesized Southern Ocean circulation modes in the Atlantic sector of Soutern Ocean during the last deglaciation. a, LGM overturning configuration with northward-shifted Southern Ocean circulation cell and absence of Weddell Sea-derived AABW at ODP Site 1094 / Site PS1768-8, resulting in unradiogenic (low) $^{206}Pb/^{204}Pb$ and local radiogenic (high) ε_{Nd} signatures. **b,** early deglacial overturning as experienced during Heinrich Stadial 1 (HS1). Southward displacement of the deglacial SO overturning cell leading to entrainment of a Weddell Sea-sourced radiogenic (high) Pb isotope signal. **c,** Younger Dryas (YD) and Holocene overturning configuration. Reinvigoration of AABW export resulted in the convergence of ε_{Nd} inside and outside of the Weddell Sea.

become more radiogenic during the penultimate deglaciation, yet after a short radiogenic spike at 132 ka BP compositions quickly drop to intermediate values (Figure 4.11k, l). In $^{206}Pb/^{204}Pb$-$^{208}Pb/^{206}Pb$ isotope space the deglacial changes follow a parallel trajectory to changes seen during TI, yet more closely resembling western Weddell Sea compositions (Figure 4.9) as opposed to a trend towards eastern Weddell Sea compositions recorded during TI. The strong Pb isotopic similarities with Western Weddell Sea compositions could be a consequence of increased melting of the West Antarctic Ice Sheet during TII (Sutter et al. 2016), yet this observation needs further investigation. The ε_{Nd} record shows similarly radiogenic compositions in the (de)glacial section preceding 133 ka BP, followed by a less sharp switch to least radiogenic compositions coinciding with heaviest δD values seen in the Vostok ice core, followed by rather intermediate ε_{Nd} during MIS 5e. The Nd isotope record never reached compositions as unradiogenic as during the Holocene within the Eemian.

The Eemian interglacial was warmer than the Holocene and the Antarctic Ice Sheet likely smaller (Huybrechts 2002). One study investigating the authigenic uranium concentration at Site 1094 including opal flux and Th_{xs} measurements reported an apparent overturning stagnation event in the SO in the middle of the last interglacial (Hayes et al. 2014) as a consequence of increased melting of Antarctic continental ice. Both our Pb and Nd isotopic compositions follow a well-defined perturbation alongside the authigenic uranium excursion (Figure 4.11c, j), suggesting reduced Weddell Sea-derived AABW export within the Eemian. Our Eemian Nd isotope record never reaches a classical Holocene SO signature, which should be on the order of ~-8, and is remarkably similar to the early deglacial Drake Passage cold-water coral record in UCDW (Struve 2015) during the reported interval. Whether these intermediate ε_{Nd} reflect the absence of Weddell Sea derived AABW or is rather controlled by changes in SO overturning outside the Weddell Sea need further research. Analogously to TI, however, the very radiogenic ε_{Nd} signature and unradiogenic Pb isotopic compositions observed preceding TII is observable and strongly argues for the absence of Weddell Sea AABW export during the penultimate

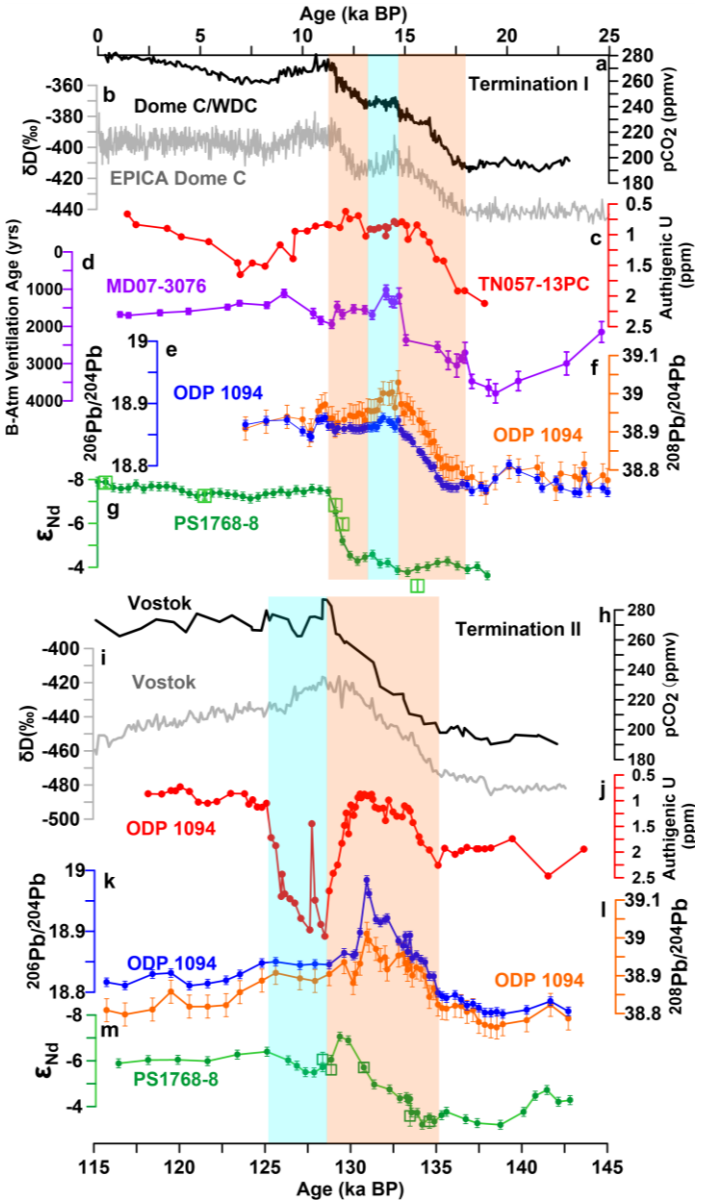

Figure 4.11 Southern Ocean authigenic U, Nd and Pb isotopic reconstructions and ice core records covering TI and TII. a, Atmospheric pCO_2 concentrations from Antarctic Dome C ice core (Monnin et al. 2004) and the West Antarctic Ice Sheet Divide ice core (WDC) (Marcott et al. 2014). **b,** δD (Parrenin et al. 2013) from Dome C and EPICA Dome C ice cores. **c,** TI sedimentary authigenic U concentrations at Site TN057-13PC (Jaccard et al. 2016). **d,** Benthic-atmospheric (B-Atm) ventilation ages (Skinner et al. 2010). **e,f,** $^{206}Pb/^{204}Pb$ and $^{208}Pb/^{204}Pb$ records in TI from ODP Site 1094. **g,** TI ε_{Nd} records extracted from bulk sediment (closed green circles) and opal (open green square) in core PS1768-8. **h, i,** Atmospheric pCO_2 (Petit et al. 1999) and δD (Waelbroeck et al. 1995) from Vostok ice core. **j,** TII sedimentary authigenic U concentrations at ODP Site 1094 (Hayes et al. 2014). **k,l,** $^{206}Pb/^{204}Pb$ and $^{208}Pb/^{204}Pb$ records in T II from ODP Site 1094. **m,** TII ε_{Nd} records extracted from bulk sediment (closed green circles) and opal (open green square) in core PS1768-8. The orange and blue boxes higlight periods of strong and diminished deglacial atmospheric pCO_2 rise.

glacial maximum.

The lack of Weddell Sea AABW export into the Atlantic sector of the SO during the last two glacial maxima does not necessarily imply that this water mass was not formed, rather that it was too dense to be exported to our northern SO core sites. Such a scenario is not unlikely since a reduced Weddell Gyre circulation could lead to reduced diapycnal mixing within the basin. The Weddell Sea is bound by the South Scotia Ridge and the Bouvet Triple Junction to the north. While Weddell Sea Bottom Water is too dense to leave the Weddell Sea today, the admixture of modified CDW within the Weddell Gyre is adding the required buoyancy to enable Weddell Sea AABW export (Huhn et al. 2013). Reduced Weddell Gyre circulation and associated lowered inflow of modified CDW as well as extended sea ice coverage may provide the boundary conditions required for the cessation of AABW export from the Weddell Sea. Given the bathymetry of the Weddell-Enderby abyssal plane we cannot exclude that a glacial equivalent of Weddell Sea AABW escaped the basin in deepest parts towards the east yet the northern export routes were closed. The clearly resolvable increase in atmospheric pCO_2 late during TI and TII (Figure 4.11) in turn illustrates how reinvigoration of Weddell Sea AABW ventilation contributed to partition carbon out of the ocean interior. As such, the resumption of AABW may have been instrumental in driving the deglacial sequence of events to completion.

4.5 Conclusions

Seawater-derived Nd and Pb isotope records extracted from three SO sites inside and outside the Weddell Sea are presented to resolve changes in the SO overturning circulation for the past two terminations. The impact of potential interferences, such as IRD and dust, on our sedimentary seawater-derived Nd and Pb isotope signal was firstly excluded as these showed no correlation. Matching Nd isotope signatures extracted from biogenic opal and bulk sediment also confirm the validity of the leaching method.

Neither deep sea Pb nor Nd isotope records revealed traces of a Weddell Sea AABW

signal during the last and penultimate glacial maximum, demonstrating the absence of AABW export out from Weddell Sea via the modern outlet in the northeast Weddell Sea basin. Following glacial maxima, the successive southward displacement of the SO overturning cell is always first recorded by increasing contributions of Weddell Sea derived Pb admixtures to regions outside the Weddell Sea for the past two terminations, coinciding with the onset of the deglacial atmospheric pCO_2 rise. The export of Weddell Sea AABW resumed late during glacial terminations and coincided with the last major atmospheric CO_2 rise in the transition to the Holocene and the Eemian. Our records also suggest that AABW was perturbed during the peak Eemian interglacial which lend strong support for a recently inferred overturning stagnation event. Overall, deep sea Pb isotope records generated in suitable SO settings should hold great potential to track Antarctic ice sheet dynamics. The Pb isotopic evolution clearly and gradually shifted towards different Antarctic continental source compositions during two different terminations in $^{206}Pb/^{204}Pb$-$^{208}Pb/^{206}Pb$ isotope space.

Acknowledgements

Sediment material for this study was obtained from the AWI core repository in Bremerhaven and the ODP/IODP core repository Bremen. We thank T. Goepfert, A. Kolevica and M. Seebeck for technical support. This manuscript benefited from discussions with S. Jaccard, M. Frank and J. Lippold. H. Huang acknowledges the China Scholarship Council (CSC) for providing financial support to his overseas study.

5. Evolution of the Antarctic Circumpolar Current in the Pacific sector of the Southern Ocean over the past 19 million years

Under preparation for publication.

Abstract

The Antarctic Circumpolar Current (ACC) is thought to play an important role in the establishment of a permanent Antarctic ice sheet, but the timing of onset of a full depth ACC and its following evolution remains mysterious. In this chapter, high-resolution, down to millennial timescales, seawater Pb isotope records are presented to reconstruct the ACC history for the past 19 million years recovered from a Fe-Mn crust grown on the Marie Byrd Seamont in the Pacific sector of the Southern Ocean based on laser ablation technique. Our data show five major circulation reorganization events during the past 19 million years and suggest a final establishment of a clockwise and eastward flowing ACC at 14 Ma. The timing of the full-depth ACC establishment coincided with the end of the Middle Miocene Climatic Optimum, likely suggesting a link between ACC establishment, intensification of Antarctic glaciations and global cooling in the middle Miocene.

3.1 Introduction

The Antarctic Circumpolar Current (ACC) is an eastward flowing, wind-driven current circulating around Antarctica and connecting all three major oceans. The formation of the ACC was thought to allow permanent ice accumulation on Antarctica by preventing polarward heat transport from low latitude regions (Kennett 1977, Zachos et al. 2001, Barker and Thomas 2004). Although the ACC plays a significant role in controlling global climate, its evolution remains poorly resolved. The formation of the circumpolar ACC requires seawater to pass around Antarctica both through the Tasman Gateway (TG) south of Australia and the Drake Passage (DP) south of South America. Therefore, the progressive tectonic opening of these two

oceanic gateways was essential for ACC evolution. Timing of TG deepening beginning around 35.5 Ma and completed by ~30.2 Ma is well constrained (Stickley et al. 2004) and seawater passing through the TG was also confirmed with help of a seawater Nd isotope record (Scher et al. 2015). The first shallow Pacific seawater influx trough the DP was found approximately at 41 Ma (Martin and Scher 2004), but the timing of deep water circulation through the DP and ACC establishment is still not resolved. A wide range of suggestions for the onset of deep water advection through the DP has been suggested encompassing a time window spanning from the Eocene-Oligocene Transition to the middle Miocene. The two popular alternative age estimates – mainly based on palaeomagnetic tectonic reconstructions – are ~31-28.5 Ma (Lawver and Gahagan 2003) and ~22-17 Ma (Barker 2001). A recent study also suggested a very late DP deepening after the middle Miocene (Dalziel et al. 2013). The drilling attemption in the DP was rather unsuccessful to date due to the rough sea conditions and lack of sediment, so there is very little sedimentary evidence to test these proposed DP opening dates.

We address the issue of ACC evolution with a lead (Pb) isotope record in ferromanganese (Fe-Mn) crust PS75/247-2 (69°8.53'S, 123°13.13'W; water depth: 1504-1708 m) dredged on the Marie Byrd Seamount in the Pacific sector of the SO. Past seawater Pb isotopic compositions recorded in Fe-Mn crusts are very sensitive tracers for tracking water mass mixing and changes in ocean circulation. Due to the very short residence time of Pb (50- 200 years) (Schaule and Patterson 1981, Cochran et al. 1990, Henderson and Maier-Reimer 2002), this proxy is ideal to reconstruct local or short distance changes. Pb has three radiogenic isotopes (^{206}Pb, ^{207}Pb and ^{208}Pb) which are produced by the decay of ^{238}U (4.47 Gyr), ^{235}U (0. 704 Gyr) and ^{232}Th (14 Gyr) and one primordial isotope ^{204}Pb. The crustal Pb isotopic ratio, i.e. ^{206}Pb/^{204}Pb, is dependent on the age and (U or Th)/Pb ratio of continental source rocks and is constant on relatively short Cenozoic timescales. Dissolved Pb in the oceans is mainly supplied by continental weathering sources with different Pb isotopic compositions (Martin 2002, Goldstein and Hemming 2003). The very distinct regional

Pb isotope signatures around the TG and DP (Abouchami and Goldstein 1995) (Figure 5.5c) suggest that Fe-Mn crust based Pb isotope records should hold great potential to identify multi-millennial scale ACC variability in the past.

In this study, we present high-resolution seawater Pb isotope records for the past 19 Ma in a Fe-Mn crust analysed by laser ablation coupled multicollector ICP-MS (LA-MC-ICPMS). The age of the Fe-Mn crust was dated by $^{10}Be/^{9}Be$ and high-resolution cobalt (Co) flux methods, and the corresponding Fe and Mn concentrations were also measured by the Electron Microprobe analysis (EMP). Our aims are to constrain seawater Pb sourcing in the Pacific sector of Southern Ocean (SO) and reconstruct the ACC evolution from a new perspective.

3.2 Sample and methods

3.2.1 Sample

The Fe-Mn crust PS75/247-2 (69° 8.53' S, 123° 13.13' W; approximate water depth 1504-1708 m) was dregded from the Marie Byrd Seamount during expedition PS75 from January to March 2010 on board the German research vessel RV Polarstern (sample location is shown in Figure 5.5). The Fe and Mn compositions in this crust show typical hydrogenous growth (Figure 5.2). A 50 mm long and 20 mm wide slab was sub-sampled and polished for further microprobe and LA-MC-ICPMS measurement. The methodological approach is detailed in Chapter 2.6.

3.2.2 Age model

The age model for the crust is based on $^{10}Be/^{9}Be$ and high-resolution cobalt (Co) flux methods. The average crust growth rates and age–depth relationships were determined directly for the last about 10 Myr using $^{10}Be/^{9}Be$ profiles. Due to the half-life for ^{10}Be of 1.5 Myr, the ^{10}Be at ages greater than 10–12 Ma is no detectable, and the ages prior to 10–12 Ma have to be estimated based on the Co-flux model (Manheim 1986, Frank et al. 1999). The samples for ^{10}Be and ^{9}Be analysis were manually drilled from 10 different depths in the Fe-Mn crust section. The samples were then dissolved in 6

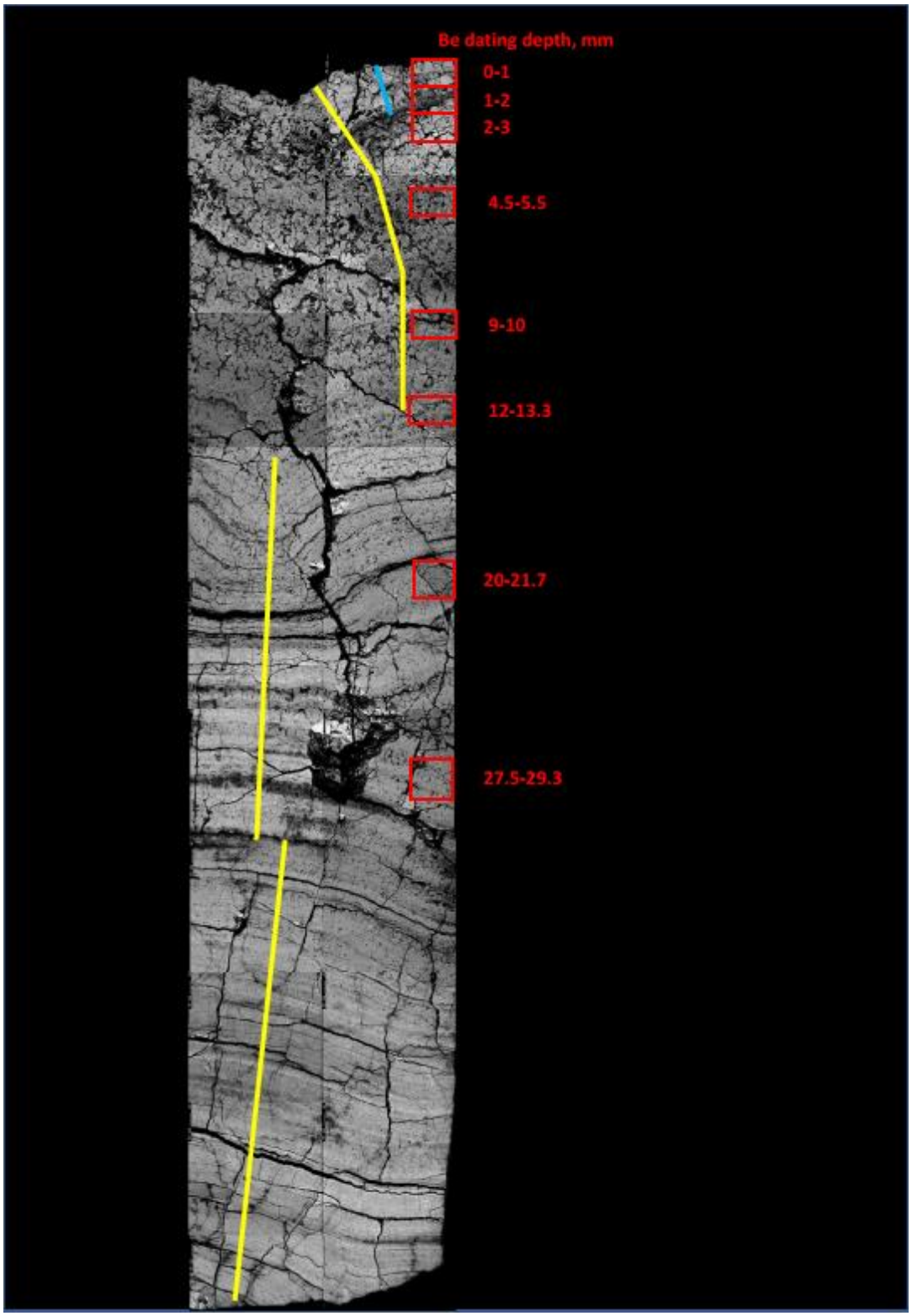

Figure 5.1 Backscatter Electron (BSE) image of the analysed Fe-Mn crust PS75/247-2. The locations of the laser ablation (LA) analyses are indicated by coloured lines (yellow lines indicate 50 microns LA tracks and blue line indicates 15 microns LA track). The red squares indicate the $^{10}Be/^{9}Be$ dating depths.

M HCl and split into two aliquots for separate ^{10}Be and ^{9}Be measurements. The ^{9}Be concentration was determined using the AGILENT 7500cs ICP-MS at the Institute of Geosciences, Christian Albrechts University of Kiel, Germany following standard procedures (Garbe-Schönberg 1993). The 1σ uncertainties of the ^{9}Be measurements are 5%. The ^{10}Be concentration in the second aliquot was measured using an isotope dilution method. After adding a known amount of ^{9}Be carrier in the weighed sample aliquot, the sample solution was purified for Accelerator Mass Spectrometry (AMS) analysis according to an established method (Henken-Mellies et al. 1990, Frank et al. 1994). The ^{10}Be concentrations were measured at the AMS Tandy facility at ETH Zürich, Switzerland. The repeatedly measured ^{10}Be/^{9}Be ratios of standards were normalized to the internal AMS standard S555N with a nominal ^{10}Be/^{9}Be ratio of 87.1×10^{-12} (Christl et al. 2013). The given statistical 1σ uncertainties include counting statistics and reproducibility of repeated measurements. The results are shown in Figure 5.3 and Table 5.1.

The microprobe measurement for Fe, Mn, Co and BSE images was carried out at GEOMAR Kiel, Germany, using a JEOL JXA 8200 "Superprobe" (Detailed in Chapter 2.8). The Co-flux data was calculated by following equation modified from previous studies (Manheim 1986, Frank et al. 1999):

$$\text{Growth rate (mm/Ma)} = \frac{0.31}{(\text{Co}_{\text{Intensity}}/142)^{2.5}}$$

$\text{Co}_{\text{intensity}}$ is the average measured Co signal intensity of ten data points which are in parallel with the laser track (Figure 5.1). The results are shown in Figure 5.3 and Table 5.2.

3.2.3 ε_{Nd} measurement

Approximately 30 mg of Fe-Mn oxyhydroxide powder was sampled from the Fe-Mn crust at depths of 0.5 mm (0.29 Ma) and 44 mm (18 Ma). The samples were then dissolved 6 M HCl and refluxed on the hotplate for 6 hours. The Nd in the solution

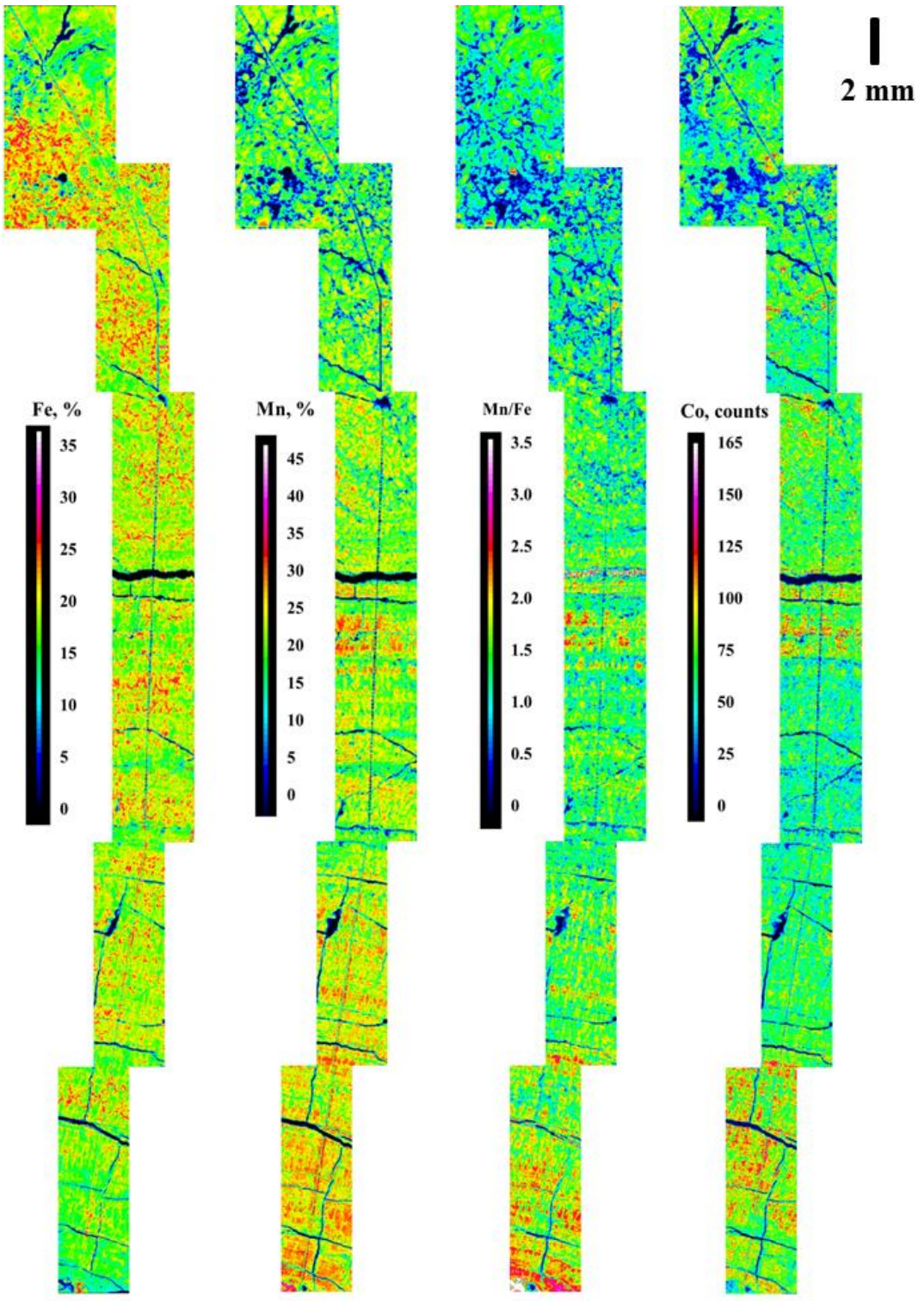

Figure 5.2 Fe and Mn concentrations, Co intensity (shown as counts per dwell time (20ms)) and Fe/Mn ratio maps of Fe-Mn crust PS75/247-2 acquired by EMP. The maps were chosen to match the laser ablation tracks. The instrumental parameters are decribed in the Chapter 2.8.

was purified by ion exchange chromatography (detailed in Chapter 2.4.3) and the ε_{Nd} value was determined by MC-ICP-MS on a Thermo Scientific Neptune Plus at GEOMAR Kiel (detailed in Chapter 2.5.2). The $\varepsilon_{Nd(T)}$ values were calculated using $^{147}Sm/^{144}Nd = 0.115$ which was taken from a nearby Fe-Mn crust DR153 (Frank et al. 2002). The results are listed in the Appendix Table 17.

5.2.4 Pb isotopic compositions analysed by LA-MC-ICPMS

Pb isotopic composition analysis was carried out using a Teledyne CETAC Analyte Excite Excimer Laser Ablation System coupled with a Thermo Scientific Neptune Plus MC-ICP-MS at GEOMAR, Kiel, Germany. The instrumental parameters and data reduction method are detailed in Chapter 2.7 and 2.8.

5.3 Results

5.3.1 Age model of the Crust PS75/247-2

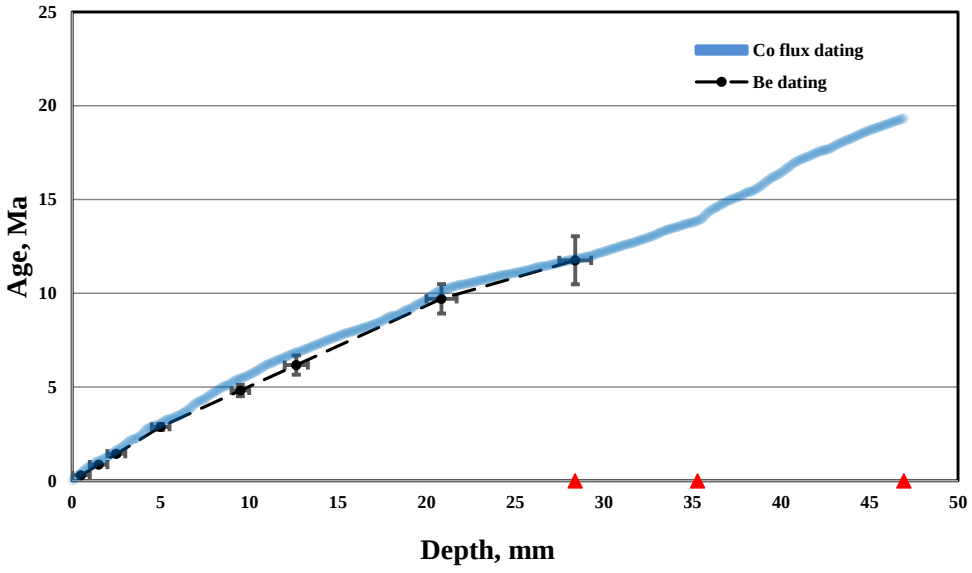

Figure 5.3 Calculated ages versus sample depth of Fe-Mn crust PS75/247-2. The $^{10}Be/^{9}Be$ dated ages were calculated with a half-life for ^{10}Be of 1.5 Myr by assuming a constant initial $^{10}Be/^{9}Be$ ratio. The growth rates and ages beyond the age range covered by $^{10}Be/^{9}Be$ dating have been calculated using a constant Co-growth rate relationship (Manheim 1986) which was calibrated to match the $^{10}Be/^{9}Be$ dating of the younger part. The dashed lines represent the Be-derived age model. The blue line shows the Co-flux derived age model. The red triangles indicate the tie points for calculating Co-flux derived growth rates.

The measured ^{9}Be and ^{10}Be concentrations, ^{10}Be/^{9}Be ratios and dated ages are listed in Table 5.1. The surface ^{10}Be/^{9}Be ratio of 0.7×10^{-8} is very close to the surface ^{10}Be/^{9}Be ratios in the Fe-Mn nodules ($0.9\text{-}1.3 \times 10^{-8}$) (Inoue et al. 1983) and crusts ($0.8\text{-}1.2\times 10^{-8}$) (van de Flierdt et al. 2004) in the Pacific Ocean. The growth rates calculated based on ^{10}Be/^{9}Be dated age and Co-flux model are presented in Table 5.2 and Figure 5.3. The ^{10}Be/^{9}Be results show three different growth rates in the top 28.4 mm of the crust and no ^{10}Be was detected below 28.5 mm depth. The top four sections and following three sections show identical growth rates of 1.74 and 2.32 mm/Ma. The growth rate then increased to 3.68 mm/Ma in the last section to 28.4 mm. Below 28.4 mm, the growth rates are estimated via the Co-flux model. As shown in Figure 5.3, the Co flux age model is calculated with an average value of the two sections with similar Co growth pattern constrained by tie points instead of using high resolution record in each 30 microns. The fast growth rate of 3.6 mm/Ma between 28.4 and 35.3 mm is also certified by Co-flux data. From 35.3 mm to the bottom of the sections, growth rate decreased to 2 mm/Ma. The ^{10}Be/^{9}Be and Co-flux derived growth rates showed similar covariation, especially at 5 mm and 20.85 mm where both showed changes into faster growth rates, indicating that the age model is robust.

Table 5.1 Be concentrations and ^{10}Be/^{9}Be-based ages for Fe-Mn crust PS75/247-2

Depth Interval (mm)	^{10}Be ([atoms/g]*10^{-7}), ±1 SE	^{9}Be, ppm	^{10}Be/^{9}Be (*10^{-7}), ± 1 SE	Age (Ma) ±SE
0-1.0	1924.27 ± 38.83	4.517	0.7074 ± 0.038	0.29 ± 0.02
1-2	1739.00 ± 35.12	5.044	0.5725 ± 0.031	0.86 ± 0.05
2-3	1191.46 ± 24.14	4.663	0.4243 ± 0.023	1.44 ± 0.08
4.5-5.5	705.38 ± 14.42	5.825	0.2011 ± 0.011	2.87 ± 0.16
9-10	375.72 ± 14.24	7.746	0.0805 ± 0.005	4.81 ± 0.30
12-13.3	128.73 ± 8.50	5.829	0.0367 ± 0.003	6.17 ± 0.51
20-21.7	26.64 ± 1.70	6.764	0.0065 ± 0.001	9.70 ± 0.79
27.5-29.3	10.72 ± 1.04	7.528	0.0024 ± 0.000	11.75 ± 1.28

Table 5.2 Incremental growth rates of Fe-Mn crust PS75/247-2. The growth rates were calculated directly by using the depth dividing the age. The depths of the Be dating ages are taken from the median of the depth interval in Table 5.1 and the depths for the Co-flux model are taken from the tie points in the Figure 5.3

Depth Interval (mm)	Growth Rate, mm/Ma	Comments
0-0.5	1.72	Derived from $^{10}Be/^{9}Be$ data
0.5-1.5	1.75	Derived from $^{10}Be/^{9}Be$ data
1.5-2.5	1.72	Derived from $^{10}Be/^{9}Be$ data
2.5-5	1.75	Derived from $^{10}Be/^{9}Be$ data
5-9.5	2.32	Derived from $^{10}Be/^{9}Be$ data
9.5-12.65	2.32	Derived from $^{10}Be/^{9}Be$ data
12.65-20.85	2.32	Derived from $^{10}Be/^{9}Be$ data
20.85-28.4	3.68	Derived from $^{10}Be/^{9}Be$ data
28.4-35.3	3.60	Derived from Co-flux model
35.3-46.95	2.00	Derived from Co-flux model

5.3.2 Standard material Pb isotope precision and accuracy using linear regression normalization

As shown in Figure 5.4, the $^{206}Pb/^{204}Pb$ ratios of standards NIST610, NOD-A-1 and NOD-P-1 normalized with the linear regression method agree with the literature data (Baker et al. 2004) throughout the analytical sequences. No significant Pb isotopic drift was found among these three standards during entire the LA-MC-ICPMS measurements (n=230). Two hundred-thirty repeat analyses of these three standards over several analytical sessions yielded the following ratios and uncertainties: $^{206}Pb/^{204}Pb$ = 17.053 ± 0.020 and $^{208}Pb/^{206}Pb$ = 2.169 ± 0.001 for NIST610, $^{206}Pb/^{204}Pb$ = 18.953 ± 0.040 and $^{208}Pb/^{206}Pb$ = 2.054 ± 0.003 for NOD-A and $^{206}Pb/^{204}Pb$ = 18.710 ± 0.124 and $^{208}Pb/^{206}Pb$ = 2.070 ± 0.005 for NOD-P (all uncertainties are quoted as 2 SD). Clearly, the good agreement between the double spike solution data (Baker et al. 2004) and the LA-MC-ICPMS data for three different standards show that our measurements were reliable. More outliers were found in NOD standards than in the NIST610 glass due tothe inhomogeneous NOD standard

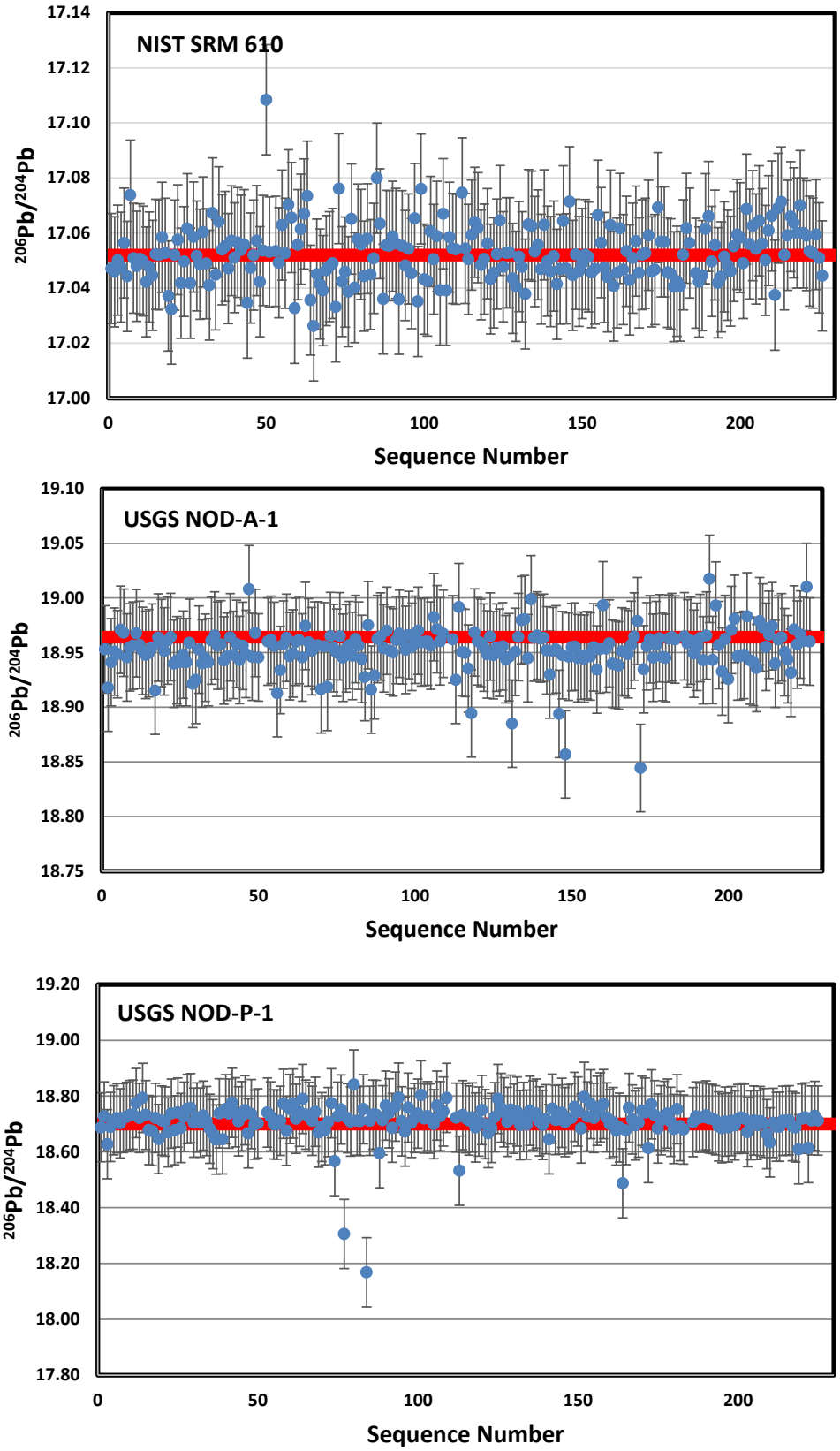

Figure 5.4 $^{206}Pb/^{204}Pb$ ratios of standard NIST610, NOD-A and NOD-P normalized by linear regression normalizing method during the LA-MC-ICPMS measurements. The red lines in each figure indicate the literature value (Baker et al. 2004).

pellet compositions. We found that the matrix had a negligible effect on the Pb isotope analysis by LA-MC-ICPMS. However, the signal intensity and Hg interference largely controlled the measurement accuracy and precision, and high Pb isotope signal intensities alongside low Hg interferences resulted in highest precision measurements. For instance, although the two NOD standards consisted of similar materials, measured Pb isotope data in NOD-A-1 showed smaller standard deviation than in NOD-P-1 because of higher Pb concentration and lower Hg concentrations in NOD-A-1 pellet than NOD-P-1. The sample has very similar Pb and Hg concentrations with NIST610 glass so we use NIST610 as the principal standard to evaluate the measurement precision (2SD = ± 0.020 in $^{206}Pb/^{204}Pb$ and 2SD = ± 0.001 in $^{208}Pb/^{206}Pb$), and NOD-A-1 / NOD-P-1 as secondary standards.

5.3.3 Pb and Nd isotope data

High-resolution past seawater laser ablation-derived Pb isotopic records in crust PS75/247-2 for the past 19 Ma were determined in 930 sampled depths at 50 micron resolution. As shown in Figure 5.5b, $^{206}Pb/^{204}Pb$ and $^{208}Pb/^{206}Pb$ show a smooth yet very variable evolution. The $^{206}Pb/^{204}Pb$ and $^{208}Pb/^{206}Pb$ ratios in PS75/247-2 (water depth: 1504-1708 m) are identical to previously reported Pb isotopic compositions in nearby but deeper Fe-Mn crust DR153 (water depth: 3300-3150 m) (Frank et al. 2002) over the past 5 Ma. Before 5 Ma, seawater Pb isotope signatures were decoupled in these two Fe-Mn crusts with the Pb isotope signal in DR153 shifted to the modern RSBW signature and where the Pb isotope composition in PS75/247-2 changed to the modern S. Pacific signature. The most noticeable feature in the PS75/247-2 Pb record is that the $^{206}Pb/^{204}Pb$ ratio increased to a plateau at about 18.90 and $^{208}Pb/^{206}Pb$ dropped to about 2.061 during the same period between 10 and 12 Ma. At 12 Ma, $^{206}Pb/^{204}Pb$ quickly decreased to another plateau at $^{206}Pb/^{204}Pb$=18.84 until 14 Ma and then, from 16 Ma to 17.5 Ma, gradully declined to 18.75 and remained constant to 19 Ma. Similar to $^{206}Pb/^{204}Pb$, $^{208}Pb/^{206}Pb$ gradually rose from 2.061 to 2.066 from 12 to 19 Ma. Similar to Pb, the topmost ε_{Nd} of PS75/247-2 (at 0.29 Ma) and ε_{Nd} in DR153

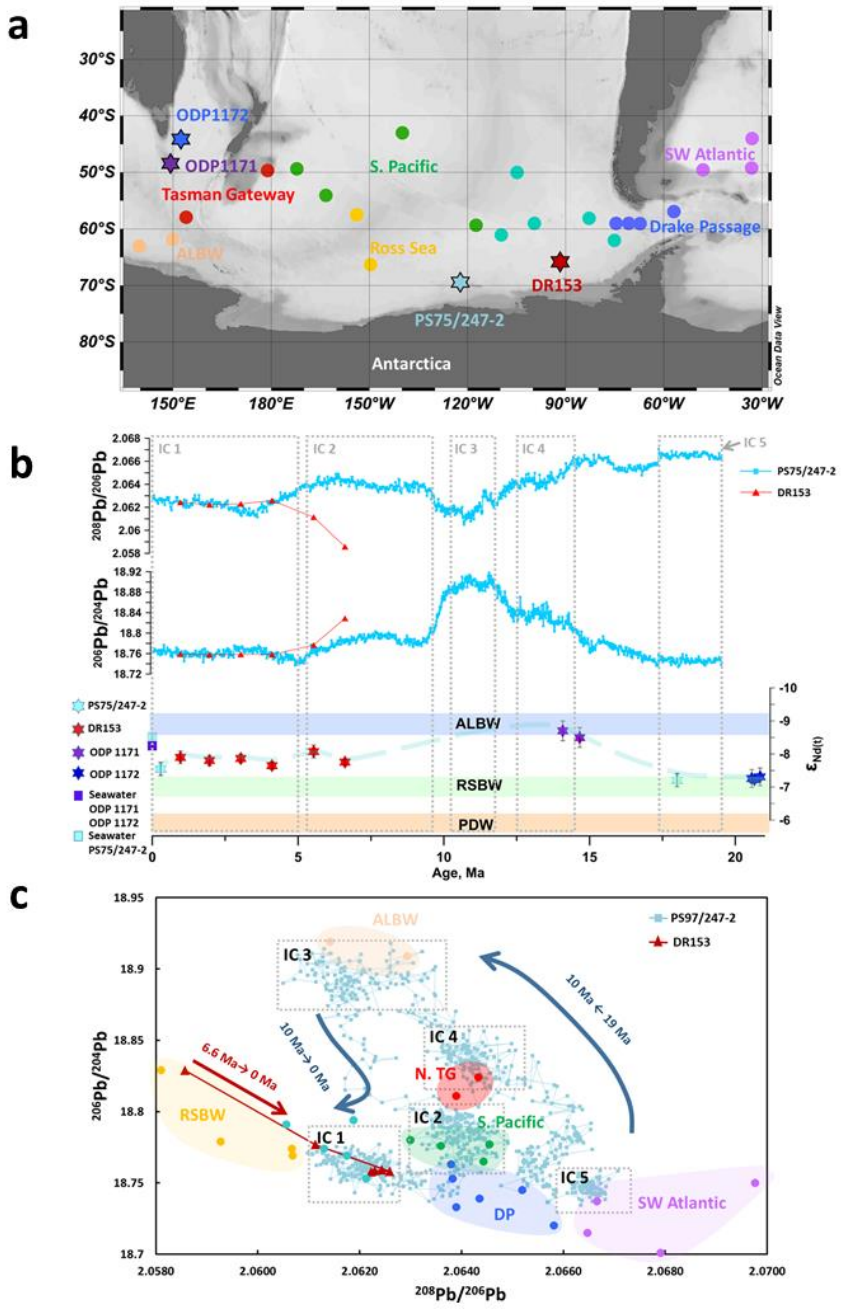

Figure 5.5 Compilation of seawater Pb and Nd isotope records in the Pacific sector of Southern Ocean for the past 19 Ma. Locations of Fe-Mn crusts (PS75/247-2 (water depth: 1504-1708 m) and DR153 (water depth: 3300-3150 m)), sediment cores (ODP Site 1172 (water depth: 2620 m) and ODP Site 1171 (water depth: 2150 m)) and Fe-Mn nodules used in this study. b, comparison of Pb isotope records in Fe-Mn crusts (PS75/247-2 and DR153) and Nd isotope records in the Pacific sector of SO. The colour bars of ε_{Nd} indicate present-day seawater signatures of ALBW (Lambelet et al. 2016), RSBW (Basak et al. 2015) and PDW (Molina-Kescher et al. 2014). The ε_{Nd} values of PS75/247-2 (this study) and DR153 (Frank et al. 2002) were derived from Fe-Mn crusts. The ε_{Nd} data of Site ODP 1172 were extracted from fossil fish teeth (Scher et al. 2015). The ε_{Nd} data of ODP Site 1171 were extracted from bulk sediments (Holbourn et al. 2013). The present-day seawater Nd isotope signature at Site ODP1171/Site ODP1172 (Lambelet et al. 2016) and PS75/247-2 (Rickli et al. 2014) are taken from a nearby stations. c, Seawater Pb isotopic evolution recorded in Fe-Mn crust PS75/247-2 and DR153 compared with Pb isotopic signatures in surface Fe-Mn nodules in $^{206}Pb/^{204}Pb$-$^{208}Pb/^{206}Pb$ spacing (Abouchami and Goldstein 1995). The regionally characteristic Pb isotopic signatures for various endmembers are marked by different colours. The blue and red arrows delineate the Pb isotopic evolution in PS75/247-2 and DR153, respectively. The dashed squares indicate the Pb Isotopic Cloud (IC) as also shown in b. PDW: Pacific Deep Water, RSBW: Ross Sea Bottom Water, ALBW: Adélie Land Bottom Water, S. Pacific: South Pacific, N. TG: Northern Tasman Gateway, DP: Drake Passage, SW Atlantic: Southwest Atlantic.

for the past 6.6 Ma (Frank et al. 2002) were also within error. However, the ε_{Nd} values at the topmost and bottom parts of PS75/247-2 are almost identical at about -7.4, while $^{208}Pb/^{206}Pb$ in the surface and bottom section of the same crust are very different (Figure 5.5b).

The top 1.5 mm of the Fe-Mn crust was also analysed with a 15 micron LA resolution setting and results are shown in Figure 5.6f and h. Its age model was slightly tuned to match the glacial and interglacial cycles with an overall growth rate of 1.6 mm/Ma, which is within error of the $^{10}Be/^{9}Be$-derived growth rate of 1.74 mm/Ma. During the past 1 Ma, both the $^{208}Pb/^{206}Pb$ and $^{206}Pb/^{204}Pb$ record show very pronounced glacial-interglacial variability. $^{206}Pb/^{204}Pb$ signals are more radiogenic (high) and $^{208}Pb/^{206}Pb$ ratios are lower in warm periods than in cold periods.

5.4 Discussion

5.4.1 ACC evolution in the Pacific sector of SO

One advantage of using the radiogenic Pb isotope system, compared with Nd isotopes, to reconstruct regional circulation changes is that Pb has three radiogenic isotopes (^{206}Pb, ^{207}Pb and ^{208}Pb), so we can use more than one isotopic ratio to accurately identify the origin of water masses. Pb isotope data are plotted in $^{206}Pb/^{204}Pb$-$^{208}Pb/^{206}Pb$ space to distinguish water mass provenance signals in crust PS75/247-2 (Figure 5.5c). The Pb isotope data in surface scrapings from Fe-Mn nodules from adjacent sites (Abouchami and Goldstein 1995) are also presented to characterise the Pb isotope signature endmembers of Adélie Land Bottom Water (ALBW), TG, DP, South Pacific (S. Pacific), Southwest Atlantic (SW Atlantic) and RSBW. As a benefit of the unprecedented high-resolution approach, the Pb isotope data covering the past 19 Ma of PS75/247-2 in $^{206}Pb/^{204}Pb$-$^{208}Pb/^{206}Pb$ spacing define five major evolution clouds and I denote these as Pb Isotopic Clouds (IC) 1 to 5 from young to old.

Continental weathering and ocean circulation changes are both potential candidates

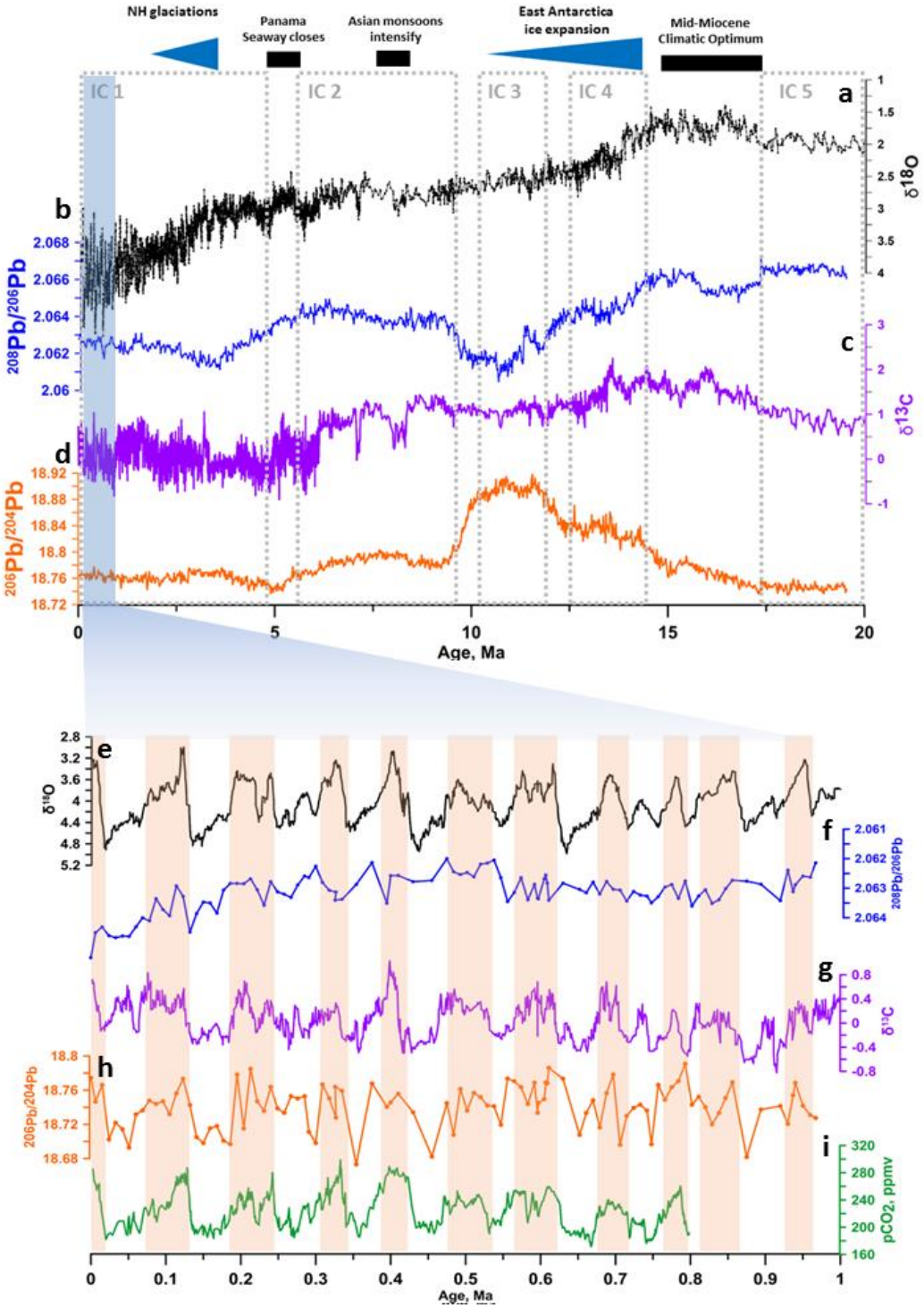

Figure 5.6 Compilation of global palaeoclimatic reconstructions and Pb isotope record in PS97/247-2 over the past 20 Ma. (a) and (e) are global deep-sea oxygen records (Zachos et al. 2001); (b), (d), (f) and (h) are Pb isotope records in PS97/247-2; (c) and (g) are global deep-sea carbon isotope records (Zachos et al. 2001); (i) Atmospheric CO_2 concentrations from Antarctic ice core (Lüthi et al. 2008). The timing of climatic and tectonic events are taken from previous study (Zachos et al. 2001). The dashed squares indicate the timing of the Pb Isotopic Clouds (ICs). The orange shades indicate the warm periods.

for shifting the Pb isotope signals from one to another cloud as suggested previously (Christensen et al. 1997, Frank 2002). Continental weathering can release Pb incongruently to the ocean during early chemical weathering which may lead to a more radiogenic Pb isotopic runoff signal (Foster and Vance 2006, Gutjahr et al. 2009, Wilson et al. 2015). This is because, in the newly-produced or freshly exposed soils and rocks generated by continental ice sheet advance and retreat, uranium- and thorium-enriched accessory mineral phases preferentially release a significantly more radiogenic Pb isotope signal than the bulk rock during early chemical weathering. This incongruent weathering Pb signal was also found along the permanent Antarctic ice cover development during the Eocene–Oligocene transition (Basak and Martin 2013). However, universal occurrence of incongruent weathering is still not quantified, as the lab-based and natural case studies in the Swiss Alps were not observed such a mechanism (Dausmann et al. 2019, Süfke et al. 2019).

Between 12.5 and 14 Ma, the Antarctic ice sheet expanded substantially as recorded by benthic oxygen isotope compositions (Figure 5.6a) while $^{206}Pb/^{204}Pb$ was invariant (Figure 5.6d). Moreover, the major $^{206}Pb/^{204}Pb$ increase between IC3 and IC4 and very large $^{206}Pb/^{204}Pb$ decrease between IC2 and IC3 (Figure 5.6d) have no corresponding Antarctic ice sheet advance and retreat events recorded by the benthic oxygen isotope record (Figure 5.6a). This lack of covariation suggests that the Pb isotopic variability was unlikely controlled by the continental incongruent Pb weathering, even though the location of PS75/247-2 is located close to the Antarctic continent. As shown in Figure5.5a and c, overall the Pb isotope signals are very variable shifting between modern SW Atlantic, South Pacific, RSBW and ALBW throughout the record. Ocean circulation changes would be capable to transfer Pb isotope signatures from different water mass endmembers to the sample sites. Therefore, I suggest that the Pb isotopic shifts were driven by larger-scale ocean circulation reorganization events and each isotopic cloud corresponds to a relatively stable ocean circulation regime.

A Proto-Ross Gyre circulation with an anti-clockwise (from east to west) circulation along the Antarctic coast in the Pacific sector of SO with seawater flowing from the DP to PS75/247-2 and then to Site ODP 1172 was suggested to have prevailed between 49 and 37 Ma (Bijl et al. 2010). The surface water of this current was found to be redirected eastwards through the DP at about 41 Ma (Scher and Martin 2006) but the timing of deep water redirection is not clear yet due to the lack of sediment in the DP (Pfuhl and McCave 2005). Because of the short residence time of Pb in the ocean (Schaule and Patterson 1981, Cochran et al. 1990, Henderson and Maier-Reimer 2002), the seawater Pb isotope signature of different water masses in the studied area is dominated by regional or local signals and should be relatively constant according to the nearby continental sources during the past 20 Ma. Comparison of Pb IC5 and SW Atlantic Pb isotope signatures indicates that deep water at about 1500 meter was still flowing in an anti-clockwise direction from the DP to PS75/247-2 during 19 Ma and 17 Ma (Figure 5.5c) in the southern reaches of the Pacific sector of the SO. In addition, the $\varepsilon_{Nd(t)}$ in crust PS75/247-2 at 18 Ma and in ODP Site 1172 at about 20 Ma was also identical (Figure 5.5b). Both Pb and Nd isotope records demonstrate that the anti-clockwise deep Proto-Ross Gyre current lasted until 17 Ma, which was possibly caused by the remnant volcanic arc barrier in the DP in the mid-Miocene (Dalziel et al. 2013).

The most striking $^{206}Pb/^{204}Pb$ and $^{208}Pb/^{206}Pb$ isotopic changes in PS75/247-2 is found in the interval between 14 and 10 Ma which was marked by IC4 (12-14 Ma) and IC3 (10-12 Ma). The Pb isotopic signature of IC4 was consistent with Pb isotope data in the deep Northern Tasman Gateway (N. TG), which is Lower Circumpolar Deep Water (LCDW) Pb signature, and the following IC3 was almost identical to the Adélie Land Bottom Water (ALBW) Pb isotope signature (Figure 5.5c), indicating the onset of ALBW and a clockwise deep ACC ran from TG to DP between 14 and 10 Ma. The initialization of ALBW formation at 14 Ma was also documented in a Nd isotope record, as ε_{Nd} at Site ODP 1171 changed to -8.7 (Holbourn et al. 2013), which corresponds to the ALBW Nd isotope signature (Lambelet et al. 2018) of -7.3 at

nearby Site ODP 1172 (Scher et al. 2015) (Figure 5.5b). Interestingly, in the modern ACC circulation mode, an ALBW signal cannot be directly delivered to PS75/247-2 because Ross Sea Bottom Water (RSBW) occupies the deep ocean of the Pacific sector of the SO today. However, between 14 and 10 Ma, the Pb isotope signal in PS75/247-2 appears to have recorded an ALBW signal and an even almost pure ALBW Pb signature range from 12 to 10 Ma, suggesting that RSBW was not yet active or as extensive before 10 Ma.

The RSBW Pb isotope signature was first recorded in Fe-Mn crust DR153 at 6.6 Ma, while the coeval Pb isotope record (IC2) of PS75/247-2 was showing a very different signal characteristic for modern S. Pacific Pb signatures (Figure 5.5c). Due to the different water depths of DR153 (3300-3150m) and PS75/247-2 (1504-1734m), the decoupling of the respective Pb isotope signals might be caused by increased stratification due to the previously suggested reduced upwelling in the SO (Marlow et al. 2000). Given that the seawater Pb isotope signal reflects the entire water column change, even if the ocean was more stratified the Pb signal in the deeper DR153 should also show an influence of the Pb signal seen in crust PS75/247-2. However, the Pb signal in these two locations is strikingly different indicating that ocean stratification is not the reason for the Pb decoupling. Another explanation is that the SO front in the Ross Sea section during this time may have been shifted towards the Antarctic continental margin and the SO front in the Bellingshausen See was more equatorial-wards extended compared with today. For example, RSBW might have circulated along the Antarctic continent with more expanded Pacific Deep Water (PDW) invading into the SO at the location of PS75/247-2 thus showing modern S. Pacific Pb signatures, while the RSBW could still reach site DR153 before passing the DP. The shift from Pb IC3 to IC2 appears to trace the vanishing of an ALBW signal at the location of PS75/247-2. Since the RSBW Pb isotope signature was documented in DR153 at 6.6 Ma, the formation of RSBW might have replaced the ALBW signal as seen in the modern ACC circulation. On the other hand, we can also speculate that the timing of Pb IC3 shifted to IC2 at 10 Ma is the timing of the onset of RSBW

formation.

Throughout the past 5 Ma, the Pb isotope record in PS75/247-2 varied within IC1. In the modern ACC circulation system, LCDW contains contributions of PDW and Antarctic Bottom Water (AABW) derived from the Ross Sea, flowing past sample locations of PS75/247-2 and DR153 and eventually through the DP, so the Pb IC1 sits in the mixing envelope of the RSBW and S. Pacific Pb signatures (in Figure 5.5c). Compared with IC2, IC1 is clearly closer to the RSBW Pb signature indicating stronger contribution of AABW from the Ross Sea and more equatorial-wards extended SO front. Moreover, the 15-micron LA Pb isotope data show high $^{206}Pb/^{204}Pb$ and low $^{208}Pb/^{206}Pb$ during interglacials and low $^{206}Pb/^{204}Pb$ and high $^{208}Pb/^{206}Pb$ in glacial periods for the past 1 Ma (Figure 5.6h and f). Although the PS75/247-2 is located at the water depth between 1504-1734m, it is still situated within the modern LCDW, so the glacial/interglacial Pb isotopic variability indicates southwards shifted SO fronts, stronger AABW export from Ross Sea and more vigorous Southern Ocean overturning circulation during warmer times and northward shifted SO fronts, reduced AABW export and likely sluggish circulation in the colder times as found in Chapter 4 for the last two glacial terminations in the Atlantic sector of the SO. Since similar Pb isotopic trends were recorded in PS75/247-2 within the IC1 range for the past 5 Ma than seen in chapter 4, we could deduce this glacial-interglacial circulation variation is the main rhythm in the Pacific sector of the Southern Ocean.

4.4.2 Climatic and tectonic implications

The deep sea $\delta^{18}O$ record delineates a global warm period during the Miocene, which peaked in the Middle Miocene Climatic Optimum (MMCO) (17-14 Ma) (Zachos et al. 2001). The ACC transition from a westward to eastward flow direction during the MMCO should lead to an interrupted and chaotic circulation scenario in the Pacific sector of Southern Ocean which could cause more poleward heat transport from low latitudes and result in enhanced ice melting in Antarctica. As seen in Figure 5.5c and

5.6, the MMCO coincided with the transition towards clockwise modern ACC circulation between IC5 and IC4 in the Pacific sector of the Southern Ocean also from 17 to 14 Ma. Establishment of the ACC is widely believed to have been a key factor in the history of Antarctic glaciation, and a full depth ACC circulation leads to Antarctic Ice Sheet expansion by preventing heat transport from low latitudes (Kennett 1977, Zachos et al. 2001, Barker and Thomas 2004). The East Antarctic Ice Sheet expansion events (14-12 Ma) (Vincent et al. 1985, Flower and Kennett 1995) was documented in deep sea oxygen isotope records (Figure 5.6a), which coincided with the timing of onset of a full depth clockwise ACC circulation regime at 14 Ma as indicated by the Fe-Mn crust Pb isotope record. The covariation of ACC establishment and global climatic cooling likely suggests a link between ACC evolution, intensification of Antarctic glaciations and global climate change in the middle Miocene.

Tectonic development of gateway regions or onset/intensification of AABW formation might lead to the large-scale reorganization of ocean circulation regimes recorded in a seawater Pb isotope record. For example, IC 4 and IC 3 were related to deepening of the DP and ALBW formation, and the shift from IC3 to IC2 is likely caused by RSBW initialization at about 10 Ma. In addition, the timing of closure of the Panama Seaway at 4.6 Ma, which led to a marked reorganization of global ocean circulation (Haug and Tiedemann 1998), matches with the timing of transition between IC1 and IC2. Other tectonic events in the DP (Dalziel et al. 2013) or in other places, i.e. Tethyan Sea (von der Heydt and Dijkstra 2006), may theoretically also have played a role for IC shifting during 12 and 19 Ma. However, it is still possible that one IC source signature in $^{206}Pb/^{204}Pb$ -$^{208}Pb/^{206}Pb$ diagram (Figure 5.5c) is made up by two or more ICs with indistinguishable Pb isotopic variations. For instance, a major change in $^{208}Pb/^{206}Pb$ and negligible variations in $^{206}Pb/^{204}Pb$ are observed at about 3 Ma together with a deep-sea $\delta^{18}O$ increase due to Northern Hemisphere (NH) glaciation, which was caused by a fundamentally altered deep ocean circulation (Shackleton and Opdyke 1977, Raymo et al. 1992, Ruddiman et al. 2017), but the Pb

isotopic difference in $^{206}Pb/^{204}Pb$-$^{208}Pb/^{206}Pb$ spacing is not resolvable during this interval.

5.5 Conclusions

A high-resolution seawater Pb isotope record was recovered from a Fe-Mn crust in the Pacific sector of Southern Ocean using the LA-MC-ICPMS technique to reconstruct the late Cenozoic ACC evolution. Our data demonstrate that the modern deep eastward-directed ACC most likely formed at 14 Ma. The Fe-Mn crust Pb isotope records also suggest five large-scale circulation reorganization senarios during the past 19 million years. The evolution of the Pb isotopic trends between the TG and DP documents water flowing from DP to the crust sampling site before 17 Ma. Due to the progressive enlargement and deepening of the DP, deep water could pass the DP and gradually a full depth ACC was established at 14 Ma. The transition from a westward to eastward directed ACC circulation regime in the Pacific sector of Southern Ocean may have led to unstable ACC circulation stages and coincided the East Antarctic Ice Sheet melting during MMCO. After modern ACC formation at 14 Ma, the poleward heat transport was reduced, leading to East Antarctic Ice Sheet expansion until 10 Ma. The Pb isotope records in DR153 and PS97/247-2 suggest that the RSBW initiated, but the SO overturning front in the Ross Sea area was likely more pulled back towards the Antarctic continent compared to today. The equatorial-wards expansion of SO overturning front started at about 5 Ma as more RSBW Pb isotope signals recorded in PS97/247-2, and this vigorous Southern Ocean overturning circulation regime continues until today. During the Pleistocene, glacial-interglacial Pb isotopic cycles observed in PS97/247-2 coincident with the atmospheric CO_2 and deep sea oxygen and carbon isotope records, indicating the circulation in Pacific sector of SO in this period was controlled by Milankovitch cycles forcing.

Acknowledgement

I thank Jutta Heinze for the $^{10}Be/^{9}Be$ dating work and also thank Mario Thöner and Jan Fietzke for microprobe analysis. Huang Huang acknowledges the China Scholarship Council (CSC) for providing financial support to his overseas study. Dieter Garbe-Schönberg at the University of Kiel analysed the ^{9}Be fraction, while Marcus Christl at ETH Zürich analysed the ^{10}Be concentrations. Jan Fietzke and Tyler Goepfert were vital for carrying out the LA-ICP-MS analyses.

6. General conclusions and outlook

6.1 Summary

The different timescale Pb and Nd isotope records have been carried out to reconstruct circulation changes in the Southern Ocean starting with the present-day Pb and Nd isotope distribution in the Atlantic sector of Southern Ocean (Chapter 3), moving on to resolve glacial-interglacial variations during the past two glacial terminations (Chapter 4) and then providing an extended insight into ACC circulation modes over the past 19 Ma (Chapter 5).

Chapter 3 aimed to present results of a series of experiments carried out to establish a refined reliable leaching method to extract hydrogenetic Pb and Nd in the Southern Ocean sediments for paleoceanographic purposes. The detailed leaching method is discussed and modified step by step. The approach is applied to Southern Ocean sediments which contained substantial quantities of immature chemically weathered continental detritus. The questionable $MgCl_2$ wash step was found to be unnessary and potentially harmful, and the use of EDTA was confirmed for its effective anti-readsorption effect. The sequential leaching experiments demonstrated that 10 seconds vortexing leaching is the best approach to extract hydrogenetic Pb and Nd from Southern Ocean sediments. Based on the results, it is recommended to leach previously untreated bulk sediments directly with vortexing leaching method with EDTA as chelating ligand. Moreover, for the first time, it could be confirmed that the extracted hydrogenetic Pb isotope signal by vortexing leaching method indeed reflects a porewater Pb isotope signature by comparing the isotopic compostions in the sediment leachates and corresponding porewater as well as overlying seawater at three stations in front of Ronne-Filchner Ice Shelf. Last but not least, the Pb and Nd isotope distributions in the Atlantic sector of Southern Ocean were studied with 70 coretop sediments. The results show that (a) the presence of preformed ferromanganese oxyhydroxides overprinted the authigenic Pb and Nd signal in several sediment samples near the Antarctic continent and (b) presence of volcanic materials

altered the hydrogenentic Nd signature in some samples, but did not significantly influence the Pb isotope signature in marine sediments.

In Chapter 4, using the vortexing leaching method and suggested core sites suitable for paleoceangraphic study in Chapter 3, we present seawater-derived downcore sedimentary Nd and Pb isotope records from three Southern Ocean sites inside and outside the Weddell Sea to reconstruct changes in Southern Ocean overturning circulation for the past two glacial terminations. While no study to date could unambiguously indicate whether Weddell Sea-derived AABW was the source of glacial Southern Source Water filling significant parts of the glacial abyssal ocean basins, our data provide strong evidence for the absence of Weddell Sea AABW during the last and penultimate glacial maximum in the Atlantic sector of the Southern Ocean. Furthermore, the deep sea Pb isotope records recovered during these intervals suggest great potential to document the water mass change in the entire overlying water column. The combination of investigating deep sea Pb and Nd isotope records provides the potential to resolve both upper and lower Southern Ocean overturning circulation changes. The successive southward displacement of the Southern Ocean overturning cell in the early deglacial is recorded by increasing contributions of Weddell Sea-derived Pb admixtures to regions outside the Weddell Sea during both glacial terminations. The export of Weddell Sea-sourced AABW resumed later during glacial terminations and was documented by both deep sea Pb and Nd isotopes. Both the last two glacial terminations experienced the same deglacial physical ocean circulation change sequence beginning with a southward shifted Southern Ocean overturning cell and followed by onset of Weddell Sea-derived AABW export, each coinciding with major atmospheric CO_2 rise events. While Holocene AABW formation and export from the Weddell Sea took place without major perturbations, our new records lend strong support for a previously inferred overturning stagnation event during the peak Eemian interglacial. Overall our data suggest that Weddell Sea AABW export can be reduced or absent during both colder and warmer climates than current.

Chapter 5 aimed to resolve Southern Ocean circulation changes for late Pleistocene and late Cenozoic timescales. For this purpose, an unprecedented continuous high-resolution Pb isotope record was generated from a Fe-Mn crust dredged from the Marie Byrd Seamont in the Pacific sector of the Southern Ocean using a LA-MC-ICPMS approach. The Pb isotope results showed similar glacial-interglacial cyclicity as the sediment-based Pb isotope records in Chapter 4 for the past two glacial terminations, featuring this pattern until at least 1 Ma. Overall the Pb isotope data covered the ACC history for the past 19 million years and indicate an establishment of the modern clockwise and eastwards flowing ACC at 14 Ma. The evolution of Pb isotopes also shows five large-scale ocean circulation reorganization events which can be related to the establishment or intensification of Ross Sea Bottom Water formation and tectonic events in ocean gateway regions, i.e. Panama Seaway and Drake Passage.

In summary, the following conclusions can be drawn from this thesis:

1) Differences in Pb and Nd isotope proxies. The first difference is sedimentary seawater-derived Pb and Nd isotope signals are affected by different mechanisms. Both authigenic Pb and Nd signatures in the sediment core near continents can be overprinted by continental signals from pre-formed ferromanganese oxyhydroxides supplied by nearby rivers and ice-streams. The hydrogenetic Nd signal can also be altered by contributions released from volcanic materials (as shown in previous studies in Elmore et al. 2011 and Blaser et al. 2016) but this effect has negligible influence on hydrogenetic Pb isotope signals. The present-day Pb isotope signal extracted from coretope sediments is heavily overprinted by anthropogenic Pb from dust. However, anthropogenic Pb can only penetrate into the topmost centimetres in the sediment and have no negative effect for paloceanographic studies. The second difference is deep sea Pb and Nd isotope compositions record different parts of the water column. While deep sea Nd only reflect bottom water change, deep sea Pb can record the water mass change in the entire water column due to their different

chemistry behaviours in the seawater.

2) Southern Ocean circulation changes during glacial terminations. Via combination of deep sea Pb and Nd isotope records, we resolved the different timing of the southward shifting Southern Ocean overturning cell and onset of AABW export during the past two glacial-interglacial transitions. The southward shifting of this upwelling cell, most likely related to southward shifting westlies, always preceded onset of Weddell Sea-derived AABW export. The well-matched deglacial atmospheric CO_2 rise events and the changes in the Southern Ocean overturning circulation show that oceanic processes in Southern Ocean governed the atmospheric CO_2 variability to a large degree, as seen in earlier studies (Anderson et al. 2009, Skinner et al. 2010).

3) *Southern Ocean circulation reorganization events.* The LA Pb isotope data in the Fe-Mn crust PS75/247-2 exhibited five large-scale circulation reorganization events in the past 19 Ma. The seawater Pb isotopic trends resolve the Southern Ocean front shifting and Antarctic Bottom Water evolution from a new perspective. The timing at 14 Ma of establishment of modern clockwise and eastward flowing ACC in the Pacific sector of Southern Ocean is suggested by the Pb isotope record which agrees with a recent suggested timing of full opening of the Drake Passage (Dalziel et al. 2013).

6.2 Outlook

The radiogenic Pb and Nd isotope systems used in this thesis not only present novel insights in paleoceanographic reconstruction but also provide new suggestion for future work as below:

1) AABW formation and evolution in the Weddell Sea. In Chapter 4, we found evidence for the lack of Weddell Sea-derived AABW export during glacial times to the northeast of the Weddell Sea basin. However, it is still possible glacial Weddell Sea-sourced AABW escaped via the eastern part towards the Weddell-Enderby abyssal plain. To test this hypothesis, downcore seawater Nd and Pb isotope records from distal northeast sites within the Weddell-Enderby abyssal plain are needed.

Moreover, the Pb isotope data defined different Pb isotopic trends of Weddell Sea sourced waters in the Atlantic sector of the SO for the past two terminations, but the mechanism controlling this variation is not clear. Variability in AABW formation in the different area along the east and west of the Antarctic continental coast and different ice melting rates of the east and west Antarctic Ice Sheet could both potentially lead to different Pb isotope signature in Southern Ocean seawater further north, but which was the dominant effect?

2) *AABW formation and its evolution in the Ross Sea.* The Ross Sea is another important area for the generation of modern AABW but the AABW evolution in this part of the Antarctic margin is also poorly understood to date. The ε_{Nd} results suggest almost simultaneous AABW export timing in the Ross Sea and Weddell Sea (Figure 4.7g and h) during Termination I. Was this just a coincidence or is AABW formation and export in these two areas following the same underlying controls?

3) *Ocean circulation reorganization events.* In Chapter 5, the laser ablation Pb isotope records showed five major ocean circulation reorganization events during the past 19 Ma in the Pacific sector of the Southern Ocean. Are these global ocean circulation changes or just a local event? Furthermore, the mechanisms controlling these events are not clear. The tectonic evolution in gateway regions surely plays a key control. What about the initialisation of AABW export/formation? Which other controls may have amplified the respective paleo-circulation changes?

References

Abbott, A. N., B. A. Haley and J. McManus (2015). "Bottoms up: Sedimentary control of the deep North Pacific Ocean's εNd signature." Geology **43**(11): 1035-1035.

Abouchami, W. and S. L. Goldstein (1995). "A lead isotopic study of circum-antarctic manganese nodules." Geochimica et Cosmochimica Acta **59**(9): 1809-1820.

Abouchami, W., S. L. Goldstein, S. J. G. Gazer, A. Eisenhauer and A. Mangini (1997). "Secular changes of lead and neodymium in central Pacific seawater recorded by a Fe-Mn crust." Geochimica et Cosmochimica Acta **61**(18): 3957-3974.

Adkins, J. F. (2013). "The role of deep ocean circulation in setting glacial climates." Paleoceanography **28**(3): 539-561.

Adkins, J. F., K. McIntyre and D. P. Schrag (2002). "The salinity, temperature, and delta O-18 of the glacial deep ocean." Science **298** (5599): 1769-1773.

Anderson, R. F., S. Ali, L. I. Bradtmiller, S. H. H. Nielsen, M. Q. Fleisher, B. E. Anderson and L. H. Burckle (2009). "Wind-driven upwelling in the Southern Ocean and the deglacial rise in atmospheric CO_2." Science **323** (5920): 1443-1448.

Arsouze, T., J. C. Dutay, F. Lacan and C. Jeandel (2009). "Reconstructing the Nd oceanic cycle using a coupled dynamical – biogeochemical model." Biogeosciences **6**(12): 2829-2846.

Baker, J., D. Peate, T. Waight and C. Meyzen (2004). "Pb isotopic analysis of standards and samples using a 207Pb–204Pb double spike and thallium to correct for mass bias with a double-focusing MC-ICP-MS." Chemical Geology **211**(3): 275-303.

Barker, P. F. (2001). "Scotia Sea regional tectonic evolution: implications for mantle flow and palaeocirculation." Earth-Science Reviews **55**(1): 1-39.

Barker, P. F. and E. Thomas (2004). "Origin, signature and palaeoclimatic influence of the Antarctic Circumpolar Current." Earth-Science Reviews **66**(1): 143-162.

Basak, C., H. Fröllje, F. Lamy, R. Gersonde, V. Benz, R. F. Anderson, M. Molina-Kescher and K. Pahnke (2018). "Breakup of last glacial deep stratification in the South Pacific." Science **359**(6378): 900-904.

Basak, C. and E. E. Martin (2013). "Antarctic weathering and carbonate compensation at the Eocene–Oligocene transition." Nature Geoscience **6**: 121.

Basak, C., E. E. Martin and G. D. Kamenov (2011). "Seawater Pb isotopes extracted

from Cenozoic marine sediments." Chemical Geology **286**(3): 94-108.

Basak, C., K. Pahnke, M. Frank, F. Lamy and R. Gersonde (2015). "Neodymium isotopic characterization of Ross Sea Bottom Water and its advection through the southern South Pacific." Earth and Planetary Science Letters **419**: 211-221.

Bayon, G., C. R. German, K. W. Burton, R. W. Nesbitt and N. Rogers (2004). "Sedimentary Fe–Mn oxyhydroxides as paleoceanographic archives and the role of aeolian flux in regulating oceanic dissolved REE." Earth and Planetary Science Letters **224**(3): 477-492.

Berger, A. and M. F. Loutre (1991). "Insolation Values for the Climate of the Last 10000000 Years." Quaternary Science Reviews **10**(4): 297-317.

Bertram, C. J. and H. Elderfield (1993). "The geochemical balance of the rare earth elements and neodymium isotopes in the oceans." Geochimica et Cosmochimica Acta **57**(9): 1957-1986.

Bijl, P. K., A. J. P. Houben, S. Schouten, S. M. Bohaty, A. Sluijs, G.-J. Reichart, J. S. Sinninghe Damsté and H. Brinkhuis (2010). "Transient Middle Eocene Atmospheric CO_2 and Temperature Variations." Science **330**(6005): 819-821.

Blaser, P., J. Lippold, M. Gutjahr, N. Frank, J. M. Link and M. Frank (2016). "Extracting foraminiferal seawater Nd isotope signatures from bulk deep sea sediment by chemical leaching." Chemical Geology **439**: 189-204.

Blaser, P., F. Pöppelmeier, H. Schulz, M. Gutjahr, M. Frank, J. Lippold, H. Heinrich, J. M. Link, J. Hoffmann, S. Szidat and N. Frank (2019). "The resilience and sensitivity of Northeast Atlantic deep water εNd to overprinting by detrital fluxes over the past 30,000 years." Geochimica et Cosmochimica Acta **245**: 79-97.

Bollhöfer, A. and K. J. R. Rosman (2000). "Isotopic source signatures for atmospheric lead: the Southern Hemisphere." Geochimica et Cosmochimica Acta **64**(19): 3251-3262.

Bollhöfer, A. and K. J. R. Rosman (2002). "The temporal stability in lead isotopic signatures at selected sites in the Southern and Northern Hemispheres." Geochimica et Cosmochimica Acta **66**(8): 1375-1386.

Broecker, W. S. and G. M. Henderson (1998). "The sequence of events surrounding Termination II and their implications for the cause of glacial-interglacial CO2 changes." Paleoceanography **13**(4): 352-364.

Buizert, C., M. Sigl, M. Severi, B. R. Markle, J. J. Wettstein, J. R. McConnell, J. B. Pedro, H. Sodemann, K. Goto-Azuma, K. Kawamura, S. Fujita, H. Motoyama, M.

Hirabayashi, R. Uemura, B. Stenni, F. Parrenin, F. He, T. J. Fudge and E. J. Steig (2018). "Abrupt ice-age shifts in southern westerly winds and Antarctic climate forced from the north." Nature **563**(7733): 681-685.

Burke, A. and L. F. Robinson (2012). "The Southern Ocean's Role in Carbon Exchange During the Last Deglaciation." Science **335**(6068): 557-561.

Burton, K. W., H.-F. Ling and R. K. O'Nions (1997). "Closure of the Central American Isthmus and its effect on deep-water formation in the North Atlantic." Nature **386**(6623): 382-385.

Carsten, M., W. Stefan, S. Erik and M. Klaus (2001). "Separation of high field strength elements (Nb, Ta, Zr, Hf) and Lu from rock samples for MC- ICPMS measurements." Geochemistry, Geophysics, Geosystems **2**(12).

Carter, L., I. N. McCave and M. J. M. Williams (2008). Chapter 4 Circulation and Water Masses of the Southern Ocean: A Review. Developments in Earth and Environmental Sciences. F. Florindo and M. Siegert, Elsevier. **8:** 85-114.

Chen, T.-Y., M. Frank, B. A. Haley, M. Gutjahr and R. F. Spielhagen (2012). "Variations of North Atlantic inflow to the central Arctic Ocean over the last 14 million years inferred from hafnium and neodymium isotopes." Earth and Planetary Science Letters **353-354**: 82-92.

Chester, R. and M. J. Hughes (1967). "A chemical technique for the separation of ferro-manganese minerals, carbonate minerals and adsorbed trace elements from pelagic sediments." Chemical Geology **2**: 249-262.

Christensen, J. N., A. N. Halliday, L. V. Godfrey, J. R. Hein and D. K. Rea (1997). "Climate and Ocean Dynamics and the Lead Isotopic Records in Pacific Ferromanganese Crusts." Science **277**(5328): 913-918.

Christl, M., C. Vockenhuber, P. W. Kubik, L. Wacker, J. Lachner, V. Alfimov and H. A. Synal (2013). "The ETH Zurich AMS facilities: Performance parameters and reference materials." Nuclear Instruments and Methods in Physics Research Section B: Beam Interactions with Materials and Atoms **294**: 29-38.

Cochran, J. K., T. McKibbin-Vaughan, M. M. Dornblaser, D. Hirschberg, H. D. Livingston and K. O. Buesseler (1990). "210Pb scavenging in the North Atlantic and North Pacific Oceans." Earth and Planetary Science Letters **97**(3): 332-352.

Colin, C., N. Frank, K. Copard and E. Douville (2010). "Neodymium isotopic composition of deep-sea corals from the NE Atlantic: implications for past hydrological changes during the Holocene." Quaternary Science Reviews **29**(19): 2509-2517.

Coxall, H. K., P. A. Wilson, H. Pälike, C. H. Lear and J. Backman (2005). "Rapid stepwise onset of Antarctic glaciation and deeper calcite compensation in the Pacific Ocean." Nature **433**(7021): 53-57.

Crocket, K. C., G. L. Foster, D. Vance, D. A. Richards and M. Tranter (2013). "A Pb isotope tracer of ocean-ice sheet interaction: the record from the NE Atlantic during the Last Glacial/Interglacial cycle." Quaternary Science Reviews **82**: 133-144.

Crocket, K. C., D. Vance, G. L. Foster, D. A. Richards and M. Tranter (2012). "Continental weathering fluxes during the last glacial/interglacial cycle: insights from the marine sedimentary Pb isotope record at Orphan Knoll, NW Atlantic." Quaternary Science Reviews **38**: 89-99.

Dalziel, I. W. D., L. A. Lawver, J. A. Pearce, P. F. Barker, A. R. Hastie, D. N. Barfod, H.-W. Schenke and M. B. Davis (2013). "A potential barrier to deep Antarctic circumpolar flow until the late Miocene?" Geology **41**(9): 947-950.

Dausmann, V., M. Gutjahr, M. Frank, K. Kouzmanov and U. Schaltegger (2019). "Experimental evidence for mineral-controlled release of radiogenic Nd, Hf and Pb isotopes from granitic rocks during progressive chemical weathering." Chemical Geology **507**: 64-84.

DeConto, R. M., D. Pollard, P. A. Wilson, H. Pälike, C. H. Lear and M. Pagani (2008). "Thresholds for Cenozoic bipolar glaciation." Nature **455**: 652.

Diekmann, B., D. K. Fütterer, H. Grobe, C.-D. Hillenbrand, G. Kuhn, K. Michels, R. Petschick and M. Pirrung (2003). Ice rafted debris distribution in 16 sediment cores from the South Atlantic. Terrigenous sediment supply in the polar to temperate South Atlantic: land-ocean links of environmental changes during the late Quaternary. In: Wefer, G; Mulitza, S & Ratmeyer, V (eds.), The South Atlantic in the Late Quaternary: Reconstruction of Material Budget and Current Systems. Springer-Verlag, Berlin, Heidelberg, New York, 375-399, hdl:10013/epic.15597.d001.

Diekmann, B. and G. Kuhn (1999). "Provenance and dispersal of glacial–marine surface sediments in the Weddell Sea and adjoining areas, Antarctica: ice-rafting versus current transport." Marine Geology **158**(1): 209-231.

Du, J., B. A. Haley and A. C. Mix (2016). "Neodymium isotopes in authigenic phases, bottom waters and detrital sediments in the Gulf of Alaska and their implications for paleo-circulation reconstruction." Geochimica et Cosmochimica Acta **193**: 14-35.

Elmore, A. C., A. M. Piotrowski, J. D. Wright and A. E. Scrivner (2011). "Testing the extraction of past seawater Nd isotopic composition from North Atlantic deep sea sediments and foraminifera." Geochemistry, Geophysics, Geosystems **12**(9).

Ferrari, R., M. F. Jansen, J. F. Adkins, A. Burke, A. L. Stewart and A. F. Thompson (2014). "Antarctic sea ice control on ocean circulation in present and glacial climates." Proceedings of the National Academy of Sciences **111**(24): 8753-8758.

Fietzke, J., V. Liebetrau, D. Günther, K. Gürs, K. Hametner, K. Zumholz, T. H. Hansteen and A. Eisenhauer (2008). "An alternative data acquisition and evaluation strategy for improved isotope ratio precision using LA-MC-ICP-MS applied to stable and radiogenic strontium isotopes in carbonates." Journal of Analytical Atomic Spectrometry **23**(7): 955-961.

Flegal, A. R., H. Maring and S. Niemeyer (1993). "Anthropogenic lead in Antarctic sea water." Nature **365**: 242.

Flower, B. P. and J. P. Kennett (1995). "Middle Miocene deepwater paleoceanography in the southwest Pacific: Relations with East Antarctic Ice Sheet development." Paleoceanography **10**(6): 1095-1112.

Flowerdew, M. J., S. Tyrrell and V. L. Peck (2013). "Inferring sites of subglacial erosion using the Pb isotopic composition of ice-rafted feldspar: Examples from the Weddell Sea, Antarctica." Geology **41**(2): 147-150.

Foldvik, A., T. Gammelsrød, S. Østerhus, E. Fahrbach, G. Rohardt, M. Schröder, K. W. Nicholls, L. Padman and R. A. Woodgate (2004). "Ice shelf water overflow and bottom water formation in the southern Weddell Sea." Journal of Geophysical Research: Oceans **109**(C2).

Foster, G. L. and D. Vance (2006). "Negligible glacial–interglacial variation in continental chemical weathering rates." Nature **444**(7121): 918-921.

Fröllje, H., K. Pahnke, B. Schnetger, H.-J. Brumsack, H. Dulai and J. N. Fitzsimmons (2016). "Hawaiian imprint on dissolved Nd and Ra isotopes and rare earth elements in the central North Pacific: Local survey and seasonal variability." Geochimica et Cosmochimica Acta **189**: 110-131.

Frank, M. (2002). "Radiogenic isotopes: tracers of past ocean circulation and erosional input." Reviews of Geophysics **40**(1): 1-1-1-38.

Frank, M., J.-D. Eckhardt, A. Eisenhauer, P. W. Kubik, B. Dittrich-Hannen, M. Segl and A. Mangini (1994). "Beryllium 10, thorium 230, and protactinium 231 in Galapagos microplate sediments: Implications of hydrothermal activity and paleoproductivity changes during the last 100,000 years." Paleoceanography **9**(4): 559-578.

Frank, M., A. Mangini, R. Gersonde, M. Rutgers van der Loeff and G. Kuhn (1996). "Late Quaternary sediment dating and quantification of lateral sediment redistribution

applying $^{230}Th_{ex}$: a study from the eastern Atlantic sector of the Southern Ocean." Geologische Rundschau **85**(3): 554-566.

Frank, M. and R. K. O'Nions (1998). "Sources of Pb for Indian Ocean ferromanganese crusts: a record of Himalayan erosion?" Earth and Planetary Science Letters **158**(3): 121-130.

Frank, M., R. K. O'Nions, J. R. Hein and V. K. Banakar (1999). "60 Myr records of major elements and Pb–Nd isotopes from hydrogenous ferromanganese crusts: reconstruction of seawater paleochemistry." Geochimica et Cosmochimica Acta **63**(11): 1689-1708.

Frank, M., N. Whiteley, S. Kasten, J. R. Hein and K. O'Nions (2002). "North Atlantic Deep Water export to the Southern Ocean over the past 14 Myr: Evidence from Nd and Pb isotopes in ferromanganese crusts." Paleoceanography **17**(2): 12-11-12-19.

Garbe-Schönberg, C.-D. (1993). "Simultaneous determination of thirty-seven trace elements in twenty-eight international rock standards by icp-ms." Geostandards Newsletter **17**(1): 81-97.

Garcia, H. E., R. A. Locarnini, T. P. Boyer, J. I. Antonov, A. V. Mishonov, O. K. Baranova, M. M. Zweng, J. R. Reagan and D. R. Johnson (2013). "Dissolved Oxygen, Apparent Oxygen Utilization, and Oxygen Saturation." World Ocean Atlas 2013. **3** 27.

Goldstein, S. J. and S. B. Jacobsen (1987). "The Nd and Sr isotopic systematics of river-water dissolved material: Implications for the sources of Nd and Sr in seawater." Chemical Geology: Isotope Geoscience section **66**(3): 245-272.

Goldstein, S. L. and S. R. Hemming (2003). 6.17 - Long-lived Isotopic Tracers in Oceanography, Paleoceanography, and Ice-sheet Dynamics. Treatise on Geochemistry. H. D. Holland and K. K. Turekian. Oxford, Pergamon**:** 453-489.

Goldstein, S. L., R. K. O'Nions and P. J. Hamilton (1984). "A Sm-Nd isotopic study of atmospheric dusts and particulates from major river systems." Earth and Planetary Science Letters **70**(2): 221-236.

Golledge, N. R., L. Menviel, L. Carter, C. J. Fogwill, M. H. England, G. Cortese and R. H. Levy (2014). "Antarctic contribution to meltwater pulse 1A from reduced Southern Ocean overturning." Nature Communications **5**: 5107.

Gordon, A. L. (2001). Current Systems in the Southern Ocean. Encyclopedia of Ocean Sciences (Second Edition). J. H. Steele. Oxford, Academic Press**:** 735-743.

Gourlan, A. T., L. Meynadier, C. J. Allègre, P. Tapponnier, J.-L. Birck and J.-L. Joron

(2010). "Northern Hemisphere climate control of the Bengali rivers discharge during the past 4 Ma." Quaternary Science Reviews **29**(19): 2484-2498.

Gutjahr, M., M. Frank, A. N. Halliday and L. D. Keigwin (2009). "Retreat of the Laurentide ice sheet tracked by the isotopic composition of Pb in western North Atlantic seawater during termination 1." Earth and Planetary Science Letters **286**(3–4): 546-555.

Gutjahr, M., M. Frank, C. H. Stirling, V. Klemm, T. Flierdt and A. N. Halliday (2007). "Reliable extraction of a deepwater trace metal isotope signal from Fe–Mn oxyhydroxide coatings of marine sediments." Chemical Geology **242**(3): 351-370.

Gutjahr, M., H. Huang, E. Hathorne, G. Kuhn and A. Eisenhauer (2019). "Formation and export of the modern Weddell Sea-sourced Antarctic Bottom Water Nd isotope signature." in prep.

Haley, B. A., M. Frank, R. F. Spielhagen and J. Fietzke (2008). "Radiogenic isotope record of Arctic Ocean circulation and weathering inputs of the past 15 million years." Paleoceanography **23**(1).

Hathorne, E. C., B. Haley, T. Stichel, P. Grasse, M. Zieringer and M. Frank (2012). "Online preconcentration ICP-MS analysis of rare earth elements in seawater." Geochemistry, Geophysics, Geosystems **13**(1).

Haug, G. H. and R. Tiedemann (1998). "Effect of the formation of the Isthmus of Panama on Atlantic Ocean thermohaline circulation." Nature **393**(6686): 673-676.

Hayes, C. T., A. Martínez-García, A. P. Hasenfratz, S. L. Jaccard, D. A. Hodell, D. M. Sigman, G. H. Haug and R. F. Anderson (2014). "A stagnation event in the deep South Atlantic during the last interglacial period." Science **346**(6216): 1514-1517.

Hellmer, H. H., M. Rhein, G. Heinemann, J. Abalichin, W. Abouchami, O. Baars, U. Cubasch, K. Dethloff, L. Ebner, E. Fahrbach, M. Frank, G. Gollan, R. J. Greatbatch, J. Grieger, V. M. Gryanik, M. Gryschka, J. Hauck, M. Hoppema, O. Huhn, T. Kanzow, B. P. Koch, G. König-Langlo, U. Langematz, G. C. Leckebusch, C. Lüpkes, S. Paul, A. Rinke, B. Rost, M. R. van der Loeff, M. Schröder, G. Seckmeyer, T. Stichel, V. Strass, R. Timmermann, S. Trimborn, U. Ulbrich, C. Venchiarutti, U. Wacker, S. Willmes and D. Wolf-Gladrow (2016). "Meteorology and oceanography of the Atlantic sector of the Southern Ocean—a review of German achievements from the last decade." Ocean Dynamics **66**(11): 1379-1413.

Henderson, G. M. and E. Maier-Reimer (2002). "Advection and removal of 210Pb and stable Pb isotopes in the oceans: a general circulation model study." Geochimica et Cosmochimica Acta **66**(2): 257-272.

Henken-Mellies, W. U., J. Beer, F. Heller, K. J. Hsü, C. Shen, G. Bonani, H. J. Hofmann, M. Suter and W. Wölfli (1990). "10Be and9Be in South Atlantic DSDP Site 519: Relation to geomagnetic reversals and to sediment composition." Earth and Planetary Science Letters **98**(3): 267-276.

Hodell, D. A., C. D. Charles, J. H. Curtis, P. G. Mortyn, U. S. Ninnemann and K. A. Venz (2003). Stable isotope record of benthic and planktonic foraminifera in sediment cores of ODP Leg 177, Southern Ocean. Proceedings of the Ocean Drilling Program, Scientific Results, College Station, TX (Ocean Drilling Program), 177, 1-26, https://doi.org/10.2973/odp.proc.sr.177.120.2003.

Hodell, D. A., R. Gersonde and P. Blum (2002). "Leg 177 synthesis: insights into Southern Ocean paleoceanography on tectonic to millennial timescales." Proc. ODP, Sci. Results **177**.

Hodell, D. A. and K. A. Venz-Curtis (2006). "Late Neogene history of deepwater ventilation in the Southern Ocean." Geochemistry, Geophysics, Geosystems **7**(9).

Holbourn, A., W. Kuhnt, M. Frank and B. A. Haley (2013). "Changes in Pacific Ocean circulation following the Miocene onset of permanent Antarctic ice cover." Earth and Planetary Science Letters **365**: 38-50.

Hu, R., T. L. Noble, A. M. Piotrowski, I. N. McCave, H. C. Bostock and H. L. Neil (2016). "Neodymium isotopic evidence for linked changes in Southeast Atlantic and Southwest Pacific circulation over the last 200 kyr." Earth and Planetary Science Letters **455**: 106-114.

Huhn, O., H. H. Hellmer, M. Rhein, C. Rodehacke, W. Roether, M. P. Schodlok and M. Schroeder (2008). "Evidence of deep- and bottom-water formation in the western Weddell Sea." Deep-Sea Research Part Ii-Topical Studies in Oceanography **55**(8-9): 1098-1116.

Huhn, O., M. Rhein, M. Hoppema and S. van Heuven (2013). "Decline of deep and bottom water ventilation and slowing down of anthropogenic carbon storage in the Weddell Sea, 1984-2011." Deep-Sea Research Part I-Oceanographic Research Papers **76**: 66-84.

Huybrechts, P. (2002). "Sea-level changes at the LGM from ice-dynamic reconstructions of the Greenland and Antarctic ice sheets during the glacial cycles." Quaternary Science Reviews **21**: 203-231.

Inoue, T., Z.-Y. Huang, M. Imamura, S. Tanaka and A. Usui (1983). "10Be and 10Be/9Be in manganese nodules." GEOCHEMICAL JOURNAL **17**(6): 307-312.

Jaccard, S. L., E. D. Galbraith, A. Martínez-García and R. F. Anderson (2016).

"Covariation of deep Southern Ocean oxygenation and atmospheric CO_2 through the last ice age." Nature **530**: 207.

Jaccard, S. L., C. T. Hayes, A. Martínez-García, D. A. Hodell, R. F. Anderson, D. M. Sigman and G. H. Haug (2013). "Two Modes of Change in Southern Ocean Productivity Over the Past Million Years." Science **339**(6126): 1419-1423.

Jacobs, S. S. (2004). "Bottom water production and its links with the thermohaline circulation." Antarctic Science **16**(4): 427-437.

Jeandel, C. and E. H. Oelkers (2015). "The influence of terrigenous particulate material dissolution on ocean chemistry and global element cycles." Chemical Geology **395**: 50-66.

Jouzel, J., V. Masson-Delmotte, O. Cattani, G. Dreyfus, S. Falourd, G. Hoffmann, B. Minster, J. Nouet, J. M. Barnola, J. Chappellaz, H. Fischer, J. C. Gallet, S. Johnsen, M. Leuenberger, L. Loulergue, D. Luethi, H. Oerter, F. Parrenin, G. Raisbeck, D. Raynaud, A. Schilt, J. Schwander, E. Selmo, R. Souchez, R. Spahni, B. Stauffer, J. P. Steffensen, B. Stenni, T. F. Stocker, J. L. Tison, M. Werner and E. W. Wolff (2007). "Orbital and Millennial Antarctic Climate Variability over the Past 800,000 Years." Science **317**(5839): 793-796.

Kawabe, M. and S. Fujio (2010). "Pacific ocean circulation based on observation." Journal of Oceanography **66**(3): 389-403.

Kennett, J. P. (1977). "Cenozoic evolution of Antarctic glaciation, the circum-Antarctic Ocean, and their impact on global paleoceanography." Journal of Geophysical Research (1896-1977) **82**(27): 3843-3860.

Kerr, R., T. S. Dotto, M. M. Mata and H. H. Hellmer (2018). "Three decades of deep water mass investigation in the Weddell Sea (1984-2014): Temporal variability and changes." Deep-Sea Research Part Ii-Topical Studies in Oceanography **149**: 70-83.

Klemm, V., B. Reynolds, M. Frank, T. Pettke and A. N. Halliday (2007). "Cenozoic changes in atmospheric lead recorded in central Pacific ferromanganese crusts." Earth and Planetary Science Letters **253**(1): 57-66.

Klevenz, V., D. Vance, D. N. Schmidt and K. Mezger (2008). "Neodymium isotopes in benthic foraminifera: Core-top systematics and a down-core record from the Neogene south Atlantic." Earth and Planetary Science Letters **265**(3): 571-587.

Kraft, S., M. Frank, E. C. Hathorne and S. Weldeab (2013). "Assessment of seawater Nd isotope signatures extracted from foraminiferal shells and authigenic phases of Gulf of Guinea sediments." Geochimica et Cosmochimica Acta **121**: 414-435.

Kurzweil, F., M. Gutjahr, D. Vance and L. Keigwin (2010). "Authigenic Pb isotopes from the Laurentian Fan: Changes in chemical weathering and patterns of North American freshwater runoff during the last deglaciation." Earth and Planetary Science Letters **299**(3): 458-465.

Lüthi, D., M. Le Floch, B. Bereiter, T. Blunier, J.-M. Barnola, U. Siegenthaler, D. Raynaud, J. Jouzel, H. Fischer, K. Kawamura and T. F. Stocker (2008). "High-resolution carbon dioxide concentration record 650,000–800,000 years before present." Nature **453**: 379.

Lacan, F. and C. Jeandel (2005). "Acquisition of the neodymium isotopic composition of the North Atlantic Deep Water." Geochemistry, Geophysics, Geosystems **6**(12).

Lacan, F. and C. Jeandel (2005). "Neodymium isotopes as a new tool for quantifying exchange fluxes at the continent–ocean interface." Earth and Planetary Science Letters **232**(3): 245-257.

Lacan, F., K. Tachikawa and C. Jeandel (2012). "Neodymium isotopic composition of the oceans: A compilation of seawater data." Chemical Geology **300-301**: 177-184.

Lambelet, M., T. van de Flierdt, E. C. V. Butler, A. R. Bowie, S. R. Rintoul, R. J. Watson, T. Remenyi, D. Lannuzel, M. Warner, L. F. Robinson, H. C. Bostock and L. I. Bradtmiller (2018). "The Neodymium Isotope Fingerprint of Adélie Coast Bottom Water." Geophysical Research Letters **45**(20): 11,247-211,256.

Lambelet, M., T. van de Flierdt, K. Crocket, M. Rehkämper, K. Kreissig, B. Coles, M. J. A. Rijkenberg, L. J. A. Gerringa, H. J. W. de Baar and R. Steinfeldt (2016). "Neodymium isotopic composition and concentration in the western North Atlantic Ocean: Results from the GEOTRACES GA02 section." Geochimica et Cosmochimica Acta **177**: 1-29.

Lambert, F., B. Delmonte, J. R. Petit, M. Bigler, P. R. Kaufmann, M. A. Hutterli, T. F. Stocker, U. Ruth, J. P. Steffensen and V. Maggi (2008). "Dust-climate couplings over the past 800,000 years from the EPICA Dome C ice core." Nature **452**: 616.

Lawver, L. A. and L. M. Gahagan (2003). "Evolution of Cenozoic seaways in the circum-Antarctic region." Palaeogeography, Palaeoclimatology, Palaeoecology **198**(1): 11-37.

Lee, J.-M., E. A. Boyle, T. Gamo, H. Obata, K. Norisuye and Y. Echegoyen (2015). "Impact of anthropogenic Pb and ocean circulation on the recent distribution of Pb isotopes in the Indian Ocean." Geochimica et Cosmochimica Acta **170**: 126-144.

Lee, J.-M., E. A. Boyle, I. Suci Nurhati, M. Pfeiffer, A. J. Meltzner and B. Suwargadi (2014). "Coral-based history of lead and lead isotopes of the surface Indian Ocean

since the mid-20th century." Earth and Planetary Science Letters **398**: 37-47.

Lee, J.-M., S. F. Eltgroth, E. A. Boyle and J. F. Adkins (2017). "The transfer of bomb radiocarbon and anthropogenic lead to the deep North Atlantic Ocean observed from a deep sea coral." Earth and Planetary Science Letters **458**: 223-232.

Lippold, J., M. Gutjahr, P. Blaser, E. Christner, M. L. de Carvalho Ferreira, S. Mulitza, M. Christl, F. Wombacher, E. Böhm, B. Antz, O. Cartapanis, H. Vogel and S. L. Jaccard (2016). "Deep water provenance and dynamics of the (de)glacial Atlantic meridional overturning circulation." Earth and Planetary Science Letters **445**: 68-78.

Lisiecki, L. E. and M. E. Raymo (2005). "A Pliocene-Pleistocene stack of 57 globally distributed benthic δ18O records." Paleoceanography **20**(1).

Liu, Z., M. Pagani, D. Zinniker, R. DeConto, M. Huber, H. Brinkhuis, S. R. Shah, R. M. Leckie and A. Pearson (2009). "Global Cooling During the Eocene-Oligocene Climate Transition." Science **323**(5918): 1187-1190.

Manheim, F. T. (1986). "Marine Cobalt Resources." Science **232**(4750): 600-608.

Marcott, S. A., T. K. Bauska, C. Buizert, E. J. Steig, J. L. Rosen, K. M. Cuffey, T. J. Fudge, J. P. Severinghaus, J. Ahn, M. L. Kalk, J. R. McConnell, T. Sowers, K. C. Taylor, J. W. C. White and E. J. Brook (2014). "Centennial-scale changes in the global carbon cycle during the last deglaciation." Nature **514**: 616.

Marlow, J. R., C. B. Lange, G. Wefer and A. Rosell-Melé (2000). "Upwelling Intensification As Part of the Pliocene-Pleistocene Climate Transition." Science **290**(5500): 2288-2291.

Martin, E. E. and H. D. Scher (2004). "Preservation of seawater Sr and Nd isotopes in fossil fish teeth: bad news and good news." Earth and Planetary Science Letters **220**(1): 25-39.

Martin, F. (2002). "RADIOGENIC ISOTOPES: TRACERS OF PAST OCEAN CIRCULATION AND EROSIONAL INPUT." Reviews of Geophysics **40**(1): 1-1-1-38.

Menviel, L., P. Spence, J. Yu, M. A. Chamberlain, R. J. Matear, K. J. Meissner and M. H. England (2018). "Southern Hemisphere westerlies as a driver of the early deglacial atmospheric CO2 rise." Nature Communications **9**(1): 2503.

Michels, K., G. Kuhn, C.-D. Hillenbrand, B. Diekmann, D. K. Fütterer, H. Grobe and G. Uenzelmann-Neben (2002). Grain size composition of sediment cores from the Weddell Sea, Antarctica. The southern Weddell Sea: combined contourite-turbidite sedimentation at the southeastern margin of the Weddell Gyre. In: Stow, D A V;

Pudsey, C; Howe, J C; Faugères, J-C & Viana, A R (eds.), Deep-water contourite systems: modern drifts and ancient series, seismic and sedimentary characteristics. Geological Society of London, Memoirs, London, 22, 305-323, hdl:10013/epic.14690.d001, PANGAEA.

Molina-Kescher, M., M. Frank and E. Hathorne (2014). "South Pacific dissolved Nd isotope compositions and rare earth element distributions: Water mass mixing versus biogeochemical cycling." Geochimica et Cosmochimica Acta **127**: 171-189.

Monnin, E., E. J. Steig, U. Siegenthaler, K. Kawamura, J. Schwander, B. Stauffer, T. F. Stocker, D. L. Morse, J.-M. Barnola, B. Bellier, D. Raynaud and H. Fischer (2004). "Evidence for substantial accumulation rate variability in Antarctica during the Holocene, through synchronization of CO2 in the Taylor Dome, Dome C and DML ice cores." Earth and Planetary Science Letters **224**(1): 45-54.

Naveira Garabato, A. C., E. L. McDonagh, D. P. Stevens, K. J. Heywood and R. J. Sanders (2002). "On the export of Antarctic Bottom Water from the Weddell Sea." Deep Sea Research Part II: Topical Studies in Oceanography **49**(21): 4715-4742.

Ndungu, K., C. M. Zurbrick, S. Stammerjohn, S. Severmann, R. M. Sherrell and A. R. Flegal (2016). "Lead Sources to the Amundsen Sea, West Antarctica." Environmental Science & Technology **50**(12): 6233-6239.

Niebler, H.-S. (1995). Stable isotope record of foraminifera from South Atlantic sediments with reconstruction of paleotemperatures and paleosalinities. Reconstruction of paleo-environmental parameters using stable isotopes and faunal assemblages of planktonic foraminifera in the South Atlantic Ocean. Reports on Polar Research, 167, 198 pp, https://doi.org/10.2312/BzP_0167_1995.

O'Nions, R. K., M. Frank, F. von Blanckenburg and H. F. Ling (1998). "Secular variation of Nd and Pb isotopes in ferromanganese crusts from the Atlantic, Indian and Pacific Oceans." Earth and Planetary Science Letters **155**(1): 15-28.

Ohr, M., A. N. Halliday and D. R. Peacor (1991). "Sr and Nd isotopic evidence for punctuated clay diagenesis, Texas Gulf Coast." Earth and Planetary Science Letters **105**(1): 110-126.

Oppo, D. W. and S. J. Lehman (1993). "Mid-depth circulation of the subpolar North Atlantic during the Last Glacial Maximum." Science **259**(5098): 1148-1152.

Orsi, A. H., G. C. Johnson and J. L. Bullister (1999). "Circulation, mixing, and production of Antarctic Bottom Water." Progress in Oceanography **43**(1): 55-109.

Orsi, A. H., T. Whitworth and W. D. Nowlin (1995). "On the meridional extent and fronts of the Antarctic Circumpolar Current." Deep Sea Research Part I:

Oceanographic Research Papers **42**(5): 641-673.

Pöppelmeier, F., M. Gutjahr, P. Blaser, L. D. Keigwin and J. Lippold (2018). "Origin of Abyssal NW Atlantic Water Masses Since the Last Glacial Maximum." Paleoceanography and Paleoclimatology **33**(5): 530-543.

Parrenin, F., V. Masson-Delmotte, P. Köhler, D. Raynaud, D. Paillard, J. Schwander, C. Barbante, A. Landais, A. Wegner and J. Jouzel (2013). "Synchronous Change of Atmospheric CO_2 and Antarctic Temperature During the Last Deglacial Warming." Science **339**(6123): 1060-1063.

Paul, M., T. van de Flierdt, M. Rehkämper, R. Khondoker, D. Weiss, M. C. Lohan and W. B. Homoky (2015). "Tracing the Agulhas leakage with lead isotopes." Geophysical Research Letters **42**(20): 8515-8521.

Pearce, C. R., M. T. Jones, E. H. Oelkers, C. Pradoux and C. Jeandel (2013). "The effect of particulate dissolution on the neodymium (Nd) isotope and Rare Earth Element (REE) composition of seawater." Earth and Planetary Science Letters **369-370**: 138-147.

Petit, J. R., J. Jouzel, D. Raynaud, N. I. Barkov, J. M. Barnola, I. Basile, M. Bender, J. Chappellaz, M. Davis, G. Delaygue, M. Delmotte, V. M. Kotlyakov, M. Legrand, V. Y. Lipenkov, C. Lorius, L. PÉpin, C. Ritz, E. Saltzman and M. Stievenard (1999). "Climate and atmospheric history of the past 420,000 years from the Vostok ice core, Antarctica." Nature **399**: 429.

Pfuhl, H. A. and I. N. McCave (2005). "Evidence for late Oligocene establishment of the Antarctic Circumpolar Current." Earth and Planetary Science Letters **235**(3): 715-728.

Pin, C. and J. S. Zalduegui (1997). "Sequential separation of light rare-earth elements, thorium and uranium by miniaturized extraction chromatography: Application to isotopic analyses of silicate rocks." Analytica Chimica Acta **339**(1): 79-89.

Piotrowski, A. M., S. L. Goldstein, S. R. Hemming and R. G. Fairbanks (2004). "Intensification and variability of ocean thermohaline circulation through the last deglaciation." Earth and Planetary Science Letters **225**(1-2): 205-220.

Piotrowski, A. M., S. L. Goldstein, S. R. Hemming and R. G. Fairbanks (2004). "Intensification and variability of ocean thermohaline circulation through the last deglaciation." Earth and Planetary Science Letters **225**(1): 205-220.

Planchon, F. A. M., K. van de Velde, K. J. R. Rosman, E. W. Wolff, C. P. Ferrari and C. F. Boutron (2003). "One hundred fifty–year record of lead isotopes in Antarctic snow from Coats Land." Geochimica et Cosmochimica Acta **67**(4): 693-708.

Purkey, S. G., W. M. Smethie, G. Gebbie, A. L. Gordon, R. E. Sonnerup, M. J. Warner and J. L. Bullister (2018). "A synoptic view of the ventilation and circulation of Antarctic Bottom Water from chlorofluorocarbons and natural tracers." Annual Review of Marine Science, Vol 10 **10**: 503-527.

Rae, J. W. B., A. Burke, L. F. Robinson, J. F. Adkins, T. Chen, C. Cole, R. Greenop, T. Li, E. F. M. Littley, D. C. Nita, J. A. Stewart and B. J. Taylor (2018). "CO_2 storage and release in the deep Southern Ocean on millennial to centennial timescales." Nature **562**(7728): 569.

Raymo, M. E., D. Hodell and E. Jansen (1992). "Response of deep ocean circulation to initiation of northern hemisphere glaciation (3–2 MA)." Paleoceanography **7**(5): 645-672.

Rempfer, J., T. F. Stocker, F. Joos, J.-C. Dutay and M. Siddall (2011). "Modelling Nd-isotopes with a coarse resolution ocean circulation model: Sensitivities to model parameters and source/sink distributions." Geochimica et Cosmochimica Acta **75**(20): 5927-5950.

Reynolds, B. C., M. Frank and R. K. O'Nions (1999). "Nd- and Pb-isotope time series from Atlantic ferromanganese crusts: implications for changes in provenance and paleocirculation over the last 8 Myr." Earth and Planetary Science Letters **173**(4): 381-396.

Rickli, J., M. Gutjahr, D. Vance, M. Fischer-Gödde, C.-D. Hillenbrand and G. Kuhn (2014). "Neodymium and hafnium boundary contributions to seawater along the West Antarctic continental margin." Earth and Planetary Science Letters **394**: 99-110.

Rignot, E., J. Mouginot and B. Scheuchl (2011). "Ice Flow of the Antarctic Ice Sheet." Science **333**(6048): 1427-1430.

Roberts, N. L. and A. M. Piotrowski (2015). "Radiogenic Nd isotope labeling of the northern NE Atlantic during MIS 2." Earth and Planetary Science Letters **423**: 125-133.

Roberts, N. L., A. M. Piotrowski, J. F. McManus and L. D. Keigwin (2010). "Synchronous Deglacial Overturning and Water Mass Source Changes." Science **327**(5961): 75-78.

Rohling, E. J., K. Grant, C. Hemleben, M. Siddall, B. A. A. Hoogakker, M. Bolshaw and M. Kucera (2007). "High rates of sea-level rise during the last interglacial period." Nature Geoscience **1**: 38.

Ruddiman, W. F., A. McIntyre, V. Niebler-Hunt and J. T. Durazzi (2017). "Oceanic Evidence for the Mechanism of Rapid Northern Hemisphere Glaciation." Quaternary

Research **13**(1): 33-64.

Süfke, F., M. Gutjahr, A. Gilli, F. S. Anselmetti, L. Glur and A. Eisenhauer (2019). "Early stage weathering systematics of Pb and Nd isotopes derived from a high-Alpine Holocene lake sediment record." Chemical Geology **507**: 42-53.

Schaule, B. K. and C. C. Patterson (1981). "Lead concentrations in the northeast Pacific: evidence for global anthropogenic perturbations." Earth and Planetary Science Letters **54**(1): 97-116.

Scher, H. D. and E. E. Martin (2006). "Timing and Climatic Consequences of the Opening of Drake Passage." Science **312**(5772): 428-430.

Scher, H. D., J. M. Whittaker, S. E. Williams, J. C. Latimer, W. E. C. Kordesch and M. L. Delaney (2015). "Onset of Antarctic Circumpolar Current 30 million years ago as Tasmanian Gateway aligned with westerlies." Nature **523**: 580.

Schlitzer, R. (2011). Ocean Data View. http://odv.awi.de.

Schlitzer, R., R. F. Anderson, E. M. Dodas, M. Lohan, W. Geibert, A. Tagliabue, A. Bowie, C. Jeandel, M. T. Maldonado, W. M. Landing, D. Cockwell, C. Abadie, W. Abouchami, E. P. Achterberg, A. Agather, A. Aguliar-Islas, H. M. van Aken, M. Andersen, C. Archer, M. Auro, H. J. de Baar, O. Baars, A. R. Baker, K. Bakker, C. Basak, M. Baskaran, N. R. Bates, D. Bauch, P. van Beek, M. K. Behrens, E. Black, K. Bluhm, L. Bopp, H. Bouman, K. Bowman, J. Bown, P. Boyd, M. Boye, E. A. Boyle, P. Branellec, L. Bridgestock, G. Brissebrat, T. Browning, K. W. Bruland, H.-J. Brumsack, M. Brzezinski, C. S. Buck, K. N. Buck, K. Buesseler, A. Bull, E. Butler, P. Cai, P. C. Mor, D. Cardinal, C. Carlson, G. Carrasco, N. Casacuberta, K. L. Casciotti, M. Castrillejo, E. Chamizo, R. Chance, M. A. Charette, J. E. Chaves, H. Cheng, F. Chever, M. Christl, T. M. Church, I. Closset, A. Colman, T. M. Conway, D. Cossa, P. Croot, J. T. Cullen, G. A. Cutter, C. Daniels, F. Dehairs, F. Deng, H. T. Dieu, B. Duggan, G. Dulaquais, C. Dumousseaud, Y. Echegoyen-Sanz, R. L. Edwards, M. Ellwood, E. Fahrbach, J. N. Fitzsimmons, A. Russell Flegal, M. Q. Fleisher, T. van de Flierdt, M. Frank, J. Friedrich, F. Fripiat, H. Fröllje, S. J. G. Galer, T. Gamo, R. S. Ganeshram, J. Garcia-Orellana, E. Garcia-Solsona, M. Gault-Ringold, E. George, L. J. A. Gerringa, M. Gilbert, J. M. Godoy, S. L. Goldstein, S. R. Gonzalez, K. Grissom, C. Hammerschmidt, A. Hartman, C. S. Hassler, E. C. Hathorne, M. Hatta, N. Hawco, C. T. Hayes, L.-E. Heimbürger, J. Helgoe, M. Heller, G. M. Henderson, P. B. Henderson, S. van Heuven, P. Ho, T. J. Horner, Y.-T. Hsieh, K.-F. Huang, M. P. Humphreys, K. Isshiki, J. E. Jacquot, D. J. Janssen, W. J. Jenkins, S. John, E. M. Jones, J. L. Jones, D. C. Kadko, R. Kayser, T. C. Kenna, R. Khondoker, T. Kim, L. Kipp, J. K. Klar, M. Klunder, S. Kretschmer, Y. Kumamoto, P. Laan, M. Labatut, F. Lacan, P. J. Lam, M. Lambelet, C. H. Lamborg, F. A. C. Le Moigne, E. Le Roy, O. J. Lechtenfeld, J.-M. Lee, P. Lherminier, S. Little, M. López-Lora, Y. Lu, P. Masque, E. Mawji, C. R. McClain, C. Measures, S. Mehic, J.-L. M. Barraqueta, P. van der Merwe, R. Middag,

S. Mieruch, A. Milne, T. Minami, J. W. Moffett, G. Moncoiffe, W. S. Moore, P. J. Morris, P. L. Morton, Y. Nakaguchi, N. Nakayama, J. Niedermiller, J. Nishioka, A. Nishiuchi, A. Noble, H. Obata, S. Ober, D. C. Ohnemus, J. van Ooijen, J. O'Sullivan, S. Owens, K. Pahnke, M. Paul, F. Pavia, L. D. Pena, B. Peters, F. Planchon, H. Planquette, C. Pradoux, V. Puigcorbé, P. Quay, F. Queroue, A. Radic, S. Rauschenberg, M. Rehkämper, R. Rember, T. Remenyi, J. A. Resing, J. Rickli, S. Rigaud, M. J. A. Rijkenberg, S. Rintoul, L. F. Robinson, M. Roca-Martí, V. Rodellas, T. Roeske, J. M. Rolison, M. Rosenberg, S. Roshan, M. M. Rutgers van der Loeff, E. Ryabenko, M. A. Saito, L. A. Salt, V. Sanial, G. Sarthou, C. Schallenberg, U. Schauer, H. Scher, C. Schlosser, B. Schnetger, P. Scott, P. N. Sedwick, I. Semiletov, R. Shelley, R. M. Sherrell, A. M. Shiller, D. M. Sigman, S. K. Singh, H. A. Slagter, E. Slater, W. M. Smethie, H. Snaith, Y. Sohrin, B. Sohst, J. E. Sonke, S. Speich, R. Steinfeldt, G. Stewart, T. Stichel, C. H. Stirling, J. Stutsman, G. J. Swarr, J. H. Swift, A. Thomas, K. Thorne, C. P. Till, R. Till, A. T. Townsend, E. Townsend, R. Tuerena, B. S. Twining, D. Vance, S. Velazquez, C. Venchiarutti, M. Villa-Alfageme, S. M. Vivancos, A. H. L. Voelker, B. Wake, M. J. Warner, R. Watson, E. van Weerlee, M. Alexandra Weigand, Y. Weinstein, D. Weiss, A. Wisotzki, E. M. S. Woodward, J. Wu, Y. Wu, K. Wuttig, N. Wyatt, Y. Xiang, R. C. Xie, Z. Xue, H. Yoshikawa, J. Zhang, P. Zhang, Y. Zhao, L. Zheng, X.-Y. Zheng, M. Zieringer, L. A. Zimmer, P. Ziveri, P. Zunino and C. Zurbrick (2018). "The GEOTRACES Intermediate Data Product 2017." Chemical Geology **493**: 210-223.

Schlosser, C., J. Karstensen and E. M. S. Woodward (2019). "Distribution of dissolved and leachable particulate Pb in the water column along the GEOTRACES section GA10 in the South Atlantic." Deep Sea Research Part I: Oceanographic Research Papers.

Shackleton, N. J. and N. D. Opdyke (1977). "Oxygen isotope and palaeomagnetic evidence for early Northern Hemisphere glaciation." Nature **270**(5634): 216-219.

Shakun, J. D., P. U. Clark, F. He, S. A. Marcott, A. C. Mix, Z. Y. Liu, B. Otto-Bliesner, A. Schmittner and E. Bard (2012). "Global warming preceded by increasing carbon dioxide concentrations during the last deglaciation." Nature **484**(7392): 49-55.

Shen, G. T. and E. A. Boyle (1987). "Lead in corals: reconstruction of historical industrial fluxes to the surface ocean." Earth and Planetary Science Letters **82**(3): 289-304.

Sigman, D. M. and E. A. Boyle (2000). "Glacial/interglacial variations in atmospheric carbon dioxide." Nature **407**(6806): 859-869.

Sigman, D. M., M. P. Hain and G. H. Haug (2010). "The polar ocean and glacial cycles in atmospheric CO2 concentration." Nature **466**: 47.

Skinner, L. C. (2009). "Glacial-interglacial atmospheric CO2 change: a possible

"standing volume" effect on deep-ocean carbon sequestration." Climate of the Past **5**(3): 537-550.

Skinner, L. C., S. Fallon, C. Waelbroeck, E. Michel and S. Barker (2010). "Ventilation of the deep Southern Ocean and deglacial CO2 rise." Science **328** (5982): 1147-1151.

Skinner, L. C., A. E. Scrivner, D. Vance, S. Barker, S. Fallon and C. Waelbroeck (2013). "North Atlantic versus Southern Ocean contributions to a deglacial surge in deep ocean ventilation." Geology **41**(6): 667-670.

Smith, J. A., C.-D. Hillenbrand, C. J. Pudsey, C. S. Allen and A. G. C. Graham (2010). "The presence of polynyas in the Weddell Sea during the Last Glacial Period with implications for the reconstruction of sea-ice limits and ice sheet history." Earth and Planetary Science Letters **296**(3): 287-298.

Staudigel, H., P. Doyle and A. Zindler (1985). "Sr and Nd isotope systematics in fish teeth." Earth and Planetary Science Letters **76**(1): 45-56.

Stichel, T., M. Frank, J. Rickli and B. A. Haley (2012). "The hafnium and neodymium isotope composition of seawater in the Atlantic sector of the Southern Ocean." Earth and Planetary Science Letters **317-318**: 282-294.

Stichel, T., M. Frank, J. Rickli, E. C. Hathorne, B. A. Haley, C. Jeandel and C. Pradoux (2012). "Sources and input mechanisms of hafnium and neodymium in surface waters of the Atlantic sector of the Southern Ocean." Geochimica et Cosmochimica Acta **94**: 22-37.

Stickley, C. E., H. Brinkhuis, S. A. Schellenberg, A. Sluijs, U. Röhl, M. Fuller, M. Grauert, M. Huber, J. Warnaar and G. L. Williams (2004). "Timing and nature of the deepening of the Tasmanian Gateway." Paleoceanography **19**(4).

Strawn, D. G. and D. L. Sparks (2000). "Effects of Soil Organic Matter on the Kinetics and Mechanisms of Pb(II) Sorption and Desorption in Soil." Soil Science Society of America Journal **64**(1): 144-156.

Struve, T. (2015). Deciphering glacial-interglacial Southern Ocean dynamics with deep-sea corals. Doctor of Philosophy (PhD), Imperial College London.

Struve, T., T. van de Flierdt, A. Burke, L. F. Robinson, S. J. Hammond, K. C. Crocket, L. I. Bradtmiller, M. E. Auro, K. J. Mohamed and N. J. White (2017). "Neodymium isotopes and concentrations in aragonitic scleractinian cold-water coral skeletons - Modern calibration and evaluation of palaeo-applications." Chemical Geology **453**: 146-168.

Sutter, J., P. Gierz, K. Grosfeld, M. Thoma and G. Lohmann (2016). "Ocean

temperature thresholds for Last Interglacial West Antarctic Ice Sheet collapse." Geophysical Research Letters **43**(6): 2675-2682.

Tachikawa, K., V. Athias and C. Jeandel (2003). "Neodymium budget in the modern ocean and paleo-oceanographic implications." Journal of Geophysical Research-Oceans **108** (C8): Art. No. 3254.

Tachikawa, K., C. Jeandel and M. Roy-Barman (1999). "A new approach to the Nd residence time in the ocean: the role of atmospheric inputs." Earth and Planetary Science Letters **170**(4): 433-446.

Talley, L. (2018). "Southern Ocean - circulation and water properties." SIO 210: Introduction to Physical Oceanography.

Tanaka, T., S. Togashi, H. Kamioka, H. Amakawa, H. Kagami, T. Hamamoto, M. Yuhara, Y. Orihashi, S. Yoneda, H. Shimizu, T. Kunimaru, K. Takahashi, T. Yanagi, T. Nakano, H. Fujimaki, R. Shinjo, Y. Asahara, M. Tanimizu and C. Dragusanu (2000). "JNdi-1: a neodymium isotopic reference in consistency with LaJolla neodymium." Chemical Geology **168**(3): 279-281.

Tessier, A., P. G. C. Campbell and M. Bisson (1979). "Sequential extraction procedure for the speciation of particulate trace metals." Analytical Chemistry **51**(7): 844-851.

Thirlwall, M. F. (2002). "Multicollector ICP-MS analysis of Pb isotopes using a 207pb-204pb double spike demonstrates up to 400 ppm/amu systematic errors in Tl-normalization." Chemical Geology **184**(3): 255-279.

Toggweiler, J. R. (1999). "Variation of atmospheric CO2 by ventilation of the ocean's deepest water." Paleoceanography **14**(5): 571-588.

Vallelonga, P., P. Gabrielli, E. Balliana, A. Wegner, B. Delmonte, C. Turetta, G. Burton, F. Vanhaecke, K. J. R. Rosman, S. Hong, C. F. Boutron, P. Cescon and C. Barbante (2010). "Lead isotopic compositions in the EPICA Dome C ice core and Southern Hemisphere Potential Source Areas." Quaternary Science Reviews **29**(1): 247-255.

van de Flierdt, T., M. Frank, A. N. Halliday, J. R. Hein, B. Hattendorf, D. Günther and P. W. Kubik (2004). "Deep and bottom water export from the Southern Ocean to the Pacific over the past 38 million years." Paleoceanography **19**(1).

van de Flierdt, T., M. Frank, D.-C. Lee, A. N. Halliday, B. C. Reynolds and J. R. Hein (2004). "New constraints on the sources and behavior of neodymium and hafnium in seawater from Pacific Ocean ferromanganese crusts." Geochimica et Cosmochimica Acta **68**(19): 3827-3843.

van de Flierdt, T., L. F. Robinson and J. F. Adkins (2010). "Deep-sea coral aragonite as a recorder for the neodymium isotopic composition of seawater." Geochimica et Cosmochimica Acta **74**(21): 6014-6032.

van de Flierdt, T., L. F. Robinson, J. F. Adkins, S. R. Hemming and S. L. Goldstein (2006). "Temporal stability of the neodymium isotope signature of the Holocene to glacial North Atlantic." Paleoceanography **21**(4).

van Sebille, E., P. Spence, M. R. Mazloff, M. H. England, S. R. Rintoul and O. A. Saenko (2013). "Abyssal connections of Antarctic Bottom Water in a Southern Ocean State Estimate." Geophysical Research Letters **40**(10): 2177-2182.

Vance, D. and K. Burton (1999). "Neodymium isotopes in planktonic foraminifera: a record of the response of continental weathering and ocean circulation rates to climate change." Earth and Planetary Science Letters **173**(4): 365-379.

Vance, D. and M. Thirlwall (2002). "An assessment of mass discrimination in MC-ICPMS using Nd isotopes." Chemical Geology **185** (3-4): 227-240.

Vincent, E., J. S. Killingley and W. H. Berger (1985). Miocene oxygen and carbon isotope stratigraphy of the tropical Indian Ocean

The Miocene Ocean: Paleoceanography and Biogeography. J. P. Kennett, Geological Society of America. **163:** 0.

von der Heydt, A. and H. A. Dijkstra (2006). "Effect of ocean gateways on the global ocean circulation in the late Oligocene and early Miocene." Paleoceanography **21**(1).

Waelbroeck, C., J. Jouzel1, L. Labeyrie, C. Lorius, M. Labracherie, M. Stiévenard and N. I. Barkov (1995). "A comparison of the Vostok ice deuterium record and series from Southern Ocean core MD 88-770 over the last two glacial-interglacial cycles." Climate Dynamics **12**(2): 113-123.

Watson, A. J. and A. C. N. Garabato (2006). "The role of Southern Ocean mixing and upwelling in glacial-interglacial atmospheric CO2 change." Tellus Series B-Chemical and Physical Meteorology **58**(1): 73-87.

Weber, M. E., P. U. Clark, G. Kuhn, A. Timmermann, D. Sprenk, R. Gladstone, X. Zhang, G. Lohmann, L. Menviel, M. O. Chikamoto, T. Friedrich and C. Ohlwein (2014). "Millennial-scale variability in Antarctic ice-sheet discharge during the last deglaciation." Nature **510**: 134.

Weber, M. E., P. U. Clark, W. Ricken, J. X. Mitrovica, S. W. Hostetler and G. Kuhn (2011). "Interhemispheric Ice-Sheet Synchronicity During the Last Glacial Maximum." Science **334**(6060): 1265-1269.

Wei, R., W. Abouchami, R. Zahn and P. Masque (2016). "Deep circulation changes in the South Atlantic since the Last Glacial Maximum from Nd isotope and multi-proxy records." Earth and Planetary Science Letters **434**: 18-29.

Wilson, D. J., K. C. Crocket, T. van de Flierdt, L. F. Robinson and J. F. Adkins (2014). "Dynamic intermediate ocean circulation in the North Atlantic during Heinrich Stadial 1: A radiocarbon and neodymium isotope perspective." Paleoceanography **29**(11): 1072-1093.

Wilson, D. J., A. Galy, A. M. Piotrowski and V. K. Banakar (2015). "Quaternary climate modulation of Pb isotopes in the deep Indian Ocean linked to the Himalayan chemical weathering." Earth and Planetary Science Letters **424**: 256-268.

Wilson, D. J., A. M. Piotrowski, A. Galy and J. A. Clegg (2013). "Reactivity of neodymium carriers in deep sea sediments: Implications for boundary exchange and paleoceanography." Geochimica et Cosmochimica Acta **109**: 197-221.

Wilson, D. J., T. van de Flierdt and J. F. Adkins (2017). "Lead isotopes in deep-sea coral skeletons: Ground-truthing and a first deglacial Southern Ocean record." Geochimica et Cosmochimica Acta **204**: 350-374.

Wu, J., R. Rember, M. Jin, E. A. Boyle and A. R. Flegal (2010). "Isotopic evidence for the source of lead in the North Pacific abyssal water." Geochimica et Cosmochimica Acta **74**(16): 4629-4638.

Xiao, W., O. Esper and R. Gersonde (2016). "Last Glacial - Holocene climate variability in the Atlantic sector of the Southern Ocean." Quaternary Science Reviews **135**: 115-137.

Xiao, W. S., O. Esper and R. Gersonde (2016). "Last Glacial - Holocene climate variability in the Atlantic sector of the Southern Ocean." Quaternary Science Reviews **135**: 115-137.

Zachos, J., M. Pagani, L. Sloan, E. Thomas and K. Billups (2001). "Trends, Rhythms, and Aberrations in Global Climate 65 Ma to Present." Science **292**(5517): 686-693.

Zweng, M. M., J. R. Reagan, J. I. Antonov, R. A. Locarnini, A. V. Mishonov, T. P. Boyer, H. E. Garcia, O.K. Baranova, D.R. Johnson, D. Seidov and M. M. Biddle (2013). "Salinity." World Ocean Atlas 2013. **2**.

Appendix.

Table 1 The coordinate, water depth and sample depth information of coretop samples in Chapter 3.

Nr.	Latitude, °	Longitude, °	Water Depth, m	Sample depth, cm
PS1010-1	-77.24	-34.54	476	3
PS1012-1	-77.30	-35.81	1021	3
PS1013-1	-77.41	-37.92	1074	2
PS1016-1	-77.28	-40.83	701	2
PS1167-5	-63.96	-44.07	4515	2
PS1202-1	-75.14	-59.64	630	1
PS1207-1	-75.78	-56.86	352	2
PS1210-1	-76.15	-54.42	414	2
PS1215-1	-77.57	-38.55	1108	2
PS1224-3	-70.62	-13.97	2811	7
PS1226-1	-54.53	10.31	4033	2
PS1275-1	-77.53	-46.00	242	2
PS1276-1	-77.65	-44.89	253	3
PS1277-1	-77.53	-43.66	415	3
PS1278-1	-77.54	-42.13	635	2
PS1279-1	-77.31	-40.14	729	2
PS1367-2	-72.33	-16.50	307	4
PS1368-1	-71.75	-18.98	4007	3
PS1370-1	-72.05	-17.44	2279	3
PS1375-2	-72.17	-17.13	1762	2
PS1377-1	-69.27	-10.73	3802	2
PS1380-1	-70.01	-9.99	2062	2
PS1386-1	-68.33	-5.62	4395	2
PS1388-1	-69.03	-5.89	2521	3
PS1398-2	-76.77	-50.57	284	2
PS1423-1	-74.70	-61.32	468	2
PS1435-1	-49.16	15.03	4320	1
PS1436-1	-51.98	15.01	2230	1
PS1442-4	-54.00	11.10	3600	1
PS1448-3	-58.64	7.97	4970	5
PS1451-1	-64.56	5.45	3596	2
PS1461-1	-64.50	3.70	2370	2
PS1498-1	-73.49	-35.53	2825	2
PS1506-2	-68.75	-5.87	2405	2
PS1508-2	-66.99	-32.36	4655	1
PS1575-2	-62.85	-43.34	3461	3
PS1599-1	-74.07	-27.69	2482	2
PS1606-1	-73.50	-34.01	2933	1
PS1607-1	-74.10	-33.68	1610	1
PS1609-2	-74.69	-38.25	423	1
PS1612-1	-74.40	-37.02	815	3
PS1613-2	-74.24	-36.68	1541	1
PS1649-1	-54.91	3.29	2446	4
PS1653-2	-52.21	9.49	3202	2
PS1768-8	-52.59	4.48	3299	2
PS1778-5	-49.01	-12.70	3407	1
PS1780-5	-51.70	-15.30	4280	1
PS1782-5	-55.19	-18.61	5160	2
PS1789-1	-74.24	-27.30	2411	1
PS1790-1	-73.78	-28.50	2598	1
PS1800-2	-70.02	-14.98	4696	2
PS2028-1	-70.01	11.75	209	4
PS2038-2	-69.35	6.29	1603	2
PS2039-1	-69.02	6.23	2073	3
PS2040-2	-68.84	6.24	2625	2
PS2045-3	-69.68	0.93	1392	2
PS2046-1	-69.62	1.04	1798	2
PS2047-3	-69.49	1.21	2375	1
PS2049-4	-69.09	0.89	3264	3
PS2050-1	-68.77	0.87	3903	3
PS2055-2	-68.29	6.25	3606	1
PS2056-1	-68.74	6.13	3060	3
PS2070-1	-65.11	3.62	2611	2
PS2102-2	-53.07	-4.99	2390	2
PS2104-2	-50.74	-3.23	2611	2
PS2319-1	-59.79	-42.68	4323	2
PS2575-5	-59.48	-3.20	5069	2
PS2813-1	-66.73	-50.00	3499	1
PS63/068-1	-61.00	0.01	5427	1
PS97/85-3	-58.35	-62.17	3091	3

Table 2 Pb and Nd isotopic compositions of coretop samples in Chapter 3.

Nr.	$^{206}Pb/^{204}Pb$	$^{207}Pb/^{204}Pb$	$^{208}Pb/^{204}Pb$	$^{208}Pb/^{206}Pb$	$^{207}Pb/^{206}Pb$	$^{208}Pb/^{207}Pb$	$^{143}Nd/^{144}Nd$	ε_{Nd}
PS1010-1	18.39	15.63	38.19	2.08	0.85	2.44	0.512234	-7.9
PS1012-1	18.90	15.67	38.79	2.05	0.83	2.48	0.512219	-8.2
PS1013-1	18.72	15.66	38.63	2.06	0.84	2.47	0.512210	-8.4
PS1016-1	18.64	15.65	38.56	2.07	0.84	2.46	0.512167	-9.2
PS1167-5	18.84	15.66	38.83	2.06	0.83	2.48	0.512259	-7.4
PS1202-1	18.75	15.65	38.73	2.06	0.83	2.47	0.512262	-7.3
PS1207-1	18.75	15.65	38.71	2.06	0.83	2.47	0.512225	-8.1
PS1210-1	18.76	15.66	38.72	2.06	0.83	2.47	0.512208	-8.4
PS1215-1	18.86	15.67	38.78	2.06	0.83	2.48	0.512190	-8.7
PS1224-3	19.28	15.71	39.66	2.06	0.82	2.52	0.512046	-11.5
PS1226-1	18.86	15.67	38.98	2.07	0.83	2.49	0.512348	-5.7
PS1275-1	18.45	15.64	38.42	2.08	0.85	2.46	0.512196	-8.6
PS1276-1	18.49	15.64	38.39	2.08	0.85	2.45	0.512206	-8.4
PS1277-1	19.00	15.68	39.09	2.06	0.83	2.49	0.512057	-11.3
PS1278-1	18.46	15.64	38.42	2.08	0.85	2.46	0.512148	-9.6
PS1279-1	18.82	15.66	38.75	2.06	0.83	2.47	0.512142	-9.7
PS1367-2	18.71	15.66	38.91	2.08	0.84	2.49	0.512221	-8.1
PS1368-1	18.72	15.67	38.93	2.08	0.84	2.48	0.512051	-11.4
PS1370-1	19.02	15.69	39.28	2.06	0.82	2.50	0.512070	-11.1
PS1375-2	19.07	15.69	39.33	2.06	0.82	2.51	0.512101	-10.5
PS1377-1	19.22	15.72	39.66	2.06	0.82	2.52	0.512020	-12.1
PS1380-1	19.26	15.71	39.60	2.06	0.82	2.52	0.512021	-12.0
PS1386-1	19.31	15.71	39.69	2.05	0.81	2.53	0.512023	-12.0
PS1388-1	19.19	15.71	39.59	2.06	0.82	2.52	0.512037	-11.7
PS1398-2	18.85	15.67	38.83	2.06	0.83	2.48	0.512227	-8.0
PS1423-1	18.75	15.65	38.71	2.06	0.83	2.47	0.512248	-7.6
PS1435-1	18.59	15.65	38.57	2.07	0.84	2.46	0.512206	-8.4
PS1436-1	18.80	15.66	38.83	2.07	0.83	2.48	0.512266	-7.3
PS1442-4	18.82	15.66	38.91	2.07	0.83	2.48	0.512376	-5.1
PS1448-3	18.85	15.66	38.88	2.06	0.83	2.48	0.512266	-7.3
PS1451-1	19.06	15.70	39.40	2.07	0.82	2.51	0.512191	-8.7
PS1461-1	18.97	15.69	39.20	2.07	0.83	2.50	0.512129	-9.9
PS1498-1	18.80	15.67	38.82	2.07	0.83	2.48	0.512199	-8.6
PS1506-2	19.30	15.71	39.67	2.06	0.81	2.53	0.512045	-11.6
PS1508-2	18.87	15.67	38.92	2.06	0.83	2.48	0.512189	-8.8
PS1575-2	18.83	15.66	38.82	2.06	0.83	2.48	0.512312	-6.4
PS1599-1	19.12	15.68	39.25	2.05	0.82	2.50	0.512107	-10.3
PS1606-1	19.14	15.70	39.39	2.06	0.82	2.51	0.512097	-10.5
PS1607-1	18.87	15.67	38.87	2.06	0.83	2.48	0.512183	-8.9
PS1609-2	18.66	15.65	38.60	2.07	0.84	2.47	0.512247	-7.6
PS1612-1	18.67	15.65	38.66	2.07	0.84	2.47	0.512195	-8.6
PS1613-2	18.72	15.65	38.66	2.07	0.84	2.47	0.512214	-8.3
PS1649-1	18.90	15.68	38.88	2.06	0.83	2.48	0.512556	-1.6
PS1653-2	18.47	15.64	38.44	2.08	0.85	2.46	0.512296	-6.7
PS1768-8	18.80	15.66	38.85	2.07	0.83	2.48	0.512232	-7.9
PS1778-5	18.85	15.66	38.89	2.06	0.83	2.48	0.512226	-8.0
PS1780-5	18.83	15.66	38.88	2.06	0.83	2.48	0.512240	-7.8
PS1782-5	18.56	15.65	38.60	2.08	0.84	2.47	0.512233	-7.9
PS1789-1	18.42	15.64	38.49	2.09	0.85	2.46	0.512130	-9.9
PS1790-1	19.11	15.68	38.92	2.04	0.82	2.48	0.512221	-8.1
PS1800-2	19.14	15.70	39.44	2.06	0.82	2.51	0.512056	-11.4
PS2028-1	19.62	15.72	40.11	2.04	0.80	2.55	0.512056	-11.4
PS2038-2	19.48	15.70	39.78	2.04	0.81	2.53	0.512017	-12.1
PS2039-1	19.49	15.70	39.83	2.04	0.81	2.54	0.512017	-12.1
PS2040-2	19.16	15.69	39.39	2.06	0.82	2.51	0.512060	-11.3
PS2045-3	19.25	15.69	39.44	2.05	0.82	2.51	0.512044	-11.6
PS2046-1	19.77	15.72	40.11	2.03	0.80	2.55	0.511999	-12.5
PS2047-3	19.46	15.71	39.83	2.05	0.81	2.54	0.512044	-11.6
PS2049-4	19.54	15.71	40.02	2.05	0.80	2.55	0.512043	-11.6
PS2050-1	19.65	15.70	40.13	2.04	0.80	2.56	0.512003	-12.4
PS2055-2	19.60	15.71	39.97	2.04	0.80	2.54	0.512029	-11.9
PS2056-1	19.23	15.70	39.58	2.06	0.82	2.52	0.512047	-11.5
PS2070-1	18.88	15.69	39.11	2.07	0.83	2.49	0.512184	-8.8
PS2102-2	18.03	15.59	37.82	2.10	0.86	2.43	0.512227	-8.0
PS2104-2	18.73	15.66	38.74	2.07	0.84	2.47	0.512213	-8.3
PS2319-1	18.86	15.67	38.91	2.06	0.83	2.48	0.512392	-4.8
PS2575-5	18.92	15.68	39.02	2.06	0.83	2.49	0.512281	-7.0
PS2813-1	18.83	15.66	38.80	2.06	0.83	2.48	0.512223	-8.1
PS63/068-1	18.91	15.67	39.02	2.06	0.83	2.49	0.512208	-8.4
PS97-1	18.79	15.65	38.79	2.06	0.83	2.48	0.512264	-7.3

Table 3 Pb isotopic compositions of CTD seawater and MUC seawater samples in Chapter 3.

Stat.	Depth, m	Lat., °	Long., °	$^{206}Pb/^{204}Pb$	±2SE	$^{207}Pb/^{204}Pb$	±2SE	$^{208}Pb/^{204}Pb$	±2SE	$^{208}Pb/^{206}Pb$	±2SE	$^{207}Pb/^{206}Pb$	±2SE	$^{208}Pb/^{207}Pb$	±2SE
PS111_42-3	150	-76.14	-53.36	18.51	0.01	15.65	0.01	38.59	0.01	2.084	0.000	0.845	0.000	2.466	0.000
PS111_42-3	472	-76.14	-53.36	18.67	0.00	15.65	0.00	38.65	0.01	2.070	0.000	0.838	0.000	2.470	0.000
PS111_42-1	493	-76.14	-53.36	17.83	0.00	15.58	0.00	37.74	0.00	2.117	0.000	0.874	0.000	2.422	0.000
PS111_60-1	20	-77.02	-45.40	18.57	0.01	15.65	0.01	38.62	0.01	2.080	0.000	0.843	0.000	2.468	0.000
PS111_60-1	100	-77.02	-45.40	18.30	0.00	15.62	0.00	38.27	0.01	2.091	0.000	0.854	0.000	2.449	0.000
PS111_60-1	313	-77.02	-45.40	18.65	0.00	15.64	0.00	38.63	0.01	2.071	0.000	0.839	0.000	2.469	0.000
PS111_60-3	330	-77.02	-45.41	17.85	0.00	15.58	0.00	37.77	0.00	2.115	0.000	0.873	0.000	2.423	0.000
PS111_80-1	20	-76.65	-35.43	18.18	0.00	15.61	0.00	38.15	0.01	2.098	0.000	0.859	0.000	2.444	0.000
PS111_80-1	220	-76.65	-35.43	18.53	0.01	15.64	0.01	38.56	0.02	2.080	0.000	0.844	0.000	2.466	0.000
PS111_80-1	490	-76.65	-35.43	18.66	0.00	15.65	0.00	38.61	0.01	2.069	0.000	0.839	0.000	2.467	0.000
PS111_80-1	896	-76.65	-35.43	18.72	0.00	15.65	0.00	38.68	0.01	2.066	0.000	0.836	0.000	2.472	0.000
PS111_80-3	930	-76.64	-35.43	17.86	0.00	15.58	0.00	37.77	0.00	2.115	0.000	0.873	0.000	2.424	0.000

Table 4 Nd isotopic compositions of CTD seawater and MUC seawater samples in Chapter 3.

Stations	Water Depth, m	Latitude, °	Longitude, °	$^{143}Nd/^{144}Nd$	±2SE	ε_{Nd}	±2SE
PS111_42-3	150	-76.14	-53.36	0.512166	0.000012	-9.21	0.23
PS111_42-3	472	-76.14	-53.36	0.512158	0.000011	-9.35	0.22
PS111_42-1	493	-76.14	-53.36	0.512253	0.000048	-7.51	0.94
PS111_60-1	20	-77.02	-45.40	0.512157	0.000011	-9.39	0.21
PS111_60-1	313	-77.02	-45.40	0.512177	0.000012	-8.99	0.24
PS111_60-3	330	-77.02	-45.41	0.512152	0.000041	-9.48	0.81
PS111_80-1	20	-76.65	-35.43	0.512176	0.000016	-9.02	0.31
PS111_80-1	220	-76.65	-35.43	0.512151	0.000016	-9.49	0.30
PS111_80-1	490	-76.65	-35.43	0.512162	0.000011	-9.28	0.22
PS111_80-1	896	-76.65	-35.43	0.512163	0.000014	-9.26	0.28
PS111_80-3	930	-76.64	-35.43	0.512138	0.000029	-9.75	0.56

Table 5 Pb isotopic compositions of MUC porewater samples in Chapter 3.

Stations	Water Depth, m	Latitude, °	Longitude, °	Sample depth, cm	$^{208}Pb/^{206}Pb$	±2SE
PS111_40-2	493	-76.00	-54.24	17	2.050	0.018
PS111_40-2	493	-76.00	-54.24	39	2.065	0.003
PS111_60-2	330	-77.02	-45.41	1	2.087	0.009
PS111_60-2	330	-77.02	-45.41	3	2.067	0.012
PS111_60-2	330	-77.02	-45.41	7	2.055	0.002
PS111_60-2	330	-77.02	-45.41	11	2.050	0.003
PS111_60-2	330	-77.02	-45.41	13	2.050	0.002
PS111_60-2	330	-77.02	-45.41	17	2.052	0.001
PS111_60-2	330	-77.02	-45.41	19	2.052	0.002
PS111_60-2	330	-77.02	-45.41	21	2.056	0.000
PS111_60-2	330	-77.02	-45.41	23	2.056	0.001
PS111_80-3	930	-76.64	-35.43	19	2.061	0.008
PS111_80-3	930	-76.64	-35.43	21	2.062	0.008

Table 6 Pb and Nd isotopic compositions in MUC sediment leacahtes in Chapter 3.

Stations	Water Depth,m	Latitude, °	Longitude, °	Sample depth,cm	$^{206}Pb/^{204}Pb$	±2SE	$^{207}Pb/^{204}Pb$	±2SE	$^{208}Pb/^{204}Pb$	±2SE	$^{208}Pb/^{206}Pb$	±2SE	$^{207}Pb/^{206}Pb$	±2SE	$^{208}Pb/^{207}Pb$	±2SE	$^{143}Nd/^{144}Nd$	±2SE	ε_{Nd}	±2SE
PS111_40-2	493	-76.00	-54.24	1	18.81	0.00	15.66	0.00	38.76	0.00	2.061	0.000	0.832	0.000	2.475	0.000	0.5122074	0.000003	-8.40	0.06
PS111_40-2	493	-76.00	-54.24	3	18.81	0.00	15.66	0.00	38.76	0.00	2.060	0.000	0.832	0.000	2.476	0.000	0.5122040	0.000004	-8.47	0.08
PS111_40-2	493	-76.00	-54.24	5	18.82	0.00	15.66	0.00	38.76	0.00	2.060	0.000	0.832	0.000	2.476	0.000	0.5122005	0.000003	-8.53	0.07
PS111_40-2	493	-76.00	-54.24	7	18.82	0.00	15.66	0.00	38.77	0.00	2.060	0.000	0.832	0.000	2.476	0.000	0.5122037	0.000005	-8.47	0.09
PS111_40-2	493	-76.00	-54.24	9	18.82	0.00	15.66	0.00	38.76	0.00	2.060	0.000	0.832	0.000	2.476	0.000	0.5122070	0.000004	-8.41	0.07
PS111_40-2	493	-76.00	-54.24	11	18.82	0.00	15.66	0.00	38.76	0.00	2.060	0.000	0.832	0.000	2.475	0.000	0.5121849	0.000005	-8.84	0.09
PS111_40-2	493	-76.00	-54.24	13	18.81	0.00	15.66	0.00	38.75	0.00	2.060	0.000	0.832	0.000	2.475	0.000	0.5121748	0.000004	-9.03	0.08
PS111_40-2	493	-76.00	-54.24	15	18.81	0.00	15.66	0.00	38.75	0.00	2.060	0.000	0.832	0.000	2.475	0.000	0.5121972	0.000004	-8.60	0.09
PS111_40-2	493	-76.00	-54.24	17	18.81	0.00	15.66	0.00	38.75	0.00	2.060	0.000	0.832	0.000	2.475	0.000	0.5122126	0.000005	-8.30	0.09
PS111_40-2	493	-76.00	-54.24	19	18.81	0.00	15.66	0.00	38.76	0.00	2.060	0.000	0.832	0.000	2.475	0.000	0.5122100	0.000004	-8.35	0.07
PS111_40-2	493	-76.00	-54.24	21	18.81	0.00	15.66	0.00	38.75	0.00	2.060	0.000	0.832	0.000	2.475	0.000	0.5121945	0.000005	-8.65	0.09
PS111_40-2	493	-76.00	-54.24	23	18.80	0.00	15.66	0.00	38.75	0.00	2.061	0.000	0.833	0.000	2.475	0.000	0.5121812	0.000005	-8.91	0.09
PS111_40-2	493	-76.00	-54.24	25	18.80	0.00	15.66	0.00	38.75	0.00	2.061	0.000	0.833	0.000	2.475	0.000	0.5121838	0.000004	-8.86	0.08
PS111_40-2	493	-76.00	-54.24	27	18.80	0.00	15.66	0.00	38.74	0.00	2.061	0.000	0.833	0.000	2.475	0.000	0.5121940	0.000003	-8.66	0.06
PS111_40-2	493	-76.00	-54.24	29	18.80	0.00	15.66	0.00	38.74	0.00	2.061	0.000	0.833	0.000	2.475	0.000	0.5121753	0.000004	-9.03	0.07
PS111_40-2	493	-76.00	-54.24	31	18.80	0.00	15.65	0.00	38.74	0.00	2.061	0.000	0.833	0.000	2.474	0.000	0.5121920	0.000004	-8.70	0.09
PS111_40-2	493	-76.00	-54.24	33	18.78	0.00	15.66	0.00	38.73	0.00	2.062	0.000	0.834	0.000	2.474	0.000	0.5121815	0.000004	-8.91	0.08
PS111_40-2	493	-76.00	-54.24	35	18.75	0.00	15.65	0.00	38.71	0.00	2.065	0.000	0.835	0.000	2.473	0.000	0.5121915	0.000004	-8.71	0.08
PS111_40-2	493	-76.00	-54.24	37	18.75	0.00	15.65	0.00	38.71	0.00	2.065	0.000	0.835	0.000	2.473	0.000	0.5121930	0.000004	-8.68	0.08
PS111_40-2	493	-76.00	-54.24	39	18.78	0.00	15.65	0.00	38.72	0.00	2.062	0.000	0.834	0.000	2.474	0.000	0.5121966	0.000004	-8.61	0.08
PS111_60-2	330	-77.02	-45.41	1	18.86	0.00	15.67	0.00	38.82	0.00	2.058	0.000	0.831	0.000	2.478	0.000	0.5121946	0.000004	-8.65	0.07
PS111_60-2	330	-77.02	-45.41	3	18.87	0.00	15.67	0.00	38.82	0.00	2.057	0.000	0.830	0.000	2.478	0.000	0.5121885	0.000003	-8.77	0.06
PS111_60-2	330	-77.02	-45.41	5	18.88	0.00	15.67	0.00	38.83	0.00	2.057	0.000	0.830	0.000	2.478	0.000	0.5121940	0.000004	-8.66	0.07
PS111_60-2	330	-77.02	-45.41	7	18.88	0.00	15.67	0.00	38.83	0.00	2.057	0.000	0.830	0.000	2.478	0.000	0.5121983	0.000004	-8.58	0.09
PS111_60-2	330	-77.02	-45.41	9	18.88	0.00	15.67	0.00	38.83	0.00	2.057	0.000	0.830	0.000	2.478	0.000	0.5121981	0.000004	-8.58	0.08
PS111_60-2	330	-77.02	-45.41	11	18.87	0.00	15.67	0.00	38.82	0.00	2.057	0.000	0.830	0.000	2.478	0.000	0.5121965	0.000004	-8.61	0.07
PS111_60-2	330	-77.02	-45.41	13	18.87	0.00	15.67	0.00	38.82	0.00	2.057	0.000	0.830	0.000	2.478	0.000	0.5121972	0.000004	-8.60	0.08
PS111_60-2	330	-77.02	-45.41	15	18.86	0.00	15.67	0.00	38.81	0.00	2.058	0.000	0.830	0.000	2.478	0.000	0.5122031	0.000005	-8.48	0.09
PS111_60-2	330	-77.02	-45.41	17	18.85	0.00	15.66	0.00	38.80	0.00	2.058	0.000	0.831	0.000	2.477	0.000	0.5122118	0.000004	-8.31	0.08
PS111_60-2	330	-77.02	-45.41	19	18.85	0.00	15.66	0.00	38.80	0.00	2.058	0.000	0.831	0.000	2.477	0.000	0.5122055	0.000005	-8.44	0.09
PS111_60-2	330	-77.02	-45.41	21	18.86	0.00	15.66	0.00	38.80	0.00	2.058	0.000	0.831	0.000	2.477	0.000	0.5122032	0.000004	-8.48	0.08
PS111_80-3	930	-76.64	-35.43	1	18.88	0.00	15.67	0.00	38.80	0.002	2.055	0.000	0.830	0.000	2.477	0.000	0.5122055	0.000006	-8.44	0.11
PS111_80-3	930	-76.64	-35.43	3	18.88	0.00	15.66	0.00	38.80	0.001	2.055	0.000	0.830	0.000	2.477	0.000	0.5122000	0.000004	-8.54	0.08
PS111_80-3	930	-76.64	-35.43	5	18.88	0.00	15.66	0.00	38.79	0.002	2.055	0.000	0.830	0.000	2.477	0.000	0.5121997	0.000004	-8.55	0.09
PS111_80-3	930	-76.64	-35.43	7	18.88	0.00	15.66	0.00	38.79	0.001	2.054	0.000	0.830	0.000	2.476	0.000	0.5122020	0.000004	-8.50	0.09
PS111_80-3	930	-76.64	-35.43	9	18.88	0.00	15.66	0.00	38.79	0.002	2.054	0.000	0.830	0.000	2.476	0.000	0.5122034	0.000004	-8.48	0.08
PS111_80-3	930	-76.64	-35.43	11	18.88	0.00	15.66	0.00	38.76	0.002	2.053	0.000	0.830	0.000	2.475	0.000	0.5121984	0.000003	-8.58	0.06
PS111_80-3	930	-76.64	-35.43	13	18.87	0.00	15.66	0.00	38.75	0.001	2.053	0.000	0.830	0.000	2.474	0.000	0.5121909	0.000004	-8.72	0.08
PS111_80-3	930	-76.64	-35.43	15	18.91	0.00	15.67	0.00	38.80	0.002	2.051	0.000	0.828	0.000	2.476	0.000	0.5122013	0.000004	-8.52	0.07
PS111_80-3	930	-76.64	-35.43	17	18.90	0.00	15.67	0.00	38.77	0.002	2.052	0.000	0.829	0.000	2.475	0.000	0.5121930	0.000005	-8.68	0.09
PS111_80-3	930	-76.64	-35.43	19	18.85	0.00	15.67	0.00	38.70	0.001	2.053	0.000	0.831	0.000	2.471	0.000	0.5121617	0.000005	-9.29	0.09
PS111_80-3	930	-76.64	-35.43	21	18.84	0.00	15.67	0.00	38.67	0.002	2.053	0.000	0.831	0.000	2.469	0.000	0.5121432	0.000004	-9.65	0.07
PS111_80-3	930	-76.64	-35.43	23	19.08	0.00	15.69	0.00	38.92	0.002	2.040	0.000	0.822	0.000	2.481	0.000	0.5121196	0.000004	-10.11	0.07
PS111_80-3	930	-76.64	-35.43	25	19.10	0.00	15.69	0.00	38.95	0.002	2.039	0.000	0.821	0.000	2.482	0.000	0.5121090	0.000004	-10.32	0.07
PS111_80-3	930	-76.64	-35.43	27	19.06	0.00	15.69	0.00	38.90	0.002	2.041	0.000	0.823	0.000	2.480	0.000	0.5121225	0.000004	-10.06	0.07

Table 7 Effect of $MgCl_2$ pre-wash on normalized element concentrations, Pb and Nd isotopic compositions in sediment leacahtes in Chapter 3.

Nr.	Stations	$MgCl_2$ pre-wash	$^{206}Pb/^{204}Pb$	±2SE	$^{207}Pb/^{204}Pb$	±2SE	$^{208}Pb/^{204}Pb$	±2SE	$^{208}Pb/^{206}Pb$	±2SE	$^{207}Pb/^{206}Pb$	±2SE	$^{208}Pb/^{207}Pb$	±2SE	$^{143}Nd/^{144}Nd$	±2SE	ε_{Nd}	±2SE	Al, µg/g	Nd, ng/g	Pb, ng/g	Al/Nd	Al/Pb
S1	PS1377-1	Yes	19.22	0.00	15.71	0.00	39.65	0.00	2.06	0.00	0.82	0.00	2.52	0.00	0.5120495	0.000005	-8.40	0.06	260	1686	1583	154	164
		No	19.22	0.00	15.71	0.00	39.65	0.00	2.06	0.00	0.82	0.00	2.52	0.00	0.5120474	0.000004	-8.47	0.08	191	1325	1563	144	122
S2	PS1398-2	Yes	18.84	0.00	15.66	0.00	38.80	0.00	2.06	0.00	0.83	0.00	2.48	0.00	0.5122558	0.000005	-8.53	0.07	28	374	622	75	45
		No	18.86	0.00	15.67	0.00	38.83	0.00	2.06	0.00	0.83	0.00	2.48	0.00	0.5122423	0.000004	-8.47	0.09	33	363	740	90	44
S3	PS1768-8	Yes	18.82	0.00	15.66	0.00	38.85	0.00	2.06	0.00	0.83	0.00	2.48	0.00	0.5122353	0.000005	-8.41	0.07	54	966	555	56	98
		No	18.82	0.00	15.66	0.00	38.86	0.00	2.06	0.00	0.83	0.00	2.48	0.00	0.5122412	0.000004	-8.84	0.09	36	873	564	41	63
S4	PS2070-1	Yes	18.69	0.00	15.67	0.00	38.84	0.00	2.08	0.00	0.84	0.00	2.48	0.00	0.5121978	0.000005	-9.03	0.08	16	2230	1214	7	13
		No	18.92	0.00	15.69	0.00	39.14	0.00	2.07	0.00	0.83	0.00	2.50	0.00	0.5121963	0.000003	-8.60	0.09	7	2180	1112	3	7
S5	PS2319-1	Yes	18.85	0.00	15.67	0.00	38.90	0.00	2.06	0.00	0.83	0.00	2.48	0.00	0.5124787	0.000005	-8.30	0.09	95	542	884	175	107
		No	18.87	0.00	15.67	0.00	38.93	0.00	2.06	0.00	0.83	0.00	2.48	0.00	0.5124757	0.000003	-8.35	0.07	108	543	1063	198	101
S6	PS2575-5	Yes	18.90	0.00	15.67	0.00	38.99	0.00	2.06	0.00	0.83	0.00	2.49	0.00	0.5123297	0.000004	-8.65	0.09	417	957	3565	436	117
		No	18.91	0.00	15.67	0.00	39.00	0.00	2.06	0.00	0.83	0.00	2.49	0.00	0.5122973	0.000003	-8.91	0.09	311	911	3559	341	87
S7	NOD-A-1	Yes	18.96	0.00	15.68	0.00	38.95	0.00	2.05	0.00	0.83	0.00	2.48	0.00	0.5121576	0.000006	-8.86	0.08	408	14100	5114	29	80
		No	18.97	0.00	15.69	0.00	38.95	0.00	2.05	0.00	0.83	0.00	2.48	0.00	0.5121472	0.000003	-8.66	0.06	474	14762	4755	32	100

Table 8 Effect of chelating ligands on normalized element concentrations, Pb and Nd isotopic compositions in sediment leacahtes in Chapter 3.

Nr.	Stations	ligand	$^{206}Pb/^{204}Pb$	±2SE	$^{207}Pb/^{204}Pb$	±2SE	$^{208}Pb/^{204}Pb$	±2SE	$^{208}Pb/^{206}Pb$	±2SE	$^{207}Pb/^{206}Pb$	±2SE	$^{208}Pb/^{207}Pb$	±2SE	$^{143}Nd/^{144}Nd$	±2SE	ε_{Nd}	±2SE	Al, µg/g	Nd, ng/g	Pb, ng/g	Al/Nd	Al/Pb
S1	PS1377-1	EDTA	19.22	0.00	15.71	0.00	39.65	0.00	2.06	0.00	0.82	0.00	2.52	0.00	0.5120202	0.000003	-12.1	0.1	260	1686	1583	154	164
		DTPA	19.22	0.00	15.72	0.00	39.67	0.00	2.06	0.00	0.82	0.00	2.52	0.00	0.5120167	0.000004	-12.1	0.1	113	1137	1224	99	92
		none	19.23	0.00	15.72	0.00	39.68	0.00	2.06	0.00	0.82	0.00	2.52	0.00	0.5120147	0.000007	-12.2	0.1	43	184	54	231	787
S2	PS1398-2	EDTA	18.86	0.00	15.67	0.00	38.83	0.00	2.06	0.00	0.83	0.00	2.48	0.00	0.5122269	0.000004	-8.0	0.1	28	374	622	75	45
		DTPA	18.84	0.00	15.67	0.00	38.82	0.00	2.06	0.00	0.83	0.00	2.48	0.00	0.5122134	0.000004	-8.3	0.1	50	280	690	180	73
		none	18.86	0.00	15.68	0.00	39.07	0.00	2.07	0.00	0.83	0.00	2.49	0.00	0.5122365	0.000013	-7.8	0.3	20	59	158	332	124
S3	PS1768-8	EDTA	18.80	0.00	15.66	0.00	38.85	0.00	2.07	0.00	0.83	0.00	2.48	0.00	0.5122320	0.000004	-7.9	0.1	54	966	555	56	98
		DTPA	18.78	0.00	15.66	0.00	38.82	0.00	2.07	0.00	0.83	0.00	2.48	0.00	0.5122358	0.000004	-7.8	0.1	31	875	422	35	73
		none	18.80	0.00	15.66	0.00	38.84	0.00	2.07	0.00	0.83	0.00	2.48	0.00	0.5122358	0.000004	-7.8	0.1	29	508	238	58	123
S4	PS2070-1	EDTA	18.92	0.00	15.69	0.00	39.14	0.00	2.07	0.00	0.83	0.00	2.50	0.00	0.5121844	0.000004	-8.8	0.1	16	2230	1214	7	13
		DTPA	18.76	0.00	15.67	0.00	38.82	0.08	2.07	0.00	0.84	0.00	2.48	0.00	0.5121915	0.000004	-8.7	0.1	16	1956	998	8	16
		none	18.68	0.00	15.66	0.00	38.61	0.00	2.07	0.00	0.84	0.00	2.47	0.00	0.5121870	0.000002	-8.8	0.0	6	2405	635	2	9
S5	PS2319-1	EDTA	18.87	0.00	15.67	0.00	38.93	0.00	2.06	0.00	0.83	0.00	2.48	0.00	0.5123924	0.000005	-4.8	0.1	95	542	884	175	107
		DTPA	18.87	0.00	15.67	0.00	38.92	0.00	2.06	0.00	0.83	0.00	2.48	0.00	0.5124048	0.000006	-4.5	0.1	153	352	770	435	199
		none	18.86	0.00	15.67	0.00	38.93	0.00	2.06	0.00	0.83	0.00	2.48	0.00	0.5124048	0.000006	-4.5	0.1	58	103	97	560	596
S6	PS2575-5	EDTA	18.91	0.00	15.67	0.00	39.00	0.00	2.06	0.00	0.83	0.00	2.49	0.00	0.5122814	0.000004	-7.0	0.1	417	957	3565	436	117
		DTPA	18.92	0.00	15.67	0.00	39.01	0.00	2.06	0.00	0.83	0.00	2.49	0.00	0.5122687	0.000004	-7.2	0.1	123	422	1328	290	92
		none	18.92	0.00	15.68	0.00	39.03	0.00	2.06	0.00	0.83	0.00	2.49	0.00	0.5122908	0.000006	-6.8	0.1	48	69	150	705	322
S7	NOD-A-1	EDTA	18.97	0.00	15.69	0.00	38.96	0.00	2.05	0.00	0.83	0.00	2.48	0.00	0.5121435	0.000004	-9.6	0.1	408	5223	24917	78	16
		DTPA	18.97	0.00	15.70	0.00	38.99	0.00	2.05	0.00	0.83	0.00	2.48	0.00	0.5121476	0.000004	-9.6	0.1	62	4860	373	13	166
		none	18.97	0.00	15.69	0.00	38.95	0.00	2.05	0.00	0.83	0.00	2.48	0.00	0.5121464	0.000004	-9.6	0.1	71	1542	7	46	10122

Table 9 Effect of leaching time on normalized element concentrations, Pb and Nd isotopic compositions in sediment leacahtes in Chapter 3.

Nr.	Stations	Leaching time	$^{206}Pb/^{204}Pb$	±2SE	$^{207}Pb/^{204}Pb$	±2SE	$^{208}Pb/^{204}Pb$	±2SE	$^{208}Pb/^{206}Pb$	±2SE	$^{207}Pb/^{206}Pb$	±2SE	$^{207}Pb/^{206}Pb$	±2SE	$^{143}Nd/^{144}Nd$	±2SE	ε_{Nd}	±2SE	Al, µg/g	Nd, ng/g	Pb, ng/g	Al/Nd	Al/Pb
S1	PS1377-1	10 seconds	19.22	0.00	15.72	0.00	39.66	0.00	2.06	0.00	0.82	0.00	2.52	0.00	0.5120202	0.000003	-12.1	0.1	135	1117	1197	120	112
		30 minutes	19.22	0.00	15.71	0.00	39.65	0.00	2.06	0.00	0.82	0.00	2.52	0.00	0.5120474	0.000004	-11.5	0.1	191	1325	1563	144	122
		60 minutes	19.35	0.00	15.72	0.00	39.77	0.00	2.06	0.00	0.81	0.00	2.53	0.00	0.5120906	0.000004	-10.7	0.1	138	1066	369	129	373
		180 minutes	19.51	0.00	15.73	0.00	39.89	0.00	2.05	0.00	0.81	0.00	2.54	0.00	0.5120631	0.000004	-11.2	0.1	115	1244	175	92	653
S2	PS1398-2	10 seconds	18.85	0.00	15.67	0.00	38.83	0.00	2.06	0.00	0.83	0.00	2.48	0.00	0.5122269	0.000004	-8.0	0.1	117	301	743	387	157
		30 minutes	18.86	0.00	15.67	0.00	38.83	0.00	2.06	0.00	0.83	0.00	2.48	0.00	0.5122423	0.000004	-7.7	0.1	33	363	740	90	44
		60 minutes	18.95	0.00	15.67	0.00	38.97	0.00	2.06	0.00	0.83	0.00	2.49	0.00	0.5123130	0.000004	-6.3	0.1	46	274	132	167	346
		180 minutes	19.00	0.00	15.68	0.00	39.01	0.00	2.05	0.00	0.83	0.00	2.49	0.00	0.5123054	0.000008	-6.5	0.2	42	277	58	153	726
S3	PS1768-8	10 seconds	18.80	0.00	15.66	0.00	38.85	0.00	2.07	0.00	0.83	0.00	2.48	0.00	0.5122320	0.000004	-7.9	0.1	31	940	478	33	64
		30 minutes	18.82	0.00	15.66	0.00	38.86	0.00	2.06	0.00	0.83	0.00	2.48	0.00	0.5122412	0.000004	-7.7	0.1	36	873	564	41	63
		60 minutes	18.83	0.00	15.66	0.00	38.87	0.00	2.06	0.00	0.83	0.00	2.48	0.00	0.5124043	0.000008	-4.6	0.2	59	101	59	579	1000
		180 minutes	18.83	0.00	15.66	0.00	38.88	0.00	2.06	0.00	0.83	0.00	2.48	0.00	0.5126620	0.000013	0.5	0.3	57	80	3	715	16555
S4	PS2070-1	10 seconds	18.88	0.00	15.69	0.00	39.11	0.00	2.07	0.00	0.83	0.00	2.49	0.00	0.5121844	0.000004	-8.8	0.1	20	1746	949	11	21
		30 minutes	18.92	0.00	15.69	0.00	39.14	0.00	2.07	0.00	0.83	0.00	2.50	0.00	0.5121963	0.000003	-8.6	0.1	7	2180	1112	3	7
		60 minutes	18.94	0.00	15.69	0.00	39.17	0.00	2.07	0.00	0.83	0.00	2.50	0.00	0.5121952	0.000007	-8.6	0.1	40	263	333	152	120
		180 minutes	18.98	0.00	15.69	0.00	39.25	0.00	2.07	0.00	0.83	0.00	2.50	0.00	0.5120152	0.000010	-12.1	0.2	102	115	156	887	656
S5	PS2319-1	10 seconds	18.86	0.00	15.67	0.00	38.91	0.00	2.06	0.00	0.83	0.00	2.48	0.00	0.5123924	0.000005	-4.8	0.1	157	332	840	473	187
		30 minutes	18.87	0.00	15.67	0.00	38.93	0.00	2.06	0.00	0.83	0.00	2.48	0.00	0.5124757	0.000003	-3.2	0.1	108	543	1063	198	101
		60 minutes	18.89	0.00	15.67	0.00	38.96	0.00	2.06	0.00	0.83	0.00	2.49	0.00	0.5125216	0.000006	-2.3	0.1	84	293	240	288	351
		180 minutes	18.90	0.00	15.67	0.00	38.96	0.00	2.06	0.00	0.83	0.00	2.49	0.00	0.5124883	0.000009	-2.9	0.2	80	221	214	359	372
S6	PS2575-5	10 seconds	18.92	0.00	15.68	0.00	39.02	0.00	2.06	0.00	0.83	0.00	2.49	0.00	0.5122814	0.000004	-7.0	0.1	151	518	2085	292	72
		30 minutes	18.91	0.00	15.67	0.00	39.00	0.00	2.06	0.00	0.83	0.00	2.49	0.00	0.5122973	0.000003	-6.6	0.1	311	911	3559	341	87
		60 minutes	18.92	0.00	15.68	0.00	39.02	0.00	2.06	0.00	0.83	0.00	2.49	0.00	0.5122966	0.000004	-6.7	0.1	295	402	868	733	340
		180 minutes	18.91	0.00	15.68	0.00	39.02	0.00	2.06	0.00	0.83	0.00	2.49	0.00	0.5121693	0.000007	-9.1	0.1	258	304	365	850	708
S7	Nod-A-1	10 seconds	18.97	0.00	15.69	0.00	38.96	0.00	2.05	0.00	0.83	0.00	2.48	0.00	0.5121435	0.000004	-9.6	0.1	88	4477	5481	20	16
		30 minutes	18.97	0.00	15.69	0.00	38.95	0.00	2.05	0.00	0.83	0.00	2.48	0.00	0.5121472	0.000003	-9.6	0.1	474	14762	4755	32	100
		60 minutes	18.97	0.00	15.69	0.00	38.98	0.00	2.05	0.00	0.83	0.00	2.48	0.00	0.5121560	0.000004	-9.4	0.1	767	5049	509	152	1506
		180 minutes	18.97	0.00	15.69	0.00	38.97	0.00	2.05	0.00	0.83	0.00	2.48	0.00	0.5121558	0.000003	-9.4	0.1	969	7361	109	132	8883

Table 10 Seawater Pb concentration data of PS111 stations in Chapter 3.

Station	Latitude, °	Longitude, °	Water Depth, m	Pb concentration, pmol/kg	Reference
PS111_09-3	-64.0	5.0	2000	16	Chapter 3
PS111_09-3	-64.0	5.0	3000	24	Chapter 3
PS111_09-3	-64.0	5.0	3500	15	Chapter 3
PS111_09-3	-64.0	5.0	3800	16	Chapter 3
PS111_100-1	-77.2	-42.9	20	15	Chapter 3
PS111_100-1	-77.2	-42.9	260	18	Chapter 3
PS111_100-1	-77.2	-42.9	448	36	Chapter 3
PS111_12-2	-66.7	0.0	100	12	Chapter 3
PS111_12-2	-66.7	0.0	1000	20	Chapter 3
PS111_12-2	-66.7	0.0	2000	10	Chapter 3
PS111_12-2	-66.7	0.0	3000	29	Chapter 3
PS111_12-2	-66.7	0.0	3500	10	Chapter 3
PS111_12-2	-66.7	0.0	4200	15	Chapter 3
PS111_12-2	-66.7	0.0	4550	17	Chapter 3
PS111_12-2	-66.7	0.0	4654	12	Chapter 3
PS111_123-1	-74.9	-31.0	40	59	Chapter 3
PS111_123-1	-74.9	-31.0	140	74	Chapter 3
PS111_123-1	-74.9	-31.0	500	10	Chapter 3
PS111_123-1	-74.9	-31.0	543	19	Chapter 3
PS111_128-1	-74.6	-34.3	20	14	Chapter 3
PS111_128-1	-74.6	-34.3	330	14	Chapter 3
PS111_128-1	-74.6	-34.3	528	21	Chapter 3
PS111_131-1	-74.6	-36.9	25	21	Chapter 3
PS111_131-1	-74.6	-36.9	310	14	Chapter 3
PS111_131-1	-74.6	-36.9	368	15	Chapter 3
PS111_132-1	-74.0	-32.4	20	12	Chapter 3
PS111_132-1	-74.0	-32.4	860	30	Chapter 3
PS111_132-1	-74.0	-32.4	1200	274	Chapter 3
PS111_132-1	-74.0	-32.4	1500	770	Chapter 3
PS111_132-1	-74.0	-32.4	1747	11	Chapter 3
PS111_133-1	-75.0	-29.5	30	80	Chapter 3
PS111_133-1	-75.0	-29.5	160	20	Chapter 3
PS111_133-1	-75.0	-29.5	385	446	Chapter 3
PS111_135-1	-75.1	-28.3	20	9	Chapter 3
PS111_135-1	-75.1	-28.3	200	24	Chapter 3
PS111_135-1	-75.1	-28.3	400	14	Chapter 3
PS111_135-1	-75.1	-28.3	462	446	Chapter 3
PS111_141-1	-75.5	-26.9	10	102	Chapter 3
PS111_141-1	-75.5	-26.9	0	162	Chapter 3
PS111_147-1	-63.6	-48.7	30	15	Chapter 3
PS111_147-1	-63.6	-48.7	1300	180	Chapter 3
PS111_147-1	-63.6	-48.7	2200	691	Chapter 3
PS111_147-1	-63.6	-48.7	2800	38	Chapter 3
PS111_147-1	-63.6	-48.7	3000	14	Chapter 3
PS111_147-1	-63.6	-48.7	3200	53	Chapter 3
PS111_147-1	-63.6	-48.7	3276	20	Chapter 3
PS111_16-1	-72.4	-17.8	150	16	Chapter 3
PS111_16-1	-72.4	-17.8	1000	14	Chapter 3
PS111_16-1	-72.4	-17.8	1360	29	Chapter 3
PS111_17-4	-73.7	-25.7	20	18	Chapter 3
PS111_17-4	-73.7	-25.7	300	7	Chapter 3
PS111_17-4	-73.7	-25.7	1100	14	Chapter 3
PS111_17-4	-73.7	-25.7	1800	18	Chapter 3
PS111_17-4	-73.7	-25.7	2500	18	Chapter 3
PS111_17-4	-73.7	-25.7	2900	13	Chapter 3
PS111_17-4	-73.7	-25.7	3170	11	Chapter 3
PS111_18-1	-76.2	-30.0	20	10	Chapter 3
PS111_18-1	-76.2	-30.0	390	9	Chapter 3
PS111_23-1	-76.0	-32.0	20	6	Chapter 3
PS111_23-1	-76.0	-32.0	200	60	Chapter 3
PS111_23-1	-76.0	-32.0	500	14	Chapter 3
PS111_23-1	-76.0	-32.0	716	13	Chapter 3
PS111_29-1	-76.0	-27.7	20	55	Chapter 3
PS111_29-1	-76.0	-27.7	200	18	Chapter 3
PS111_29-1	-76.0	-27.7	390	8	Chapter 3
PS111_33-1	-74.8	-32.5	140	52	Chapter 3
PS111_33-1	-74.8	-32.5	360	13	Chapter 3
PS111_33-1	-74.8	-32.5	480	11	Chapter 3
PS111_33-1	-74.8	-32.5	576	10	Chapter 3
PS111_35-2	-76.7	-52.1	50	8	Chapter 3
PS111_35-2	-76.7	-52.1	285	42	Chapter 3
PS111_37-2	-76.5	-52.6	1	11	Chapter 3
PS111_37-2	-76.5	-52.6	50	8	Chapter 3
PS111_37-2	-76.5	-52.6	260	29	Chapter 3
PS111_37-2	-76.5	-52.6	376	11	Chapter 3
PS111_39-1	-76.0	-54.7	20	16	Chapter 3
PS111_39-1	-76.0	-54.7	240		Chapter 3
PS111_39-1	-76.0	-54.7	479	13	Chapter 3
PS111_42-3	-76.1	-53.4	150	18	Chapter 3

PS111_42-3	-76.1	-53.4	472	13	Chapter 3
PS111_46-1	-75.3	-58.6	100	8	Chapter 3
PS111_46-1	-75.3	-58.6	320	17	Chapter 3
PS111_46-1	-75.3	-58.6	599	14	Chapter 3
PS111_48-1	-74.8	-60.8	25	15	Chapter 3
PS111_48-1	-74.8	-60.8	200	10	Chapter 3
PS111_48-1	-74.8	-60.8	616	11	Chapter 3
PS111_52-1	-75.4	-57.7	20	7	Chapter 3
PS111_52-1	-75.4	-57.7	140	11	Chapter 3
PS111_52-1	-75.4	-57.7	360	38	Chapter 3
PS111_52-1	-75.4	-57.7	529	13	Chapter 3
PS111_55-1	-76.9	-50.9	50	25	Chapter 3
PS111_55-1	-76.9	-50.9	276	8	Chapter 3
PS111_58-1	-77.1	-48.4	30	12	Chapter 3
PS111_58-1	-77.1	-48.4	237	35	Chapter 3
PS111_60-1	-77.0	-45.4	20	7	Chapter 3
PS111_60-1	-77.0	-45.4	100	19	Chapter 3
PS111_60-1	-77.0	-45.4	313	10	Chapter 3
PS111_63-1	-75.3	-41.1	20	16	Chapter 3
PS111_63-1	-75.3	-41.1	100	15	Chapter 3
PS111_63-1	-75.3	-41.1	357	21	Chapter 3
PS111_64-2	-75.6	-39.7	60	31	Chapter 3
PS111_64-2	-75.6	-39.7	190	40	Chapter 3
PS111_67-1	-76.1	-36.6	80	37	Chapter 3
PS111_67-1	-76.1	-36.6	260	19	Chapter 3
PS111_67-1	-76.1	-36.6	540	25	Chapter 3
PS111_67-1	-76.1	-36.6	650	22	Chapter 3
PS111_70-1	-76.1	-33.7	10	17	Chapter 3
PS111 70-1	-76.1	-33.7	220	37	Chapter 3
PS111_70-1	-76.1	-33.7	380	51	Chapter 3
PS111_70-1	-76.1	-33.7	756	20	Chapter 3
PS111_80-1	-76.6	-35.4	220	12	Chapter 3
PS111_80-1	-76.6	-35.4	490	16	Chapter 3
PS111_80-1	-76.6	-35.4	896	20	Chapter 3
PS111_91-1	-77.9	-37.2	20	13	Chapter 3
PS111_91-1	-77.9	-37.2	300	35	Chapter 3
PS111_91-1	-77.9	-37.2	660	19	Chapter 3
PS111_91-1	-77.9	-37.2	1078	21	Chapter 3
PS111_94-1	-77.8	-39.2	20	13	Chapter 3
PS111_94-1	-77.8	-39.2	300	19	Chapter 3
PS111_94-1	-77.8	-39.2	660	60	Chapter 3
PS111_94-1	-77.8	-39.2	1078	35	Chapter 3
PS111_97-1	-77.8	-41.3	20	31	Chapter 3
PS111_97-1	-77.8	-41.3	300	17	Chapter 3
PS111_97-1	-77.8	-41.3	569	26	Chapter 3
PS111_97-1	-77.8	-41.3	805	40	Chapter 3
GIPY04	-57.6	0.0	30.3	31	Schlitzer et al. 2018
GIPY04	-57.6	0.0	60.6	20	Schlitzer et al. 2018
GIPY04	-57.6	0.0	121.2	27	Schlitzer et al. 2018
GIPY04	-57.6	0.0	141.4	23	Schlitzer et al. 2018
GIPY04	-57.6	0.0	252.5	24	Schlitzer et al. 2018
GIPY04	-57.6	0.0	555.9	26	Schlitzer et al. 2018
GIPY04	-57.6	0.0	809	27	Schlitzer et al. 2018
GIPY04	-57.6	0.0	1265.5	18	Schlitzer et al. 2018
GIPY04	-57.6	0.0	1722.9	24	Schlitzer et al. 2018
GIPY04	-57.6	0.0	2181.3	17	Schlitzer et al. 2018
GIPY04	-57.6	0.0	2640.7	26	Schlitzer et al. 2018
GIPY04	-57.6	0.0	3101.1	17	Schlitzer et al. 2018
GIPY04	-57.6	0.0	3562.3	17	Schlitzer et al. 2018
GIPY04	-57.6	0.0	3911.5	21	Schlitzer et al. 2018
GIPY04	-55.3	0.0	30	12	Schlitzer et al. 2018
GIPY04	-55.3	0.0	61	12	Schlitzer et al. 2018
GIPY04	-55.3	0.0	101	12	Schlitzer et al. 2018
GIPY04	-55.3	0.0	121	12	Schlitzer et al. 2018
GIPY04	-55.3	0.0	202	12	Schlitzer et al. 2018
GIPY04	-55.3	0.0	303	11	Schlitzer et al. 2018
GIPY04	-55.3	0.0	657	9	Schlitzer et al. 2018
GIPY04	-55.3	0.0	1012	7	Schlitzer et al. 2018
GIPY04	-55.3	0.0	1519	7	Schlitzer et al. 2018
GIPY04	-55.3	0.0	2130	9	Schlitzer et al. 2018

Table 11 Nd isotope results extracted from PS1768-8 in the Chapter 4.

Depth, cm	Age, kyr	Material	$^{143}Nd/^{144}Nd$	±2SE	ε_{Nd}	±2SE
0	0.0	sediment	0.512232	0.000004	-7.91	0.07
2	0.4	sediment	0.512234	0.000005	-7.88	0.10
4	0.7	sediment	0.512246	0.000003	-7.64	0.06
6	1.1	sediment	0.512249	0.000003	-7.59	0.06
8	1.5	sediment	0.512248	0.000003	-7.61	0.06
10	1.9	sediment	0.512239	0.000004	-7.79	0.08
12	2.2	sediment	0.512250	0.000004	-7.57	0.08
14	2.6	sediment	0.512243	0.000004	-7.70	0.07
16	3.0	sediment	0.512245	0.000003	-7.67	0.07
18	3.4	sediment	0.512244	0.000004	-7.69	0.08
20	3.7	sediment	0.512246	0.000004	-7.65	0.07
22	4.1	sediment	0.512254	0.000003	-7.49	0.06
24	4.5	sediment	0.512261	0.000004	-7.36	0.08
26	4.8	sediment	0.512266	0.000005	-7.25	0.09
28	5.2	sediment	0.512262	0.000003	-7.34	0.06
30	5.6	sediment	0.512259	0.000004	-7.39	0.08
32	6.0	sediment	0.512259	0.000004	-7.39	0.08
34	6.3	sediment	0.512263	0.000003	-7.32	0.06
36	6.7	sediment	0.512264	0.000003	-7.30	0.06
38	7.1	sediment	0.512267	0.000004	-7.23	0.07
40	7.5	sediment	0.512273	0.000004	-7.12	0.08
42	7.8	sediment	0.512268	0.000003	-7.21	0.06
44	8.2	sediment	0.512261	0.000003	-7.35	0.06
46	8.6	sediment	0.512260	0.000004	-7.37	0.07
48	8.9	sediment	0.512255	0.000012	-7.48	0.24
50	9.3	sediment	0.512261	0.000010	-7.35	0.19
52	9.7	sediment	0.512252	0.000004	-7.53	0.08
54	10.1	sediment	0.512257	0.000004	-7.42	0.09
62	10.5	sediment	0.512249	0.000005	-7.59	0.09
70	10.9	sediment	0.512252	0.000003	-7.53	0.06
78	11.3	sediment	0.512256	0.000006	-7.45	0.11
86	11.6	sediment	0.512303	0.000004	-6.53	0.09
94	12.0	sediment	0.512371	0.000005	-5.21	0.10
102	12.3	sediment	0.512405	0.000005	-4.54	0.10
110	12.7	sediment	0.512418	0.000007	-4.28	0.14
118	13.1	sediment	0.512409	0.000008	-4.46	0.16
126	13.4	sediment	0.512403	0.000004	-4.58	0.08
134	13.8	sediment	0.512425	0.000008	-4.16	0.15
142	14.2	sediment	0.512422	0.000004	-4.21	0.07
147	14.6	sediment	0.512440	0.000005	-3.87	0.09
152	15.1	sediment	0.512445	0.000006	-3.77	0.11
157	15.6	sediment	0.512435	0.000005	-3.95	0.10
162	16.1	sediment	0.512431	0.000005	-4.04	0.10
167	16.6	sediment	0.512422	0.000009	-4.21	0.17
172	17.1	sediment	0.512418	0.000008	-4.28	0.15
177	17.6	sediment	0.512429	0.000015	-4.07	0.30
182	18.1	sediment	0.512438	0.000004	-3.90	0.08
187	18.5	sediment	0.512431	0.000004	-4.04	0.08
192	19.0	sediment	0.512452	0.000004	-3.63	0.07
732	116.4	sediment	0.512336	0.000004	-5.89	0.08
737	118.2	sediment	0.512329	0.000005	-6.03	0.10
742	119.9	sediment	0.512328	0.000005	-6.04	0.09
747	121.6	sediment	0.512331	0.000005	-5.99	0.10
752	123.4	sediment	0.512317	0.000005	-6.27	0.10
757	125.1	sediment	0.512310	0.000005	-6.40	0.10
762	126.4	sediment	0.512329	0.000004	-6.02	0.08
767	126.9	sediment	0.512341	0.000004	-5.79	0.08
772	127.4	sediment	0.512356	0.000006	-5.50	0.11
777	127.9	sediment	0.512357	0.000005	-5.49	0.10
782	128.4	sediment	0.512345	0.000007	-5.72	0.13
787	128.9	sediment	0.512328	0.000004	-6.04	0.07
792	129.4	sediment	0.512276	0.000003	-7.06	0.06
797	129.9	sediment	0.512285	0.000004	-6.89	0.08
802	130.8	sediment	0.512345	0.000004	-5.71	0.08
804	131.4	sediment	0.512383	0.000007	-4.97	0.14
807	132.3	sediment	0.512394	0.000009	-4.75	0.17
809	132.9	sediment	0.512414	0.000007	-4.36	0.13
812	133.3	sediment	0.512412	0.000006	-4.42	0.11
814	133.3	sediment	0.512419	0.000006	-4.26	0.12
817	133.5	sediment	0.512416	0.000009	-4.33	0.17
819	133.6	sediment	0.512446	0.000013	-3.74	0.25
822	133.9	sediment	0.512447	0.000007	-3.72	0.14
824	134.2	sediment	0.512473	0.000007	-3.21	0.13
827	134.6	sediment	0.512458	0.000004	-3.51	0.08
829	134.9	sediment	0.512466	0.000004	-3.35	0.08
832	135.3	sediment	0.512452	0.000004	-3.62	0.07
834	135.6	sediment	0.512445	0.000004	-3.77	0.08
842	136.7	sediment	0.512461	0.000003	-3.45	0.07
847	137.4	sediment	0.512470	0.000003	-3.28	0.07
857	138.8	sediment	0.512474	0.000006	-3.20	0.12
867	140.1	sediment	0.512445	0.000005	-3.77	0.10
872	140.8	sediment	0.512409	0.000005	-4.47	0.10
877	141.5	sediment	0.512396	0.000003	-4.72	0.06
882	142.1	sediment	0.512422	0.000005	-4.21	0.09
887	142.8	sediment	0.512419	0.000005	-4.28	0.10
2	0.4	opal	0.512235	0.000007	-7.86	0.13
28	5.2	opal	0.512266	0.000006	-7.26	0.12
86	11.6	opal	0.512288	0.000015	-6.84	0.29
94	12.0	opal	0.512332	0.000013	-5.96	0.26
157	15.6	opal	0.512476	0.000015	-3.15	0.29
782	128.4	opal	0.512327	0.000016	-6.06	0.32
787	128.9	opal	0.512350	0.000012	-5.61	0.23
802	130.8	opal	0.512345	0.000010	-5.71	0.19
817	133.5	opal	0.512454	0.000023	-3.59	0.45
827	134.6	opal	0.512466	0.000015	-3.35	0.29
0	0.0	detrital	0.512477	0.000003	-3.14	0.06
48	8.9	detrital	0.512422	0.000003	-4.21	0.07

86	**11.6**	**detrital**	**0.512483**	**0.000005**	**-3.03**	**0.10**
94	**12.0**	**detrital**	**0.512506**	**0.000005**	**-2.57**	**0.09**
147	**14.6**	**detrital**	**0.512553**	**0.000003**	**-1.66**	**0.05**
172	**17.1**	**detrital**	**0.512470**	**0.000003**	**-3.28**	**0.06**
747	**121.6**	**detrital**	**0.512411**	**0.000004**	**-4.43**	**0.08**
772	**127.4**	**detrital**	**0.512503**	**0.000005**	**-2.63**	**0.09**
792	**129.4**	**detrital**	**0.512420**	**0.000005**	**-4.25**	**0.09**
802	**130.8**	**detrital**	**0.512395**	**0.000006**	**-4.75**	**0.12**
847	**137.4**	**detrital**	**0.512410**	**0.000005**	**-4.44**	**0.10**

Table 12 Nd isotope results extracted from PS1599-3 in Chapter 4.

Depth, cm	Age, kyr	Material	$^{143}Nd/^{144}Nd$	±2SE	ε_{Nd}	±2SE
100	5.7	sediment	0.512241	0.000004	-7.74	0.07
123	7.0	sediment	0.512244	0.000003	-7.69	0.07
149	8.5	sediment	0.512245	0.000003	-7.67	0.07
186	10.6	sediment	0.512241	0.000003	-7.74	0.06
211	12.0	sediment	0.512220	0.000003	-8.16	0.06
236	13.4	sediment	0.512208	0.000003	-8.40	0.06
249	14.2	sediment	0.512236	0.000003	-7.84	0.07
265	15.1	sediment	0.512225	0.000003	-8.06	0.05
275	15.7	sediment	0.512231	0.000003	-7.95	0.07
298	17.0	sediment	0.512227	0.000003	-8.01	0.07
325	18.5	sediment	0.512225	0.000004	-8.06	0.08
350	19.9	sediment	0.512234	0.000003	-7.89	0.06
400	21.7	sediment	0.512223	0.000003	-8.10	0.07
450	22.2	sediment	0.512229	0.000003	-7.98	0.06
500	22.7	sediment	0.512221	0.000003	-8.13	0.06
550	23.1	sediment	0.512224	0.000003	-8.08	0.05
600	23.4	sediment	0.512203	0.000003	-8.49	0.06
650	23.7	sediment	0.512210	0.000003	-8.34	0.06
702	23.9	sediment	0.512215	0.000004	-8.26	0.08
750	24.2	sediment	0.512205	0.000004	-8.45	0.08
800	24.4	sediment	0.512190	0.000004	-8.74	0.08
850	24.6	sediment	0.512206	0.000004	-8.43	0.07

Table 13 Pb isotope results extracted from ODP1094 in Chapter 4.

Depth ,mcd	Age ,kyr	$^{206}Pb/^{204}Pb$	±2SE	$^{207}Pb/^{204}Pb$	±2SE	$^{208}Pb/^{204}Pb$	±2SE	$^{208}Pb/^{206}Pb$	±2SE	$^{207}Pb/^{206}Pb$	±2SE	$^{208}Pb/^{207}Pb$	±2SE
4.13	7.2	18.87	0.00	15.67	0.00	38.91	0.00	2.062	0.000	0.830	0.000	2.484	0.000
4.73	8.2	18.87	0.00	15.67	0.00	38.93	0.00	2.063	0.000	0.830	0.000	2.485	0.000
5.33	9.2	18.87	0.00	15.67	0.00	38.94	0.00	2.063	0.000	0.830	0.000	2.485	0.000
5.78	10.0	18.86	0.00	15.67	0.00	38.93	0.00	2.065	0.000	0.831	0.000	2.485	0.000
5.98	10.3	18.85	0.00	15.67	0.00	38.89	0.00	2.063	0.000	0.831	0.000	2.482	0.000
6.03	10.4	18.85	0.00	15.67	0.00	38.90	0.00	2.064	0.000	0.831	0.000	2.483	0.000
6.23	10.8	18.87	0.00	15.67	0.00	38.95	0.00	2.064	0.000	0.830	0.000	2.486	0.000
6.33	10.9	18.87	0.00	15.67	0.00	38.97	0.00	2.065	0.000	0.830	0.000	2.487	0.000
6.43	11.1	18.88	0.00	15.67	0.00	38.97	0.00	2.065	0.000	0.830	0.000	2.487	0.000
6.53	11.3	18.86	0.00	15.67	0.00	38.93	0.00	2.064	0.000	0.830	0.000	2.485	0.000
6.63	11.4	18.86	0.00	15.67	0.00	38.94	0.00	2.064	0.000	0.830	0.000	2.485	0.000
6.68	11.6	18.85	0.00	15.67	0.00	38.92	0.00	2.064	0.000	0.831	0.000	2.484	0.000
6.73	11.7	18.86	0.00	15.67	0.00	38.92	0.00	2.064	0.000	0.831	0.000	2.485	0.000
6.83	12.0	18.86	0.00	15.67	0.00	38.93	0.00	2.064	0.000	0.831	0.000	2.485	0.000
6.93	12.3	18.86	0.00	15.67	0.00	38.94	0.00	2.065	0.000	0.831	0.000	2.486	0.000
6.98	12.5	18.86	0.00	15.67	0.00	38.94	0.00	2.065	0.000	0.831	0.000	2.485	0.000
7.03	12.6	18.86	0.00	15.66	0.00	38.94	0.00	2.065	0.000	0.831	0.000	2.486	0.000
7.08	12.8	18.86	0.00	15.66	0.00	38.95	0.00	2.065	0.000	0.831	0.000	2.486	0.000
7.13	12.9	18.86	0.00	15.66	0.00	38.95	0.00	2.065	0.000	0.831	0.000	2.486	0.000
7.18	13.1	18.86	0.00	15.67	0.00	38.93	0.00	2.064	0.000	0.831	0.000	2.485	0.000
7.23	13.2	18.86	0.00	15.67	0.00	38.96	0.00	2.065	0.000	0.831	0.000	2.487	0.000
7.28	13.4	18.86	0.00	15.67	0.00	38.95	0.00	2.065	0.000	0.831	0.000	2.487	0.000
7.33	13.5	18.86	0.00	15.67	0.00	38.95	0.00	2.065	0.000	0.831	0.000	2.486	0.000
7.38	13.6	18.86	0.00	15.67	0.00	38.96	0.00	2.065	0.000	0.831	0.000	2.486	0.000
7.43	13.8	18.87	0.00	15.67	0.00	38.98	0.00	2.066	0.000	0.830	0.000	2.488	0.000
7.48	13.9	18.88	0.00	15.67	0.00	39.00	0.00	2.066	0.000	0.830	0.000	2.489	0.000
7.58	14.2	18.87	0.00	15.67	0.00	39.00	0.00	2.067	0.000	0.830	0.000	2.489	0.000
7.63	14.4	18.87	0.00	15.67	0.00	39.00	0.00	2.067	0.000	0.831	0.000	2.489	0.000
7.68	14.5	18.86	0.00	15.67	0.00	38.96	0.00	2.066	0.000	0.831	0.000	2.487	0.000
7.73	14.7	18.87	0.00	15.67	0.00	39.03	0.00	2.068	0.000	0.830	0.000	2.490	0.000
7.78	14.8	18.86	0.00	15.67	0.00	38.97	0.00	2.067	0.000	0.831	0.000	2.488	0.000
7.83	15.0	18.85	0.00	15.67	0.00	38.95	0.00	2.066	0.000	0.831	0.000	2.486	0.000
7.88	15.1	18.85	0.00	15.67	0.00	38.97	0.00	2.068	0.000	0.831	0.000	2.487	0.000
7.93	15.3	18.84	0.00	15.67	0.00	38.96	0.00	2.068	0.000	0.831	0.000	2.487	0.000
7.98	15.4	18.84	0.00	15.67	0.00	38.95	0.00	2.068	0.000	0.832	0.000	2.486	0.000
8.08	15.7	18.82	0.00	15.66	0.00	38.93	0.00	2.068	0.000	0.832	0.000	2.485	0.000
8.13	15.8	18.82	0.00	15.66	0.00	38.92	0.00	2.068	0.000	0.832	0.000	2.485	0.000
8.18	16.0	18.81	0.00	15.66	0.00	38.90	0.00	2.068	0.000	0.833	0.000	2.484	0.000
8.23	16.1	18.81	0.00	15.66	0.00	38.89	0.00	2.068	0.000	0.833	0.000	2.483	0.000
8.28	16.3	18.80	0.00	15.66	0.00	38.87	0.00	2.068	0.000	0.833	0.000	2.482	0.000
8.33	16.4	18.80	0.00	15.66	0.00	38.88	0.00	2.068	0.000	0.833	0.000	2.482	0.000
8.38	16.6	18.78	0.00	15.66	0.00	38.84	0.00	2.068	0.000	0.834	0.000	2.480	0.000
8.43	16.7	18.78	0.00	15.66	0.00	38.83	0.00	2.068	0.000	0.834	0.000	2.480	0.000
8.48	16.9	18.77	0.00	15.66	0.00	38.81	0.00	2.068	0.000	0.834	0.000	2.479	0.000
8.53	17.0	18.77	0.00	15.66	0.00	38.81	0.00	2.068	0.000	0.834	0.000	2.479	0.000
8.58	17.2	18.77	0.00	15.65	0.00	38.80	0.00	2.068	0.000	0.834	0.000	2.479	0.000
8.63	17.3	18.76	0.00	15.65	0.00	38.80	0.00	2.068	0.000	0.834	0.000	2.479	0.000
8.68	17.5	18.76	0.00	15.65	0.00	38.81	0.00	2.068	0.000	0.834	0.000	2.479	0.000
8.74	17.8	18.77	0.00	15.65	0.00	38.79	0.00	2.067	0.000	0.834	0.000	2.478	0.000
8.79	18.0	18.77	0.00	15.65	0.00	38.78	0.00	2.066	0.000	0.834	0.000	2.477	0.000
8.84	18.3	18.76	0.00	15.65	0.00	38.78	0.00	2.067	0.000	0.834	0.000	2.478	0.000
8.94	18.7	18.77	0.00	15.65	0.00	38.76	0.00	2.066	0.000	0.834	0.000	2.477	0.000
8.99	19.0	18.76	0.00	15.65	0.00	38.74	0.00	2.065	0.000	0.834	0.000	2.475	0.000
9.09	19.4	18.78	0.00	15.65	0.00	38.78	0.00	2.065	0.000	0.833	0.000	2.478	0.000
9.24	20.1	18.80	0.00	15.66	0.00	38.81	0.00	2.064	0.000	0.833	0.000	2.479	0.000
9.34	20.6	18.79	0.00	15.65	0.00	38.80	0.00	2.065	0.000	0.833	0.000	2.478	0.000
9.54	21.5	18.78	0.00	15.66	0.00	38.81	0.00	2.066	0.000	0.834	0.000	2.479	0.000
9.59	21.7	18.76	0.00	15.65	0.00	38.79	0.00	2.067	0.000	0.834	0.000	2.478	0.000
9.74	22.4	18.78	0.00	15.66	0.00	38.75	0.00	2.064	0.000	0.834	0.000	2.475	0.000
9.79	22.6	18.76	0.00	15.65	0.00	38.79	0.00	2.067	0.000	0.834	0.000	2.478	0.000
9.94	23.3	18.76	0.00	15.65	0.00	38.78	0.00	2.068	0.000	0.835	0.000	2.478	0.000
9.99	23.5	18.76	0.00	15.65	0.00	38.78	0.00	2.067	0.000	0.834	0.000	2.477	0.000
10.04	23.8	18.79	0.00	15.66	0.00	38.82	0.00	2.066	0.000	0.833	0.000	2.479	0.000
10.09	24.0	18.76	0.00	15.65	0.00	38.76	0.00	2.066	0.000	0.834	0.000	2.476	0.000
10.24	24.7	18.76	0.00	15.65	0.00	38.79	0.00	2.067	0.000	0.834	0.000	2.478	0.000
10.29	24.9	18.76	0.00	15.65	0.00	38.77	0.00	2.067	0.000	0.834	0.000	2.477	0.000
22.32	115.7	18.82	0.00	15.66	0.00	38.81	0.00	2.062	0.000	0.832	0.000	2.478	0.000
22.52	116.8	18.81	0.00	15.66	0.00	38.80	0.00	2.062	0.000	0.832	0.000	2.477	0.000
22.82	118.4	18.83	0.00	15.66	0.00	38.81	0.00	2.061	0.000	0.832	0.000	2.478	0.000
23.02	119.5	18.83	0.00	15.66	0.00	38.86	0.00	2.063	0.000	0.832	0.000	2.481	0.000
23.22	120.6	18.81	0.00	15.66	0.00	38.82	0.00	2.064	0.000	0.832	0.000	2.479	0.000
23.42	121.7	18.81	0.00	15.66	0.00	38.82	0.00	2.063	0.000	0.832	0.000	2.479	0.000
23.62	122.7	18.82	0.00	15.66	0.00	38.82	0.00	2.063	0.000	0.832	0.000	2.480	0.000
23.77	123.5	18.83	0.00	15.66	0.00	38.86	0.00	2.064	0.000	0.832	0.000	2.481	0.000
24.01	124.8	18.85	0.00	15.66	0.00	38.89	0.00	2.063	0.000	0.831	0.000	2.482	0.000
24.16	125.6	18.85	0.00	15.67	0.00	38.91	0.00	2.064	0.000	0.831	0.000	2.484	0.000
24.41	127.0	18.84	0.00	15.66	0.00	38.89	0.00	2.064	0.000	0.831	0.000	2.483	0.000
24.56	127.9	18.85	0.00	15.67	0.00	38.89	0.00	2.063	0.000	0.831	0.000	2.482	0.000
24.71	128.7	18.85	0.00	15.67	0.00	38.90	0.00	2.064	0.000	0.831	0.000	2.483	0.000
24.91	129.6	18.86	0.00	15.67	0.00	38.94	0.00	2.064	0.000	0.831	0.000	2.484	0.000
25.11	130.1	18.86	0.00	15.67	0.00	38.88	0.00	2.062	0.000	0.831	0.000	2.482	0.000
25.16	130.3	18.86	0.00	15.67	0.00	38.91	0.00	2.063	0.000	0.831	0.000	2.483	0.000
25.26	130.5	18.90	0.00	15.67	0.00	38.93	0.00	2.060	0.000	0.829	0.000	2.484	0.000
25.41	130.9	18.98	0.00	15.68	0.00	39.01	0.00	2.055	0.000	0.826	0.000	2.487	0.000
25.46	131.1	18.96	0.00	15.68	0.00	38.99	0.00	2.056	0.000	0.827	0.000	2.487	0.000
25.61	131.5	18.92	0.00	15.68	0.00	38.97	0.00	2.060	0.000	0.829	0.000	2.486	0.000
25.71	131.7	18.91	0.00	15.68	0.00	38.94	0.01	2.059	0.000	0.829	0.000	2.484	0.000
25.81	132.0	18.92	0.00	15.68	0.00	38.95	0.00	2.059	0.000	0.829	0.000	2.485	0.000
25.86	132.1	18.92	0.00	15.68	0.00	38.92	0.00	2.057	0.000	0.829	0.000	2.482	0.000
26.11	132.8	18.88	0.00	15.67	0.00	38.95	0.00	2.063	0.000	0.830	0.000	2.485	0.000
26.21	133.1	18.88	0.00	15.67	0.00	38.96	0.00	2.064	0.000	0.830	0.000	2.486	0.000
26.26	133.2	18.89	0.00	15.67	0.00	38.93	0.00	2.061	0.000	0.830	0.000	2.484	0.000
26.31	133.3	18.87	0.00	15.67	0.00	38.92	0.00	2.063	0.000	0.830	0.000	2.484	0.000
26.36	133.5	18.89	0.00	15.67	0.00	38.94	0.00	2.061	0.000	0.829	0.000	2.485	0.000
26.41	133.6	18.86	0.00	15.66	0.00	38.90	0.00	2.063	0.000	0.831	0.000	2.483	0.000
26.46	133.9	18.86	0.00	15.67	0.00	38.92	0.00	2.064	0.000	0.831	0.000	2.484	0.000

26.51	**134.1**	**18.85**	**0.00**	**15.67**	**0.00**	**38.92**	**0.00**	**2.064**	**0.000**	**0.831**	**0.000**	**2.484**	**0.000**
26.56	**134.4**	**18.85**	**0.00**	**15.67**	**0.00**	**38.90**	**0.00**	**2.064**	**0.000**	**0.831**	**0.000**	**2.483**	**0.000**
26.61	**134.6**	**18.83**	**0.00**	**15.66**	**0.00**	**38.84**	**0.00**	**2.063**	**0.000**	**0.832**	**0.000**	**2.480**	**0.000**
26.66	**134.9**	**18.83**	**0.00**	**15.66**	**0.00**	**38.87**	**0.00**	**2.065**	**0.000**	**0.832**	**0.000**	**2.482**	**0.000**
26.71	**135.1**	**18.80**	**0.00**	**15.66**	**0.00**	**38.82**	**0.00**	**2.065**	**0.000**	**0.833**	**0.000**	**2.479**	**0.000**
26.76	**135.4**	**18.79**	**0.00**	**15.66**	**0.00**	**38.81**	**0.00**	**2.065**	**0.000**	**0.833**	**0.000**	**2.479**	**0.000**
26.81	**135.6**	**18.79**	**0.00**	**15.66**	**0.00**	**38.81**	**0.00**	**2.066**	**0.000**	**0.833**	**0.000**	**2.479**	**0.000**
26.91	**136.1**	**18.80**	**0.00**	**15.66**	**0.00**	**38.82**	**0.00**	**2.065**	**0.000**	**0.833**	**0.000**	**2.479**	**0.000**
26.96	**136.5**	**18.79**	**0.00**	**15.66**	**0.00**	**38.82**	**0.00**	**2.066**	**0.000**	**0.833**	**0.000**	**2.479**	**0.000**
27.01	**136.8**	**18.78**	**0.00**	**15.66**	**0.00**	**38.80**	**0.00**	**2.066**	**0.000**	**0.834**	**0.000**	**2.478**	**0.000**
27.06	**137.1**	**18.78**	**0.00**	**15.66**	**0.00**	**38.81**	**0.00**	**2.066**	**0.000**	**0.834**	**0.000**	**2.479**	**0.000**
27.11	**137.5**	**18.77**	**0.00**	**15.65**	**0.00**	**38.78**	**0.00**	**2.065**	**0.000**	**0.834**	**0.000**	**2.477**	**0.000**
27.16	**137.8**	**18.77**	**0.00**	**15.65**	**0.00**	**38.77**	**0.00**	**2.066**	**0.000**	**0.834**	**0.000**	**2.477**	**0.000**
27.21	**138.2**	**18.77**	**0.00**	**15.65**	**0.00**	**38.77**	**0.00**	**2.066**	**0.000**	**0.834**	**0.000**	**2.477**	**0.000**
27.26	**138.5**	**18.77**	**0.00**	**15.65**	**0.00**	**38.76**	**0.00**	**2.065**	**0.000**	**0.834**	**0.000**	**2.476**	**0.000**
27.31	**138.9**	**18.76**	**0.00**	**15.65**	**0.00**	**38.77**	**0.00**	**2.066**	**0.000**	**0.834**	**0.000**	**2.477**	**0.000**
27.51	**140.3**	**18.77**	**0.00**	**15.65**	**0.00**	**38.78**	**0.00**	**2.066**	**0.000**	**0.834**	**0.000**	**2.477**	**0.000**
27.71	**141.7**	**18.79**	**0.00**	**15.66**	**0.00**	**38.82**	**0.00**	**2.067**	**0.000**	**0.834**	**0.000**	**2.479**	**0.000**
27.86	**142.7**	**18.77**	**0.00**	**15.65**	**0.00**	**38.79**	**0.00**	**2.067**	**0.000**	**0.834**	**0.000**	**2.478**	**0.000**

Table 14 Pb isotopic compositions in coretop sediments and surface Fe-Mn nodules in Chapter 4.

Stations	Water Depth,m	Latitude, °	Longitude, °	Materials	Sample depth, cm	$^{206}Pb/^{204}Pb$	±2SE	$^{207}Pb/^{204}Pb$	±2SE	$^{208}Pb/^{204}Pb$	±2SE	$^{208}Pb/^{206}Pb$	±2SE	$^{207}Pb/^{206}Pb$	±2SE	$^{207}Pb/^{206}Pb$	±2SE	Reference
E1O-17	4389	-60.0	-70.2	Fe-Mn nodule	surface	18.77		15.63		38.70		2.062		0.833		2.476	18.77	Abouchami et al 1995
E1O-20	4697	-59.0	-74.7	Fe-Mn nodule	surface	18.74		15.63		38.68		2.064		0.834		2.475	18.74	Abouchami et al 1995
E1O-20-duplicate	4697	-59.0	-74.7	Fe-Mn nodule	surface	18.75		15.64		38.71		2.065		0.834		2.475	18.75	Abouchami et al 1995
E1O-20-triplicate	4697	-59.0	-74.7	Fe-Mn nodule	surface	18.73		15.62		38.66		2.064		0.834		2.475	18.73	Abouchami et al 1995
EO5-25	3841	-59.0	-70.8	Fe-Mn nodule	surface	18.72		15.63		38.67		2.066		0.835		2.475	18.72	Abouchami et al 1995
E05-07B	3475	-59.0	-67.3	Fe-Mn nodule	surface	18.75		15.63		38.70		2.064		0.834		2.476	18.75	Abouchami et al 1995
v14-46	3429	-56.9	-57.0	Fe-Mn nodule	surface	18.76		15.63		38.72		2.064		0.833		2.477	18.76	Abouchami et al 1995
Vl5-138	2725	-49.6	-48.1	Fe-Mn nodule	surface	18.74		15.64		38.72		2.067		0.835		2.476	18.74	Abouchami et al 1995
v22-99	5440	-49.2	-33.2	Fe-Mn nodule	surface	18.75		15.64		38.81		2.070		0.834		2.481	18.75	Abouchami et al 1995
IO-TCl678-117	5201	-44.0	-33.1	Fe-Mn nodule	surface	18.70		15.63		38.67		2.068		0.836		2.474	18.70	Abouchami et al 1995
IO-TC1678-117duplicate	5201	-44.0	-33.1	Fe-Mn nodule	surface	18.72		15.64		38.67		2.066		0.835		2.474	18.72	Abouchami et al 1995
PS1170-4	3803	-63.5	-44.5	sediment	2cm	18.85	0.00	15.66	0.00	38.85	0.00	2.061	0.000	0.831	0.000	2.480	0.000	Appendix Table 1 and 2
PS1167-5	4515	-64.0	-44.1	sediment	2cm	18.84	0.00	15.66	0.00	38.83	0.00	2.061	0.000	0.831	0.000	2.479	0.000	Appendix Table 1 and 2
PS1575-2	3461	-62.8	-43.3	sediment	3cm	18.83	0.00	15.66	0.00	38.82	0.00	2.062	0.000	0.832	0.000	2.479	0.000	Appendix Table 1 and 2
PS2813-1	3499	-66.7	-50.0	sediment	1cm	18.83	0.00	15.66	0.00	38.80	0.00	2.060	0.000	0.831	0.000	2.478	0.000	Appendix Table 1 and 2
PS1508-2	4655	-67.0	-32.4	sediment	1cm	18.87	0.00	15.67	0.00	38.92	0.00	2.062	0.000	0.830	0.000	2.484	0.000	Appendix Table 1 and 2
PS1507-2	4771	-68.6	-24.1	sediment	2cm	19.05	0.00	15.69	0.00	39.11	0.00	2.053	0.000	0.823	0.000	2.494	0.000	Appendix Table 1 and 2
PS1607-1	1610	-74.1	-33.7	sediment	1cm	18.87	0.00	15.67	0.00	38.87	0.00	2.060	0.000	0.830	0.000	2.481	0.000	Appendix Table 1 and 2
PS1599-1	2482	-74.1	-27.7	sediment	2cm	19.12	0.00	15.68	0.00	39.25	0.00	2.053	0.000	0.820	0.000	2.502	0.000	Appendix Table 1 and 2
PS1790-1	2598	-73.8	-28.5	sediment	1cm	19.11	0.00	15.68	0.00	38.92	0.00	2.036	0.000	0.820	0.000	2.482	0.000	Appendix Table 1 and 2
PS1498-1	2825	-73.5	-35.5	sediment	2cm	18.80	0.00	15.67	0.00	38.82	0.00	2.065	0.000	0.833	0.000	2.478	0.000	Appendix Table 1 and 2
IO-TC1578-14A	4256	-68.7	-10.2	Fe-Mn nodule	surface	18.83		15.69		39.10		2.076		0.833		2.493		Abouchami et al 1995
IO-TC1578-14A-duplicate	4256	-68.7	-10.2	Fe-Mn nodule	surface	18.85		15.69		39.12		2.076		0.832		2.494		Abouchami et al 1995
IO-TCl578-14A-triplicate	4256	-68.7	-10.2	Fe-Mn nodule	surface	18.84		15.68		39.14		2.078		0.832		2.497		Abouchami et al 1995
IO-TC1277-36	3440	-65.5	0.5	Fe-Mn nodule	surface	19.00		15.67		39.21		2.064		0.825		2.502		Abouchami et al 1995
IO-PC1277-14	4682	-58.4	18.3	Fe-Mn nodule	surface	18.94		15.67		39.03		2.061		0.827		2.491		Abouchami et al 1995
PS2575-5	5069	-59.5	-3.2	sediment	2cm	18.92	0.00	15.68	0.00	39.02	0.00	2.063	0.000	0.829	0.000	2.489	0.000	Appendix Table 1 and 2
PS63/068-1	5427	-61.0	0.0	sediment	1cm	18.91	0.00	15.67	0.00	39.02	0.00	2.063	0.000	0.829	0.000	2.490	0.000	Appendix Table 1 and 2
PS2070-1	2611	-65.1	3.6	sediment	2cm	18.88	0.00	15.69	0.00	39.11	0.00	2.071	0.000	0.831	0.000	2.493	0.000	Appendix Table 1 and 2
PS1461-1	2370	-64.5	3.7	sediment	2cm	18.97	0.00	15.69	0.00	39.20	0.00	2.066	0.000	0.827	0.000	2.499	0.000	Appendix Table 1 and 2
v29-D4	4574	-50.4	8.8	Fe-Mn nodule	surface	18.78		15.62		38.77		2.065		0.832		2.482		Abouchami et al 1995
v29-D6	2994	-51.4	13.6	Fe-Mn nodule	surface	18.80		15.64		38.82		2.065		0.832		2.482		Abouchami et al 1995
PS1768-8	3299	-52.6	4.5	sediment	2cm	18.80	0.00	15.66	0.00	38.85	0.00	2.066	0.000	0.836	0.000	2.474	0.000	Appendix Table 1 and 2
PS1226-1	4033	-54.5	10.3	sediment	2cm	18.86	0.00	15.67	0.00	38.98	0.00	2.066	0.000	0.833	0.000	2.480	0.000	Appendix Table 1 and 2
PS1442-4	3600	-54.0	11.1	sediment	1cm	18.82	0.00	15.66	0.00	38.91	0.00	2.067	0.000	0.831	0.000	2.487	0.000	Appendix Table 1 and 2
PS1436-1	2230	-52.0	15.0	sediment	1cm	18.80	0.00	15.66	0.00	38.83	0.00	2.065	0.000	0.832	0.000	2.484	0.000	Appendix Table 1 and 2
PS1780-5	4280	-51.7	-15.3	sediment	1cm	18.83	0.00	15.66	0.00	38.88	0.00	2.065	0.000	0.833	0.000	2.480	0.000	Appendix Table 1 and 2
PS1778-5	3407	-49.0	-12.7	sediment	1cm	18.85	0.00	15.66	0.00	38.89	0.00	2.063	0.000	0.832	0.000	2.482	0.000	Appendix Table 1 and 2

Table 15 Pb isotope results of 50 microns LA-MC-ICPMS in Chapter 5.

Age , Ma	Depth, mm	$^{206}Pb/^{204}Pb$	±2SE	$^{207}Pb/^{204}Pb$	±2SE	$^{208}Pb/^{204}Pb$	±2SE	$^{208}Pb/^{206}Pb$	±2SE	$^{207}Pb/^{206}Pb$	±2SE	$^{208}Pb/^{207}Pb$	±2SE
0.029	0.050	18.764	0.009	15.626	0.007	38.702	0.020	2.063	0.000	0.833	0.000	2.477	0.000
0.057	0.100	18.763	0.009	15.626	0.008	38.704	0.020	2.063	0.000	0.833	0.000	2.477	0.000
0.086	0.150	18.769	0.010	15.632	0.008	38.711	0.022	2.062	0.000	0.833	0.000	2.476	0.000
0.115	0.200	18.765	0.010	15.623	0.008	38.700	0.021	2.062	0.000	0.833	0.000	2.477	0.000
0.144	0.250	18.765	0.009	15.627	0.007	38.700	0.018	2.062	0.000	0.833	0.000	2.476	0.000
0.172	0.300	18.766	0.007	15.627	0.006	38.699	0.015	2.062	0.000	0.833	0.000	2.476	0.000
0.201	0.350	18.759	0.011	15.619	0.008	38.682	0.024	2.062	0.000	0.833	0.000	2.477	0.000
0.230	0.400	18.767	0.008	15.631	0.007	38.705	0.017	2.062	0.000	0.833	0.000	2.476	0.000
0.259	0.450	18.765	0.010	15.627	0.008	38.703	0.022	2.062	0.000	0.833	0.000	2.477	0.000
0.287	0.500	18.757	0.008	15.622	0.007	38.684	0.016	2.062	0.000	0.833	0.000	2.476	0.000
0.316	0.550	18.768	0.009	15.630	0.007	38.708	0.019	2.062	0.000	0.833	0.000	2.477	0.000
0.345	0.600	18.759	0.008	15.621	0.007	38.684	0.018	2.062	0.000	0.833	0.000	2.476	0.000
0.374	0.650	18.764	0.009	15.627	0.007	38.697	0.019	2.062	0.000	0.833	0.000	2.476	0.000
0.402	0.700	18.777	0.011	15.639	0.009	38.725	0.023	2.062	0.000	0.833	0.000	2.476	0.000
0.431	0.750	18.765	0.008	15.627	0.006	38.691	0.016	2.062	0.000	0.833	0.000	2.476	0.000
0.460	0.800	18.759	0.010	15.622	0.008	38.688	0.022	2.062	0.000	0.833	0.000	2.476	0.000
0.489	0.850	18.761	0.009	15.627	0.007	38.692	0.018	2.062	0.000	0.833	0.000	2.476	0.000
0.517	0.900	18.772	0.011	15.633	0.009	38.719	0.022	2.063	0.000	0.833	0.000	2.477	0.000
0.546	0.950	18.766	0.011	15.633	0.010	38.703	0.023	2.062	0.000	0.833	0.000	2.476	0.000
0.575	1.000	18.765	0.015	15.636	0.011	38.704	0.027	2.063	0.001	0.833	0.001	2.475	0.001
0.603	1.050	18.767	0.009	15.629	0.008	38.700	0.018	2.062	0.000	0.833	0.000	2.476	0.000
0.632	1.100	18.755	0.010	15.619	0.009	38.669	0.022	2.062	0.000	0.833	0.000	2.476	0.000
0.661	1.150	18.763	0.010	15.623	0.008	38.680	0.021	2.061	0.000	0.833	0.000	2.476	0.000
0.690	1.200	18.753	0.012	15.620	0.010	38.671	0.025	2.062	0.000	0.833	0.000	2.476	0.000
0.718	1.250	18.762	0.007	15.626	0.006	38.689	0.015	2.062	0.000	0.833	0.000	2.476	0.000
0.747	1.300	18.761	0.010	15.628	0.008	38.690	0.021	2.062	0.000	0.833	0.000	2.476	0.000
0.776	1.350	18.764	0.009	15.629	0.007	38.695	0.019	2.062	0.000	0.833	0.000	2.476	0.000
0.805	1.400	18.761	0.010	15.627	0.008	38.690	0.020	2.062	0.000	0.833	0.000	2.476	0.000
0.833	1.450	18.772	0.011	15.638	0.009	38.720	0.023	2.063	0.000	0.833	0.000	2.476	0.000
0.862	1.500	18.757	0.008	15.625	0.007	38.687	0.017	2.063	0.000	0.833	0.000	2.476	0.000
0.891	1.550	18.768	0.009	15.633	0.007	38.705	0.019	2.062	0.000	0.833	0.000	2.476	0.000
0.920	1.600	18.758	0.009	15.623	0.007	38.682	0.019	2.062	0.000	0.833	0.000	2.476	0.000
0.948	1.650	18.756	0.012	15.622	0.010	38.676	0.027	2.062	0.000	0.833	0.000	2.476	0.000
0.977	1.700	18.763	0.008	15.628	0.007	38.689	0.017	2.062	0.000	0.833	0.000	2.476	0.000
1.006	1.750	18.764	0.013	15.630	0.011	38.693	0.027	2.062	0.000	0.833	0.000	2.476	0.000
1.034	1.800	18.761	0.011	15.627	0.009	38.687	0.022	2.062	0.000	0.833	0.000	2.476	0.000
1.063	1.850	18.760	0.012	15.626	0.010	38.680	0.026	2.062	0.000	0.833	0.000	2.475	0.000
1.092	1.900	18.745	0.017	15.614	0.014	38.659	0.036	2.062	0.000	0.833	0.000	2.476	0.001
1.121	1.950	18.766	0.013	15.631	0.011	38.694	0.027	2.062	0.000	0.833	0.000	2.476	0.000
1.149	2.000	18.754	0.012	15.622	0.011	38.665	0.027	2.062	0.000	0.833	0.000	2.475	0.000
1.178	2.050	18.763	0.012	15.634	0.010	38.695	0.026	2.062	0.000	0.833	0.000	2.475	0.000
1.207	2.100	18.762	0.010	15.628	0.008	38.685	0.021	2.062	0.000	0.833	0.000	2.475	0.000
1.236	2.150	18.761	0.011	15.626	0.009	38.681	0.023	2.062	0.000	0.833	0.000	2.475	0.000
1.264	2.200	18.754	0.011	15.620	0.009	38.665	0.022	2.062	0.000	0.833	0.000	2.475	0.000
1.293	2.250	18.754	0.010	15.623	0.009	38.669	0.020	2.062	0.000	0.833	0.000	2.475	0.000
1.322	2.300	18.760	0.009	15.626	0.008	38.682	0.021	2.062	0.000	0.833	0.000	2.475	0.001
1.351	2.350	18.754	0.007	15.625	0.006	38.673	0.014	2.062	0.000	0.833	0.000	2.475	0.000
1.379	2.400	18.755	0.007	15.623	0.006	38.672	0.015	2.062	0.000	0.833	0.000	2.475	0.000
1.408	2.450	18.761	0.007	15.631	0.006	38.695	0.016	2.062	0.000	0.833	0.000	2.475	0.000
1.437	2.500	18.761	0.007	15.631	0.006	38.690	0.015	2.062	0.000	0.833	0.000	2.475	0.000
1.466	2.550	18.757	0.009	15.629	0.007	38.691	0.018	2.063	0.000	0.833	0.000	2.476	0.000
1.494	2.600	18.766	0.010	15.633	0.008	38.700	0.022	2.062	0.000	0.833	0.000	2.476	0.000
1.523	2.650	18.758	0.010	15.627	0.008	38.686	0.021	2.062	0.000	0.833	0.000	2.476	0.000
1.552	2.700	18.755	0.009	15.624	0.008	38.680	0.020	2.062	0.000	0.833	0.000	2.476	0.000
1.580	2.750	18.756	0.010	15.628	0.008	38.682	0.023	2.062	0.000	0.833	0.000	2.475	0.000
1.609	2.800	18.764	0.011	15.633	0.010	38.706	0.024	2.063	0.000	0.833	0.000	2.476	0.000
1.638	2.850	18.753	0.011	15.624	0.009	38.671	0.023	2.062	0.000	0.833	0.000	2.475	0.000
1.667	2.900	18.764	0.010	15.630	0.009	38.692	0.021	2.062	0.000	0.833	0.000	2.476	0.000
1.695	2.950	18.761	0.013	15.631	0.011	38.688	0.027	2.062	0.000	0.833	0.000	2.475	0.000
1.724	3.000	18.768	0.013	15.634	0.010	38.704	0.027	2.062	0.000	0.833	0.000	2.476	0.001
1.753	3.050	18.743	0.009	15.617	0.007	38.647	0.019	2.062	0.000	0.833	0.000	2.475	0.000
1.782	3.100	18.757	0.010	15.624	0.008	38.673	0.021	2.062	0.000	0.833	0.000	2.475	0.000
1.810	3.150	18.770	0.010	15.637	0.008	38.705	0.020	2.062	0.000	0.833	0.000	2.475	0.001
1.839	3.200	18.756	0.011	15.625	0.009	38.675	0.023	2.062	0.000	0.833	0.000	2.475	0.000
1.868	3.250	18.754	0.013	15.625	0.010	38.674	0.028	2.062	0.000	0.833	0.000	2.475	0.001
1.897	3.300	18.764	0.014	15.632	0.011	38.696	0.029	2.062	0.000	0.833	0.000	2.475	0.000
1.925	3.350	18.759	0.012	15.625	0.010	38.682	0.025	2.062	0.000	0.833	0.000	2.476	0.000
1.954	3.400	18.753	0.010	15.621	0.008	38.668	0.020	2.062	0.000	0.833	0.000	2.475	0.000
1.983	3.450	18.761	0.009	15.629	0.008	38.685	0.019	2.062	0.000	0.833	0.000	2.475	0.000
2.011	3.500	18.761	0.010	15.630	0.009	38.691	0.022	2.062	0.000	0.833	0.000	2.475	0.000
2.040	3.550	18.758	0.007	15.628	0.006	38.683	0.015	2.062	0.000	0.833	0.000	2.475	0.000
2.069	3.600	18.748	0.010	15.623	0.007	38.666	0.019	2.062	0.000	0.833	0.000	2.475	0.000
2.098	3.650	18.752	0.008	15.620	0.007	38.661	0.018	2.062	0.000	0.833	0.000	2.475	0.000
2.126	3.700	18.757	0.009	15.625	0.008	38.678	0.020	2.062	0.000	0.833	0.000	2.475	0.000
2.155	3.750	18.755	0.008	15.625	0.007	38.674	0.018	2.062	0.000	0.833	0.000	2.475	0.000
2.184	3.800	18.761	0.011	15.629	0.010	38.688	0.025	2.062	0.000	0.833	0.000	2.475	0.000
2.213	3.850	18.760	0.008	15.626	0.006	38.680	0.018	2.062	0.000	0.833	0.000	2.475	0.000
2.241	3.900	18.762	0.009	15.631	0.008	38.690	0.020	2.062	0.000	0.833	0.000	2.475	0.000
2.270	3.950	18.767	0.011	15.638	0.009	38.701	0.023	2.062	0.000	0.833	0.000	2.475	0.000
2.299	4.000	18.765	0.011	15.631	0.009	38.694	0.022	2.062	0.000	0.833	0.000	2.475	0.000
2.328	4.050	18.758	0.011	15.627	0.009	38.681	0.024	2.062	0.000	0.833	0.000	2.475	0.000
2.356	4.100	18.759	0.010	15.628	0.008	38.680	0.021	2.062	0.000	0.833	0.000	2.475	0.000
2.385	4.150	18.755	0.011	15.624	0.009	38.667	0.024	2.062	0.000	0.833	0.000	2.475	0.000
2.414	4.200	18.754	0.017	15.623	0.014	38.670	0.035	2.062	0.000	0.833	0.000	2.475	0.000
2.443	4.250	18.768	0.013	15.633	0.011	38.696	0.027	2.062	0.000	0.833	0.000	2.475	0.000
2.471	4.300	18.755	0.015	15.622	0.012	38.670	0.031	2.062	0.000	0.833	0.000	2.475	0.000
2.500	4.350	18.760	0.009	15.627	0.007	38.684	0.018	2.062	0.000	0.833	0.000	2.475	0.001
2.529	4.400	18.766	0.011	15.634	0.010	38.695	0.024	2.062	0.000	0.833	0.000	2.475	0.000
2.557	4.450	18.764	0.014	15.633	0.011	38.696	0.029	2.062	0.000	0.833	0.000	2.475	0.001
2.586	4.500	18.770	0.020	15.636	0.016	38.710	0.041	2.062	0.000	0.833	0.000	2.476	0.000
2.615	4.550	18.752	0.016	15.620	0.013	38.661	0.032	2.062	0.000	0.833	0.000	2.475	0.000
2.644	4.600	18.768	0.017	15.632	0.013	38.690	0.034	2.061	0.000	0.833	0.000	2.475	0.000
2.672	4.650	18.756	0.015	15.621	0.012	38.668	0.030	2.062	0.000	0.833	0.000	2.475	0.000
2.701	4.700	18.764	0.013	15.630	0.010	38.685	0.027	2.062	0.000	0.833	0.000	2.475	0.000
2.730	4.750	18.757	0.015	15.621	0.012	38.670	0.031	2.062	0.000	0.833	0.000	2.475	0.000
2.759	4.800	18.757	0.012	15.622	0.010	38.671	0.024	2.062	0.000	0.833	0.000	2.475	0.000

2.787	4.850	18.753	0.012	15.618	0.010	38.657	0.026	2.061	0.000	0.833	0.000	2.475	0.000
2.816	4.900	18.775	0.012	15.636	0.010	38.706	0.026	2.062	0.000	0.833	0.000	2.475	0.000
2.845	4.950	18.774	0.012	15.636	0.009	38.708	0.026	2.062	0.000	0.833	0.000	2.476	0.001
2.874	5.000	18.770	0.012	15.632	0.010	38.697	0.026	2.062	0.000	0.833	0.000	2.476	0.000
2.896	5.050	18.766	0.013	15.627	0.010	38.685	0.028	2.061	0.000	0.833	0.000	2.476	0.001
2.917	5.100	18.766	0.008	15.630	0.007	38.682	0.018	2.061	0.000	0.833	0.000	2.475	0.000
2.939	5.150	18.774	0.009	15.637	0.008	38.708	0.019	2.062	0.000	0.833	0.000	2.475	0.000
2.960	5.200	18.766	0.012	15.629	0.011	38.685	0.026	2.061	0.000	0.833	0.000	2.475	0.000
2.982	5.250	18.765	0.010	15.628	0.008	38.684	0.020	2.061	0.000	0.833	0.000	2.475	0.000
3.003	5.300	18.772	0.008	15.630	0.007	38.694	0.018	2.061	0.000	0.833	0.000	2.476	0.000
3.025	5.350	18.770	0.014	15.628	0.012	38.686	0.030	2.061	0.000	0.833	0.000	2.476	0.001
3.046	5.400	18.772	0.008	15.627	0.006	38.692	0.018	2.061	0.000	0.832	0.000	2.476	0.000
3.068	5.450	18.771	0.007	15.627	0.005	38.687	0.015	2.061	0.000	0.833	0.000	2.476	0.001
3.090	5.500	18.774	0.008	15.632	0.006	38.699	0.017	2.061	0.000	0.833	0.000	2.476	0.000
3.111	5.550	18.771	0.006	15.628	0.005	38.702	0.013	2.062	0.000	0.833	0.000	2.476	0.001
3.133	5.600	18.764	0.007	15.622	0.005	38.679	0.016	2.061	0.000	0.833	0.000	2.476	0.001
3.154	5.650	18.763	0.009	15.622	0.007	38.674	0.019	2.061	0.000	0.833	0.000	2.476	0.000
3.176	5.700	18.768	0.006	15.627	0.005	38.693	0.013	2.062	0.000	0.833	0.000	2.476	0.000
3.197	5.750	18.763	0.006	15.620	0.004	38.681	0.013	2.062	0.000	0.832	0.000	2.476	0.000
3.219	5.800	18.768	0.009	15.625	0.006	38.690	0.019	2.061	0.000	0.833	0.000	2.476	0.000
3.262	5.900	18.769	0.007	15.628	0.005	38.690	0.014	2.061	0.000	0.833	0.000	2.476	0.000
3.283	5.950	18.768	0.007	15.628	0.006	38.690	0.015	2.061	0.000	0.833	0.000	2.476	0.000
3.305	6.000	18.764	0.007	15.624	0.006	38.682	0.015	2.062	0.000	0.833	0.000	2.476	0.000
3.327	6.050	18.768	0.008	15.627	0.007	38.699	0.017	2.062	0.000	0.833	0.000	2.476	0.000
3.348	6.100	18.764	0.010	15.621	0.008	38.678	0.022	2.061	0.000	0.832	0.000	2.476	0.000
3.370	6.150	18.769	0.007	15.626	0.006	38.689	0.016	2.061	0.000	0.833	0.000	2.476	0.000
3.391	6.200	18.764	0.008	15.621	0.007	38.679	0.016	2.061	0.000	0.833	0.000	2.476	0.000
3.413	6.250	18.765	0.007	15.622	0.006	38.683	0.015	2.061	0.000	0.833	0.000	2.476	0.000
3.434	6.300	18.771	0.007	15.629	0.005	38.698	0.015	2.062	0.000	0.833	0.000	2.476	0.000
3.456	6.350	18.762	0.007	15.623	0.005	38.678	0.014	2.062	0.000	0.833	0.000	2.476	0.000
3.477	6.400	18.770	0.008	15.626	0.006	38.698	0.017	2.062	0.000	0.833	0.000	2.476	0.000
3.499	6.450	18.766	0.006	15.624	0.005	38.685	0.014	2.061	0.000	0.833	0.000	2.476	0.000
3.521	6.500	18.772	0.007	15.627	0.006	38.694	0.015	2.061	0.000	0.832	0.000	2.476	0.000
3.542	6.550	18.769	0.007	15.625	0.006	38.691	0.015	2.061	0.000	0.832	0.000	2.476	0.000
3.564	6.600	18.771	0.007	15.626	0.005	38.692	0.015	2.061	0.000	0.832	0.000	2.476	0.000
3.585	6.650	18.766	0.007	15.622	0.006	38.685	0.014	2.061	0.000	0.832	0.000	2.476	0.000
3.607	6.700	18.762	0.005	15.619	0.004	38.672	0.011	2.061	0.000	0.832	0.000	2.476	0.000
3.628	6.750	18.769	0.005	15.627	0.004	38.699	0.010	2.062	0.000	0.833	0.000	2.476	0.000
3.650	6.800	18.776	0.006	15.630	0.004	38.713	0.014	2.062	0.000	0.832	0.000	2.477	0.000
3.671	6.850	18.770	0.006	15.625	0.005	38.700	0.013	2.062	0.000	0.832	0.000	2.477	0.000
3.693	6.900	18.773	0.008	15.627	0.006	38.709	0.019	2.062	0.000	0.832	0.000	2.477	0.001
3.715	6.950	18.764	0.008	15.627	0.006	38.691	0.018	2.062	0.000	0.833	0.000	2.476	0.000
3.736	7.000	18.771	0.006	15.633	0.004	38.705	0.013	2.062	0.000	0.833	0.000	2.476	0.000
3.758	7.050	18.759	0.006	15.622	0.005	38.687	0.014	2.062	0.000	0.833	0.000	2.476	0.000
3.779	7.100	18.765	0.006	15.625	0.005	38.686	0.013	2.062	0.000	0.833	0.000	2.476	0.000
3.801	7.150	18.759	0.008	15.620	0.007	38.673	0.018	2.062	0.000	0.833	0.000	2.476	0.000
3.822	7.200	18.764	0.007	15.627	0.005	38.693	0.014	2.062	0.000	0.833	0.000	2.476	0.000
3.844	7.250	18.770	0.007	15.632	0.006	38.705	0.016	2.062	0.000	0.833	0.000	2.476	0.000
3.865	7.300	18.763	0.006	15.625	0.005	38.689	0.013	2.062	0.000	0.833	0.000	2.476	0.000
3.887	7.350	18.761	0.008	15.623	0.006	38.683	0.017	2.062	0.000	0.833	0.000	2.476	0.000
3.908	7.400	18.770	0.009	15.634	0.007	38.704	0.019	2.062	0.000	0.833	0.000	2.476	0.000
3.930	7.450	18.751	0.007	15.617	0.006	38.657	0.017	2.062	0.000	0.833	0.000	2.475	0.000
3.952	7.500	18.756	0.005	15.624	0.004	38.685	0.011	2.063	0.000	0.833	0.000	2.476	0.000
3.973	7.550	18.759	0.005	15.626	0.004	38.689	0.011	2.062	0.000	0.833	0.000	2.476	0.000
3.995	7.600	18.759	0.008	15.625	0.007	38.687	0.017	2.062	0.000	0.833	0.000	2.476	0.000
4.016	7.650	18.762	0.008	15.629	0.006	38.694	0.018	2.062	0.000	0.833	0.000	2.476	0.000
4.038	7.700	18.760	0.008	15.626	0.006	38.688	0.016	2.062	0.000	0.833	0.000	2.476	0.000
4.059	7.750	18.755	0.014	15.623	0.011	38.681	0.029	2.062	0.000	0.833	0.000	2.476	0.000
4.081	7.800	18.763	0.008	15.628	0.006	38.700	0.018	2.063	0.000	0.833	0.000	2.476	0.001
4.102	7.850	18.759	0.005	15.628	0.004	38.688	0.012	2.062	0.000	0.833	0.000	2.476	0.000
4.124	7.900	18.756	0.006	15.626	0.005	38.680	0.015	2.062	0.000	0.833	0.000	2.475	0.001
4.146	7.950	18.749	0.013	15.619	0.011	38.673	0.027	2.063	0.000	0.833	0.000	2.476	0.000
4.167	8.000	18.760	0.007	15.629	0.005	38.694	0.017	2.063	0.000	0.833	0.000	2.476	0.001
4.189	8.050	18.752	0.007	15.624	0.005	38.675	0.015	2.062	0.000	0.833	0.000	2.475	0.000
4.210	8.100	18.751	0.006	15.621	0.005	38.674	0.014	2.063	0.000	0.833	0.000	2.476	0.000
4.232	8.150	18.753	0.005	15.621	0.004	38.678	0.013	2.062	0.000	0.833	0.000	2.476	0.001
4.253	8.200	18.762	0.006	15.630	0.005	38.696	0.016	2.063	0.000	0.833	0.000	2.476	0.000
4.275	8.250	18.756	0.008	15.628	0.006	38.686	0.017	2.063	0.000	0.833	0.000	2.475	0.000
4.296	8.300	18.763	0.006	15.631	0.005	38.698	0.013	2.062	0.000	0.833	0.000	2.476	0.000
4.318	8.350	18.746	0.008	15.617	0.006	38.662	0.017	2.062	0.000	0.833	0.000	2.476	0.000
4.340	8.400	18.741	0.009	15.617	0.007	38.652	0.019	2.062	0.000	0.833	0.000	2.475	0.000
4.361	8.450	18.748	0.007	15.622	0.006	38.669	0.015	2.063	0.000	0.833	0.000	2.475	0.000
4.383	8.500	18.749	0.007	15.621	0.006	38.674	0.015	2.063	0.000	0.833	0.000	2.476	0.000
4.404	8.550	18.758	0.008	15.630	0.006	38.703	0.019	2.063	0.000	0.833	0.000	2.476	0.000
4.426	8.600	18.751	0.012	15.626	0.010	38.683	0.024	2.063	0.000	0.833	0.000	2.476	0.000
4.447	8.650	18.755	0.006	15.630	0.005	38.687	0.014	2.063	0.000	0.833	0.000	2.475	0.000
4.469	8.700	18.742	0.012	15.619	0.010	38.659	0.027	2.063	0.000	0.833	0.000	2.475	0.001
4.490	8.750	18.752	0.008	15.626	0.007	38.682	0.016	2.063	0.000	0.833	0.000	2.475	0.000
4.512	8.800	18.751	0.006	15.626	0.005	38.683	0.014	2.063	0.000	0.833	0.000	2.476	0.000
4.533	8.850	18.747	0.005	15.623	0.004	38.673	0.011	2.063	0.000	0.833	0.000	2.475	0.000
4.555	8.900	18.751	0.008	15.624	0.006	38.687	0.017	2.063	0.000	0.833	0.000	2.476	0.000
4.577	8.950	18.761	0.007	15.634	0.005	38.704	0.016	2.063	0.000	0.833	0.000	2.476	0.000
4.598	9.000	18.754	0.008	15.628	0.006	38.686	0.016	2.063	0.000	0.833	0.000	2.475	0.000
4.620	9.050	18.758	0.008	15.633	0.006	38.698	0.017	2.063	0.000	0.833	0.000	2.475	0.001
4.641	9.100	18.754	0.008	15.629	0.006	38.683	0.017	2.063	0.000	0.833	0.000	2.475	0.000
4.663	9.150	18.748	0.008	15.621	0.006	38.674	0.018	2.063	0.000	0.833	0.000	2.476	0.000
4.684	9.200	18.758	0.008	15.631	0.007	38.696	0.018	2.063	0.000	0.833	0.000	2.476	0.000
4.706	9.250	18.749	0.008	15.625	0.007	38.682	0.018	2.063	0.000	0.833	0.000	2.476	0.000
4.727	9.300	18.757	0.007	15.631	0.006	38.699	0.016	2.063	0.000	0.833	0.000	2.476	0.000
4.749	9.350	18.756	0.008	15.627	0.007	38.694	0.017	2.063	0.000	0.833	0.000	2.476	0.000
4.771	9.400	18.748	0.006	15.623	0.005	38.678	0.015	2.063	0.000	0.833	0.000	2.476	0.001
4.792	9.450	18.750	0.007	15.626	0.006	38.682	0.014	2.063	0.000	0.833	0.000	2.475	0.000
4.814	9.500	18.757	0.007	15.632	0.005	38.698	0.017	2.063	0.000	0.833	0.000	2.476	0.000
4.835	9.550	18.751	0.006	15.628	0.005	38.689	0.012	2.063	0.000	0.833	0.000	2.476	0.000
4.857	9.600	18.749	0.006	15.624	0.004	38.682	0.014	2.063	0.000	0.833	0.000	2.476	0.000
4.878	9.650	18.750	0.006	15.624	0.005	38.682	0.013	2.063	0.000	0.833	0.000	2.476	0.000
4.900	9.700	18.737	0.005	15.617	0.004	38.661	0.012	2.063	0.000	0.833	0.000	2.476	0.000
4.921	9.750	18.746	0.005	15.623	0.004	38.673	0.013	2.063	0.000	0.833	0.000	2.475	0.000
4.943	9.800	18.746	0.007	15.625	0.005	38.684	0.015	2.064	0.000	0.834	0.000	2.476	0.000
4.965	9.850	18.739	0.006	15.623	0.005	38.667	0.013	2.063	0.000	0.834	0.000	2.475	0.000
4.986	9.900	18.745	0.008	15.625	0.007	38.682	0.017	2.064	0.000	0.834	0.000	2.476	0.000

5.008	9.950	18.745	0.008	15.627	0.007	38.682	0.019	2.064	0.000	0.834	0.000	2.475	0.001
5.029	10.000	18.749	0.006	15.627	0.005	38.690	0.014	2.064	0.000	0.834	0.000	2.476	0.001
5.051	10.050	18.741	0.006	15.623	0.005	38.674	0.013	2.064	0.000	0.834	0.000	2.475	0.000
5.072	10.100	18.752	0.006	15.632	0.005	38.700	0.014	2.064	0.000	0.834	0.000	2.476	0.000
5.094	10.150	18.748	0.007	15.627	0.006	38.687	0.016	2.064	0.000	0.834	0.000	2.476	0.000
5.115	10.200	18.742	0.009	15.622	0.006	38.680	0.019	2.064	0.000	0.834	0.000	2.476	0.000
5.137	10.250	18.744	0.007	15.627	0.005	38.685	0.014	2.064	0.000	0.834	0.000	2.476	0.000
5.158	10.300	18.747	0.006	15.629	0.005	38.692	0.014	2.064	0.000	0.834	0.000	2.476	0.000
5.180	10.350	18.743	0.005	15.626	0.004	38.683	0.012	2.064	0.000	0.834	0.000	2.476	0.000
5.202	10.400	18.741	0.005	15.623	0.004	38.677	0.011	2.064	0.000	0.834	0.000	2.476	0.000
5.223	10.450	18.751	0.007	15.628	0.006	38.697	0.016	2.064	0.000	0.833	0.000	2.476	0.000
5.245	10.500	18.747	0.006	15.625	0.004	38.692	0.012	2.064	0.000	0.833	0.000	2.476	0.000
5.266	10.550	18.755	0.005	15.630	0.004	38.711	0.012	2.064	0.000	0.833	0.000	2.477	0.000
5.288	10.600	18.756	0.007	15.628	0.006	38.711	0.015	2.064	0.000	0.833	0.000	2.477	0.000
5.309	10.650	18.757	0.005	15.629	0.004	38.711	0.011	2.064	0.000	0.833	0.000	2.477	0.000
5.331	10.700	18.758	0.005	15.630	0.005	38.713	0.012	2.064	0.000	0.833	0.000	2.477	0.000
5.352	10.750	18.759	0.005	15.629	0.004	38.717	0.012	2.064	0.000	0.833	0.000	2.477	0.000
5.374	10.800	18.758	0.006	15.629	0.005	38.714	0.013	2.064	0.000	0.833	0.000	2.477	0.000
5.396	10.850	18.755	0.006	15.625	0.005	38.706	0.012	2.064	0.000	0.833	0.000	2.477	0.000
5.417	10.900	18.759	0.006	15.626	0.005	38.707	0.014	2.063	0.000	0.833	0.000	2.477	0.000
5.439	10.950	18.764	0.008	15.630	0.006	38.720	0.016	2.064	0.000	0.833	0.000	2.477	0.000
5.460	11.000	18.777	0.009	15.637	0.008	38.753	0.020	2.064	0.000	0.833	0.000	2.478	0.000
5.482	11.050	18.761	0.007	15.627	0.005	38.721	0.015	2.064	0.000	0.833	0.000	2.478	0.000
5.503	11.100	18.767	0.006	15.630	0.006	38.736	0.013	2.064	0.000	0.833	0.000	2.478	0.001
5.525	11.150	18.769	0.005	15.631	0.004	38.735	0.010	2.064	0.000	0.833	0.000	2.478	0.000
5.546	11.200	18.772	0.008	15.637	0.006	38.744	0.018	2.064	0.000	0.833	0.000	2.478	0.000
5.568	11.250	18.762	0.007	15.629	0.005	38.724	0.016	2.064	0.000	0.833	0.000	2.478	0.000
5.590	11.300	18.762	0.007	15.628	0.006	38.726	0.014	2.064	0.000	0.833	0.000	2.478	0.000
5.611	11.350	18.770	0.004	15.635	0.004	38.740	0.009	2.064	0.000	0.833	0.000	2.478	0.000
5.633	11.400	18.759	0.006	15.624	0.005	38.718	0.013	2.064	0.000	0.833	0.000	2.478	0.000
5.654	11.450	18.757	0.005	15.623	0.004	38.722	0.012	2.064	0.000	0.833	0.000	2.479	0.000
5.676	11.500	18.765	0.006	15.631	0.005	38.735	0.013	2.064	0.000	0.833	0.000	2.478	0.000
5.697	11.550	18.771	0.006	15.637	0.005	38.755	0.014	2.065	0.000	0.833	0.000	2.478	0.000
5.719	11.600	18.768	0.007	15.634	0.006	38.751	0.017	2.065	0.000	0.833	0.000	2.479	0.001
5.740	11.650	18.766	0.006	15.630	0.005	38.736	0.014	2.064	0.000	0.833	0.000	2.478	0.000
5.762	11.700	18.771	0.007	15.632	0.005	38.742	0.014	2.064	0.000	0.833	0.000	2.478	0.000
5.783	11.750	18.773	0.006	15.634	0.005	38.748	0.012	2.064	0.000	0.833	0.000	2.478	0.000
5.805	11.800	18.772	0.005	15.633	0.004	38.748	0.011	2.064	0.000	0.833	0.000	2.479	0.000
5.827	11.850	18.771	0.006	15.633	0.005	38.746	0.013	2.064	0.000	0.833	0.000	2.478	0.000
5.848	11.900	18.766	0.006	15.630	0.005	38.730	0.013	2.064	0.000	0.833	0.000	2.478	0.000
5.870	11.950	18.768	0.007	15.634	0.006	38.738	0.016	2.064	0.000	0.833	0.000	2.478	0.000
5.891	12.000	18.768	0.006	15.635	0.005	38.740	0.014	2.064	0.000	0.833	0.000	2.478	0.000
5.913	12.050	18.771	0.008	15.638	0.006	38.753	0.016	2.064	0.000	0.833	0.000	2.478	0.000
5.934	12.100	18.770	0.005	15.637	0.005	38.745	0.011	2.064	0.000	0.833	0.000	2.478	0.000
5.956	12.150	18.764	0.007	15.631	0.006	38.731	0.015	2.064	0.000	0.833	0.000	2.478	0.000
5.977	12.200	18.766	0.008	15.632	0.006	38.736	0.016	2.064	0.000	0.833	0.000	2.478	0.000
5.999	12.250	18.767	0.006	15.634	0.004	38.728	0.024	2.064	0.001	0.833	0.000	2.477	0.002
6.021	12.300	18.770	0.009	15.640	0.007	38.755	0.019	2.065	0.000	0.833	0.000	2.478	0.000
6.042	12.350	18.766	0.008	15.631	0.006	38.734	0.018	2.064	0.000	0.833	0.000	2.478	0.000
6.064	12.400	18.768	0.007	15.633	0.005	38.739	0.014	2.064	0.000	0.833	0.000	2.478	0.000
6.085	12.450	18.771	0.007	15.636	0.006	38.750	0.015	2.064	0.000	0.833	0.000	2.478	0.000
6.107	12.500	18.773	0.004	15.633	0.006	38.755	0.015	2.064	0.000	0.833	0.000	2.479	0.000
6.128	12.550	18.774	0.004	15.631	0.006	38.755	0.016	2.064	0.000	0.833	0.000	2.479	0.000
6.150	12.600	18.786	0.002	15.644	0.004	38.785	0.011	2.065	0.000	0.833	0.000	2.479	0.000
6.171	12.650	18.775	0.003	15.634	0.005	38.760	0.014	2.065	0.000	0.833	0.000	2.479	0.001
6.193	12.700	18.780	0.004	15.641	0.006	38.771	0.016	2.064	0.000	0.833	0.000	2.479	0.000
6.215	12.750	18.775	0.004	15.636	0.006	38.756	0.017	2.064	0.000	0.833	0.000	2.479	0.001
6.236	12.800	18.772	0.004	15.635	0.007	38.754	0.016	2.064	0.000	0.833	0.000	2.479	0.000
6.258	12.850	18.774	0.003	15.630	0.005	38.750	0.014	2.064	0.000	0.833	0.000	2.479	0.000
6.279	12.900	18.776	0.004	15.635	0.007	38.764	0.019	2.065	0.000	0.833	0.000	2.479	0.001
6.301	12.950	18.779	0.003	15.640	0.005	38.777	0.015	2.065	0.000	0.833	0.000	2.479	0.000
6.322	13.000	18.778	0.004	15.641	0.005	38.768	0.016	2.065	0.000	0.833	0.000	2.479	0.001
6.344	13.050	18.781	0.003	15.642	0.006	38.773	0.015	2.064	0.000	0.833	0.000	2.479	0.001
6.365	13.100	18.786	0.004	15.642	0.006	38.788	0.016	2.065	0.000	0.833	0.000	2.480	0.001
6.387	13.150	18.778	0.003	15.636	0.004	38.775	0.013	2.065	0.000	0.833	0.000	2.480	0.001
6.408	13.200	18.785	0.003	15.644	0.005	38.785	0.014	2.065	0.000	0.833	0.000	2.479	0.000
6.430	13.250	18.785	0.006	15.641	0.009	38.782	0.024	2.065	0.000	0.833	0.000	2.479	0.000
6.452	13.300	18.792	0.004	15.647	0.006	38.791	0.019	2.064	0.000	0.833	0.000	2.479	0.000
6.473	13.350	18.778	0.005	15.635	0.009	38.756	0.022	2.064	0.000	0.833	0.000	2.479	0.001
6.495	13.400	18.786	0.004	15.644	0.006	38.781	0.016	2.064	0.000	0.833	0.000	2.479	0.000
6.516	13.450	18.786	0.004	15.644	0.007	38.783	0.018	2.064	0.000	0.833	0.000	2.479	0.000
6.538	13.500	18.787	0.004	15.644	0.007	38.783	0.018	2.064	0.000	0.833	0.000	2.479	0.000
6.559	13.550	18.781	0.004	15.637	0.006	38.770	0.016	2.064	0.000	0.833	0.000	2.479	0.000
6.581	13.600	18.787	0.003	15.641	0.004	38.780	0.015	2.064	0.000	0.833	0.000	2.479	0.001
6.602	13.650	18.782	0.004	15.636	0.005	38.772	0.016	2.064	0.000	0.833	0.000	2.480	0.000
6.624	13.700	18.781	0.004	15.637	0.006	38.773	0.019	2.064	0.000	0.833	0.000	2.480	0.000
6.646	13.750	18.788	0.004	15.642	0.007	38.781	0.017	2.064	0.000	0.833	0.000	2.479	0.000
6.667	13.800	18.784	0.004	15.639	0.006	38.775	0.016	2.064	0.000	0.833	0.000	2.479	0.000
6.689	13.850	18.789	0.004	15.641	0.006	38.787	0.016	2.064	0.000	0.832	0.000	2.480	0.000
6.710	13.900	18.784	0.003	15.639	0.005	38.776	0.014	2.064	0.000	0.833	0.000	2.479	0.000
6.732	13.950	18.787	0.003	15.642	0.006	38.785	0.015	2.064	0.000	0.833	0.000	2.480	0.000
6.753	14.000	18.778	0.003	15.633	0.005	38.755	0.015	2.064	0.000	0.833	0.000	2.479	0.000
6.775	14.050	18.782	0.003	15.638	0.005	38.768	0.014	2.064	0.000	0.833	0.000	2.479	0.000
6.796	14.100	18.781	0.003	15.638	0.006	38.770	0.016	2.064	0.000	0.833	0.000	2.479	0.001
6.818	14.150	18.786	0.003	15.641	0.004	38.779	0.011	2.064	0.000	0.833	0.000	2.479	0.000
6.840	14.200	18.793	0.003	15.645	0.005	38.801	0.014	2.065	0.000	0.832	0.000	2.480	0.000
6.861	14.250	18.790	0.003	15.641	0.006	38.793	0.015	2.065	0.000	0.832	0.000	2.480	0.001
6.883	14.300	18.786	0.004	15.637	0.007	38.780	0.018	2.064	0.000	0.832	0.000	2.480	0.000
6.904	14.350	18.786	0.004	15.638	0.007	38.780	0.018	2.064	0.000	0.832	0.000	2.480	0.000
6.926	14.400	18.791	0.003	15.642	0.005	38.788	0.014	2.064	0.000	0.832	0.000	2.480	0.000
6.947	14.450	18.787	0.003	15.640	0.005	38.779	0.014	2.064	0.000	0.832	0.000	2.480	0.000
6.969	14.500	18.787	0.004	15.638	0.006	38.778	0.017	2.064	0.000	0.832	0.000	2.480	0.000
6.990	14.550	18.781	0.003	15.633	0.005	38.761	0.014	2.064	0.000	0.832	0.000	2.479	0.000
7.012	14.600	18.785	0.004	15.636	0.007	38.766	0.019	2.064	0.000	0.832	0.000	2.479	0.000
7.033	14.650	18.789	0.004	15.636	0.006	38.779	0.016	2.064	0.000	0.832	0.000	2.480	0.000
7.055	14.700	18.792	0.004	15.638	0.007	38.793	0.017	2.064	0.000	0.832	0.000	2.481	0.000
7.077	14.750	18.792	0.003	15.637	0.005	38.790	0.014	2.064	0.000	0.832	0.000	2.481	0.001
7.098	14.800	18.795	0.004	15.639	0.006	38.792	0.017	2.064	0.000	0.832	0.000	2.480	0.000
7.120	14.850	18.797	0.003	15.644	0.005	38.800	0.016	2.064	0.000	0.832	0.000	2.480	0.001
7.141	14.900	18.792	0.004	15.641	0.005	38.789	0.016	2.064	0.000	0.832	0.000	2.480	0.000
7.163	14.950	18.797	0.003	15.645	0.005	38.801	0.014	2.064	0.000	0.832	0.000	2.480	0.000

7.184	15.000	18.787	0.004	15.635	0.006	38.783	0.016	2.064	0.000	0.832	0.000	2.481	0.000
7.206	15.050	18.791	0.004	15.636	0.006	38.784	0.015	2.064	0.000	0.832	0.000	2.480	0.000
7.227	15.100	18.790	0.003	15.637	0.005	38.782	0.015	2.064	0.000	0.832	0.000	2.480	0.000
7.249	15.150	18.789	0.003	15.640	0.005	38.787	0.015	2.064	0.000	0.832	0.000	2.480	0.000
7.271	15.200	18.798	0.003	15.645	0.005	38.802	0.015	2.064	0.000	0.832	0.000	2.480	0.001
7.292	15.250	18.782	0.004	15.634	0.007	38.769	0.018	2.064	0.000	0.832	0.000	2.480	0.000
7.314	15.300	18.785	0.003	15.637	0.006	38.776	0.015	2.064	0.000	0.832	0.000	2.480	0.000
7.335	15.350	18.786	0.003	15.636	0.005	38.769	0.013	2.064	0.000	0.832	0.000	2.480	0.001
7.357	15.400	18.790	0.004	15.639	0.007	38.780	0.018	2.064	0.000	0.832	0.000	2.480	0.000
7.378	15.450	18.790	0.004	15.638	0.006	38.781	0.016	2.064	0.000	0.832	0.000	2.480	0.000
7.400	15.500	18.795	0.003	15.639	0.005	38.792	0.013	2.064	0.000	0.832	0.000	2.480	0.000
7.421	15.550	18.798	0.004	15.640	0.007	38.798	0.018	2.064	0.000	0.832	0.000	2.481	0.000
7.443	15.600	18.793	0.004	15.636	0.006	38.783	0.015	2.064	0.000	0.832	0.000	2.480	0.000
7.465	15.650	18.795	0.004	15.641	0.007	38.792	0.019	2.064	0.000	0.832	0.000	2.480	0.000
7.486	15.700	18.791	0.003	15.636	0.005	38.782	0.013	2.064	0.000	0.832	0.000	2.480	0.000
7.508	15.750	18.795	0.004	15.640	0.006	38.789	0.015	2.064	0.000	0.832	0.000	2.480	0.000
7.529	15.800	18.795	0.004	15.638	0.007	38.788	0.020	2.064	0.000	0.832	0.000	2.480	0.000
7.551	15.850	18.795	0.003	15.639	0.004	38.786	0.012	2.064	0.000	0.832	0.000	2.480	0.000
7.572	15.900	18.799	0.003	15.640	0.005	38.802	0.014	2.064	0.000	0.832	0.000	2.481	0.000
7.594	15.950	18.790	0.004	15.636	0.007	38.779	0.019	2.064	0.000	0.832	0.000	2.480	0.000
7.615	16.000	18.797	0.004	15.641	0.007	38.796	0.018	2.064	0.000	0.832	0.000	2.480	0.000
7.637	16.050	18.795	0.004	15.640	0.006	38.790	0.017	2.064	0.000	0.832	0.000	2.480	0.001
7.658	16.100	18.803	0.004	15.645	0.006	38.804	0.019	2.064	0.000	0.832	0.000	2.480	0.000
7.680	16.150	18.799	0.003	15.642	0.006	38.799	0.015	2.064	0.000	0.832	0.000	2.480	0.000
7.702	16.200	18.801	0.003	15.643	0.005	38.803	0.014	2.064	0.000	0.832	0.000	2.481	0.000
7.723	16.250	18.800	0.004	15.642	0.007	38.794	0.019	2.064	0.000	0.832	0.000	2.480	0.000
7.745	16.300	18.790	0.004	15.632	0.006	38.773	0.017	2.063	0.000	0.832	0.000	2.480	0.000
7.766	16.350	18.798	0.004	15.639	0.006	38.787	0.017	2.063	0.000	0.832	0.000	2.480	0.001
7.788	16.400	18.797	0.003	15.638	0.005	38.789	0.013	2.064	0.000	0.832	0.000	2.480	0.000
7.809	16.450	18.789	0.004	15.632	0.006	38.776	0.017	2.064	0.000	0.832	0.000	2.480	0.000
7.831	16.500	18.789	0.004	15.630	0.006	38.774	0.017	2.064	0.000	0.832	0.000	2.481	0.001
7.852	16.550	18.799	0.003	15.640	0.005	38.794	0.014	2.064	0.000	0.832	0.000	2.480	0.000
7.874	16.600	18.791	0.003	15.637	0.005	38.777	0.012	2.064	0.000	0.832	0.000	2.480	0.000
7.896	16.650	18.796	0.004	15.639	0.006	38.790	0.016	2.064	0.000	0.832	0.000	2.480	0.000
7.917	16.700	18.795	0.004	15.637	0.005	38.789	0.015	2.064	0.000	0.832	0.000	2.481	0.000
7.939	16.750	18.796	0.004	15.639	0.007	38.790	0.017	2.064	0.000	0.832	0.000	2.480	0.000
7.960	16.800	18.795	0.004	15.636	0.006	38.787	0.017	2.064	0.000	0.832	0.000	2.481	0.000
7.982	16.850	18.793	0.003	15.635	0.005	38.782	0.017	2.064	0.000	0.832	0.000	2.480	0.000
8.003	16.900	18.797	0.004	15.636	0.006	38.785	0.017	2.063	0.000	0.832	0.000	2.480	0.000
8.025	16.950	18.792	0.004	15.634	0.007	38.780	0.018	2.064	0.000	0.832	0.000	2.481	0.000
8.046	17.000	18.794	0.003	15.636	0.005	38.786	0.015	2.064	0.000	0.832	0.000	2.481	0.000
8.068	17.050	18.789	0.003	15.631	0.006	38.773	0.015	2.064	0.000	0.832	0.000	2.481	0.000
8.090	17.100	18.799	0.004	15.634	0.007	38.792	0.018	2.064	0.000	0.832	0.000	2.481	0.000
8.111	17.150	18.801	0.004	15.638	0.007	38.798	0.019	2.064	0.000	0.832	0.000	2.481	0.000
8.133	17.200	18.797	0.004	15.636	0.006	38.791	0.016	2.064	0.000	0.832	0.000	2.481	0.000
8.154	17.250	18.790	0.003	15.631	0.005	38.779	0.016	2.064	0.000	0.832	0.000	2.481	0.001
8.176	17.300	18.798	0.003	15.637	0.005	38.797	0.014	2.064	0.000	0.832	0.000	2.481	0.000
8.197	17.350	18.796	0.004	15.636	0.006	38.793	0.018	2.064	0.000	0.832	0.000	2.481	0.000
8.219	17.400	18.797	0.003	15.638	0.005	38.794	0.016	2.064	0.000	0.832	0.000	2.481	0.001
8.240	17.450	18.792	0.004	15.637	0.006	38.784	0.016	2.064	0.000	0.832	0.000	2.480	0.000
8.262	17.500	18.795	0.004	15.637	0.006	38.785	0.018	2.064	0.000	0.832	0.000	2.480	0.000
8.283	17.550	18.796	0.004	15.639	0.007	38.790	0.017	2.064	0.000	0.832	0.000	2.480	0.000
8.305	17.600	18.796	0.004	15.640	0.006	38.785	0.017	2.064	0.000	0.832	0.000	2.480	0.000
8.327	17.650	18.789	0.004	15.636	0.007	38.770	0.019	2.063	0.000	0.832	0.000	2.480	0.001
8.348	17.700	18.797	0.004	15.642	0.006	38.800	0.016	2.064	0.000	0.832	0.000	2.480	0.000
8.370	17.750	18.790	0.004	15.639	0.006	38.779	0.016	2.064	0.000	0.832	0.000	2.480	0.000
8.391	17.800	18.785	0.004	15.635	0.006	38.763	0.018	2.064	0.000	0.832	0.000	2.479	0.000
8.413	17.850	18.780	0.004	15.630	0.006	38.758	0.015	2.064	0.000	0.832	0.000	2.480	0.000
8.434	17.900	18.785	0.004	15.634	0.006	38.770	0.015	2.064	0.000	0.832	0.000	2.480	0.000
8.456	17.950	18.780	0.004	15.634	0.007	38.771	0.018	2.064	0.000	0.832	0.000	2.480	0.000
8.477	18.000	18.788	0.004	15.639	0.007	38.785	0.021	2.064	0.000	0.832	0.000	2.480	0.000
8.499	18.050	18.783	0.004	15.631	0.007	38.758	0.018	2.063	0.000	0.832	0.000	2.480	0.001
8.521	18.100	18.778	0.006	15.631	0.009	38.753	0.026	2.064	0.000	0.832	0.000	2.479	0.000
8.542	18.150	18.777	0.005	15.629	0.008	38.742	0.020	2.063	0.000	0.832	0.000	2.479	0.000
8.671	18.450	18.787	0.004	15.641	0.006	38.780	0.015	2.064	0.004	0.833	0.000	2.479	0.000
8.693	18.500	18.779	0.003	15.634	0.005	38.759	0.012	2.064	0.003	0.832	0.000	2.479	0.000
8.715	18.550	18.782	0.004	15.634	0.007	38.760	0.016	2.064	0.004	0.832	0.000	2.479	0.000
8.736	18.600	18.795	0.004	15.646	0.006	38.795	0.016	2.064	0.004	0.832	0.000	2.480	0.000
8.758	18.650	18.783	0.004	15.632	0.007	38.758	0.019	2.063	0.004	0.832	0.000	2.479	0.000
8.779	18.700	18.785	0.004	15.636	0.006	38.767	0.016	2.064	0.004	0.832	0.000	2.479	0.000
8.801	18.750	18.789	0.004	15.641	0.006	38.780	0.016	2.064	0.004	0.832	0.000	2.479	0.000
8.822	18.800	18.777	0.005	15.625	0.007	38.743	0.019	2.063	0.005	0.832	0.000	2.480	0.000
8.844	18.850	18.782	0.004	15.632	0.006	38.756	0.017	2.063	0.004	0.832	0.000	2.479	0.000
8.865	18.900	18.787	0.003	15.640	0.006	38.776	0.015	2.064	0.003	0.832	0.000	2.479	0.000
8.887	18.950	18.782	0.003	15.634	0.005	38.762	0.014	2.064	0.003	0.832	0.000	2.479	0.000
8.908	19.000	18.788	0.003	15.640	0.005	38.777	0.013	2.064	0.003	0.832	0.000	2.479	0.000
8.930	19.050	18.776	0.012	15.631	0.020	38.756	0.050	2.064	0.012	0.832	0.000	2.479	0.000
8.952	19.100	18.773	0.004	15.626	0.007	38.735	0.017	2.063	0.004	0.832	0.000	2.479	0.000
8.973	19.150	18.780	0.004	15.634	0.007	38.768	0.019	2.064	0.004	0.832	0.000	2.480	0.000
8.995	19.200	18.789	0.004	15.639	0.006	38.783	0.016	2.064	0.004	0.832	0.000	2.480	0.001
9.016	19.250	18.780	0.004	15.634	0.006	38.756	0.016	2.064	0.004	0.832	0.000	2.479	0.000
9.038	19.300	18.782	0.003	15.636	0.005	38.767	0.012	2.064	0.003	0.833	0.000	2.479	0.000
9.059	19.350	18.777	0.003	15.632	0.005	38.758	0.012	2.064	0.003	0.832	0.000	2.479	0.000
9.081	19.400	18.780	0.002	15.638	0.004	38.765	0.011	2.064	0.002	0.833	0.000	2.479	0.000
9.102	19.450	18.784	0.004	15.637	0.005	38.771	0.016	2.064	0.004	0.832	0.000	2.479	0.001
9.124	19.500	18.776	0.004	15.633	0.006	38.745	0.019	2.064	0.004	0.833	0.000	2.478	0.000
9.146	19.550	18.785	0.003	15.638	0.005	38.759	0.014	2.063	0.003	0.833	0.000	2.478	0.000
9.167	19.600	18.778	0.003	15.631	0.006	38.754	0.016	2.064	0.003	0.832	0.000	2.479	0.000
9.189	19.650	18.780	0.003	15.634	0.005	38.760	0.014	2.064	0.003	0.832	0.000	2.479	0.000
9.210	19.700	18.780	0.003	15.635	0.005	38.760	0.013	2.064	0.003	0.833	0.000	2.479	0.000
9.232	19.750	18.775	0.003	15.633	0.005	38.750	0.013	2.064	0.003	0.833	0.000	2.479	0.000
9.253	19.800	18.782	0.004	15.636	0.006	38.762	0.015	2.064	0.004	0.833	0.000	2.479	0.000
9.275	19.850	18.783	0.005	15.636	0.009	38.767	0.023	2.064	0.005	0.832	0.000	2.479	0.000
9.296	19.900	18.791	0.004	15.643	0.006	38.783	0.016	2.064	0.004	0.832	0.000	2.479	0.000
9.318	19.950	18.783	0.003	15.636	0.005	38.768	0.013	2.064	0.003	0.832	0.000	2.479	0.000
9.340	20.000	18.789	0.003	15.640	0.005	38.776	0.015	2.064	0.003	0.832	0.000	2.479	0.000
9.361	20.050	18.788	0.003	15.638	0.005	38.774	0.014	2.064	0.003	0.832	0.000	2.480	0.000
9.383	20.100	18.788	0.004	15.635	0.006	38.769	0.016	2.063	0.004	0.832	0.000	2.480	0.000
9.404	20.150	18.783	0.004	15.629	0.007	38.758	0.017	2.064	0.004	0.832	0.000	2.480	0.000
9.426	20.200	18.781	0.004	15.628	0.006	38.746	0.016	2.063	0.004	0.832	0.000	2.479	0.001
9.447	20.250	18.791	0.003	15.637	0.005	38.773	0.015	2.063	0.003	0.832	0.000	2.480	0.000

9.469	20.300	18.794	0.002	15.637	0.004	38.780	0.011	2.063	0.002	0.832	0.000	2.480	0.000
9.490	20.350	18.791	0.004	15.630	0.006	38.776	0.018	2.064	0.004	0.832	0.000	2.481	0.000
9.512	20.400	18.799	0.003	15.638	0.006	38.794	0.017	2.064	0.003	0.832	0.000	2.481	0.000
9.533	20.450	18.809	0.003	15.645	0.006	38.813	0.014	2.064	0.003	0.832	0.000	2.481	0.001
9.555	20.500	18.811	0.005	15.646	0.007	38.815	0.021	2.063	0.005	0.832	0.000	2.481	0.000
9.577	20.550	18.801	0.004	15.635	0.006	38.782	0.018	2.063	0.004	0.832	0.000	2.480	0.000
9.598	20.600	18.802	0.004	15.638	0.006	38.793	0.016	2.063	0.004	0.832	0.000	2.481	0.001
9.620	20.650	18.802	0.003	15.635	0.004	38.788	0.012	2.063	0.003	0.832	0.000	2.481	0.000
9.641	20.700	18.802	0.004	15.632	0.006	38.789	0.016	2.063	0.004	0.831	0.000	2.481	0.000
9.663	20.750	18.811	0.004	15.638	0.006	38.805	0.017	2.063	0.004	0.831	0.000	2.481	0.000
9.684	20.800	18.806	0.003	15.633	0.005	38.787	0.016	2.062	0.003	0.831	0.000	2.481	0.000
9.706	20.850	18.812	0.004	15.634	0.007	38.794	0.019	2.062	0.004	0.831	0.000	2.481	0.000
9.720	20.900	18.816	0.005	15.633	0.008	38.801	0.020	2.062	0.005	0.831	0.000	2.482	0.000
9.733	20.950	18.815	0.004	15.629	0.006	38.791	0.018	2.062	0.004	0.831	0.000	2.482	0.001
9.747	21.000	18.823	0.004	15.636	0.008	38.808	0.020	2.062	0.004	0.831	0.000	2.482	0.000
9.760	21.050	18.833	0.003	15.638	0.005	38.830	0.013	2.062	0.003	0.830	0.000	2.483	0.000
9.774	21.100	18.837	0.004	15.641	0.007	38.842	0.018	2.062	0.004	0.830	0.000	2.483	0.000
9.788	21.150	18.831	0.003	15.635	0.005	38.833	0.014	2.062	0.003	0.830	0.000	2.484	0.000
9.801	21.200	18.835	0.005	15.642	0.008	38.843	0.020	2.062	0.005	0.830	0.000	2.483	0.000
9.815	21.250	18.837	0.005	15.647	0.009	38.856	0.022	2.063	0.005	0.831	0.000	2.483	0.001
9.828	21.300	18.837	0.005	15.644	0.009	38.847	0.021	2.062	0.005	0.831	0.000	2.483	0.000
9.842	21.350	18.839	0.004	15.644	0.008	38.851	0.019	2.062	0.004	0.830	0.000	2.483	0.000
9.855	21.400	18.843	0.006	15.645	0.009	38.857	0.025	2.062	0.006	0.830	0.000	2.484	0.000
9.869	21.450	18.851	0.005	15.651	0.009	38.872	0.023	2.062	0.005	0.830	0.000	2.484	0.000
9.883	21.500	18.847	0.004	15.644	0.007	38.864	0.019	2.062	0.004	0.830	0.000	2.484	0.000
9.896	21.550	18.853	0.004	15.644	0.007	38.870	0.019	2.062	0.004	0.830	0.000	2.485	0.000
9.910	21.600	18.851	0.004	15.640	0.007	38.868	0.019	2.062	0.004	0.830	0.000	2.485	0.000
9.923	21.650	18.860	0.004	15.642	0.006	38.882	0.018	2.062	0.004	0.829	0.000	2.486	0.000
9.937	21.700	18.867	0.007	15.646	0.011	38.903	0.029	2.062	0.007	0.829	0.000	2.486	0.001
9.951	21.750	18.872	0.006	15.653	0.009	38.919	0.026	2.062	0.006	0.829	0.000	2.486	0.000
9.964	21.800	18.866	0.007	15.648	0.011	38.897	0.030	2.062	0.007	0.829	0.000	2.486	0.000
9.978	21.850	18.864	0.005	15.646	0.008	38.895	0.019	2.062	0.005	0.829	0.000	2.486	0.000
9.991	21.900	18.880	0.004	15.655	0.007	38.924	0.018	2.062	0.004	0.829	0.000	2.486	0.000
10.005	21.950	18.871	0.004	15.653	0.007	38.911	0.016	2.062	0.004	0.829	0.000	2.486	0.000
10.019	22.000	18.868	0.004	15.647	0.007	38.904	0.018	2.062	0.004	0.829	0.000	2.486	0.000
10.032	22.050	18.865	0.004	15.643	0.006	38.884	0.017	2.061	0.004	0.829	0.000	2.486	0.000
10.046	22.100	18.868	0.004	15.644	0.006	38.899	0.016	2.062	0.004	0.829	0.000	2.486	0.000
10.059	22.150	18.874	0.003	15.645	0.005	38.907	0.014	2.061	0.003	0.829	0.000	2.487	0.000
10.073	22.200	18.882	0.004	15.652	0.006	38.931	0.015	2.062	0.004	0.829	0.000	2.487	0.000
10.086	22.250	18.879	0.003	15.653	0.005	38.927	0.014	2.062	0.003	0.829	0.000	2.487	0.000
10.100	22.300	18.874	0.003	15.645	0.005	38.911	0.015	2.062	0.003	0.829	0.000	2.487	0.000
10.114	22.350	18.879	0.006	15.651	0.009	38.927	0.026	2.062	0.006	0.829	0.000	2.487	0.000
10.141	22.450	18.879	0.005	15.649	0.008	38.921	0.023	2.062	0.005	0.829	0.000	2.487	0.000
10.154	22.500	18.885	0.004	15.652	0.007	38.930	0.017	2.061	0.004	0.829	0.000	2.487	0.000
10.168	22.550	18.892	0.005	15.656	0.008	38.953	0.020	2.062	0.005	0.829	0.000	2.488	0.001
10.182	22.600	18.882	0.004	15.648	0.006	38.932	0.015	2.062	0.004	0.829	0.000	2.488	0.000
10.195	22.650	18.883	0.004	15.651	0.007	38.934	0.019	2.062	0.004	0.829	0.000	2.488	0.000
10.209	22.700	18.881	0.004	15.649	0.006	38.922	0.016	2.061	0.004	0.829	0.000	2.487	0.000
10.222	22.750	18.878	0.006	15.648	0.010	38.927	0.026	2.062	0.006	0.829	0.000	2.488	0.000
10.236	22.800	18.887	0.004	15.655	0.007	38.936	0.019	2.062	0.004	0.829	0.000	2.487	0.000
10.249	22.850	18.889	0.004	15.651	0.006	38.944	0.015	2.062	0.004	0.829	0.000	2.488	0.000
10.263	22.900	18.885	0.004	15.654	0.006	38.942	0.019	2.062	0.004	0.829	0.000	2.488	0.000
10.277	22.950	18.882	0.005	15.651	0.009	38.932	0.023	2.062	0.005	0.829	0.000	2.487	0.001
10.290	23.000	18.886	0.004	15.651	0.007	38.937	0.018	2.062	0.004	0.829	0.000	2.488	0.000
10.304	23.050	18.892	0.004	15.653	0.006	38.948	0.017	2.062	0.004	0.829	0.000	2.488	0.000
10.317	23.100	18.891	0.004	15.654	0.006	38.950	0.018	2.062	0.004	0.829	0.000	2.488	0.000
10.331	23.150	18.883	0.005	15.650	0.008	38.931	0.023	2.062	0.005	0.829	0.000	2.488	0.000
10.345	23.200	18.879	0.005	15.649	0.008	38.932	0.022	2.062	0.005	0.829	0.000	2.488	0.000
10.358	23.250	18.891	0.004	15.657	0.007	38.953	0.018	2.062	0.004	0.829	0.000	2.488	0.000
10.372	23.300	18.898	0.006	15.661	0.009	38.969	0.025	2.062	0.006	0.829	0.000	2.488	0.000
10.385	23.350	18.888	0.005	15.650	0.008	38.935	0.021	2.061	0.005	0.829	0.000	2.488	0.000
10.399	23.400	18.891	0.005	15.653	0.008	38.949	0.019	2.062	0.005	0.829	0.000	2.488	0.000
10.413	23.450	18.877	0.006	15.649	0.010	38.920	0.024	2.062	0.006	0.829	0.000	2.487	0.000
10.426	23.500	18.883	0.004	15.650	0.007	38.930	0.018	2.062	0.004	0.829	0.000	2.488	0.000
10.440	23.550	18.878	0.004	15.646	0.006	38.917	0.017	2.061	0.004	0.829	0.000	2.487	0.000
10.453	23.600	18.889	0.004	15.656	0.007	38.944	0.018	2.062	0.004	0.829	0.000	2.487	0.000
10.467	23.650	18.881	0.005	15.650	0.008	38.925	0.022	2.062	0.005	0.829	0.000	2.487	0.000
10.480	23.700	18.890	0.005	15.657	0.007	38.950	0.020	2.062	0.005	0.829	0.000	2.488	0.000
10.494	23.750	18.885	0.004	15.653	0.006	38.937	0.016	2.062	0.004	0.829	0.000	2.487	0.000
10.508	23.800	18.889	0.005	15.650	0.009	38.943	0.024	2.062	0.005	0.829	0.000	2.488	0.000
10.521	23.850	18.894	0.005	15.654	0.007	38.956	0.021	2.062	0.005	0.828	0.000	2.489	0.001
10.548	23.950	18.894	0.005	15.656	0.009	38.956	0.023	2.062	0.005	0.829	0.000	2.488	0.000
10.562	24.000	18.889	0.005	15.653	0.009	38.945	0.023	2.062	0.005	0.829	0.000	2.488	0.000
10.576	24.050	18.890	0.005	15.651	0.008	38.942	0.020	2.062	0.005	0.829	0.000	2.488	0.000
10.589	24.100	18.896	0.004	15.652	0.007	38.954	0.018	2.062	0.004	0.828	0.000	2.489	0.001
10.603	24.150	18.898	0.004	15.653	0.006	38.960	0.016	2.062	0.004	0.828	0.000	2.489	0.000
10.616	24.200	18.888	0.005	15.653	0.009	38.944	0.024	2.062	0.005	0.829	0.000	2.488	0.000
10.630	24.250	18.910	0.004	15.670	0.007	38.993	0.018	2.062	0.004	0.829	0.000	2.488	0.000
10.644	24.300	18.886	0.005	15.645	0.009	38.930	0.023	2.061	0.005	0.828	0.000	2.488	0.000
10.657	24.350	18.897	0.005	15.648	0.008	38.950	0.024	2.061	0.005	0.828	0.000	2.489	0.001
10.671	24.400	18.891	0.007	15.651	0.011	38.937	0.030	2.061	0.007	0.829	0.000	2.488	0.001
10.684	24.450	18.893	0.006	15.646	0.010	38.933	0.027	2.061	0.006	0.828	0.000	2.488	0.000
10.698	24.500	18.890	0.008	15.639	0.013	38.923	0.034	2.061	0.008	0.828	0.000	2.489	0.000
10.711	24.550	18.898	0.008	15.648	0.013	38.946	0.031	2.061	0.008	0.828	0.000	2.489	0.000
10.725	24.600	18.907	0.006	15.656	0.009	38.964	0.023	2.061	0.006	0.828	0.000	2.489	0.000
10.739	24.650	18.903	0.006	15.654	0.010	38.963	0.027	2.061	0.006	0.828	0.000	2.489	0.000
10.752	24.700	18.901	0.007	15.653	0.011	38.962	0.030	2.061	0.007	0.828	0.000	2.489	0.000
10.766	24.750	18.911	0.007	15.660	0.013	38.974	0.032	2.061	0.007	0.828	0.000	2.489	0.000
10.779	24.800	18.905	0.005	15.654	0.009	38.968	0.024	2.061	0.005	0.828	0.000	2.489	0.000
10.793	24.850	18.905	0.006	15.654	0.009	38.968	0.025	2.061	0.006	0.828	0.000	2.489	0.001
10.807	24.900	18.890	0.005	15.643	0.009	38.938	0.021	2.061	0.005	0.828	0.000	2.489	0.000
10.820	24.950	18.911	0.004	15.658	0.007	38.976	0.019	2.061	0.004	0.828	0.000	2.489	0.000
10.834	25.000	18.911	0.004	15.660	0.007	38.983	0.018	2.061	0.004	0.828	0.000	2.489	0.000
10.847	25.050	18.904	0.006	15.656	0.009	38.964	0.024	2.061	0.006	0.828	0.000	2.489	0.000
10.861	25.100	18.907	0.007	15.659	0.012	38.979	0.032	2.062	0.007	0.828	0.000	2.489	0.001
10.874	25.150	18.899	0.006	15.652	0.009	38.953	0.023	2.061	0.006	0.828	0.000	2.489	0.001
10.888	25.200	18.914	0.007	15.660	0.011	38.988	0.028	2.061	0.007	0.828	0.000	2.490	0.001
10.902	25.250	18.908	0.006	15.658	0.009	38.975	0.025	2.061	0.006	0.828	0.000	2.489	0.000
10.915	25.300	18.911	0.005	15.664	0.008	38.983	0.020	2.061	0.005	0.828	0.000	2.489	0.000
10.929	25.350	18.910	0.005	15.655	0.009	38.969	0.023	2.061	0.005	0.828	0.000	2.489	0.000
10.942	25.400	18.896	0.013	15.644	0.022	38.943	0.055	2.061	0.013	0.828	0.000	2.489	0.001

10.956	25.450	18.896	0.007	15.649	0.012	38.946	0.030	2.061	0.007	0.828	0.000	2.489	0.000
10.970	25.500	18.901	0.008	15.654	0.013	38.969	0.032	2.062	0.008	0.828	0.000	2.489	0.000
10.983	25.550	18.896	0.006	15.652	0.010	38.952	0.025	2.061	0.006	0.828	0.000	2.489	0.000
10.997	25.600	18.894	0.006	15.650	0.009	38.946	0.024	2.061	0.006	0.828	0.000	2.489	0.000
11.010	25.650	18.905	0.003	15.659	0.006	38.969	0.015	2.061	0.003	0.828	0.000	2.489	0.000
11.024	25.700	18.905	0.004	15.659	0.008	38.975	0.020	2.062	0.004	0.828	0.000	2.489	0.001
11.038	25.750	18.903	0.004	15.654	0.006	38.959	0.017	2.061	0.004	0.828	0.000	2.489	0.001
11.051	25.800	18.903	0.005	15.659	0.009	38.970	0.023	2.062	0.005	0.828	0.000	2.489	0.000
11.065	25.850	18.906	0.004	15.660	0.006	38.980	0.017	2.062	0.004	0.828	0.000	2.489	0.000
11.078	25.900	18.906	0.003	15.661	0.005	38.984	0.014	2.062	0.003	0.828	0.000	2.489	0.000
11.092	25.950	18.892	0.005	15.655	0.008	38.954	0.022	2.062	0.005	0.829	0.000	2.488	0.000
11.105	26.000	18.899	0.004	15.657	0.007	38.963	0.017	2.062	0.004	0.828	0.000	2.489	0.000
11.119	26.050	18.896	0.004	15.656	0.006	38.965	0.016	2.062	0.004	0.829	0.000	2.489	0.000
11.133	26.100	18.892	0.004	15.651	0.006	38.954	0.016	2.062	0.004	0.828	0.000	2.489	0.000
11.146	26.150	18.899	0.003	15.659	0.005	38.971	0.014	2.062	0.003	0.829	0.000	2.489	0.000
11.160	26.200	18.900	0.004	15.658	0.006	38.966	0.017	2.062	0.004	0.828	0.000	2.489	0.000
11.173	26.250	18.895	0.005	15.655	0.008	38.956	0.021	2.062	0.005	0.829	0.000	2.488	0.000
11.187	26.300	18.894	0.004	15.660	0.007	38.956	0.018	2.062	0.004	0.829	0.000	2.488	0.000
11.201	26.350	18.886	0.005	15.653	0.008	38.943	0.021	2.062	0.005	0.829	0.000	2.488	0.000
11.214	26.400	18.882	0.004	15.650	0.007	38.938	0.019	2.062	0.004	0.829	0.000	2.488	0.000
11.228	26.450	18.886	0.004	15.652	0.007	38.951	0.019	2.062	0.004	0.829	0.000	2.489	0.000
11.241	26.500	18.889	0.006	15.654	0.009	38.957	0.024	2.062	0.006	0.829	0.000	2.489	0.000
11.255	26.550	18.898	0.004	15.657	0.007	38.969	0.019	2.062	0.004	0.828	0.000	2.489	0.000
11.269	26.600	18.900	0.006	15.657	0.011	38.972	0.027	2.062	0.006	0.828	0.000	2.489	0.000
11.282	26.650	18.893	0.007	15.649	0.012	38.951	0.029	2.062	0.007	0.828	0.000	2.489	0.000
11.296	26.700	18.892	0.005	15.646	0.009	38.947	0.023	2.062	0.005	0.828	0.000	2.489	0.000
11.309	26.750	18.885	0.015	15.646	0.012	38.931	0.031	2.061	0.000	0.828	0.000	2.488	0.000
11.323	26.800	18.883	0.014	15.643	0.012	38.931	0.031	2.062	0.000	0.828	0.000	2.489	0.000
11.336	26.850	18.896	0.012	15.660	0.010	38.981	0.026	2.063	0.000	0.829	0.000	2.489	0.000
11.350	26.900	18.893	0.014	15.654	0.012	38.974	0.030	2.063	0.000	0.829	0.000	2.490	0.000
11.364	26.950	18.899	0.013	15.667	0.011	38.998	0.028	2.063	0.000	0.829	0.000	2.489	0.000
11.377	27.000	18.892	0.012	15.659	0.010	38.978	0.026	2.063	0.000	0.829	0.000	2.489	0.001
11.391	27.050	18.894	0.009	15.659	0.008	38.984	0.019	2.063	0.000	0.829	0.000	2.490	0.000
11.404	27.100	18.898	0.010	15.664	0.008	38.985	0.021	2.063	0.000	0.829	0.000	2.489	0.000
11.418	27.150	18.882	0.008	15.652	0.006	38.963	0.017	2.063	0.000	0.829	0.000	2.489	0.000
11.432	27.200	18.901	0.011	15.666	0.009	39.003	0.024	2.063	0.000	0.829	0.000	2.490	0.000
11.445	27.250	18.896	0.015	15.662	0.012	38.988	0.031	2.063	0.000	0.829	0.000	2.489	0.001
11.459	27.300	18.892	0.010	15.659	0.008	38.979	0.022	2.063	0.000	0.829	0.000	2.489	0.001
11.472	27.350	18.891	0.011	15.650	0.009	38.972	0.024	2.063	0.000	0.828	0.000	2.490	0.001
11.486	27.400	18.896	0.012	15.660	0.009	38.979	0.026	2.063	0.000	0.829	0.000	2.489	0.001
11.499	27.450	18.897	0.011	15.660	0.009	38.979	0.023	2.063	0.000	0.829	0.000	2.489	0.000
11.513	27.500	18.890	0.010	15.651	0.008	38.963	0.022	2.063	0.000	0.829	0.000	2.489	0.001
11.527	27.550	18.911	0.010	15.663	0.008	39.005	0.021	2.063	0.000	0.828	0.000	2.490	0.000
11.540	27.600	18.913	0.013	15.669	0.011	39.011	0.028	2.063	0.000	0.829	0.000	2.490	0.000
11.554	27.650	18.918	0.014	15.675	0.012	39.020	0.031	2.063	0.000	0.829	0.000	2.489	0.000
11.567	27.700	18.897	0.010	15.656	0.009	38.978	0.022	2.063	0.000	0.828	0.000	2.490	0.000
11.581	27.750	18.904	0.011	15.664	0.009	38.995	0.023	2.063	0.000	0.829	0.000	2.489	0.001
11.595	27.800	18.904	0.012	15.664	0.010	39.000	0.025	2.063	0.000	0.829	0.000	2.490	0.000
11.608	27.850	18.902	0.010	15.658	0.009	38.988	0.022	2.063	0.000	0.828	0.000	2.490	0.000
11.622	27.900	18.912	0.014	15.665	0.011	39.020	0.030	2.063	0.000	0.828	0.000	2.491	0.001
11.635	27.950	18.906	0.012	15.655	0.009	38.994	0.025	2.063	0.000	0.828	0.000	2.491	0.000
11.649	28.000	18.895	0.011	15.652	0.009	38.972	0.024	2.063	0.000	0.828	0.000	2.490	0.001
11.663	28.050	18.896	0.009	15.650	0.007	38.970	0.019	2.062	0.000	0.828	0.000	2.490	0.000
11.676	28.100	18.901	0.010	15.662	0.008	38.985	0.020	2.063	0.000	0.829	0.000	2.489	0.000
11.690	28.150	18.900	0.010	15.657	0.009	38.975	0.023	2.062	0.000	0.828	0.000	2.489	0.000
11.703	28.200	18.890	0.032	15.639	0.027	38.956	0.068	2.062	0.000	0.828	0.000	2.491	0.001
11.717	28.250	18.905	0.022	15.654	0.018	38.983	0.048	2.062	0.000	0.828	0.000	2.490	0.001
11.730	28.300	18.887	0.011	15.649	0.008	38.955	0.024	2.063	0.000	0.829	0.000	2.489	0.001
11.744	28.350	18.894	0.010	15.653	0.008	38.963	0.020	2.062	0.000	0.828	0.000	2.489	0.000
11.803	28.400	18.893	0.009	15.651	0.008	38.963	0.019	2.062	0.000	0.828	0.000	2.490	0.000
11.817	28.450	18.890	0.009	15.650	0.007	38.958	0.020	2.062	0.000	0.828	0.000	2.489	0.000
11.831	28.500	18.890	0.009	15.654	0.007	38.956	0.018	2.062	0.000	0.829	0.000	2.489	0.000
11.845	28.550	18.868	0.011	15.638	0.009	38.914	0.023	2.062	0.000	0.829	0.000	2.488	0.001
11.887	28.700	18.893	0.013	15.645	0.011	38.974	0.027	2.063	0.000	0.828	0.000	2.491	0.001
11.900	28.750	18.889	0.014	15.652	0.011	38.963	0.030	2.063	0.000	0.829	0.000	2.489	0.000
11.914	28.800	18.890	0.012	15.659	0.010	38.966	0.026	2.063	0.000	0.829	0.000	2.488	0.000
11.928	28.850	18.879	0.016	15.651	0.013	38.952	0.033	2.063	0.000	0.829	0.000	2.489	0.001
11.942	28.900	18.875	0.016	15.646	0.012	38.940	0.034	2.063	0.000	0.829	0.000	2.489	0.001
11.956	28.950	18.881	0.014	15.651	0.012	38.954	0.030	2.063	0.000	0.829	0.000	2.489	0.001
11.970	29.000	18.863	0.011	15.642	0.009	38.918	0.023	2.063	0.000	0.829	0.000	2.488	0.001
11.984	29.050	18.870	0.016	15.651	0.012	38.925	0.035	2.063	0.000	0.829	0.000	2.487	0.001
11.998	29.100	18.866	0.010	15.648	0.008	38.926	0.022	2.063	0.000	0.829	0.000	2.488	0.001
12.012	29.150	18.863	0.009	15.644	0.006	38.917	0.017	2.063	0.000	0.829	0.000	2.488	0.000
12.025	29.200	18.859	0.011	15.643	0.009	38.915	0.023	2.063	0.000	0.829	0.000	2.488	0.000
12.039	29.250	18.869	0.010	15.651	0.008	38.928	0.021	2.063	0.000	0.829	0.000	2.487	0.000
12.053	29.300	18.860	0.012	15.646	0.009	38.919	0.026	2.064	0.000	0.830	0.000	2.487	0.000
12.067	29.350	18.871	0.011	15.651	0.009	38.937	0.024	2.063	0.000	0.829	0.000	2.488	0.001
12.081	29.400	18.863	0.019	15.646	0.016	38.929	0.040	2.064	0.000	0.829	0.000	2.488	0.000
12.095	29.450	18.881	0.009	15.661	0.008	38.961	0.020	2.063	0.000	0.829	0.000	2.488	0.000
12.109	29.500	18.869	0.008	15.652	0.006	38.935	0.018	2.063	0.000	0.830	0.000	2.488	0.001
12.123	29.550	18.870	0.016	15.649	0.013	38.927	0.034	2.063	0.000	0.829	0.000	2.488	0.001
12.137	29.600	18.856	0.017	15.644	0.014	38.915	0.037	2.064	0.000	0.830	0.000	2.488	0.001
12.150	29.650	18.862	0.012	15.648	0.010	38.919	0.025	2.063	0.000	0.830	0.000	2.487	0.000
12.164	29.700	18.864	0.010	15.653	0.008	38.926	0.021	2.063	0.000	0.830	0.000	2.487	0.000
12.178	29.750	18.859	0.012	15.647	0.010	38.922	0.026	2.064	0.000	0.830	0.000	2.487	0.000
12.192	29.800	18.854	0.014	15.646	0.012	38.906	0.030	2.064	0.000	0.830	0.000	2.487	0.000
12.206	29.850	18.842	0.013	15.637	0.010	38.884	0.027	2.064	0.000	0.830	0.000	2.487	0.000
12.220	29.900	18.845	0.015	15.647	0.012	38.894	0.031	2.064	0.000	0.830	0.000	2.486	0.001
12.234	29.950	18.842	0.013	15.643	0.011	38.887	0.027	2.064	0.000	0.830	0.000	2.486	0.001
12.248	30.000	18.842	0.017	15.644	0.014	38.878	0.035	2.063	0.000	0.830	0.000	2.485	0.001
12.262	30.050	18.842	0.009	15.646	0.007	38.894	0.020	2.064	0.000	0.830	0.000	2.486	0.000
12.275	30.100	18.852	0.012	15.654	0.010	38.911	0.026	2.064	0.000	0.830	0.000	2.486	0.001
12.289	30.150	18.845	0.016	15.645	0.013	38.891	0.033	2.064	0.000	0.830	0.000	2.486	0.001
12.303	30.200	18.834	0.014	15.636	0.012	38.872	0.030	2.064	0.000	0.830	0.000	2.486	0.000
12.317	30.250	18.843	0.017	15.644	0.014	38.884	0.036	2.064	0.000	0.830	0.000	2.486	0.000
12.331	30.300	18.845	0.012	15.645	0.010	38.889	0.026	2.064	0.000	0.830	0.000	2.486	0.000
12.345	30.350	18.848	0.013	15.651	0.009	38.911	0.028	2.064	0.000	0.830	0.000	2.486	0.001
12.359	30.400	18.830	0.010	15.642	0.008	38.869	0.021	2.064	0.000	0.831	0.000	2.485	0.000
12.373	30.450	18.830	0.011	15.645	0.008	38.869	0.023	2.064	0.000	0.831	0.000	2.484	0.001
12.387	30.500	18.847	0.011	15.654	0.009	38.901	0.023	2.064	0.000	0.831	0.000	2.485	0.000
12.400	30.550	18.823	0.015	15.638	0.013	38.846	0.033	2.064	0.000	0.831	0.000	2.484	0.000

12.414	30.600	18.844	0.012	15.654	0.010	38.894	0.025	2.064	0.000	0.831	0.000	2.485	0.000
12.428	30.650	18.835	0.011	15.643	0.009	38.876	0.024	2.064	0.000	0.831	0.000	2.485	0.000
12.442	30.700	18.835	0.014	15.644	0.011	38.877	0.029	2.064	0.000	0.831	0.000	2.485	0.000
12.456	30.750	18.844	0.009	15.646	0.008	38.899	0.020	2.064	0.000	0.830	0.000	2.486	0.001
12.470	30.800	18.841	0.013	15.646	0.010	38.890	0.027	2.064	0.000	0.830	0.000	2.486	0.001
12.484	30.850	18.843	0.010	15.646	0.008	38.894	0.021	2.064	0.000	0.830	0.000	2.486	0.001
12.498	30.900	18.841	0.008	15.644	0.007	38.892	0.017	2.064	0.000	0.830	0.000	2.486	0.000
12.512	30.950	18.835	0.008	15.642	0.006	38.876	0.017	2.064	0.000	0.830	0.000	2.485	0.000
12.525	31.000	18.824	0.010	15.634	0.007	38.854	0.023	2.064	0.000	0.831	0.000	2.485	0.001
12.539	31.050	18.845	0.008	15.651	0.007	38.895	0.017	2.064	0.000	0.830	0.000	2.485	0.000
12.553	31.100	18.828	0.008	15.641	0.006	38.856	0.017	2.064	0.000	0.831	0.000	2.484	0.000
12.567	31.150	18.837	0.008	15.642	0.007	38.875	0.017	2.064	0.000	0.830	0.000	2.485	0.000
12.581	31.200	18.843	0.010	15.645	0.008	38.887	0.021	2.064	0.000	0.830	0.000	2.486	0.000
12.595	31.250	18.843	0.010	15.644	0.009	38.885	0.021	2.064	0.000	0.830	0.000	2.486	0.001
12.609	31.300	18.839	0.010	15.644	0.007	38.879	0.020	2.064	0.000	0.830	0.000	2.485	0.000
12.623	31.350	18.870	0.011	15.667	0.009	38.947	0.023	2.064	0.000	0.830	0.000	2.486	0.000
12.637	31.400	18.847	0.007	15.648	0.006	38.894	0.014	2.064	0.000	0.830	0.000	2.485	0.000
12.650	31.450	18.837	0.018	15.649	0.015	38.884	0.040	2.064	0.000	0.831	0.000	2.485	0.001
12.664	31.500	18.844	0.010	15.649	0.008	38.899	0.021	2.064	0.000	0.830	0.000	2.486	0.000
12.678	31.550	18.833	0.008	15.644	0.007	38.879	0.018	2.064	0.000	0.831	0.000	2.485	0.000
12.692	31.600	18.837	0.013	15.644	0.011	38.890	0.026	2.064	0.000	0.830	0.000	2.486	0.001
12.706	31.650	18.835	0.016	15.641	0.013	38.882	0.033	2.064	0.000	0.830	0.000	2.486	0.000
12.720	31.700	18.835	0.014	15.643	0.012	38.878	0.028	2.064	0.000	0.831	0.000	2.485	0.001
12.734	31.750	18.841	0.015	15.652	0.012	38.896	0.031	2.064	0.000	0.831	0.000	2.485	0.001
12.748	31.800	18.844	0.012	15.652	0.009	38.894	0.025	2.064	0.000	0.831	0.000	2.485	0.000
12.762	31.850	18.836	0.011	15.644	0.009	38.877	0.025	2.064	0.000	0.831	0.000	2.485	0.000
12.775	31.900	18.836	0.014	15.646	0.012	38.879	0.031	2.064	0.000	0.831	0.000	2.485	0.000
12.789	31.950	18.840	0.015	15.641	0.012	38.883	0.031	2.064	0.000	0.830	0.000	2.486	0.000
12.803	32.000	18.826	0.012	15.633	0.011	38.861	0.026	2.064	0.000	0.830	0.000	2.486	0.000
12.817	32.050	18.827	0.011	15.643	0.009	38.869	0.023	2.065	0.000	0.831	0.000	2.485	0.001
12.831	32.100	18.831	0.011	15.646	0.009	38.883	0.024	2.065	0.000	0.831	0.000	2.485	0.001
12.845	32.150	18.817	0.013	15.636	0.011	38.846	0.026	2.064	0.000	0.831	0.000	2.485	0.001
12.859	32.200	18.830	0.010	15.645	0.009	38.872	0.023	2.064	0.000	0.831	0.000	2.485	0.001
12.873	32.250	18.824	0.009	15.641	0.008	38.861	0.020	2.064	0.000	0.831	0.000	2.485	0.000
12.887	32.300	18.824	0.013	15.638	0.010	38.860	0.027	2.064	0.000	0.831	0.000	2.485	0.001
12.900	32.350	18.836	0.012	15.648	0.011	38.882	0.026	2.064	0.000	0.831	0.000	2.485	0.001
12.914	32.400	18.843	0.020	15.653	0.017	38.909	0.042	2.065	0.000	0.831	0.000	2.486	0.000
12.928	32.450	18.833	0.008	15.646	0.007	38.879	0.018	2.064	0.000	0.831	0.000	2.485	0.000
12.942	32.500	18.827	0.012	15.643	0.010	38.870	0.025	2.065	0.000	0.831	0.000	2.485	0.000
12.956	32.550	18.821	0.008	15.638	0.006	38.853	0.017	2.064	0.000	0.831	0.000	2.485	0.000
12.970	32.600	18.827	0.010	15.643	0.008	38.865	0.021	2.064	0.000	0.831	0.000	2.484	0.000
12.984	32.650	18.830	0.012	15.645	0.010	38.871	0.024	2.064	0.000	0.831	0.000	2.485	0.001
12.998	32.700	18.833	0.010	15.649	0.008	38.875	0.021	2.064	0.000	0.831	0.000	2.484	0.000
13.012	32.750	18.840	0.011	15.649	0.010	38.893	0.023	2.064	0.000	0.831	0.000	2.485	0.000
13.025	32.800	18.836	0.013	15.646	0.012	38.882	0.028	2.064	0.000	0.831	0.000	2.485	0.000
13.039	32.850	18.839	0.012	15.650	0.010	38.892	0.026	2.064	0.000	0.831	0.000	2.485	0.000
13.053	32.900	18.843	0.013	15.654	0.011	38.902	0.027	2.065	0.000	0.831	0.000	2.485	0.001
13.067	32.950	18.856	0.012	15.666	0.010	38.928	0.028	2.064	0.000	0.831	0.000	2.485	0.001
13.081	33.000	18.829	0.017	15.645	0.014	38.865	0.037	2.064	0.000	0.831	0.000	2.484	0.001
13.095	33.050	18.834	0.014	15.650	0.011	38.874	0.029	2.064	0.000	0.831	0.000	2.484	0.000
13.109	33.100	18.846	0.015	15.653	0.013	38.907	0.031	2.064	0.000	0.831	0.000	2.486	0.000
13.123	33.150	18.848	0.013	15.652	0.011	38.920	0.027	2.065	0.000	0.830	0.000	2.487	0.001
13.137	33.200	18.846	0.010	15.649	0.008	38.900	0.022	2.064	0.000	0.830	0.000	2.486	0.001
13.150	33.250	18.841	0.014	15.643	0.012	38.890	0.030	2.064	0.000	0.830	0.000	2.486	0.001
13.164	33.300	18.837	0.017	15.642	0.014	38.870	0.037	2.064	0.000	0.830	0.000	2.485	0.001
13.178	33.350	18.845	0.011	15.649	0.010	38.898	0.025	2.064	0.000	0.830	0.000	2.486	0.000
13.192	33.400	18.846	0.007	15.648	0.006	38.899	0.015	2.064	0.000	0.830	0.000	2.486	0.000
13.206	33.450	18.846	0.010	15.651	0.009	38.899	0.022	2.064	0.000	0.830	0.000	2.485	0.000
13.220	33.500	18.847	0.008	15.647	0.006	38.895	0.017	2.064	0.000	0.830	0.000	2.486	0.000
13.234	33.550	18.838	0.008	15.643	0.006	38.877	0.016	2.064	0.000	0.830	0.000	2.485	0.000
13.248	33.600	18.850	0.007	15.653	0.006	38.908	0.017	2.064	0.000	0.830	0.000	2.486	0.001
13.262	33.650	18.844	0.010	15.650	0.008	38.895	0.022	2.064	0.000	0.830	0.000	2.485	0.001
13.275	33.700	18.841	0.012	15.647	0.010	38.882	0.026	2.064	0.000	0.830	0.000	2.485	0.001
13.289	33.750	18.827	0.025	15.639	0.021	38.876	0.052	2.065	0.000	0.831	0.000	2.486	0.001
13.303	33.800	18.840	0.008	15.646	0.007	38.882	0.018	2.064	0.000	0.830	0.000	2.485	0.000
13.317	33.850	18.830	0.011	15.641	0.009	38.871	0.022	2.064	0.000	0.831	0.000	2.485	0.000
13.331	33.900	18.831	0.010	15.636	0.008	38.869	0.022	2.064	0.000	0.830	0.000	2.486	0.000
13.345	33.950	18.833	0.012	15.640	0.010	38.877	0.025	2.064	0.000	0.830	0.000	2.486	0.001
13.359	34.000	18.854	0.009	15.656	0.007	38.916	0.019	2.064	0.000	0.830	0.000	2.486	0.000
13.373	34.050	18.835	0.011	15.639	0.008	38.872	0.023	2.064	0.000	0.830	0.000	2.486	0.000
13.387	34.100	18.829	0.008	15.638	0.006	38.866	0.018	2.064	0.000	0.831	0.000	2.485	0.001
13.400	34.150	18.834	0.007	15.648	0.006	38.872	0.016	2.064	0.000	0.831	0.000	2.484	0.000
13.414	34.200	18.814	0.012	15.635	0.010	38.836	0.026	2.064	0.000	0.831	0.000	2.484	0.000
13.428	34.250	18.857	0.031	15.666	0.025	38.924	0.064	2.064	0.000	0.831	0.000	2.485	0.000
13.442	34.300	18.836	0.011	15.647	0.009	38.878	0.023	2.064	0.000	0.831	0.000	2.485	0.000
13.456	34.350	18.841	0.012	15.646	0.010	38.896	0.026	2.064	0.000	0.830	0.000	2.486	0.000
13.470	34.400	18.836	0.013	15.643	0.011	38.880	0.027	2.064	0.000	0.830	0.000	2.485	0.000
13.484	34.450	18.833	0.009	15.641	0.007	38.866	0.019	2.064	0.000	0.830	0.000	2.485	0.000
13.498	34.500	18.829	0.010	15.645	0.009	38.864	0.023	2.064	0.000	0.831	0.000	2.484	0.000
13.512	34.550	18.838	0.013	15.652	0.010	38.887	0.027	2.064	0.000	0.831	0.000	2.484	0.000
13.525	34.600	18.860	0.018	15.668	0.015	38.920	0.039	2.064	0.000	0.831	0.000	2.484	0.001
13.567	34.750	18.851	0.017	15.659	0.014	38.923	0.036	2.065	0.000	0.831	0.000	2.486	0.001
13.581	34.800	18.823	0.018	15.633	0.016	38.865	0.038	2.065	0.000	0.831	0.000	2.486	0.000
13.595	34.850	18.838	0.011	15.650	0.010	38.894	0.024	2.065	0.000	0.831	0.000	2.485	0.000
13.609	34.900	18.842	0.014	15.653	0.011	38.892	0.028	2.064	0.000	0.831	0.000	2.485	0.001
13.623	34.950	18.827	0.013	15.643	0.012	38.863	0.029	2.064	0.000	0.831	0.000	2.484	0.001
13.637	35.000	18.826	0.014	15.644	0.011	38.865	0.030	2.064	0.000	0.831	0.000	2.484	0.001
13.650	35.050	18.820	0.014	15.638	0.011	38.853	0.029	2.064	0.000	0.831	0.000	2.484	0.000
13.664	35.100	18.836	0.026	15.653	0.022	38.891	0.055	2.065	0.000	0.831	0.000	2.485	0.000
13.678	35.150	18.843	0.013	15.657	0.010	38.912	0.027	2.065	0.000	0.831	0.000	2.485	0.001
13.692	35.200	18.820	0.016	15.643	0.013	38.861	0.034	2.065	0.000	0.831	0.000	2.484	0.001
13.706	35.250	18.823	0.010	15.649	0.008	38.863	0.021	2.065	0.000	0.831	0.000	2.483	0.001
13.720	35.300	18.823	0.009	15.651	0.007	38.860	0.018	2.064	0.000	0.831	0.000	2.483	0.000
13.743	35.350	18.822	0.010	15.648	0.009	38.854	0.022	2.064	0.000	0.831	0.000	2.483	0.000
13.770	35.400	18.818	0.010	15.642	0.008	38.851	0.021	2.065	0.000	0.831	0.000	2.484	0.001
13.795	35.450	18.803	0.011	15.632	0.009	38.816	0.024	2.064	0.000	0.831	0.000	2.483	0.000
13.820	35.500	18.823	0.010	15.644	0.008	38.853	0.020	2.064	0.000	0.831	0.000	2.484	0.001
13.845	35.550	18.821	0.007	15.643	0.006	38.850	0.015	2.064	0.000	0.831	0.000	2.483	0.000
13.870	35.600	18.819	0.009	15.637	0.007	38.845	0.019	2.064	0.000	0.831	0.000	2.484	0.001
13.895	35.650	18.824	0.010	15.646	0.008	38.865	0.022	2.065	0.000	0.831	0.000	2.484	0.001
13.920	35.700	18.817	0.015	15.641	0.012	38.849	0.032	2.065	0.000	0.831	0.000	2.484	0.001

13.945	35.750	18.831	0.009	15.654	0.007	38.881	0.018	2.065	0.000	0.831	0.000	2.484	0.000
13.970	35.800	18.819	0.007	15.645	0.006	38.859	0.016	2.065	0.000	0.831	0.000	2.484	0.000
13.995	35.850	18.820	0.013	15.642	0.011	38.867	0.027	2.065	0.000	0.831	0.000	2.485	0.001
14.020	35.900	18.823	0.017	15.648	0.014	38.874	0.038	2.065	0.000	0.831	0.000	2.484	0.001
14.045	35.950	18.822	0.016	15.645	0.013	38.865	0.034	2.065	0.000	0.831	0.000	2.484	0.001
14.070	36.000	18.832	0.018	15.656	0.014	38.888	0.037	2.065	0.000	0.831	0.000	2.484	0.001
14.095	36.050	18.809	0.011	15.635	0.008	38.831	0.025	2.065	0.000	0.831	0.000	2.484	0.001
14.120	36.100	18.813	0.010	15.637	0.008	38.845	0.023	2.065	0.000	0.831	0.000	2.484	0.001
14.145	36.150	18.809	0.013	15.638	0.011	38.841	0.027	2.065	0.000	0.831	0.000	2.484	0.000
14.170	36.200	18.823	0.012	15.647	0.010	38.873	0.025	2.065	0.000	0.831	0.000	2.484	0.000
14.195	36.250	18.819	0.014	15.643	0.011	38.876	0.029	2.066	0.000	0.831	0.000	2.485	0.001
14.220	36.300	18.823	0.012	15.640	0.007	38.873	0.020	2.065	0.001	0.831	0.000	2.485	0.001
14.245	36.350	18.834	0.009	15.656	0.007	38.903	0.021	2.066	0.000	0.831	0.000	2.485	0.001
14.270	36.400	18.817	0.009	15.643	0.006	38.864	0.020	2.065	0.000	0.831	0.000	2.484	0.001
14.295	36.450	18.839	0.012	15.667	0.010	38.910	0.025	2.065	0.000	0.832	0.000	2.484	0.001
14.320	36.500	18.810	0.014	15.641	0.011	38.855	0.029	2.066	0.000	0.832	0.000	2.484	0.000
14.345	36.550	18.814	0.012	15.647	0.010	38.863	0.025	2.066	0.000	0.832	0.000	2.484	0.000
14.370	36.600	18.818	0.013	15.647	0.010	38.875	0.026	2.066	0.000	0.831	0.000	2.485	0.000
14.395	36.650	18.806	0.016	15.637	0.013	38.849	0.034	2.066	0.000	0.831	0.000	2.484	0.000
14.420	36.700	18.811	0.010	15.645	0.009	38.865	0.021	2.066	0.000	0.832	0.000	2.484	0.001
14.445	36.750	18.801	0.012	15.645	0.010	38.851	0.028	2.066	0.000	0.832	0.000	2.483	0.001
14.470	36.800	18.808	0.006	15.646	0.005	38.849	0.014	2.066	0.000	0.832	0.000	2.483	0.000
14.495	36.850	18.804	0.007	15.646	0.006	38.852	0.015	2.066	0.000	0.832	0.000	2.483	0.000
14.520	36.900	18.804	0.010	15.644	0.008	38.851	0.021	2.066	0.000	0.832	0.000	2.483	0.000
14.545	36.950	18.808	0.013	15.646	0.010	38.845	0.026	2.065	0.000	0.832	0.000	2.483	0.000
14.570	37.000	18.800	0.015	15.646	0.012	38.845	0.033	2.066	0.000	0.832	0.000	2.483	0.001
14.595	37.050	18.799	0.010	15.645	0.008	38.834	0.022	2.066	0.000	0.832	0.000	2.482	0.001
14.620	37.100	18.804	0.016	15.650	0.014	38.854	0.034	2.066	0.000	0.832	0.000	2.483	0.001
14.645	37.150	18.796	0.012	15.642	0.010	38.824	0.025	2.066	0.000	0.832	0.000	2.482	0.001
14.670	37.200	18.785	0.012	15.638	0.009	38.806	0.028	2.066	0.000	0.832	0.000	2.481	0.001
14.695	37.250	18.783	0.010	15.635	0.008	38.802	0.022	2.066	0.000	0.832	0.000	2.482	0.000
14.720	37.300	18.803	0.015	15.651	0.013	38.851	0.031	2.066	0.000	0.832	0.000	2.482	0.000
14.745	37.350	18.781	0.016	15.636	0.012	38.801	0.032	2.066	0.000	0.833	0.000	2.482	0.000
14.770	37.400	18.789	0.007	15.640	0.006	38.820	0.015	2.066	0.000	0.832	0.000	2.482	0.000
14.795	37.450	18.775	0.013	15.630	0.011	38.790	0.030	2.066	0.000	0.833	0.000	2.482	0.000
14.820	37.500	18.792	0.011	15.648	0.009	38.834	0.024	2.067	0.000	0.833	0.000	2.482	0.000
14.845	37.550	18.789	0.009	15.643	0.007	38.821	0.021	2.066	0.000	0.833	0.000	2.482	0.001
14.870	37.600	18.779	0.007	15.642	0.006	38.803	0.015	2.066	0.000	0.833	0.000	2.481	0.000
14.895	37.650	18.781	0.011	15.641	0.009	38.804	0.023	2.066	0.000	0.833	0.000	2.481	0.000
14.920	37.700	18.783	0.008	15.638	0.007	38.810	0.018	2.066	0.000	0.833	0.000	2.482	0.000
14.945	37.750	18.789	0.011	15.645	0.009	38.823	0.023	2.066	0.000	0.833	0.000	2.482	0.000
14.970	37.800	18.779	0.010	15.640	0.008	38.800	0.021	2.066	0.000	0.833	0.000	2.481	0.000
14.995	37.850	18.764	0.013	15.629	0.010	38.764	0.027	2.066	0.000	0.833	0.000	2.480	0.000
15.020	37.900	18.762	0.007	15.629	0.005	38.754	0.017	2.066	0.000	0.833	0.000	2.480	0.000
15.045	37.950	18.770	0.010	15.637	0.008	38.778	0.022	2.066	0.000	0.833	0.000	2.480	0.001
15.070	38.000	18.785	0.011	15.647	0.009	38.807	0.024	2.066	0.000	0.833	0.000	2.480	0.001
15.095	38.050	18.765	0.010	15.631	0.008	38.762	0.021	2.066	0.000	0.833	0.000	2.480	0.000
15.120	38.100	18.769	0.018	15.631	0.015	38.773	0.040	2.066	0.000	0.833	0.000	2.481	0.000
15.145	38.150	18.774	0.014	15.643	0.011	38.797	0.029	2.067	0.000	0.833	0.000	2.480	0.000
15.170	38.200	18.770	0.015	15.639	0.012	38.780	0.031	2.066	0.000	0.833	0.000	2.480	0.001
15.195	38.250	18.767	0.009	15.639	0.008	38.769	0.019	2.066	0.000	0.833	0.000	2.479	0.001
15.220	38.300	18.777	0.021	15.642	0.018	38.792	0.046	2.066	0.000	0.833	0.000	2.480	0.000
15.320	38.500	18.788	0.009	15.637	0.008	38.825	0.020	2.067	0.000	0.832	0.000	2.483	0.001
15.345	38.550	18.781	0.008	15.637	0.007	38.806	0.018	2.066	0.000	0.833	0.000	2.482	0.000
15.370	38.600	18.780	0.007	15.636	0.005	38.806	0.015	2.066	0.000	0.833	0.000	2.482	0.000
15.395	38.650	18.784	0.006	15.643	0.006	38.814	0.014	2.066	0.000	0.833	0.000	2.481	0.001
15.420	38.700	18.784	0.007	15.642	0.005	38.812	0.016	2.066	0.000	0.833	0.000	2.481	0.000
15.445	38.750	18.782	0.008	15.643	0.007	38.805	0.018	2.066	0.000	0.833	0.000	2.481	0.000
15.470	38.800	18.794	0.008	15.649	0.007	38.829	0.019	2.066	0.000	0.833	0.000	2.481	0.000
15.495	38.850	18.786	0.009	15.645	0.008	38.816	0.019	2.066	0.000	0.833	0.000	2.481	0.000
15.520	38.900	18.783	0.006	15.643	0.005	38.811	0.013	2.066	0.000	0.833	0.000	2.481	0.000
15.545	38.950	18.780	0.006	15.642	0.005	38.805	0.013	2.066	0.000	0.833	0.000	2.481	0.000
15.570	39.000	18.782	0.006	15.648	0.004	38.811	0.013	2.066	0.000	0.833	0.000	2.480	0.000
15.595	39.050	18.779	0.007	15.641	0.005	38.803	0.016	2.066	0.000	0.833	0.000	2.481	0.001
15.620	39.100	18.783	0.009	15.646	0.007	38.804	0.019	2.066	0.000	0.833	0.000	2.480	0.000
15.645	39.150	18.778	0.005	15.644	0.004	38.803	0.012	2.066	0.000	0.833	0.000	2.480	0.000
15.670	39.200	18.775	0.006	15.641	0.005	38.788	0.012	2.066	0.000	0.833	0.000	2.480	0.000
15.695	39.250	18.780	0.007	15.646	0.005	38.801	0.016	2.066	0.000	0.833	0.000	2.480	0.000
15.720	39.300	18.771	0.005	15.636	0.004	38.777	0.011	2.066	0.000	0.833	0.000	2.480	0.000
15.745	39.350	18.780	0.006	15.644	0.005	38.796	0.013	2.066	0.000	0.833	0.000	2.480	0.000
15.770	39.400	18.773	0.008	15.641	0.007	38.783	0.018	2.066	0.000	0.833	0.000	2.480	0.000
15.795	39.450	18.768	0.008	15.637	0.007	38.772	0.017	2.066	0.000	0.833	0.000	2.480	0.000
15.820	39.500	18.778	0.011	15.646	0.007	38.791	0.019	2.066	0.000	0.833	0.000	2.479	0.000
15.845	39.550	18.772	0.006	15.640	0.005	38.770	0.014	2.065	0.000	0.833	0.000	2.479	0.000
15.870	39.600	18.770	0.005	15.639	0.004	38.766	0.011	2.065	0.000	0.833	0.000	2.479	0.000
15.895	39.650	18.775	0.008	15.643	0.006	38.778	0.017	2.065	0.000	0.833	0.000	2.479	0.000
15.920	39.700	18.771	0.009	15.642	0.007	38.767	0.018	2.065	0.000	0.833	0.000	2.478	0.000
15.945	39.750	18.771	0.009	15.642	0.008	38.769	0.020	2.065	0.000	0.833	0.000	2.478	0.000
15.970	39.800	18.765	0.009	15.636	0.007	38.755	0.020	2.065	0.000	0.833	0.000	2.479	0.000
15.995	39.850	18.758	0.009	15.634	0.007	38.738	0.019	2.065	0.000	0.833	0.000	2.478	0.000
16.020	39.900	18.775	0.008	15.648	0.007	38.780	0.019	2.066	0.000	0.833	0.000	2.478	0.000
16.045	39.950	18.774	0.010	15.646	0.008	38.773	0.021	2.065	0.000	0.833	0.000	2.478	0.000
16.070	40.000	18.775	0.008	15.649	0.006	38.778	0.017	2.065	0.000	0.833	0.000	2.478	0.000
16.095	40.050	18.770	0.008	15.645	0.006	38.764	0.018	2.065	0.000	0.834	0.000	2.478	0.000
16.120	40.100	18.766	0.006	15.644	0.005	38.761	0.015	2.065	0.000	0.834	0.000	2.478	0.000
16.145	40.150	18.764	0.006	15.642	0.004	38.752	0.012	2.065	0.000	0.834	0.000	2.477	0.000
16.170	40.200	18.765	0.006	15.643	0.005	38.753	0.013	2.065	0.000	0.834	0.000	2.477	0.000
16.195	40.250	18.758	0.006	15.640	0.005	38.739	0.014	2.065	0.000	0.834	0.000	2.477	0.000
16.220	40.300	18.765	0.006	15.644	0.005	38.758	0.013	2.065	0.000	0.834	0.000	2.478	0.000
16.245	40.350	18.772	0.010	15.648	0.007	38.766	0.020	2.065	0.000	0.834	0.000	2.477	0.000
16.270	40.400	18.772	0.010	15.642	0.008	38.767	0.023	2.065	0.000	0.833	0.000	2.478	0.001
16.295	40.450	18.756	0.011	15.635	0.009	38.734	0.025	2.065	0.000	0.834	0.000	2.477	0.001
16.320	40.500	18.765	0.007	15.641	0.006	38.756	0.016	2.065	0.000	0.834	0.000	2.478	0.000
16.345	40.550	18.761	0.007	15.642	0.006	38.754	0.015	2.066	0.000	0.834	0.000	2.478	0.001
16.370	40.600	18.770	0.009	15.648	0.007	38.770	0.020	2.066	0.000	0.834	0.000	2.478	0.000
16.395	40.650	18.767	0.009	15.645	0.006	38.767	0.019	2.066	0.000	0.834	0.000	2.478	0.001
16.420	40.700	18.754	0.006	15.636	0.005	38.735	0.014	2.065	0.000	0.834	0.000	2.477	0.000
16.445	40.750	18.766	0.006	15.645	0.005	38.759	0.014	2.065	0.000	0.834	0.000	2.477	0.000
16.470	40.800	18.752	0.004	15.634	0.004	38.726	0.010	2.065	0.000	0.834	0.000	2.477	0.000
16.495	40.850	18.766	0.006	15.643	0.005	38.757	0.014	2.065	0.000	0.834	0.000	2.478	0.000
16.520	40.900	18.764	0.006	15.642	0.005	38.753	0.012	2.065	0.000	0.834	0.000	2.477	0.000

16.545	40.950	18.760	0.006	15.642	0.005	38.749	0.015	2.066	0.000	0.834	0.000	2.477	0.000
16.570	41.000	18.762	0.007	15.642	0.006	38.749	0.016	2.065	0.000	0.834	0.000	2.477	0.000
16.595	41.050	18.760	0.007	15.642	0.006	38.743	0.016	2.065	0.000	0.834	0.000	2.477	0.000
16.620	41.100	18.758	0.006	15.644	0.005	38.741	0.014	2.065	0.000	0.834	0.000	2.476	0.000
16.645	41.150	18.763	0.010	15.642	0.008	38.757	0.024	2.066	0.000	0.834	0.000	2.478	0.001
16.670	41.200	18.752	0.009	15.639	0.007	38.734	0.019	2.066	0.000	0.834	0.000	2.477	0.000
16.695	41.250	18.761	0.008	15.646	0.006	38.750	0.017	2.065	0.000	0.834	0.000	2.477	0.000
16.720	41.300	18.758	0.006	15.644	0.005	38.743	0.014	2.065	0.000	0.834	0.000	2.477	0.000
16.745	41.350	18.764	0.008	15.646	0.006	38.760	0.018	2.066	0.000	0.834	0.000	2.477	0.000
16.770	41.400	18.756	0.007	15.642	0.006	38.739	0.015	2.065	0.000	0.834	0.000	2.477	0.000
16.795	41.450	18.748	0.013	15.634	0.011	38.711	0.027	2.065	0.000	0.834	0.000	2.476	0.000
16.820	41.500	18.743	0.019	15.632	0.016	38.708	0.041	2.065	0.000	0.834	0.000	2.476	0.000
16.845	41.550	18.753	0.008	15.640	0.007	38.728	0.018	2.065	0.000	0.834	0.000	2.476	0.000
16.870	41.600	18.757	0.006	15.645	0.005	38.745	0.014	2.066	0.000	0.834	0.000	2.476	0.000
16.895	41.650	18.748	0.006	15.638	0.005	38.720	0.013	2.065	0.000	0.834	0.000	2.476	0.000
16.920	41.700	18.755	0.006	15.644	0.005	38.738	0.012	2.065	0.000	0.834	0.000	2.476	0.000
16.945	41.750	18.753	0.005	15.643	0.004	38.734	0.011	2.065	0.000	0.834	0.000	2.476	0.000
16.970	41.800	18.750	0.004	15.640	0.003	38.724	0.009	2.065	0.000	0.834	0.000	2.476	0.000
16.995	41.850	18.748	0.005	15.638	0.004	38.726	0.011	2.066	0.000	0.834	0.000	2.476	0.000
17.020	41.900	18.748	0.006	15.638	0.005	38.727	0.012	2.066	0.000	0.834	0.000	2.476	0.000
17.045	41.950	18.751	0.007	15.640	0.005	38.730	0.014	2.065	0.000	0.834	0.000	2.476	0.000
17.070	42.000	18.755	0.004	15.644	0.004	38.743	0.010	2.066	0.000	0.834	0.000	2.477	0.000
17.095	42.050	18.748	0.008	15.639	0.006	38.728	0.017	2.066	0.000	0.834	0.000	2.476	0.000
17.120	42.100	18.748	0.005	15.639	0.004	38.726	0.013	2.066	0.000	0.834	0.000	2.476	0.000
17.145	42.150	18.747	0.008	15.640	0.006	38.724	0.016	2.066	0.000	0.834	0.000	2.476	0.000
17.170	42.200	18.745	0.007	15.640	0.006	38.724	0.014	2.066	0.000	0.834	0.000	2.476	0.000
17.195	42.250	18.748	0.009	15.642	0.007	38.728	0.019	2.066	0.000	0.834	0.000	2.476	0.000
17.220	42.300	18.749	0.007	15.643	0.006	38.730	0.017	2.066	0.000	0.834	0.000	2.476	0.000
17.245	42.350	18.744	0.006	15.642	0.005	38.723	0.011	2.066	0.000	0.834	0.000	2.476	0.000
17.270	42.400	18.742	0.005	15.637	0.005	38.717	0.012	2.066	0.000	0.834	0.000	2.476	0.000
17.295	42.450	18.737	0.006	15.633	0.006	38.704	0.015	2.066	0.000	0.834	0.000	2.476	0.000
17.320	42.500	18.740	0.006	15.638	0.005	38.714	0.015	2.066	0.000	0.834	0.000	2.476	0.000
17.345	42.550	18.736	0.005	15.635	0.004	38.703	0.011	2.066	0.000	0.834	0.000	2.475	0.000
17.370	42.600	18.759	0.006	15.657	0.004	38.775	0.016	2.067	0.000	0.835	0.000	2.477	0.001
17.395	42.650	18.742	0.010	15.648	0.008	38.735	0.021	2.067	0.000	0.835	0.000	2.475	0.000
17.420	42.700	18.754	0.007	15.654	0.007	38.758	0.016	2.067	0.000	0.835	0.000	2.476	0.000
17.445	42.750	18.754	0.011	15.653	0.009	38.752	0.025	2.066	0.000	0.835	0.000	2.476	0.000
17.470	42.800	18.747	0.009	15.653	0.008	38.743	0.021	2.067	0.000	0.835	0.000	2.475	0.001
17.495	42.850	18.754	0.007	15.655	0.006	38.760	0.016	2.067	0.000	0.835	0.000	2.476	0.000
17.520	42.900	18.743	0.007	15.649	0.005	38.734	0.015	2.067	0.000	0.835	0.000	2.475	0.000
17.545	42.950	18.746	0.007	15.649	0.006	38.740	0.016	2.067	0.000	0.835	0.000	2.476	0.000
17.570	43.000	18.751	0.006	15.655	0.005	38.749	0.015	2.067	0.000	0.835	0.000	2.475	0.001
17.595	43.050	18.746	0.007	15.649	0.006	38.742	0.017	2.067	0.000	0.835	0.000	2.476	0.000
17.620	43.100	18.746	0.007	15.650	0.006	38.739	0.015	2.066	0.000	0.835	0.000	2.475	0.000
17.645	43.150	18.748	0.008	15.649	0.006	38.739	0.017	2.066	0.000	0.835	0.000	2.475	0.000
17.670	43.200	18.746	0.008	15.650	0.007	38.743	0.018	2.067	0.000	0.835	0.000	2.475	0.000
17.695	43.250	18.750	0.008	15.652	0.007	38.747	0.017	2.067	0.000	0.835	0.000	2.475	0.000
17.720	43.300	18.751	0.008	15.652	0.007	38.744	0.017	2.066	0.000	0.835	0.000	2.475	0.000
17.745	43.350	18.752	0.007	15.654	0.005	38.750	0.016	2.066	0.000	0.835	0.000	2.475	0.000
17.770	43.400	18.743	0.006	15.646	0.005	38.727	0.014	2.066	0.000	0.835	0.000	2.475	0.000
17.795	43.450	18.738	0.011	15.644	0.009	38.719	0.024	2.066	0.000	0.835	0.000	2.475	0.000
17.820	43.500	18.753	0.010	15.654	0.009	38.760	0.022	2.067	0.000	0.835	0.000	2.476	0.001
17.845	43.550	18.743	0.008	15.647	0.006	38.731	0.017	2.066	0.000	0.835	0.000	2.475	0.000
17.870	43.600	18.751	0.011	15.654	0.009	38.747	0.023	2.066	0.000	0.835	0.000	2.475	0.000
17.895	43.650	18.747	0.009	15.648	0.008	38.741	0.020	2.067	0.000	0.835	0.000	2.476	0.000
17.920	43.700	18.743	0.010	15.646	0.009	38.733	0.023	2.067	0.000	0.835	0.000	2.476	0.000
17.945	43.750	18.740	0.010	15.646	0.008	38.726	0.023	2.067	0.000	0.835	0.000	2.475	0.001
17.970	43.800	18.743	0.009	15.649	0.008	38.739	0.020	2.067	0.000	0.835	0.000	2.475	0.000
17.995	43.850	18.750	0.012	15.653	0.010	38.746	0.024	2.066	0.000	0.835	0.000	2.475	0.000
18.020	43.900	18.748	0.012	15.648	0.010	38.741	0.026	2.066	0.000	0.835	0.000	2.476	0.000
18.045	43.950	18.734	0.010	15.639	0.009	38.711	0.022	2.066	0.000	0.835	0.000	2.475	0.000
18.095	44.050	18.737	0.011	15.643	0.009	38.721	0.023	2.067	0.000	0.835	0.000	2.475	0.000
18.120	44.100	18.751	0.011	15.652	0.009	38.751	0.023	2.067	0.000	0.835	0.000	2.476	0.001
18.145	44.150	18.742	0.011	15.647	0.009	38.735	0.024	2.067	0.000	0.835	0.000	2.476	0.000
18.170	44.200	18.752	0.011	15.657	0.009	38.755	0.024	2.067	0.000	0.835	0.000	2.475	0.000
18.195	44.250	18.759	0.011	15.659	0.009	38.769	0.024	2.067	0.000	0.835	0.000	2.476	0.000
18.220	44.300	18.749	0.010	15.651	0.009	38.744	0.021	2.066	0.000	0.835	0.000	2.476	0.000
18.245	44.350	18.749	0.010	15.651	0.008	38.746	0.022	2.067	0.000	0.835	0.000	2.476	0.000
18.270	44.400	18.744	0.009	15.648	0.008	38.734	0.020	2.066	0.000	0.835	0.000	2.475	0.000
18.295	44.450	18.741	0.009	15.646	0.008	38.733	0.021	2.067	0.000	0.835	0.000	2.476	0.000
18.320	44.500	18.757	0.011	15.658	0.009	38.757	0.024	2.066	0.000	0.835	0.000	2.475	0.000
18.345	44.550	18.745	0.010	15.646	0.007	38.737	0.021	2.067	0.000	0.835	0.000	2.476	0.000
18.370	44.600	18.750	0.010	15.652	0.008	38.743	0.022	2.066	0.000	0.835	0.000	2.475	0.000
18.395	44.650	18.744	0.009	15.647	0.007	38.734	0.019	2.067	0.000	0.835	0.000	2.475	0.000
18.420	44.700	18.745	0.010	15.648	0.008	38.734	0.022	2.066	0.000	0.835	0.000	2.475	0.000
18.445	44.750	18.740	0.009	15.645	0.008	38.729	0.019	2.067	0.000	0.835	0.000	2.475	0.000
18.470	44.800	18.743	0.012	15.646	0.009	38.732	0.026	2.066	0.000	0.835	0.000	2.475	0.001
18.495	44.850	18.750	0.011	15.653	0.009	38.749	0.025	2.067	0.000	0.835	0.000	2.476	0.000
18.520	44.900	18.747	0.008	15.651	0.007	38.743	0.017	2.067	0.000	0.835	0.000	2.475	0.000
18.545	44.950	18.743	0.008	15.648	0.007	38.735	0.018	2.067	0.000	0.835	0.000	2.475	0.000
18.570	45.000	18.745	0.007	15.649	0.005	38.736	0.015	2.066	0.000	0.835	0.000	2.475	0.000
18.595	45.050	18.742	0.007	15.647	0.006	38.737	0.018	2.067	0.000	0.835	0.000	2.476	0.001
18.620	45.100	18.743	0.007	15.650	0.005	38.731	0.016	2.066	0.000	0.835	0.000	2.475	0.000
18.645	45.150	18.750	0.008	15.654	0.007	38.751	0.018	2.067	0.000	0.835	0.000	2.475	0.000
18.670	45.200	18.744	0.009	15.650	0.008	38.739	0.020	2.067	0.000	0.835	0.000	2.475	0.000
18.695	45.250	18.743	0.009	15.648	0.008	38.738	0.021	2.067	0.000	0.835	0.000	2.476	0.000
18.720	45.300	18.748	0.010	15.653	0.008	38.742	0.021	2.066	0.000	0.835	0.000	2.475	0.000
18.745	45.350	18.755	0.010	15.657	0.008	38.755	0.022	2.066	0.000	0.835	0.000	2.475	0.000
18.770	45.400	18.745	0.008	15.648	0.006	38.736	0.018	2.066	0.000	0.835	0.000	2.475	0.000
18.795	45.450	18.749	0.008	15.655	0.007	38.746	0.017	2.067	0.000	0.835	0.000	2.475	0.000
18.820	45.500	18.746	0.008	15.651	0.007	38.737	0.017	2.066	0.000	0.835	0.000	2.475	0.000
18.845	45.550	18.742	0.007	15.648	0.006	38.734	0.016	2.067	0.000	0.835	0.000	2.475	0.000
18.870	45.600	18.743	0.007	15.652	0.006	38.737	0.016	2.067	0.000	0.835	0.000	2.475	0.000
18.895	45.650	18.741	0.005	15.648	0.004	38.732	0.011	2.067	0.000	0.835	0.000	2.475	0.000
18.920	45.700	18.747	0.016	15.655	0.013	38.748	0.034	2.067	0.000	0.835	0.000	2.475	0.001
18.945	45.750	18.738	0.008	15.645	0.006	38.729	0.018	2.067	0.000	0.835	0.000	2.475	0.000
18.970	45.800	18.737	0.009	15.645	0.007	38.723	0.019	2.067	0.000	0.835	0.000	2.475	0.000
18.995	45.850	18.745	0.008	15.651	0.006	38.742	0.018	2.067	0.000	0.835	0.000	2.475	0.000
19.020	45.900	18.743	0.007	15.648	0.005	38.735	0.015	2.067	0.000	0.835	0.000	2.475	0.000
19.045	45.950	18.742	0.005	15.647	0.004	38.734	0.013	2.067	0.000	0.835	0.000	2.476	0.000
19.070	46.000	18.750	0.006	15.655	0.005	38.747	0.012	2.067	0.000	0.835	0.000	2.475	0.000

19.095	**46.050**	**18.750**	**0.010**	**15.653**	**0.008**	**38.746**	**0.021**	**2.066**	**0.000**	**0.835**	**0.000**	**2.475**	**0.000**
19.120	**46.100**	**18.746**	**0.006**	**15.648**	**0.005**	**38.733**	**0.013**	**2.066**	**0.000**	**0.835**	**0.000**	**2.475**	**0.000**
19.145	**46.150**	**18.748**	**0.007**	**15.653**	**0.006**	**38.743**	**0.016**	**2.066**	**0.000**	**0.835**	**0.000**	**2.475**	**0.000**
19.170	**46.200**	**18.743**	**0.007**	**15.649**	**0.006**	**38.732**	**0.017**	**2.067**	**0.000**	**0.835**	**0.000**	**2.475**	**0.000**
19.195	**46.250**	**18.742**	**0.007**	**15.646**	**0.006**	**38.732**	**0.016**	**2.067**	**0.000**	**0.835**	**0.000**	**2.475**	**0.000**
19.220	**46.300**	**18.743**	**0.007**	**15.648**	**0.006**	**38.733**	**0.016**	**2.066**	**0.000**	**0.835**	**0.000**	**2.475**	**0.000**
19.245	**46.350**	**18.744**	**0.008**	**15.647**	**0.006**	**38.731**	**0.016**	**2.066**	**0.000**	**0.835**	**0.000**	**2.475**	**0.000**
19.270	**46.400**	**18.749**	**0.007**	**15.654**	**0.005**	**38.741**	**0.016**	**2.066**	**0.000**	**0.835**	**0.000**	**2.475**	**0.001**
19.295	**46.450**	**18.743**	**0.007**	**15.644**	**0.006**	**38.727**	**0.015**	**2.066**	**0.000**	**0.835**	**0.000**	**2.476**	**0.000**
19.320	**46.500**	**18.752**	**0.007**	**15.656**	**0.006**	**38.749**	**0.014**	**2.066**	**0.000**	**0.835**	**0.000**	**2.475**	**0.000**
19.345	**46.550**	**18.747**	**0.006**	**15.649**	**0.005**	**38.738**	**0.014**	**2.066**	**0.000**	**0.835**	**0.000**	**2.475**	**0.000**
19.370	**46.600**	**18.747**	**0.009**	**15.650**	**0.007**	**38.735**	**0.019**	**2.066**	**0.000**	**0.835**	**0.000**	**2.475**	**0.000**
19.395	**46.650**	**18.749**	**0.008**	**15.651**	**0.006**	**38.739**	**0.017**	**2.066**	**0.000**	**0.835**	**0.000**	**2.475**	**0.000**
19.420	**46.700**	**18.749**	**0.008**	**15.651**	**0.006**	**38.740**	**0.017**	**2.066**	**0.000**	**0.835**	**0.000**	**2.475**	**0.000**
19.445	**46.750**	**18.753**	**0.006**	**15.655**	**0.005**	**38.757**	**0.015**	**2.067**	**0.000**	**0.835**	**0.000**	**2.476**	**0.000**
19.470	**46.800**	**18.747**	**0.007**	**15.650**	**0.005**	**38.738**	**0.014**	**2.066**	**0.000**	**0.835**	**0.000**	**2.475**	**0.000**
19.495	**46.850**	**18.749**	**0.007**	**15.649**	**0.006**	**38.739**	**0.014**	**2.066**	**0.000**	**0.835**	**0.000**	**2.475**	**0.000**
19.520	**46.900**	**18.739**	**0.008**	**15.643**	**0.007**	**38.720**	**0.018**	**2.066**	**0.000**	**0.835**	**0.000**	**2.475**	**0.000**
19.545	**46.950**	**18.743**	**0.008**	**15.644**	**0.007**	**38.724**	**0.017**	**2.066**	**0.000**	**0.835**	**0.000**	**2.475**	**0.000**

Table 16 Pb isotope results of 15 microns LA-MC-ICPMS in Chapter 5.

Age, Ma	Depth, mm	$^{206}Pb/^{204}Pb$	±2SE	$^{207}Pb/^{204}Pb$	±2SE	$^{208}Pb/^{204}Pb$	±2SE	$^{208}Pb/^{206}Pb$	±2SE	$^{207}Pb/^{206}Pb$	±2SE	$^{208}Pb/^{207}Pb$	±2SE
0.000	0.015	18.774	0.060	15.629	0.050	38.776	0.125	2.065	0.000	0.832	0.000	2.481	0.001
0.006	0.030	18.747	0.057	15.610	0.047	38.702	0.119	2.065	0.000	0.833	0.000	2.479	0.001
0.015	0.045	18.766	0.049	15.626	0.041	38.739	0.102	2.064	0.000	0.833	0.000	2.479	0.001
0.024	0.060	18.702	0.046	15.575	0.038	38.613	0.096	2.065	0.000	0.833	0.000	2.479	0.001
0.033	0.075	18.722	0.052	15.593	0.043	38.655	0.109	2.065	0.000	0.833	0.000	2.479	0.001
0.042	0.090	18.714	0.047	15.584	0.040	38.638	0.099	2.065	0.000	0.833	0.000	2.479	0.001
0.051	0.105	18.693	0.049	15.573	0.041	38.594	0.103	2.065	0.000	0.833	0.000	2.478	0.001
0.060	0.120	18.732	0.053	15.598	0.044	38.668	0.111	2.064	0.000	0.833	0.000	2.479	0.001
0.069	0.135	18.736	0.054	15.602	0.045	38.672	0.113	2.064	0.000	0.833	0.000	2.479	0.001
0.078	0.150	18.748	0.047	15.614	0.039	38.697	0.099	2.064	0.000	0.833	0.000	2.478	0.001
0.087	0.165	18.744	0.045	15.605	0.038	38.675	0.095	2.063	0.000	0.833	0.000	2.478	0.001
0.096	0.180	18.747	0.042	15.610	0.035	38.688	0.087	2.064	0.000	0.833	0.000	2.478	0.001
0.105	0.195	18.732	0.049	15.603	0.041	38.661	0.103	2.064	0.000	0.833	0.000	2.478	0.001
0.114	0.210	18.756	0.052	15.618	0.044	38.693	0.110	2.063	0.000	0.833	0.000	2.478	0.001
0.123	0.225	18.773	0.048	15.635	0.040	38.735	0.100	2.063	0.000	0.833	0.000	2.477	0.001
0.132	0.240	18.743	0.048	15.614	0.040	38.694	0.101	2.064	0.000	0.833	0.000	2.478	0.001
0.141	0.255	18.705	0.051	15.579	0.043	38.604	0.106	2.064	0.000	0.833	0.000	2.478	0.001
0.150	0.270	18.698	0.051	15.569	0.043	38.583	0.108	2.063	0.000	0.833	0.000	2.478	0.001
0.159	0.285	18.715	0.056	15.581	0.047	38.619	0.118	2.064	0.000	0.833	0.000	2.479	0.001
0.168	0.300	18.718	0.046	15.592	0.039	38.631	0.096	2.064	0.000	0.833	0.000	2.478	0.001
0.177	0.315	18.701	0.054	15.570	0.045	38.581	0.113	2.063	0.000	0.833	0.000	2.478	0.001
0.186	0.330	18.697	0.053	15.566	0.044	38.568	0.110	2.063	0.000	0.833	0.000	2.478	0.001
0.195	0.345	18.778	0.045	15.632	0.038	38.737	0.096	2.063	0.000	0.832	0.000	2.478	0.001
0.204	0.360	18.715	0.053	15.585	0.044	38.607	0.111	2.063	0.000	0.833	0.000	2.477	0.001
0.213	0.375	18.785	0.050	15.641	0.042	38.747	0.105	2.063	0.000	0.833	0.000	2.477	0.001
0.222	0.390	18.747	0.047	15.616	0.039	38.676	0.098	2.063	0.000	0.833	0.000	2.477	0.001
0.231	0.405	18.736	0.054	15.607	0.045	38.663	0.113	2.064	0.000	0.833	0.000	2.477	0.001
0.240	0.420	18.764	0.055	15.623	0.045	38.706	0.114	2.063	0.000	0.833	0.000	2.477	0.001
0.249	0.435	18.739	0.055	15.604	0.046	38.660	0.115	2.063	0.000	0.833	0.000	2.478	0.001
0.258	0.450	18.733	0.061	15.599	0.052	38.651	0.128	2.063	0.000	0.833	0.000	2.478	0.001
0.267	0.465	18.753	0.055	15.617	0.046	38.693	0.114	2.063	0.000	0.833	0.000	2.478	0.001
0.276	0.480	18.750	0.054	15.615	0.045	38.680	0.112	2.063	0.000	0.833	0.000	2.477	0.001
0.285	0.495	18.753	0.053	15.613	0.045	38.680	0.112	2.063	0.000	0.833	0.000	2.477	0.001
0.291	0.510	18.711	0.058	15.581	0.049	38.595	0.122	2.063	0.000	0.833	0.000	2.477	0.001
0.300	0.525	18.698	0.058	15.571	0.048	38.561	0.121	2.062	0.000	0.833	0.000	2.476	0.001
0.309	0.540	18.767	0.050	15.628	0.041	38.712	0.103	2.063	0.000	0.833	0.000	2.477	0.001
0.318	0.555	18.750	0.052	15.612	0.043	38.683	0.109	2.063	0.000	0.833	0.000	2.478	0.001
0.327	0.570	18.728	0.046	15.594	0.038	38.638	0.096	2.063	0.000	0.833	0.000	2.478	0.001
0.326	0.585	18.764	0.055	15.628	0.046	38.718	0.116	2.063	0.000	0.833	0.000	2.477	0.001
0.335	0.600	18.759	0.054	15.622	0.045	38.707	0.113	2.063	0.000	0.833	0.000	2.478	0.001
0.354	0.615	18.673	0.058	15.553	0.048	38.520	0.122	2.063	0.000	0.833	0.000	2.477	0.001
0.385	0.630	18.768	0.056	15.627	0.047	38.702	0.118	2.062	0.000	0.833	0.000	2.477	0.001
0.395	0.645	18.741	0.056	15.615	0.047	38.671	0.117	2.064	0.001	0.833	0.000	2.476	0.001
0.400	0.660	18.746	0.061	15.609	0.051	38.664	0.128	2.063	0.000	0.833	0.000	2.477	0.001
0.410	0.675	18.756	0.059	15.620	0.049	38.685	0.123	2.063	0.000	0.833	0.000	2.477	0.001
0.430	0.690	18.734	0.047	15.603	0.039	38.645	0.098	2.063	0.000	0.833	0.000	2.477	0.001
0.455	0.705	18.682	0.057	15.562	0.047	38.537	0.119	2.063	0.000	0.833	0.000	2.476	0.001
0.475	0.720	18.745	0.048	15.608	0.040	38.652	0.100	2.062	0.000	0.833	0.000	2.476	0.001
0.484	0.735	18.708	0.044	15.578	0.037	38.584	0.093	2.062	0.000	0.833	0.000	2.477	0.001
0.493	0.750	18.761	0.043	15.622	0.036	38.696	0.091	2.063	0.000	0.833	0.000	2.477	0.001
0.502	0.765	18.736	0.041	15.603	0.034	38.643	0.086	2.062	0.000	0.833	0.000	2.477	0.001
0.511	0.780	18.757	0.039	15.624	0.033	38.688	0.082	2.063	0.000	0.833	0.000	2.476	0.001
0.520	0.795	18.752	0.039	15.610	0.033	38.670	0.081	2.062	0.000	0.832	0.000	2.477	0.001
0.529	0.810	18.742	0.035	15.609	0.029	38.649	0.073	2.062	0.000	0.833	0.000	2.476	0.001
0.538	0.825	18.741	0.044	15.600	0.037	38.645	0.093	2.062	0.000	0.832	0.000	2.477	0.001
0.547	0.840	18.719	0.080	15.594	0.066	38.612	0.167	2.063	0.001	0.833	0.000	2.476	0.001
0.556	0.855	18.774	0.068	15.639	0.057	38.738	0.143	2.063	0.000	0.833	0.000	2.477	0.001
0.565	0.870	18.770	0.049	15.630	0.041	38.726	0.102	2.063	0.000	0.833	0.000	2.478	0.001
0.574	0.885	18.763	0.039	15.625	0.032	38.702	0.080	2.063	0.000	0.833	0.000	2.477	0.001
0.583	0.900	18.744	0.043	15.610	0.036	38.676	0.090	2.063	0.000	0.833	0.000	2.478	0.001
0.592	0.915	18.769	0.039	15.631	0.033	38.718	0.082	2.063	0.000	0.833	0.000	2.477	0.001
0.596	0.930	18.734	0.048	15.602	0.040	38.654	0.101	2.063	0.000	0.833	0.000	2.477	0.001
0.597	0.945	18.745	0.049	15.613	0.041	38.678	0.103	2.063	0.000	0.833	0.000	2.477	0.001
0.605	0.960	18.750	0.048	15.613	0.040	38.674	0.100	2.063	0.000	0.833	0.000	2.477	0.001
0.607	0.975	18.769	0.046	15.629	0.038	38.712	0.096	2.063	0.000	0.833	0.000	2.477	0.001
0.609	0.990	18.768	0.048	15.623	0.041	38.715	0.101	2.063	0.000	0.832	0.000	2.478	0.001
0.611	1.005	18.786	0.050	15.646	0.042	38.763	0.104	2.063	0.000	0.833	0.000	2.477	0.001
0.630	1.020	18.773	0.050	15.636	0.042	38.726	0.104	2.063	0.000	0.833	0.000	2.477	0.001
0.652	1.035	18.708	0.059	15.578	0.049	38.595	0.124	2.063	0.000	0.833	0.000	2.478	0.001
0.661	1.050	18.733	0.050	15.601	0.042	38.650	0.104	2.063	0.000	0.833	0.000	2.477	0.001
0.670	1.065	18.748	0.053	15.611	0.044	38.674	0.110	2.063	0.000	0.833	0.000	2.477	0.001
0.679	1.080	18.716	0.055	15.589	0.046	38.616	0.114	2.063	0.000	0.833	0.000	2.477	0.001
0.688	1.095	18.756	0.054	15.617	0.045	38.690	0.113	2.063	0.000	0.833	0.000	2.478	0.001
0.697	1.110	18.778	0.058	15.637	0.048	38.740	0.121	2.063	0.000	0.833	0.000	2.478	0.001
0.706	1.125	18.696	0.059	15.575	0.050	38.571	0.123	2.063	0.000	0.833	0.000	2.476	0.001
0.715	1.140	18.730	0.054	15.601	0.045	38.648	0.112	2.063	0.000	0.833	0.000	2.477	0.001
0.724	1.155	18.739	0.052	15.601	0.043	38.661	0.109	2.063	0.000	0.833	0.000	2.478	0.001
0.733	1.170	18.743	0.052	15.609	0.043	38.671	0.108	2.063	0.000	0.833	0.000	2.477	0.001
0.742	1.185	18.736	0.055	15.602	0.046	38.658	0.116	2.063	0.000	0.833	0.000	2.478	0.001
0.748	1.200	18.697	0.050	15.575	0.042	38.581	0.106	2.063	0.000	0.833	0.000	2.477	0.001
0.757	1.215	18.766	0.047	15.631	0.039	38.720	0.099	2.063	0.000	0.833	0.000	2.477	0.001
0.766	1.230	18.749	0.042	15.613	0.035	38.678	0.088	2.063	0.000	0.833	0.000	2.477	0.001
0.775	1.245	18.763	0.047	15.628	0.039	38.707	0.098	2.063	0.000	0.833	0.000	2.477	0.001
0.784	1.260	18.771	0.059	15.637	0.049	38.731	0.122	2.063	0.000	0.833	0.000	2.477	0.001
0.793	1.275	18.791	0.051	15.649	0.042	38.761	0.107	2.063	0.000	0.833	0.000	2.477	0.001
0.802	1.290	18.743	0.050	15.611	0.041	38.678	0.104	2.064	0.000	0.833	0.000	2.478	0.001
0.811	1.305	18.752	0.045	15.620	0.037	38.690	0.094	2.063	0.000	0.833	0.000	2.477	0.001
0.820	1.320	18.740	0.057	15.607	0.048	38.662	0.119	2.063	0.000	0.833	0.000	2.477	0.001
0.829	1.335	18.720	0.064	15.596	0.053	38.629	0.133	2.064	0.000	0.833	0.000	2.477	0.001
0.838	1.350	18.733	0.057	15.606	0.048	38.654	0.119	2.063	0.000	0.833	0.000	2.477	0.001
0.847	1.365	18.751	0.053	15.615	0.044	38.684	0.111	2.063	0.000	0.833	0.000	2.477	0.001
0.856	1.380	18.769	0.054	15.629	0.046	38.716	0.114	2.063	0.000	0.833	0.000	2.477	0.001
0.875	1.395	18.682	0.060	15.560	0.050	38.536	0.126	2.063	0.000	0.833	0.000	2.477	0.001
0.894	1.410	18.737	0.063	15.601	0.053	38.653	0.133	2.063	0.000	0.833	0.000	2.477	0.001
0.920	1.425	18.741	0.062	15.610	0.052	38.671	0.129	2.063	0.000	0.833	0.000	2.477	0.001
0.930	1.440	18.721	0.055	15.591	0.046	38.609	0.115	2.062	0.000	0.833	0.000	2.476	0.001

0.937	**1.455**	**18.754**	**0.053**	**15.620**	**0.045**	**38.692**	**0.112**	**2.063**	**0.000**	**0.833**	**0.000**	**2.477**	**0.001**
0.940	**1.470**	**18.769**	**0.057**	**15.628**	**0.048**	**38.717**	**0.120**	**2.063**	**0.000**	**0.833**	**0.000**	**2.477**	**0.001**
0.950	**1.485**	**18.742**	**0.057**	**15.605**	**0.048**	**38.656**	**0.119**	**2.063**	**0.000**	**0.833**	**0.000**	**2.477**	**0.001**
0.960	**1.500**	**18.731**	**0.054**	**15.603**	**0.046**	**38.635**	**0.114**	**2.063**	**0.000**	**0.833**	**0.000**	**2.476**	**0.001**
0.967	**1.515**	**18.727**	**0.048**	**15.592**	**0.041**	**38.619**	**0.102**	**2.062**	**0.000**	**0.833**	**0.000**	**2.477**	**0.001**
0.875	**1.395**	**18.682**	**0.060**	**15.560**	**0.050**	**38.536**	**0.126**	**2.063**	**0.000**	**0.833**	**0.000**	**2.477**	**0.001**
0.894	**1.410**	**18.737**	**0.063**	**15.601**	**0.053**	**38.653**	**0.133**	**2.063**	**0.000**	**0.833**	**0.000**	**2.477**	**0.001**
0.920	**1.425**	**18.741**	**0.062**	**15.610**	**0.052**	**38.671**	**0.129**	**2.063**	**0.000**	**0.833**	**0.000**	**2.477**	**0.001**

Table 17 the Nd isotope data in Fe-Mn crust PS97/247-2 in Chapter 5.

Depth, cm	Age, kyr	Material	$^{143}Nd/^{144}Nd$	±2SD	$\varepsilon_{Nd(0)}$	$\varepsilon_{Nd(t)}$	±2SD
0.5	0.29	Fe-Mn crust	0.512251	0.000010	-7.55	-7.55	0.19
44	18	Fe-Mn crust	0.512260	0.000010	-7.37	-7.21	0.19